AGARD-AR-308

AGARD

ADVISORY GROUP FOR AEROSPACE RESEARCH & DEVELOPMENT
7 RUE ANCELLE 92200 NEUILLY SUR SEINE FRANCE

AGARD ADVISORY REPORT 308

Propulsion and Energetics Panel Working Group 20 on Test Cases for Engine Life Assessment Technology

(Cas d'Essai pour la Gestion de la Durée de Vie des Moteurs)

This Advisory Report was prepared at the request of the Propulsion and Energetics Panel of AGARD.

NORTH ATLANTIC TREATY ORGANIZATION

Published September 1992

Distribution and Availability on Back Cover

AGARD

ADVISORY GROUP FOR AEROSPACE RESEARCH & DEVELOPMENT
7 RUE ANCELLE 92200 NEUILLY SUR SEINE FRANCE

AGARD ADVISORY REPORT 308

Propulsion and Energetics Panel Working Group 20 on

Test Cases for Engine Life Assessment Technology

(Cas d'Essai pour la Gestion
de la Durée de Vie des Moteurs)

This Advisory Report was prepared at the request of the Propulsion and Energetics Panel of AGARD.

North Atlantic Treaty Organization
Organisation du Traité de l'Atlantique Nord

The Mission of AGARD

According to its Charter, the mission of AGARD is to bring together the leading personalities of the NATO nations in the fields of science and technology relating to aerospace for the following purposes:

- Recommending effective ways for the member nations to use their research and development capabilities for the common benefit of the NATO community;
- Providing scientific and technical advice and assistance to the Military Committee in the field of aerospace research and development (with particular regard to its military application);
- Continuously stimulating advances in the aerospace sciences relevant to strengthening the common defence posture;
- Improving the co-operation among member nations in aerospace research and development;
- Exchange of scientific and technical information;
- Providing assistance to member nations for the purpose of increasing their scientific and technical potential;
- Rendering scientific and technical assistance, as requested, to other NATO bodies and to member nations in connection with research and development problems in the aerospace field.

The highest authority within AGARD is the National Delegates Board consisting of officially appointed senior representatives from each member nation. The mission of AGARD is carried out through the Panels which are composed of experts appointed by the National Delegates, the Consultant and Exchange Programme and the Aerospace Applications Studies Programme. The results of AGARD work are reported to the member nations and the NATO Authorities through the AGARD series of publications of which this is one.

Participation in AGARD activities is by invitation only and is normally limited to citizens of the NATO nations.

Published September 1992

ISBN 92-835-0686-3

Printed by Specialised Printing Services Limited
40 Chigwell Lane, Loughton, Essex IG10 3TZ

Recent Publications of the Propulsion and Energetics Panel

CONFERENCE PROCEEDINGS (CP)

Engine Cyclic Durability by Analysis and Testing
AGARD CP 368, September 1984

Gears and Power Transmission Systems for Helicopters and Turboprops
AGARD CP 369, January 1985

Heat Transfer and Cooling in Gas Turbines
AGARD CP 390, September 1985

Smokeless Propellants
AGARD CP 391, January 1986

Interior Ballistics of Guns
AGARD CP 392, January 1986

Advanced Instrumentation for Aero Engine Components
AGARD CP 399, November 1986

Engine Response to Distorted Inflow Conditions
AGARD CP 400, March 1987

Transonic and Supersonic Phenomena in Turbomachines
AGARD CP 401, March 1987

Advanced Technology for Aero Engine Components
AGARD CP 421, September 1987

Combustion and Fuels in Gas Turbine Engines
AGARD CP 422, June 1988

Engine Condition Monitoring – Technology and Experience
AGARD CP 448, October 1988

Application of Advanced Material for Turbomachinery and Rocket Propulsion
AGARD CP 449, March 1989

Combustion Instabilities in Liquid-Fuelled Propulsion Systems
AGARD CP 450, April 1989

Aircraft Fire Safety
AGARD CP 467, October 1989

Unsteady Aerodynamic Phenomena in Turbomachines
AGARD CP 468, February 1990

Secondary Flows in Turbomachines
AGARD CP 469, February 1990

Hypersonic Combined Cycle Propulsion
AGARD CP 479, December 1990

Low Temperature Environment Operations of Turboengines (Design and User's Problems)
AGARD CP 480, May 1991

CFD Techniques for Propulsion Applications
AGARD CP 510, February 1992

Insensitive Munitions
AGARD CP 511, July 1992

Combat Aircraft Noise
AGARD CP 512, April 1992

Airbreathing Propulsion for Missiles and Projectiles
AGARD CP 526, September 1992

ADVISORY REPORTS (AR)

Through Flow Calculations in Axial Turbomachines *(Results of Working Group 12)*
AGARD AR 175, October 1981

Alternative Jet Engine Fuels *(Results of Working Group 13)*
AGARD AR 181, Vol.1 and Vol.2, July 1982

Suitable Averaging Techniques in Non-Uniform Internal Flows *(Results of Working Group 14)*
AGARD AR 182 (in English and French), June/August 1983

Producibility and Cost Studies of Aviation Kerosines *(Results of Working Group 16)*
AGARD AR 227, June 1985

Performance of Rocket Motors with Metallized Propellants *(Results of Working Group 17)*
AGARD AR 230, September 1986

Recommended Practices for Measurement of Gas Path Pressures and Temperatures for Performance Assessment of Aircraft Turbine Engines and Components *(Results of Working Group 19)*
AGARD AR 245, June 1990

The Uniform Engine Test Programme *(Results of Working Group 15)*
AGARD AR 248, February 1990

Test Cases for Computation of Internal Flows in Aero Engine Components *(Results of Working Group 18)*
AGARD AR 275, July 1990

LECTURE SERIES (LS)

Ramjet and Ramrocket Propulsion Systems for Missiles
AGARD LS 136, September 1984

3-D Computation Techniques Applied to Internal Flows in Propulsion Systems
AGARD LS 140, June 1985

Engine Airframe Integration for Rotorcraft
AGARD LS 148, June 1986

Design Methods Used in Solid Rocket Motors
AGARD LS 150, April 1987
AGARD LS 150 (Revised), April 1988

Blading Design for Axial Turbomachines
AGARD LS 167, June 1989

Comparative Engine Performance Measurements
AGARD LS 169, May 1990

Combustion of Solid Propellants
AGARD LS 180, July 1991

Steady and Transient Performance Prediction of Gas Turbine Engines
AGARD LS 183, May 1992

AGARDOGRAPHS (AG)

Manual for Aeroelasticity in Turbomachines
AGARD AG 298/1, March 1987
AGARD AG 298/2, June 1988

Measurement Uncertainty within the Uniform Engine Test Programme
AGARD AG 307, May 1989

Hazard Studies for Solid Propellant Rocket Motors
AGARD AG 316, September 1990

REPORTS (R)

Application of Modified Loss and Deviation Correlations to Transonic Axial Compressors
AGARD R 745, November 1987

Rotorcraft Drivetrain Life Safety and Reliability
AGARD R 775, June 1990

Foreword

The worldwide trend toward producing lighter, more efficient aircraft propulsion systems presents a special challenge to the engine component designer. Higher cycle temperatures, increased aerodynamic loads, and higher rotating speeds coupled with reduced component weights all work in opposition to component life and durability. Basically, two technologies are available or are emerging that will enable component life and durability to be maintained at at least the present level: 1) new high temperature, high strength-to-weight ratio materials; 2) new structural design and life prediction codes and methodologies. The six test cases comprising this AGARD report address some of the developmental and validation requirements associated with the second technology.

It is the specific intent of this report to provide to the engine component design community as complete a data set and operational or test history as possible for use in exercising and validating newly emerging or developmental codes. In each case, special care was taken to assure that necessary and sufficient material data, component design information, rig or engine interface data, and test condition definition was provided. The test cases themselves, therefore, offer well characterized example problems typically incorporating the important design complexities, transient loads, and operating conditions encountered in service without the usual uncertainties associated with actual engine field experience. Also, in each case, the AGARD working group conducted a "validating analysis" to assure completeness of the data set and to identify any inconsistencies between analytical results and observed crack initiation or failure phenomena. Where appropriate, these inconsistencies were identified in the individual test case texts.

It is the hope of AGARD that use will be made of these test cases by the aero gas turbine design and development community. We solicit any feedback from users, and would appreciate a brief summary of users' experience in applying these test cases. Specific questions or comments applicable to a particular test case should be addressed to the test case author. General comments and overall feedback should be addressed to the undersigned.

Résumé

Ce rapport présente une série de six cas d'essai destinés à permettre le développement et la validation des codes pour l'analyse structurale et la prévision de la durée de vie des organes des turbines à gaz. Les cas d'essai sont basés sur des campagnes de simulation de fonctionnement de turbines.

Les bases de données des cas d'essai contiennent des informations sur la conception géométrique, permettant de définir le composant, les données d'interface sur le banc d'essais, les informations sur les matériaux et des données sur les conditions d'essai avec, en particulier, les sollicitations stationnaires, dynamiques et thermiques. Des données sur le début et la propagation de la fissuration y sont également incluses.

Pour la première fois donc, ces cas d'essai nous fournissent l'ensemble des données sur le composant et sur les sollicitations permettant ainsi de vérifier que les codes existants ou en cours d'élaboration donnent des prévisions cohérentes et significatives.

Dr Robert C. Bill
Chairman, WG-20

Propulsion and Energetics Panel
Working Group 20

Chairman: Dr Robert C. Bill
US Army Propulsion Directorate
NASA Lewis Research Center
Mail Stop 77-12
21000 Brookpark Road
Cleveland, Ohio 44135
United States

MEMBERS

Canada:
Mr D. Smith
Head, Rockets Section
Energetic Material Division
Defence Research Establishment
Valcartier, P.O. Box 8800
Courcelette, Quebec GOA 1R0

Dr Raj Thamburaj
Hawker Siddeley Canada
Orenda Division
Box 6001
Toronto AMF, Ontario
L5P 1B3

France:
Mlle Madeleine Chaudonneret
ONERA — Direction des Structures
29, avenue Division Leclerc
92322 Châtillon s/Bagneux

Mr Jean-François Chevalier
Ingenieur en Chef — Recherches
SNECMA
Centre D'Essais de Villaroche
77550 Moissy Cramayel

Mr Bruno Dambrine
Département Mécanique Avancée
SNECMA Direction Technique
77550 Moissy Cramayel
(until Oct. 92)

Mr Roland Krafft
Service YLMG
SNECMA-Villaroche
77550 Moissy Cramayel

Germany:
Dr-Ing. Jurgen Broede
Motoren- und Turbinen- Union
München GmbH
MTU GmbH
Abt. EMBM, Postfach 50 06 40
8000 München 50

Prof.-Dr Dietmar K. Hennecke
Fachgebiet Flugantriebe
Technische Hochschule Darmstadt,
Petersenstrasse 30
W-6100 Darmstadt

The Netherlands:
Mrs Anita Looije
NLR
Postbox 153
8300 AD Emmeloord

Mr Mom
NLR
Postbox 153
8300 AD Emmeloord

United Kingdom:
Dr George F. Harrison
Defence Research Agency
Farnborough, Hants GU14 0LS

Mr Lawrence M. Jenkins
Mechanical Technology
Rolls Royce plc
P.O. Box 3
Filton
Bristol BS12 7QE

Mr Michael Walsh
Rolls Royce plc
PO Box 3
Filton
Bristol BS12 7QE

United States:
Dr Leonard Beitch
Mail Stop A-333
General Electric Company
Aircraft Engine Business Group
P.O. Box 6301
Cincinnati OH 45215-6301
(until Oct. 89)

Mr William Cowie
ASD/YZEE
Wright Patterson Air Force Base
OH 45433-6503

Mr Robert Ditz
Manager, Life Management Programs
GE Aircraft Engines
Cincinnati, Ohio
(until Oct. 88)

Dr Paul A. Domas
General Electric Aircraft Engines
Mail Stop Q105
1, Neumann Way, Evendale
OH 45215-6301

Mr Thomas E. Farmer
Pratt and Whitney Aircraft
MS 713-39, P.O. Box 2691
West Palm Beach, FL 33402

Mr William H. Parker
Allison Gas Turbine Division, GMC
Speed Code T10B
PO Box 420
Indianapolis, Indiana 46206-0420

Ms Sharon Vukelich
Acting Chief, Structures and
Durability Group
Aeronautical Systems Division
(ASD/YZEE)
Wright Patterson AFB OH 45433-6503

PANEL EXECUTIVE

Dr E. Riester (GE)

Tel: (1) 4738 5785/87
Telex: 610176F
Telefax: (1) 4738 5799

Mail from Europe
AGARD-OTAN
7, rue Ancelle
92200 Neuilly sur Seine
France

Mail from US and Canada
AGARD-NATO
Attn: PEP Executive
Unit 21551
APO AE 09777

Contents

List of Symbols

a	Crack Length (m)
CPH	Cycles per Hour
dB	Decibels
da/dN	Crack Propagation Rate (m/cycle)
E	Modulus of Elasticity (GPa)
EFH	Engine Flight Hours
f	Frequency (sec^{-1})
ft	Length Unit, Feet
GPa	Gigapascal (10^9 N/m^2)
hp	Horsepower
HP	High Pressure
HPC	High Pressure Compressor
Hz	Hertz (sec^{-1})
in	Length Unit, Inch
K	Stress Intensity ($lb/in^{3/2}$; $MPam^{1/2}$)
K_t	Stress Concentration Factor
Kg	Kilogram
KN	Kilonewton
Ksi	10^3 lb/in^2
lb	Pound
LCF	Low Cycle Fatigue
M	Length Unit, Meter
MPa	Megapascal (10^6 N/m^2)
N_s	Spool Speed (rpm)
N	Number of Cycles
N_B	Cycles to Rupture
N_f	Cycles to Failure
PS	Proof Strength (yield strength) (Ksi or MPa)
R	R-ratio (min. stress/max. stress)
Rσ	Stress Ratio (min. stress/max. stress)
R_ϵ	Strain Ratio (min. stress/max. stress)
T	Temperature (°F, °C)
rpm	Revolutions per Minute
RT	Room Temperature
α	Coefficient of Expansion (T^{-1})
ΔK	Stress Intensity Range
ΔE	Strain Amplitude Range (E max. E min.)
Δσ	Stress Range (σ max. −σ min.)
ϵ	Strain
ϱ	Density (gm/cm^3; lb/ft^3)
υ	Poisson Ratio
σ	Stress (Ksi, MPa, GPa)

Chapter 1

INTRODUCTION

by

Dr Robert C. Bill
Chief, Engine & Transmission Div.
US Army Propulsion Directorate
(AVSCOM) NASA Lewis Research Center
21000 Brookpark Road
Cleveland, Ohio 44135
United States

1. BACKGROUND

The cost of maintaining fleet readiness and the trend toward higher power to weight ratio gas turbine engines has put increased importance on component structural analysis and life prediction. Over the past decade there has been considerable progress in the development of advanced structural analysis and life prediction codes for gas turbine engine components. Validation of these codes on the component level is a real challenge because of the scarcity of well documented data packages on actual engine components tested to failure. Hence, the Engine Life Assessment Working Group was formed, having as its objective the assembly of a comprehensive number of well documented test cases that would enable advanced code validation on the component level to be conducted. A summary of significant actions and meetings held in support of the Engine Life Assessment Working Group is presented in Table 1.

The scope of the working group's efforts was limited to the development of test cases involving crack initiation and crack propagation under elastic and elasto-plastic loading conditions. Test cases involving loading conditions that result in time dependent material behavior (ie. creep, cyclic creep, time dependent relaxation) were not included. The reason for this limitation in scope was the non-availability of sufficient published material data pertaining to documented component loading in the time dependent regime.

2. SUMMARY OF TEST CASES

Two formidable questions immediately faced the working group: 1) What constitutes a complete, useable test case? 2) How can assurance be provided that a test case is not only complete, but is self-consistent (ie. the database is not in some way flawed)? Addressing the completeness question first, seven categories of data were identified which, if fully addressed, would assure completeness of the data package. These categories are summarized in Table 3, and include all of the loading data, service or test history, essential environmental information, necessary material data, geometric design information pertaining to the component of interest, and sufficient definition of the interface between the component and the rest of the engine or test rig structure. In and of itself, definition of the list of seven data categories is considered a significant contribution of the Working Group, and was originated by Robert Ditz of GE Aircraft Engines.

The question of self-consistency and detail sufficiency of test case data bases was addressed through independent validating analyses that were conducted on each test case. The analyses were conducted to verify that enough information in each data category was provided, and that there was reasonable agreement between the analytically predicted and the actually observed failure mode and lifetime. It is assumed that sufficient data for the validating analytical code is roughly equivalent to sufficient data for any possible user analysis. Each individual test case write-up includes a paragraph or two summarizing the findings of the validating analysis work.

Taken as a set, the six test cases comprising this document include a collection of problems that consider crack initiation and crack propagation in hot section and cold section engine components. A broad range of component configurations and loading conditions are included. A detailed listing of test case attributes is included in Table 4. Following is a brief summary of each test case in the order in which it appears.

The first test case documents crack initiation and subsequent crack growth in the first stage gas generator turbine disk of the SNECMA Larzac engine. All of the testing was conducted in a spin pit test facility, and care was taken to fully describe the disk/rig interface, thermal and mechanical loading environment, and the number of spin cycles required for crack initiation. At periodic inspection intervals, crack growth was monitored. Initiation was at a fillet root radius associated with a labyrinth seal support cone. It is expected that this test case would be of particular interest in the validation of elasto-plastic crack initiation and growth models in a complex structural analysis environment, under multiaxial loading states.

The second test case involved crack initiation in the blade retention region and assembly bolt hole region of the third stage high pressure compressor disk of the MTU RB 199. Significant features of this test case included a substantial amount of engine field history combined with controlled spin pit test history. Observed spin pit cycles to crack initiation, and number of cracks are all documented. Validation of safe life LCF lifing models, in the presence of complex geometric stress concentrators would be appropriate applications of this test case.

The next test case, provided by GE Aircraft Engines, pertains to the CF6-6 high pressure compressor blade retention/locking features on the compressor spool. The Ti-6-4 spool was subjected to spin pit testing, with very frequent inspection intervals, resulting in detailed crack growth measurement data. It is felt that this test case provides an excellent tool for validation of fracture mechanics life prediction methodologies.

The fourth test case, offered by Rolls Royce, has as its salient feature subsurface crack propagation at inclusion sites in an RB211 HPT disk. The disk was subjected to high temperature spin pit testing, and crack growth related data included initial inclusion size, location of geometry, and final crack size. Cyclic history was well documented. This test case would be appropriate for validation of linear elastic fracture mechanics life prediction models.

Allison Gas Turbine provided the fifth test case, addressing the TF41 low pressure compressor drive shaft. Four shafts were subjected to torsional rig testing, simulating engine operating conditions. Cycles to initiation, and detailed crack growth data are well documented. The unique features of this test case include the predominantly torsional loading environment, documented multiple initiations, and controlled HCF cycling superimposed on the major cycle.

The final test case included in this document was contributed by Pratt & Whitney, and it addresses crack propagation life in the F100 engine second stage Ti-6-4 fan disk bolthole. Among the unique features of this test case are the presence of a hot spin imposed residual stress at the critical locations of one of the tested disks, artificial initiation of fatigue cracks, and rig testing of two disk design variations. With detailed crack growth documentation, this test case offers a unique opportunity to validate LEFM life models and structural analysis models in a strong residual stress field.

3. ACKNOWLEDGEMENTS

The assembly of the test cases in this report was made possible only through the exemplary cooperation and commitment of the companies and their selected representatives comprising the Engine Life Assessment Working Group. AGARD's special thanks are extended to SNECMA, for the contributions of Mr. R. Krafft and Mr. J. F. Chevalier; to MTU, for Dr. J. Broede's fine work; to General Electric Aircraft Engines for the guidance and input provided by Mr. R. Ditz, Dr. L. Beitch, and Dr. P. Domas; to Rolls Royce for Mr. L. Jenkins' and Mr. M. Walsh's contributions; to Allison Gas Turbine Division of GM for the support provided by Mr. W. Parker; to Pratt & Whitney Aircraft for the contributions of Mr. T. Farmer; and to Hawker Siddeley, Inc., of Canada, for the documented recommendations provided by Dr. R. Thamburaj. No less important to the Working Group's efforts were the technical guidance, suggestions, and editorial review support given by Mrs. A. Looye (NLR), Madame M. Chaudonneret (ONERA), Ms. S. Vukelich (USAF), Mr. W. Cowie (USAF), Dr. Harrison (DRE, Farnborough), and Prof. D. Hennecke (Univ. of Darmstadt). The support provided by all of the companies and organizations mentioned was timely and unstinting, and the work of all individuals was of the highest quality.

TABLE 1: HISTORY OF ENGINE LIFE ASSESSMENT WORKING GROUP

EVENT	DATE	OUTPUT
AHC 65-3 Mtg	8 & 9 Sept. '86	Terms of Reference: Objective, Scope of Work; Working Group Designation (WG-20)
WG-20 (P)*	5 May '87	Working Group Membership; Preliminary Test Case List
WG-20 (P)*	23 Oct '87	Long Range Schedule Developed; "Pilot Test Case" Concept
WG-20-1	30-31 May and 1, 2 June '88	Philosophical discussions; Some Candidate Test Cases Identified
WG-20-2	6, 7 Oct '88	Test Case Content Defined Additional Test Cases
WG-20-3	23, 24 May '89	Further Philosophical Discussions; Validating Analysis Concept Adopted
WG-20-4 (SMP)**	4, 5 Oct '89	Full Test Case List Developed; Three Documented Test Case Data Packages; Analyses Underway
WG-20-5	28, 29 May '90	First Completed & Validated Test Case; Four Other Completed Data Packages
WG-20-6	8, 11 Oct '90	Three Test Cases Validated and in Review; Final Documentation Format Discussed
WG-20-7	29, 30 May '91	Five Tests Cases in Review; Documentation Format Defined; Future Recommendations Discussed
WG-20-8	23, 24 Oct '91	Documentation Completed; In Review

* (P) implies meeting held prior to official AGARD approval of WG-20

** Meeting held in conjunction with 68th SMP panel meeting in Brussels

TABLE 3: TEST CASE DATA CATEGORIES

CATEGORY	DEFINITION
* Component Geometry	Sufficient Dimensional and Shape Data to Permit Structural Analysis. Precise Dimensions and Tolerances Generally not Required.
* Part Processing Info	Pertinent Heat Treatments, Surface Hardening, Residual Stresses and Surface Finishes as Appropriate.
* Operating Conditions	Full Description of Actual Test Conditions to Which Test Article (Component) Was Subjected.
* Boundary Conditions for Stress Analysis	Complete Description of Mechanical and Thermal Interface Between Test Article and Test Vehicle.
* Heat Transfer Information	Thermal Environment in Which Test Was Conducted
* Materials Data	Physical Property Data, Monotonic and Cyclic Mechanical Property Data, and Crack Growth Data Applicable to Material Heat from Which Test Article was Drawn.
* Field Data, Service History	Location on Test Article of Crack Initiation or Other Failure Sites; Crack Growth Measurements.

TABLE 4: TEST CASE SUMMARY

TEST CASE DESCRIPTION					ENVIRONMENTAL FEATURES					LIFE ELEMENTS			OTHER CONSIDERATIONS			
CASE NO.	SOURCE	ENGINE	COMPONENT	LOCATION	PLASTIC	STRESS CONC.	MULTI-AXIAL	MISSION	TEMP.	INITIATION SITE	FATIGUE	CRACK GROWTH	RESIDUAL STRESS	MAT'L	TEST METHOD	COMMENTS
1	SNECMA	LARZAC	TURBINE	AFT ARM FILLET	YES	NO	YES	NO	ELEV	DEFORMATION	YES	YES	NO	IN718	SPIN PIT	INITIATION AND PROPAGATION IN BIAXIAL STRESS FIELD
2	MTU	RB199	3RD STAGE	BOLT HOLE & RIM SLOT	YES	YES	NO	NO	RT & ELEV	DEFORMATION	YES	NO	NO	CORROSION RESIST. STEEL	SPIN PIT	HOLE AND SLOT SURFACE RESIDUAL MACHINING STRESSES MAY BE INFLUENTIAL
3	GEAE	CF6-6	COMPRESSOR	BLADE LOCK SLOT	YES	YES	NO	NO	150F 66C	ARTIFICIAL	NO	YES	YES (SHOT PEEN)	TI 6-4	SPIN PIT	MEASURED CRACK GROWTH FROM STRESS CONCENTRATION IN 200 CYCLE INCREMENTS
4	RR	RB211 -524	HP TURBINE DISK	DISK BORE REGION (SUB-SURFACE)	NO	NO	NO	NO	932F 500C	INCLUSION	NO	YES	YES (QUENCH STRESSES AT BOXE)	WASPALOY	SPIN PIT	SUBSURFACE CRACK GROWTH FROM INCLUSION
5	ALLISON	T41-A-1 T41-A-2	LOW PRESSURE COMPRESSOR DRIVE SHAFT	OIL HOLES	YES	YES	NO - TORQUE	YES MAJOR/ MINOR	ELEV	CORROSION PITS IMPERFECTIONS IN HOLES	YES (FROM FLAWS)	YES (UNDER TORSIONAL LOADING)	NO	EMS 64500 STEEL	TORQUE TEST RIG	INITIATION AND PROPAGATION FROM FLAWS IN HOLES UNDER MULTILEVEL TORQUE LOADING
6	P&WA	F100	FAN DISK (STAGE 2)	BOLTHOLE	YES	YES	NO	YES	70F 21C	ARTIFICIAL	NO	YES	YES (HOT PRESPIN)	TI 6-4	FERRIS WHEEL	CRACK GROWTH TRACKED FROM STRESS CONCENTRATIONS IN TWO TESTS

PLASTIC - Local stresses exceed yield strength.
STRESS CONC. - Stress concentration.
MISSION - Complex test stress cycle.
TEMP. - All cases were steady state.
INITIATION SITE - **DEFORMATION** - Crack initiation not associated with initial flaw.
- **ARITIFICAL** - Crack growth from artificial crack starter notch.
- **INCLUSIONS** - Crack initiation from inclusion.

FATIGUE - Case involves fatigue crack initiation.
CRACK GROWTH - Case involves fatigue crack growth.
RESIDUAL STRESS - Residual stress information provided in test case for

Chapter 2

LARZAC HP TURBINE DISK

CRACK INITIATION AND PROPAGATION SPIN PIT TEST

by

Roland KRAFFT
S.N.E.C.M.A.
Service YLEC
77550 MOISSY CRAMAYEL
FRANCE

1. INTRODUCTION

The component test of the LARZAC HP turbine disk proposed in this document provides the opportunity for validation of life prediction methodologies concerning crack initiation and propagation behaviour on a area of a nickel-based refractory alloy turbine disk subjected to multi-axial loading.

The specific characteristics of this test are listed in general introduction. It should be noted, in particular, that this test, carried out under a partial vacuum at high temperature, proposes study of the natural initiation and propagation of a low-cycle fatigue crack. This test case offers the following advantages :

- test analysis of a real turbine part,
- well defined test conditions,
- natural initiation of a crack in an area subjected to multi-axial loading leading to moderate plasticity,
- a well-known nickel-based material: INCONEL 718,
- only two-dimensional test analysis, but requiring fine elastic-plastic modeling.

The limitations of the test are as follows :

- it is a component test carried out under isothermic conditions, with a simple load cycle (non-mission),
- it involves a complex disk environment (recreating that of an engine) requiring modelling of the adjacent parts to simulate realistic boundary conditions.

ASSESSMENT ANALYSIS

From this study conducted by GE and RAE, it was concluded that the test case includes sufficient information to :

- generate a viable stress analysis model,
- make analytic predictions of fatigue crack propagation behaviour, and
- correlate life predictions with spin pit test results.

The LARZAC test case was assessed by constructing a two dimensional axisymetric finite element model of the entire spin pit structure including the forward shaft, turbine disk, aft seal, and cone. Rim loading was simulated by concentrated equivalent point loads connected to the rim elements using rigid connectors with appropriately cut load paths. Axially and tangentially fixed, radially free forward end boundary conditions were assumed. The cone was radially fixed near the aft end. Radially linear temperature gradients consistent with the measured radial disk and aft seal temperatures were used. Orthotropic zones were used to simulate the stiffness loss associated with holes.

Material mechanical property data (modulus, strength, crack growth rate, etc...) provided with the case were compared to independent sources and found to be consistent. Note that no independent data were readily available for comparison of the load controlled fatigue data.

2. COMPONENT GEOMETRY

This section provides an overall description of the basic part geometry and the specific feature to be analysed (the high pressure turbine disk). It also includes a complete description of the test facility used, together with all the drawing required for complete definition of the test rig.

Figure 2.1 shows a cross-section of the LARZAC 04 engine. The HP turbine disk which can be seen in this cross-section was tested on a component test bench in the geometrical configuration shown in figure 2.2. On this figure, you can see the components need to be known for mechanical modelling of the test rig, drawings of the following

parts are shown in figures 2.3, 2.4, 2.5 and 2.6 :

- HP turbine disk (2.3),
- shaft spacer (2.4),
- aft seal (2.5),
- cone (2.6).

The blades, blade retainers and bolts will be modelled by forces defined in section 5.

3. PART PROCESSING INFORMATION

Included in this section is general machining and processing information and information related to surface enhancements.

The part of the disk on which a crack has been initiated and propagated is an area machined by conventional lathe work. For this part no further surface reconditioning (for example by shot peening) was carried out.

4. OPERATING CONDITIONS

This chapter contains all information relating to the component test bench used.

The test rig shown in figure 2.2 was cycled between a minimum speed of 1500 r.p.m. and a maximum speed of 23685 r.p.m. The test cycle performed was a 36-second period trapezoidal symmetrical cycle with a 10-second hold-time at maximum speed and a 2-second hold-time at minimum speed.

The test facility is a vertical bench operating under low vacuum, with instruments to check the vibration level. No excessive level was recorded during testing.

The test rig is heated by induction on the dummy blades. The thermic map, held constant throughout the test, was measured by thermocouples installed on the disk at the positions indicated in figure 4.1.

5. BOUNDARY CONDITIONS FOR STRESS ANALYSIS

The boundary conditions required for calculation (loads due to external parts and thermic map) are defined in this chapter.

LOADS DUE TO EXTERNAL PARTS

*** Blades**
There are 62 blades with a mean individual static moment (i.e. mass* radius to center of gravity) of 683.4 cm.g, and therefore a total static moment of 42369 cm.g. The position of this load is indicated in figure 5.1.

*** Blade retainers**
The total static moment due to all these parts is 756 cm.g. It must be applied at the position indicated in figure 5.1.

*** Bolts**
There are twelve bolts (screws + nuts + washers), with a mean individual static moment of 104.6 cm.g., or a total static moment of 1255 cm.g. The position of this load is indicated in figure 5.1.

THERMIC MAP

During testing the temperatures were held constant. The thermic map was therefore measured spatially by thermocouples shown in figure 4.1. The values measured are those indicated in figure 5.2. The same figure shows another thermic map produced in another test with the same heating installation but at a lower overall temperature level. It will be noted that the much more numerous measurements show that the thermal gradient in the disk is radial. This is the assumption which will have to be made for thermal modelling of the proposed test.

6. HEAT TRANSFER INFORMATION

No heat transfer analysis was conducted for the test rig. The thermic map should be assumed constant during the test.

7. MATERIALS DATA

This chapter indicates all the material properties necessary for calculating the behaviour of the test rig and damage (crack initiation and propagation) to the test part.

As indicated in chapter 2, the modelling of the test rig may be limited to four parts, three of them in INCONEL 718 alloy. The fourth part, the HP turbine cone, is made of steel (AFNOR designation Z20CDV13).

The behaviour of the cone is purely elastic. Figure 7.1 indicates the physical data for Z20CDV13, along with graphs showing the material's Young's modulus and coefficient of thermal expansion as a function of temperature.

Figure 7.2 shows the same data for INCONEL 718. However, owing to the heavy loading of the disk, which leads the local plasticization of the

material, more complete data are given in figure 7.3 in the form of monotonic or cyclic stress-strain curves. Cyclic stress-strain data were obtained at half life from diametral strain control tests on hour glass specimens.

For the crack initiation low-cycle fatigue calculation, the Wöhler's curves for load ratios 0 and -1 are given in figure 7.4 for the temperature range covering the conditions of the disk. All the test conditions (test specimen, frequency, etc,) are listed in the same figure).

The crack propagation data (figure 7.4) are given for the temperature of the area in which the crack is initiated and then propagated : 450°C. They were obtained on compact tension type test specimens.

8. OPERATING HISTORY

TEST HISTORY

The test rig was tested under the conditions specified in section 4 for 16035 cycles, after which testing was interrupted to carry out a fractographic analysis of the disk.

DATA ACQUIRED DURING TEST

During the test, fluorescent penetrant inspections were performed regularly to monitor crack initiation. In the inspection carried out on the 7000th cycle, a crack was detected in the area of the neck under the rear flange of the disk (figure 8.1). This crack was monitored regularly up to the 16035th cycle, at which point, in view of the size of the crack, which was the only one detected up to the end of the test, it was decided to interrupt the test to carry out a fractographic analysis of the crack. The various measurements made during the test are listed in figure 8.1.

FAILURE ANALYSIS DATA

The results of fractographic examination of the crack at the end of the test are shown in figure 8.2. The initiation of the crack has crystallographic aspects without inclusions, porosities, nitrides, carbides, etc.

9. SUMMARY

The LARZAC HP turbine disk test is a good test case for study and validation of the mechanical methods for behaviour modelization and low-cycle fatigue crack initiation and crack propagation. This test case is particularly suitable to study the initiation and propagation of a crack in an area subjected to biaxial stresses leading to moderate plasticity.

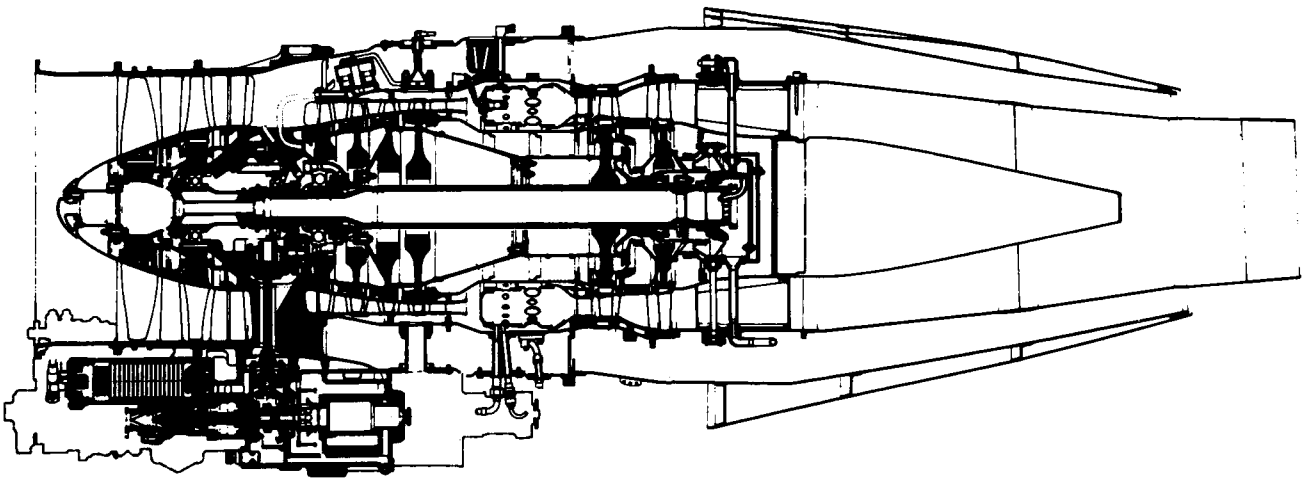

Figure 2.1 **LARZAC ENGINE**

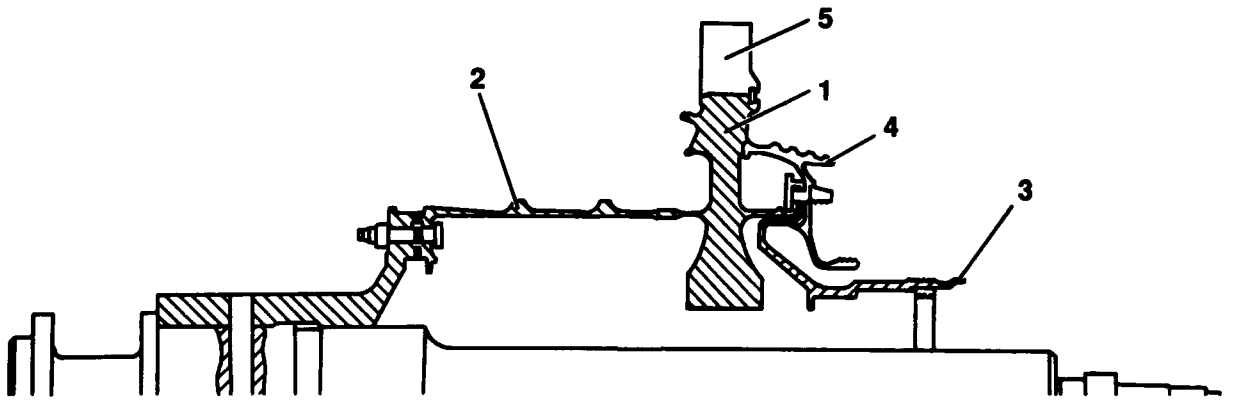

- welded disk-shaft	1
- shaft-spacer	2
- cone	3
- aft seal	4
- blades	5

Figure 2.2 **COMPONENT GEOMETRY**

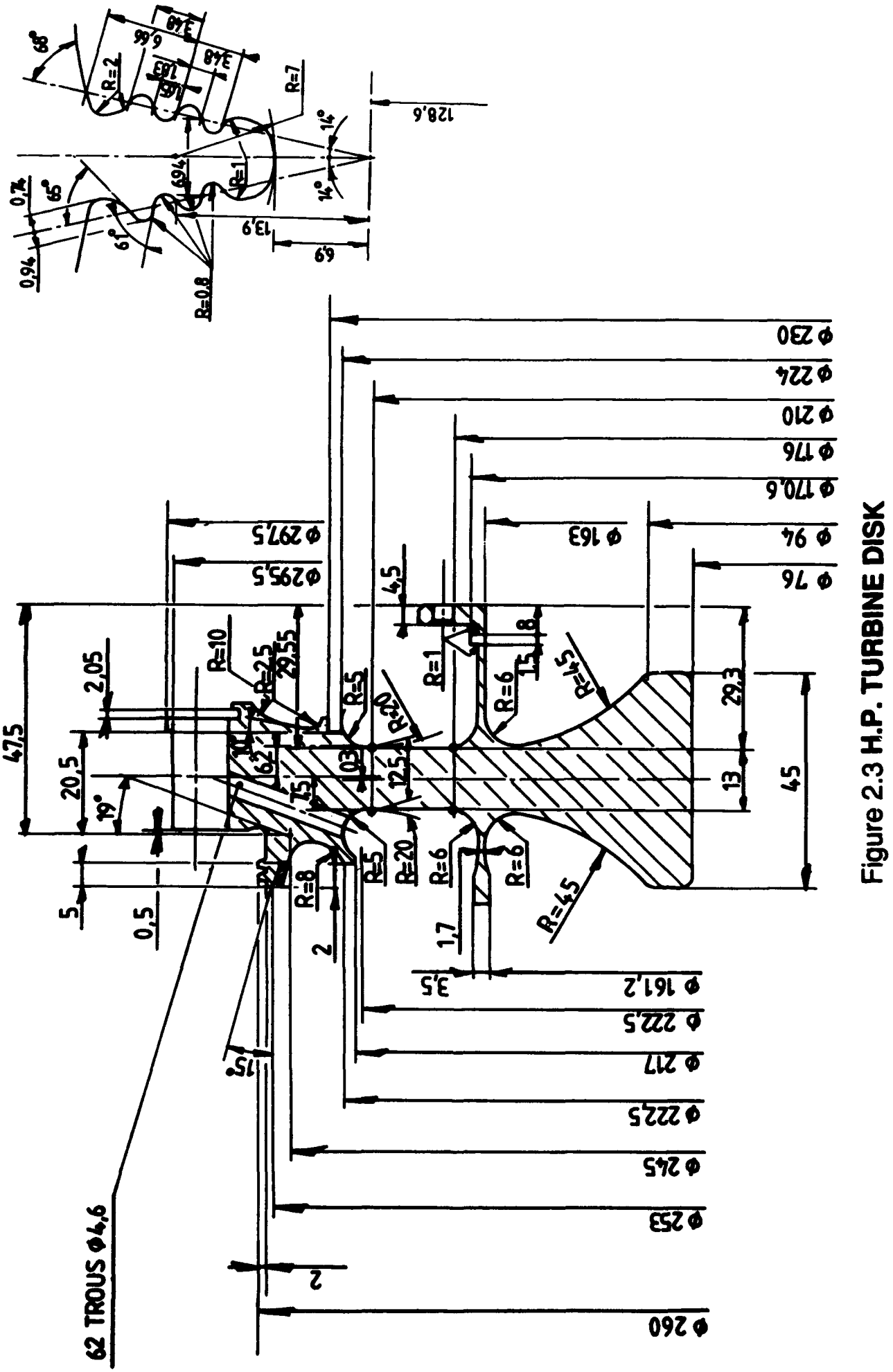

Figure 2.3 H.P. TURBINE DISK

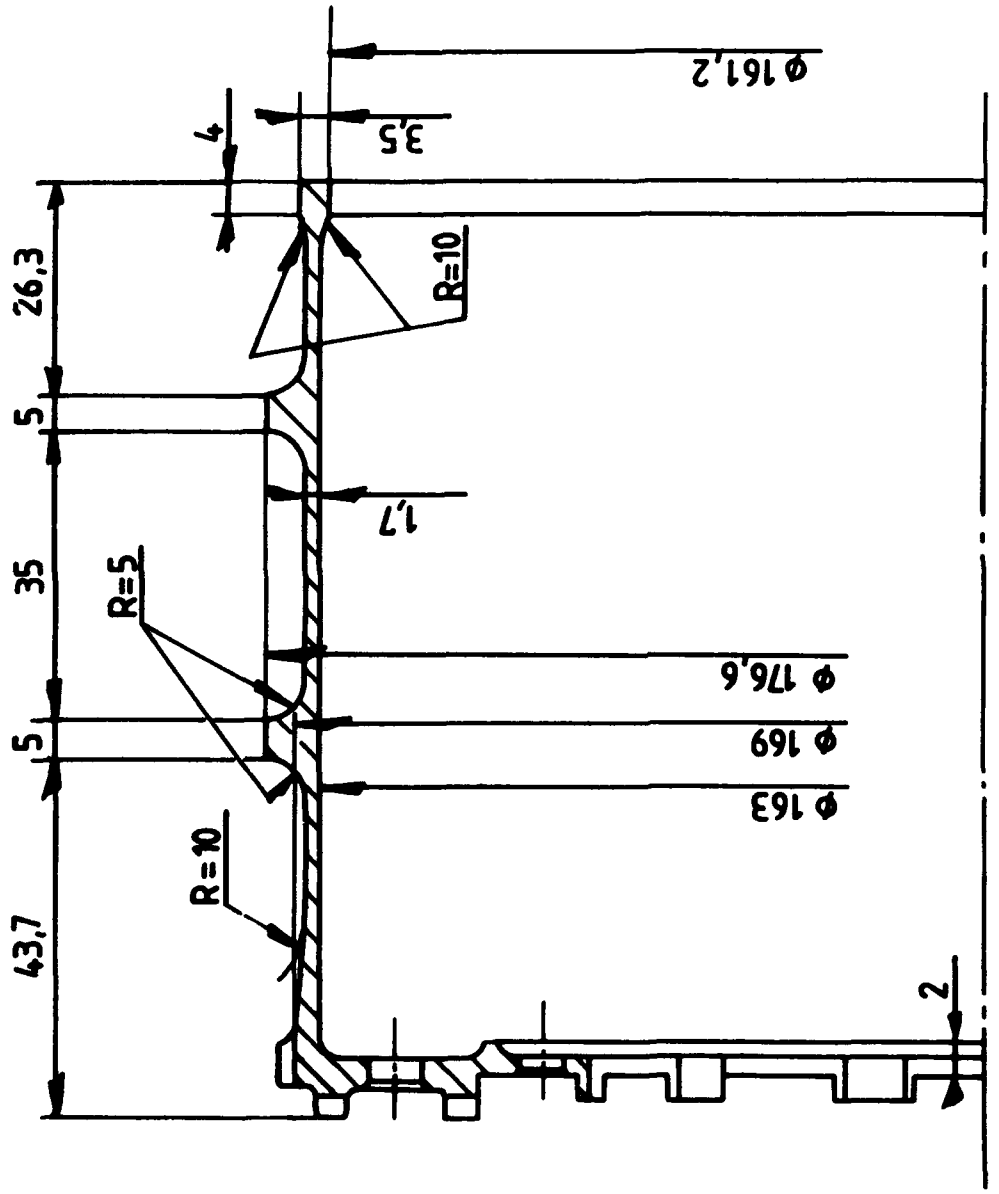

Figure 2.4 **SHAFT SPACER**

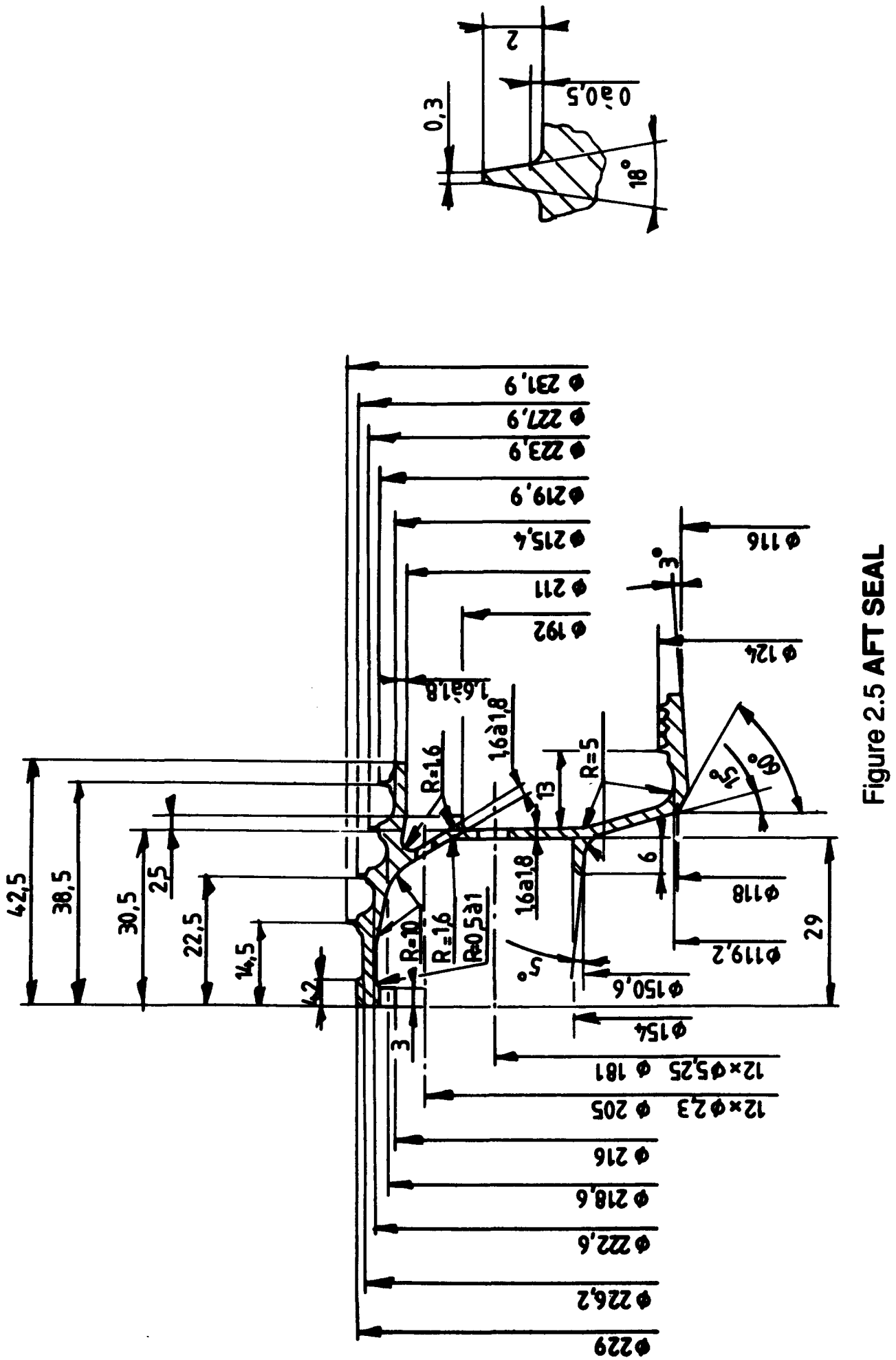

Figure 2.5 **AFT SEAL**

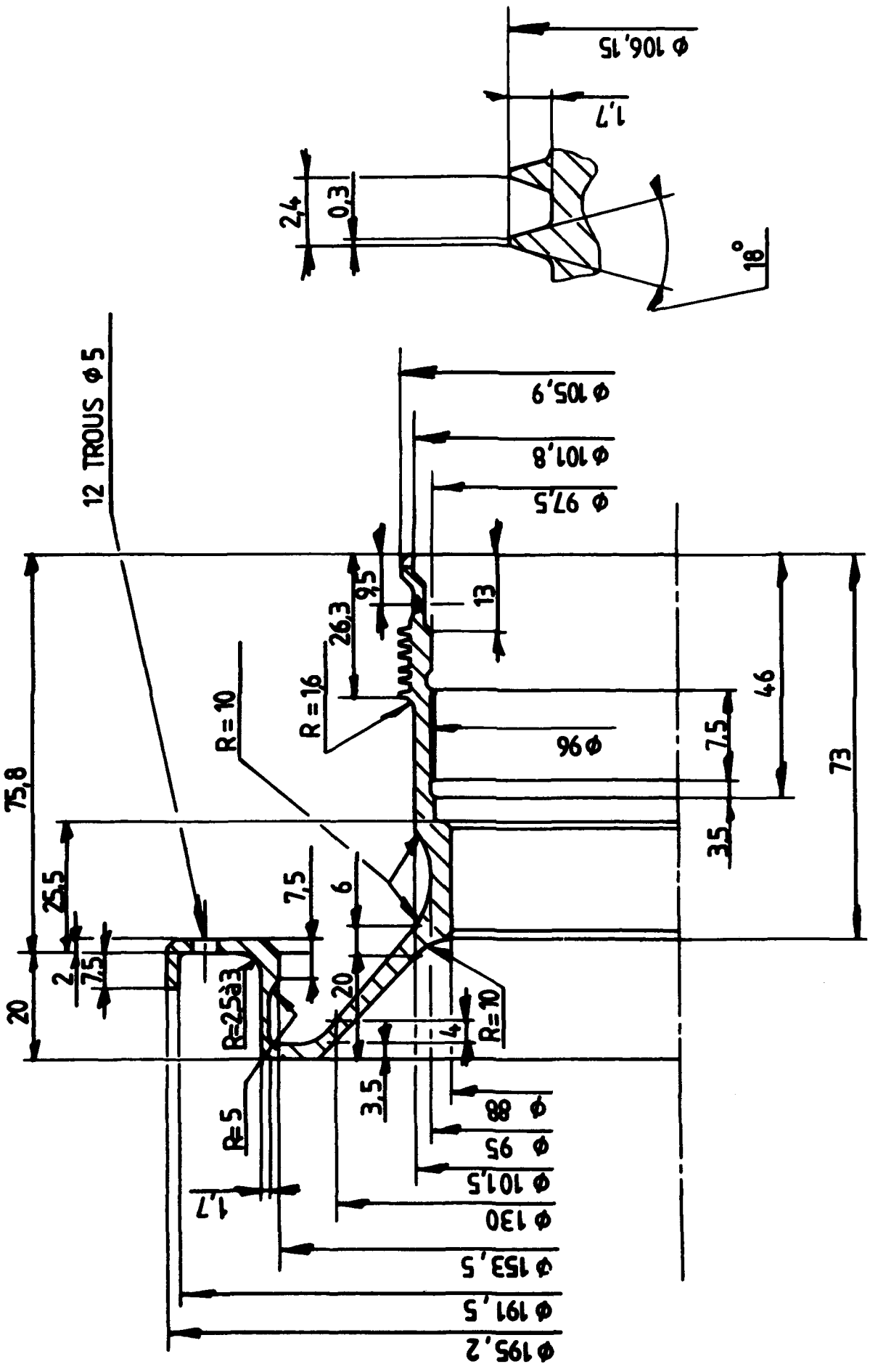

Figure 2.6 **CONE**

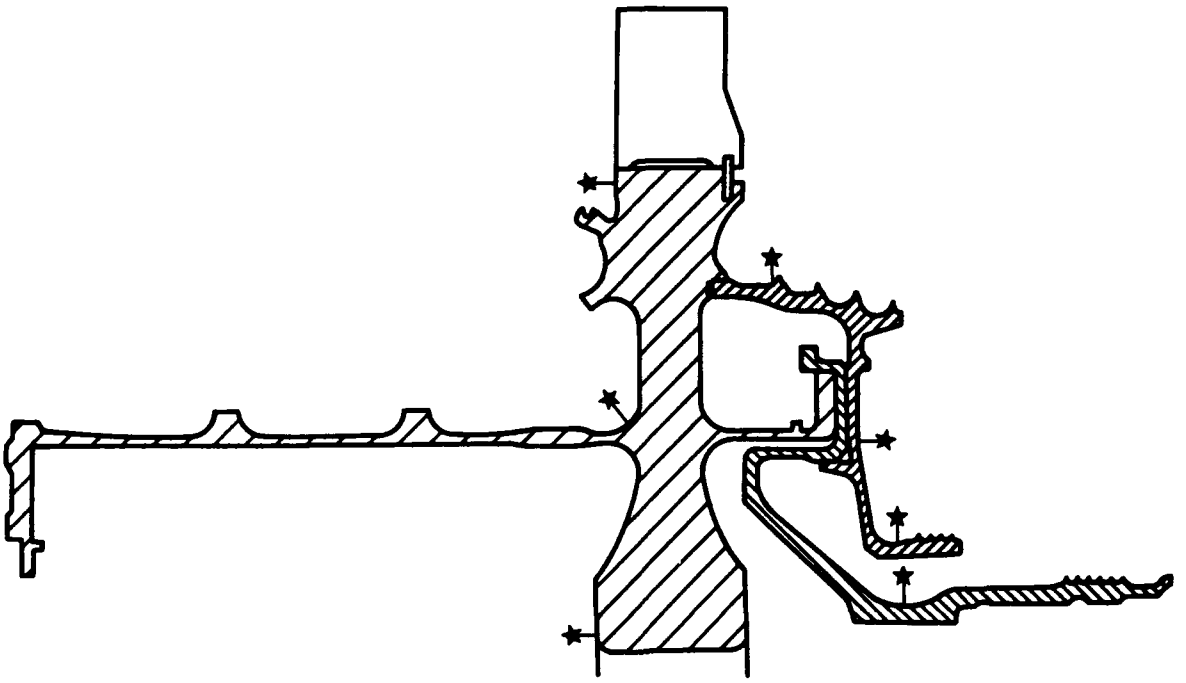

Figure 4.1 **POSITION OF THERMOCOUPLES**

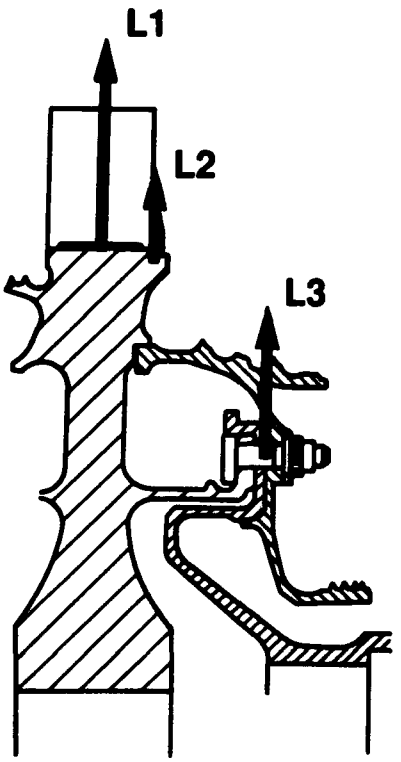

Figure 5.1 **BOUNDARY CONDITIONS FOR STRESS ANALYSIS**

Temperatures

Measured values for the test case

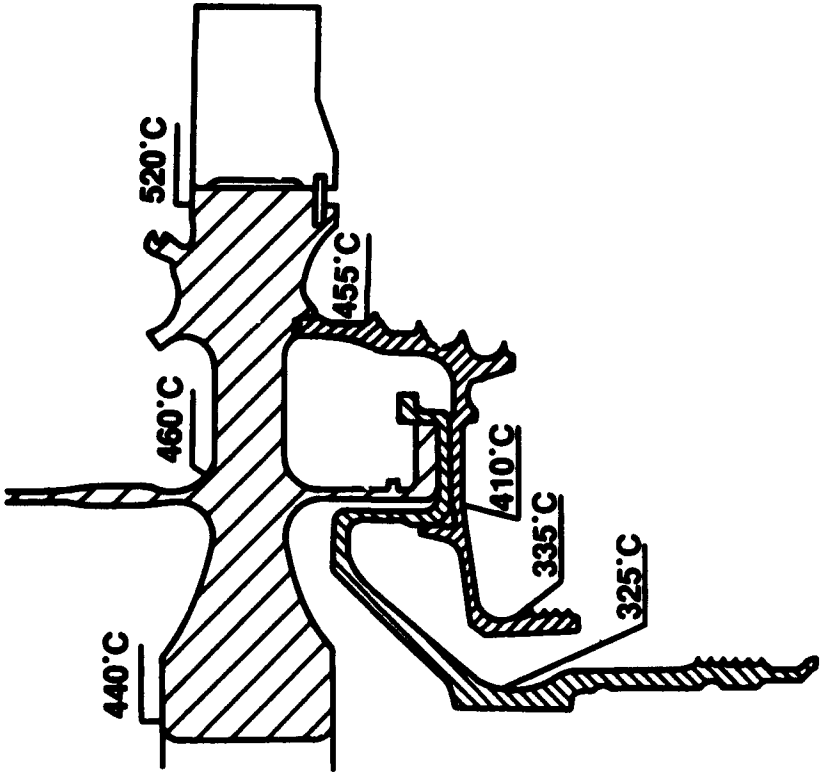

Thermic map

Temperature measurements on an other rig test show that the thermal gradient in the disk could be considered as radial

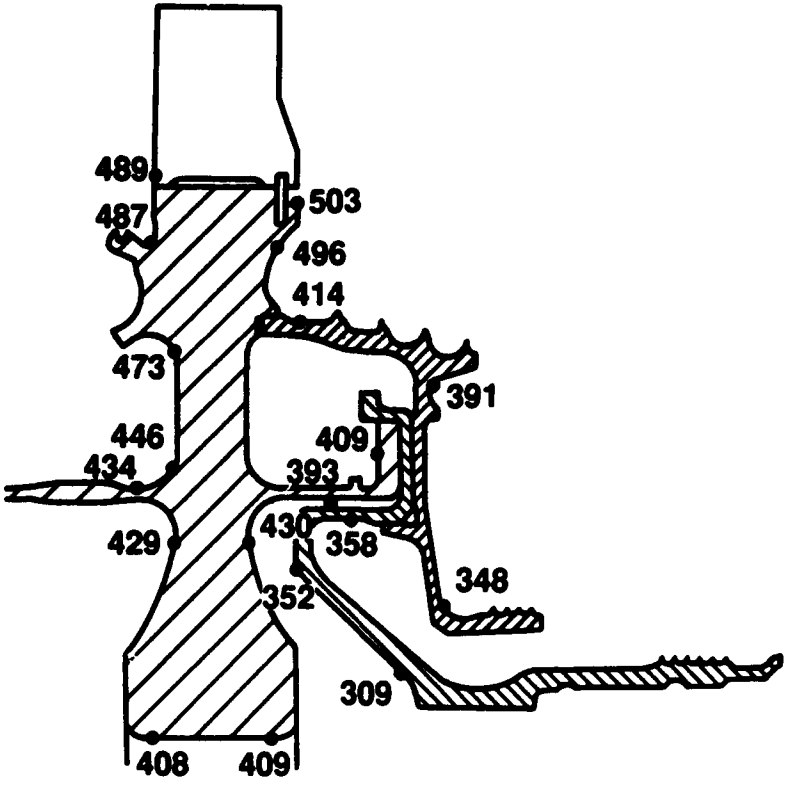

Figure 5.2 **BOUNDARY CONDITIONS FOR STRESS ANALYSIS**

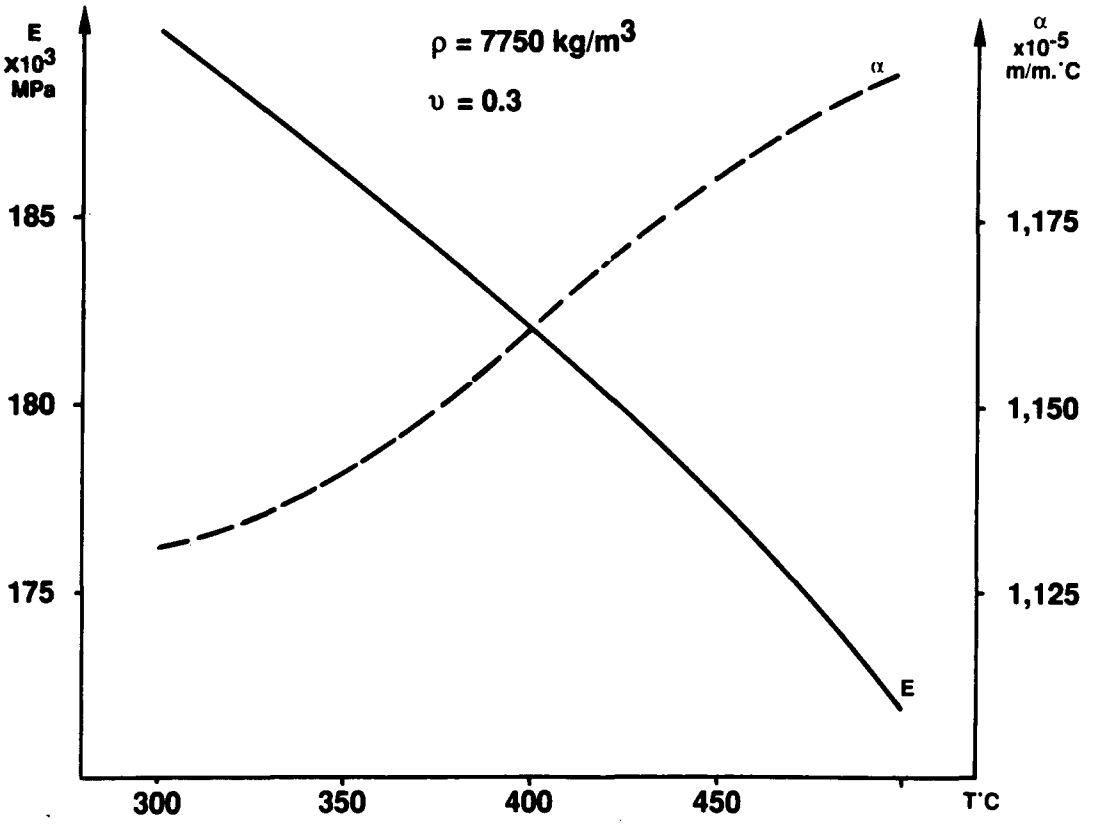

Figure 7.1 **PHYSICAL DATA Z20CDV13**

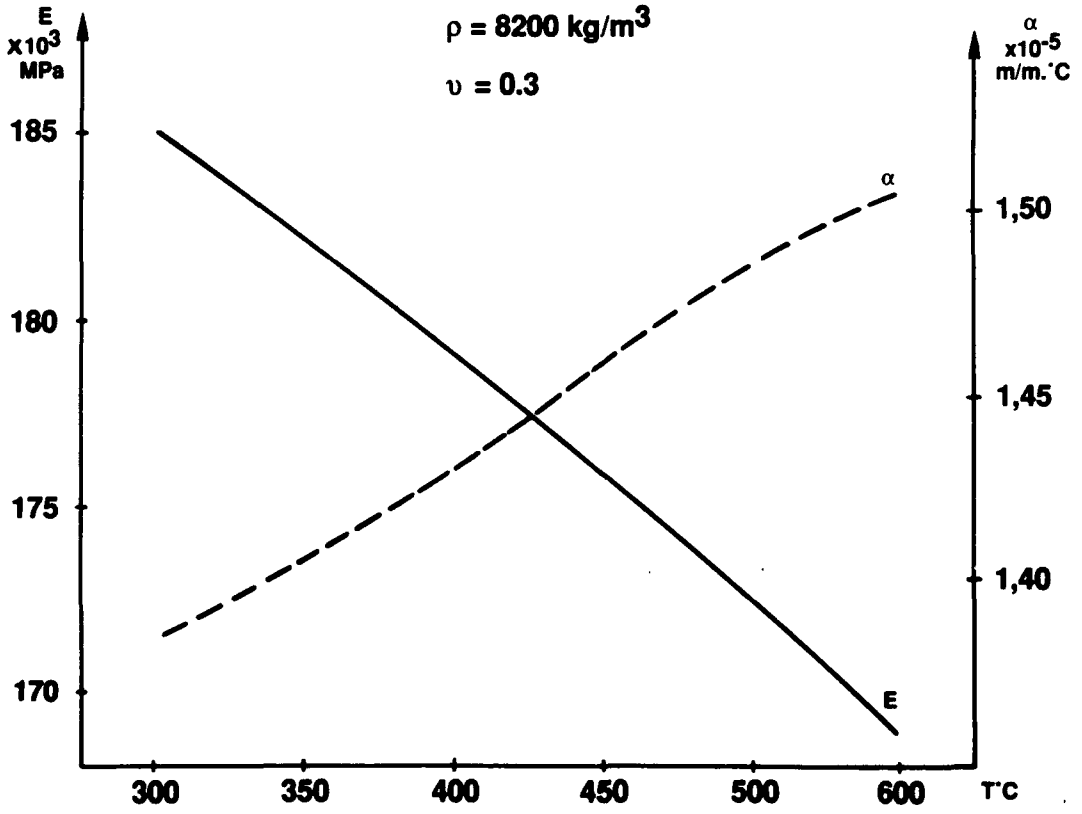

Figure 7.2 **PHYSICAL DATA INCONEL 718**

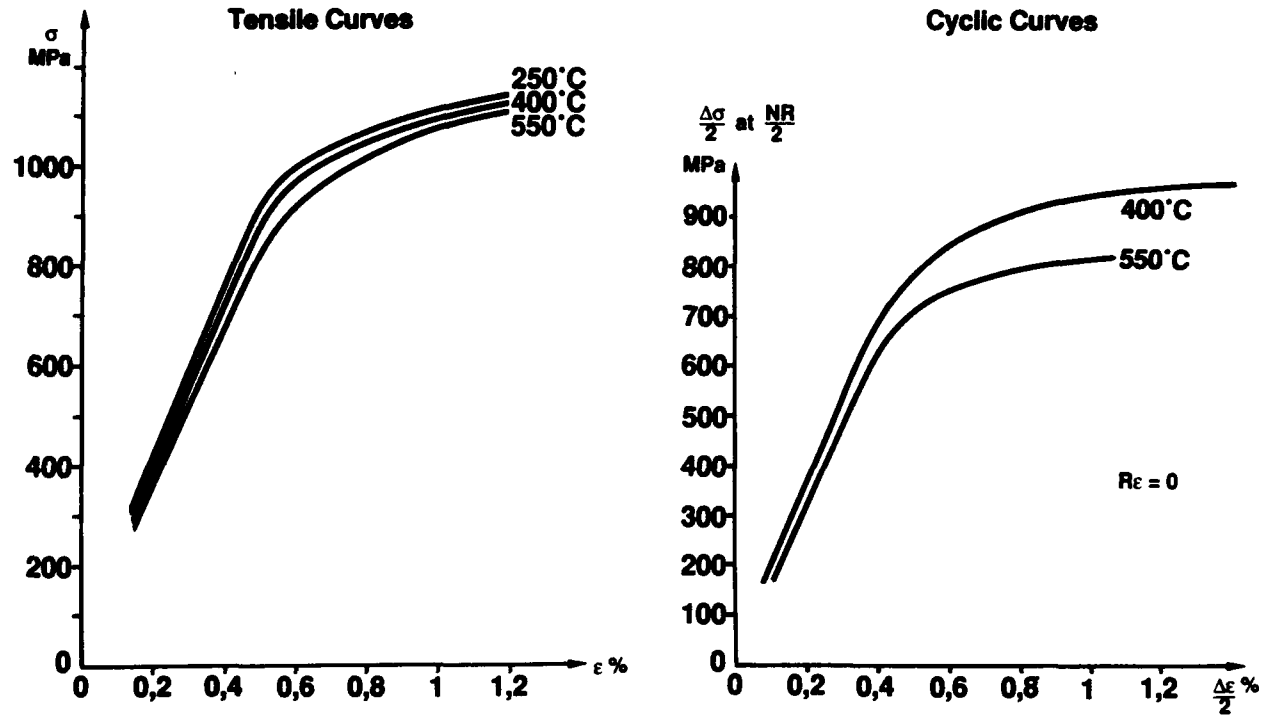

Figure 7.3 **STRESS-STRAIN DATA INCONEL 718**

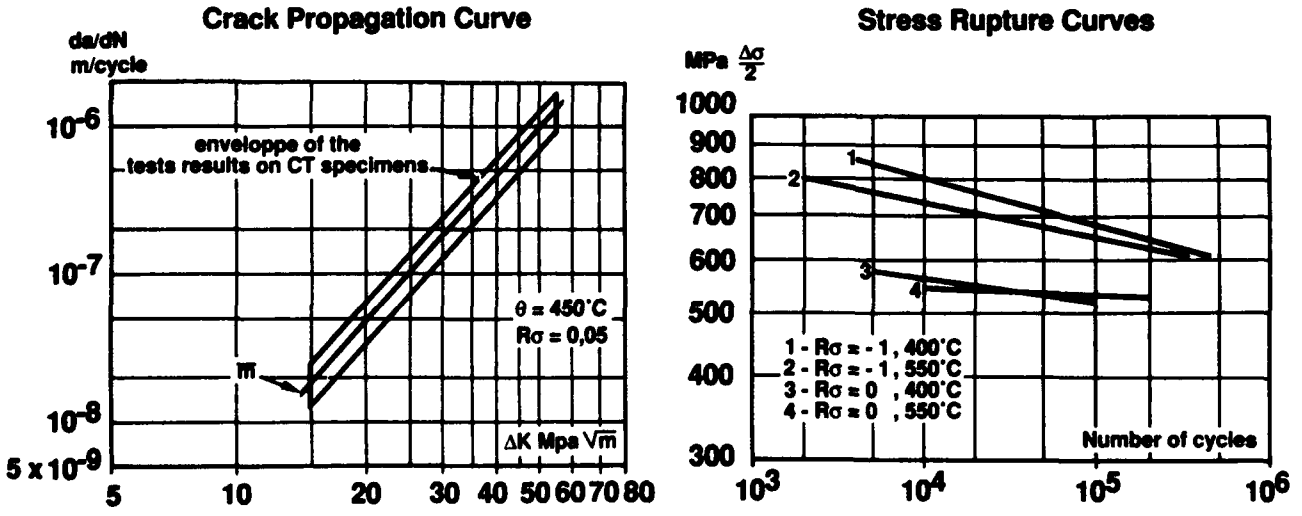

Figure 7.4 **L.C.F. DATA INCONEL 718**

Crack Location

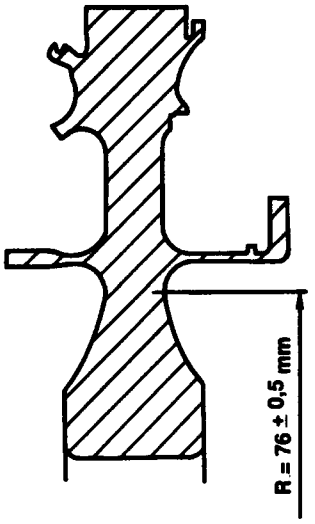

Crack Evolution During The Rig Test

Number of cycle at the inspection	Total surface length of the crack
7000	1.5 mm
9000	1.5 "
11000	2.5 "
13000	4 "
15035	6 "
16035	7 "

Figure 8.1 **OPERATING HISTORY**

Fractography Of The Crack

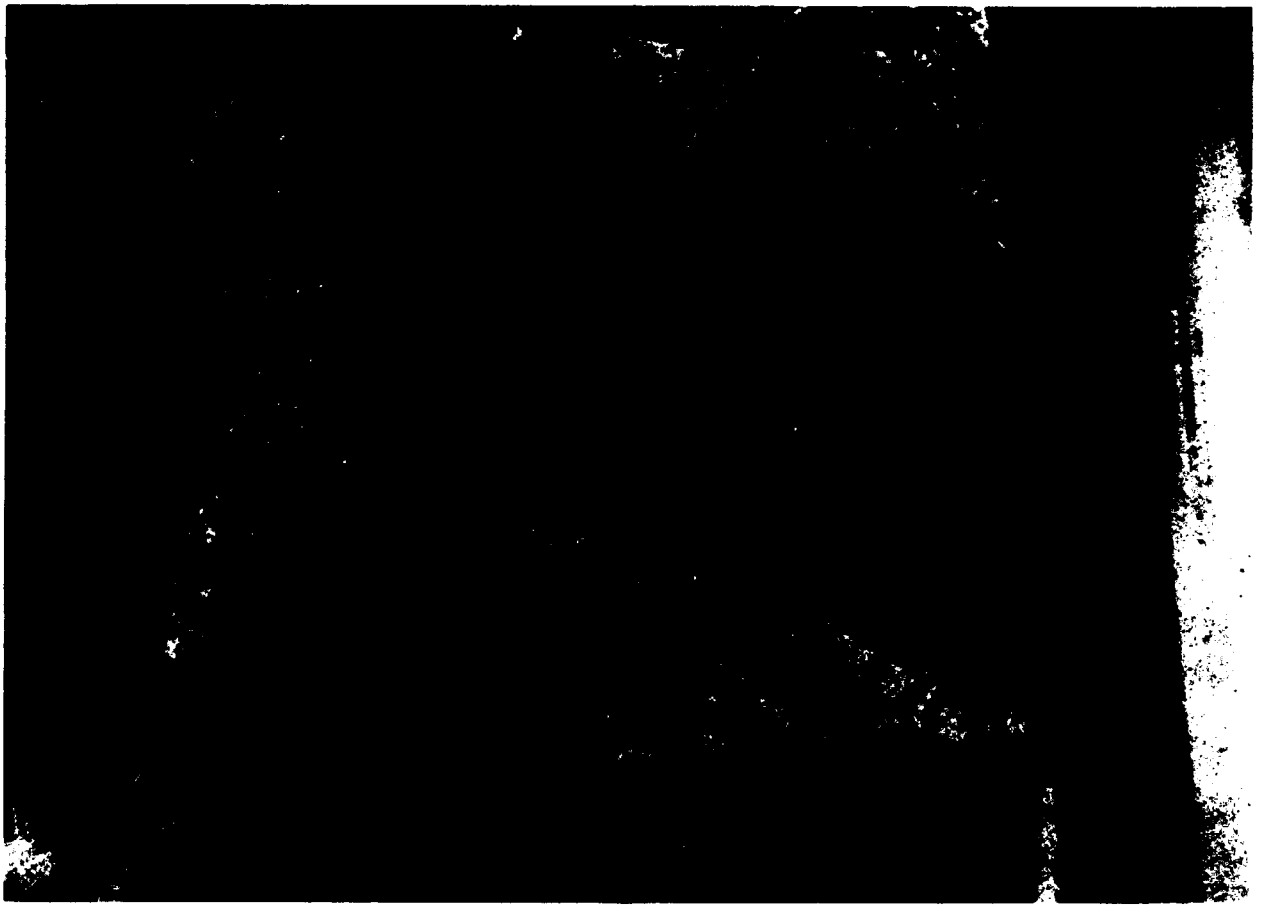

Figure 8.2 **OPERATING HISTORY**

Chapter 3

RB 199 HIGH PRESSURE COMPRESSOR
STAGE 3 SPIN PIT TESTS

J. Broede
MTU Motoren- und Turbinen-Union Muenchen GmbH
Dachauer Strasse 665
D-8000 Munich 50
Germany

1. INTRODUCTION

The data presented here are the contribution of MTU Munich to a number of test cases for the application of engine life assessment technology.

This test case deals with cyclic spin pit testing conducted on the 3rd stage HP compressor disk of the TURBO UNION RB 199 engine.

The tests have been performed to verify disk design and life prediction under a safe life LCF lifing concept.

Addressed critical areas are Bolt Holes and Rim Slots. For Bolt Hole testing the original component geometry has been modified slightly, for Rim testing significantly to ensure component failure to occur in the area under investigation and local stress distribution as under engine operating conditions.

Complexities of the test case include

- use of actual hardware (returned from service, steel material, engine part)
- complex part geometry
- local elastic-plastic stress level due to stress concentration
- realistic surface conditions
- in-service usage statistically monitored
- assessment of a significant failure mode (component classification is "fracture critical").

ASSESSMENT ANALYSIS

An independent analysis was conducted by the USAF,WPAFB (ASD/YZEE). Basesd on this effort it was concluded that the test case includes sufficient information to:

- generate a viable stress analysis model
- generate concentrated stress factors
- correlate life predictions with the spin pit test results

The rim test case was assessed by conducting a two-dimensional axisymmetric finite element analysis of the disk, adapter, and shaft. A two-dimensional finite element analysis of the concentration effect of the broach slot was also done.

The bolt hole test case was assessed by conducting a three-dimensional finite element analysis of a 36 degree sector of the disk, adapter, and shaft.

These analyses and the materials data provided in the test cases were used to predict the disk lives for the spin pit testing within 10% of the observed lives.

2. COMPONENT GEOMETRY

The geometry of the components involved in this test case is shown in several figures. Details are given only to that level that is expected of interest when running the test case.

All dimensions are given in mm. Two disk geometries (A and B) are considered. Dimensions marked with "A:" belong to geometry A and those marked with "B:" belong to geometry B. All other dimensions are common for both geometries.

In particular the following features are presented:

Figure 1 gives a general view of the TURBO UNION RB 199 engine.

Figure 2 shows the cross section of the HP compressor.

The general arrangements for testing are given in Figure 3.1 for Bolt Hole testing and in Figure 3.2 for Rim Slot testing.

Details of the original HPC St.3 Disk geometry are presented as cross section (Fig. 4.1), view to the front of the disk (Fig. 4.2) and enlarged cross section (Fig. 4.3). Rim Slot details are shown in Figure 4.4.

For testing the original part geometry has been modified. The modifications are detailed in Figure 4.5 for Bolt Hole testing and in Figure 4.6 for Rim Slot testing.

Details of the adapter and shaft parts used in the tests are shown in Figure 5.1 (adapter for Bolt Hole testing), Figure 5.2 (adapter for Rim Slot testing), Figure 5.3 (shaft (partly) for Bolt Hole testing) and Figure 5.4 (shaft (partly) for Rim Slot testing).

3. PART PROCESSING INFORMATION

This section contains part processing information which might be of interest when running the test case.

The HPC St.3 Disk is made of corrosion resistant steel X8CrCoNiMo11.

Heat treatment for this material is specified as follows:

- 1160 to 1180 deg C, oil quench
- 5 hours at 610 deg C, air cool
- 15 minutes at -70 to -80 deg C, air warm up
- 5 hours at 620 to 650 deg C, air cool

Machining and surface finishing of the areas under consideration have been performed as follows:

The bolt holes and the holes between the bolt holes were drilled and reamed, the edges were broken.

The rim slots were broached, the edges blended by hand.

4. OPERATING CONDITIONS

4.1 Usage in Service

Prior to the spin pit testing most of the disks were used in normal engine service.

4.2 Bolt Hole Tests

The cyclic Bolt Hole tests were performed in a vertical spin pit. The general arrangement is shown in Figure 3.1. The disk geometry was modified as shown in Figure 4.5.

The disk was attached to the vertical drive shaft by an adapter. Geometric details of the adapter and the relevant shaft parts are given in Figures 5.1 and 5.3.

Blades were substituted by dummies.

The spin pit was driven by an air turbine. The tests were performed under vacuum at room temperature.

4.3 Rim Slot Tests

The cyclic Rim Slot tests were performed in a horizontal spin pit. The general arrangement is shown in Figure 3.2. The disk geometry was modified as shown in Figure 4.6.

The disk was attached to the horizontal drive shaft by an adapter. Geometric details of the adapter and the relevant shaft parts are given in Figures 5.2 and 5.4.

Blades were substituted by dummies.

The spin pit was driven by an electric motor. The tests were performed in air under atmospheric pressure. The assembly was heated by air friction.

The distribution of the metal temperature was checked with thermo paints. The results are shown in Figure 6. The shaft temperature at the bearing (outside the seal) was 60 deg C.

During the tests the metal temperature at the blade dummies was monitored with a pyrometer, the air temperature around the rim was monitored with thermo couples.

5. BOUNDARY CONDITIONS FOR STRESS ANALYSIS

For stress analysis it is recommended to model the disks, the adapter parts and partly the shafts.

Further it is recommended to model the disk only to a radius of R = 156.592 mm (ground of slots) and to add an equally distributed rim load corresponding to a static moment (i.e. mass x radius to center of gravity) of 77,340 gmm in the mid plane of the disk. This includes 113 blade dummies, 113 disk humps (i.e. disk parts outside the given radius) and the blade locking plate.

The blade dummies are designed in such a way that they produce the same loads to the disk as the real blades.

For stress analysis of the Bolt Hole tests, constant temperature (room temperature) should be assumed.

For stress analysis of the Rim Slot tests, a radial and axial temperature gradient as indicated in Figure 6 should be taken into account.

Stress concentration should be accounted for by means of Kt-factors.

6. HEAT TRANSFER INFORMATION

The Bolt Hole tests were performed at room temperature. The temperature distribution within the assembly should be considered constant.

The Rim Slot tests were performed at a rim temperature of 150 deg C. The metal temperature distribution over the assembly should be derived from the thermo paint measurement results given in Figure 6.

7. MATERIALS DATA

The materials of the parts involved in this test case are

- disk :	X8CrCoNiMo11
- adapter for Bolt Hole tests:	X12CrNiMo12
- adapter for Rim Slot tests:	X12CrNiMo12
- shaft for Bolt Hole tests:	34CrNiMo6
- shaft for Rim Slot tests:	34CrNiMo6

The physical properties of these materials are given for different temperatures in Tables 1 and 2. Part specific LCF data of the disk material are given in Figure 7.

8. OPERATING HISTORY

Prior to spin pit testing, the disks experienced normal usage in service. The particular flight time (EFH: engine flying hours) was

- Bolt Hole test, geometry A :	626 EFH
- Bolt Hole test, geometry B :	941 EFH
- Rim Slot test, test 1 :	new part
- Rim Slot test, test 2 :	452 EFH
- Rim Slot test, test 3 :	757 EFH

Life usage (in terms of cycles) was not individually monitored. But a statistical investigation of in-service life usage has been performed. The data presented here are based on the average life consumption of 156 engines. The life consumption figures - originally based on engine reference cycles - have been converted to the basis of test cycles, taking into account overloads of the test cycles compared with engine cycles and compressive stresses appearing in real engine operation. It is anticipated that this simplification will not influence the results of test case application.

Average values of life usage in terms of numbers of test cycles per engine flying hours are

- Bolt Hole test, geometry A : 0.65 CPH
- Bolt Hole test, geometry B : 0.85 CPH
- Rim Slot test : 3.75 CPH

After return from service, the disks were inspected for geometry changes and cracks. The disk geometry was found within the design tolerances in all cases. All disks were crackfree, i.e. non-destructive inspections did not reveal any cracks.

For subsequent spin pit testing, the disks were modified as detailed in Figures 4.5 (Bolt Hole testing, geometry B) and 4.6 (Rim Slot testing). The test arrangements were as detailed in section 5.

The load sequence for these tests was as shown in Figure 8 with the maximum and minimum speeds and temperature as provided in Table 3.

The tests were interrupted for several inspections for geometry checks and crack appearance, where the following techniques were used:

- dye penetrant inspection
- fluorescent magnetic particle inspection
- eddy current inspection

During the tests a variety of cracks were produced.

When indications were given that the cracks were longer than defined in the applied LCF lifing concept (crack length 0.4 mm), the tests were stopped. The largest cracks were broken open for further investigation. The number of cycles to defined crack length (0.4 mm) were determined based on striation counting.

For the Bolt Hole tests a small number of cracks appeared. Most of the cracks were located at the holes between the bolt holes, mainly at the ID position propagating into the direction to the disk center. Also some cracks were found in the OD position, but these appeared later and needed more cycles to reach the failure criterion of 0.4 mm length.

In the Rim Slot tests a large number of cracks were produced. All possible crack locations were observed, i.e. front, rear and both sides of the disk. It seems to be typical that cracks started from several initiation points and grew together to single cracks.

Tables 4 and 5 give an overview of inspection intervals and findings.

To provide some general idea how and where the cracks were initiated and propagated, Figures 9.1 and 9.2 show typical examples of crack positions and shapes as found after the tests.

Since these tests were intended to address crack initiation life, no further investigation about crack propagation behaviour has been performed.

9. SUMMARY

The RB 199 test case presented here addresses areas with stress concentration to a stress level of local elastic-plastic material behaviour. The material used is a corrosion resistant steel X8CrCoNiMo11.

Information about component geometry, part processing, operating conditions and history, recommendations about stress analysis and relevant boundary and thermal conditions as well as materials data are presented.

Simplifications have been kept to a minimum. However, the data have been presented to such detail what is considered to be sufficient for running the test case and to address the full range of complexity when assessing real engine part life.

Table 1: Physical Properties of Disk Material

			Disk Material X8CrCoNiMo11		
			RT	150 deg C	300 deg C
Density	1.0E6	g/m**3	7.8	7.8	7.8
Modulus of Elasticity	1.0E9	N/m**2	215.0	210.0	201.0
Poisson's Ratio		-----	0.3	0.3	0.3
0.2 % Yield Strength	1.0E6	N/m**2	865.0	840.0	810.0
Ultimate Tensile Strength	1.0E6	N/m**2	1010.0	940.0	880.0
Coefficient of Thermal Expansion	1.0E-6	m/(m*K)	9.9	10.4	11.0
Thermal Conductivity		W/(m*K)	20.9	22.3	22.8
Specific Heat		J/(kg*K)	440.0	500.0	560.0

Table 2: Physical Properties of Adapter and Shaft Material

			Adapter X12CrNiMo12		Shaft 34CrNiMo6	
			RT	150 deg C	RT	150 deg C
Density	1.0E6	g/m**3	7.75	7.75	7.85	7.85
Modulus of Elasticity	1.0E9	N/m**2	215.0	210.0	213.0	206.0
Poisson's Ratio		-----	0.3	0.3	0.3	0.3
0.2 % Yield Strength	1.0E6	N/m**2	920.0	850.0	750.0	700.0
Ultimate Tensile Strength	1.0E6	N/m**2	1100.0	980.0	1080.0	965.0
Coefficient of Thermal Expansion	1.0E-6	m/(m*K)	10.6	10.9	11.0	12.1
Thermal Conductivity		W/(m*K)	21.0	22.2	46.0	48.0
Specific Heat		J/(kg*K)	460.0	510.0	465.0	515.0

Table 3: Test Parameters (Speeds and Temperature)

	ns_max (1/min)	ns_min (1/min)	Temp (deg C)
Bolt Hole, geometry A	26 730	500	RT
Bolt Hole, geometry B	26 730	500	RT
Rim Slot, test 1	18 400	1000	150
Rim Slot, test 2	18 400	200	150
Rim Slot, test 3	18 400	200	150

Table 4: Inspection Intervals and Findings for the Bolt Hole Areas

	Bolt Hole geometry A	Bolt Hole geometry B
Normal in-service usage	626 EFH	941 EFH
Inspection result at return from service usage	crackfree	crackfree
Spin pit tests		
Inspection after test cycles	5 200 8 000 11 000 14 000	4 500 9 000 12 000 15 000 18 000 21 000
Number of cracks at test end	5	6
Number of cycles to 0.4 mm crack length (largest crack)	7 350 hole between bolt holes, ID no cracks hole between bolt holes, OD	13 700 hole between bolt holes, ID 19 700 hole between bolt holes, OD
Crack shape and position	see Fig. 9.1	see Fig. 9.1

Table 5: Inspection Intervals and Findings for the Rim Area

	Rim Slot test 1	Rim Slot test 2	Rim Slot test 2
Normal in-service usage	---	452 EFH	757 EFH
Inspection result at return from service usage	new part	crackfree	crackfree
Spin pit tests			
Inspection after test cycles	10 2 500 5 000 7 500 9 900 12 000 16 000	10 000 11 000 12 000 13 000	5 000 8 000 10 000 12 000 14 000 15 000
Number of cracks at test end	> 100	> 30	> 100
Number of cycles to 0.4 mm crack length (largest crack)	12 700	11 150	11 800
Crack shape and position	see Fig. 9.2	see Fig. 9.2	see Fig. 9.2

Fig. 1 : General View of RB 199 Engine

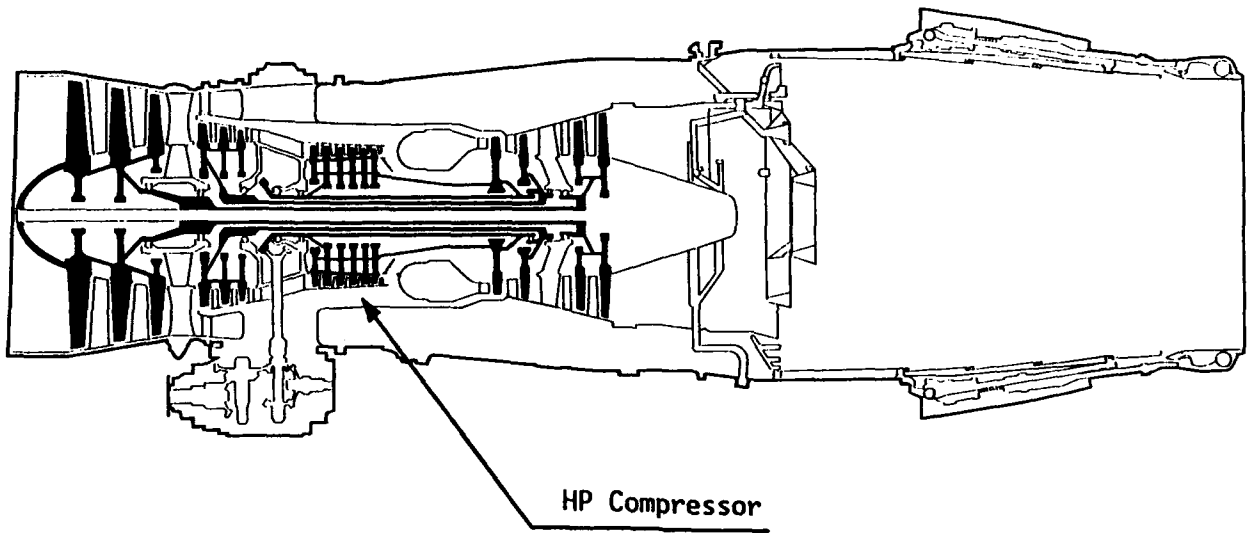

Fig. 2 : Cross Section of HP Compressor

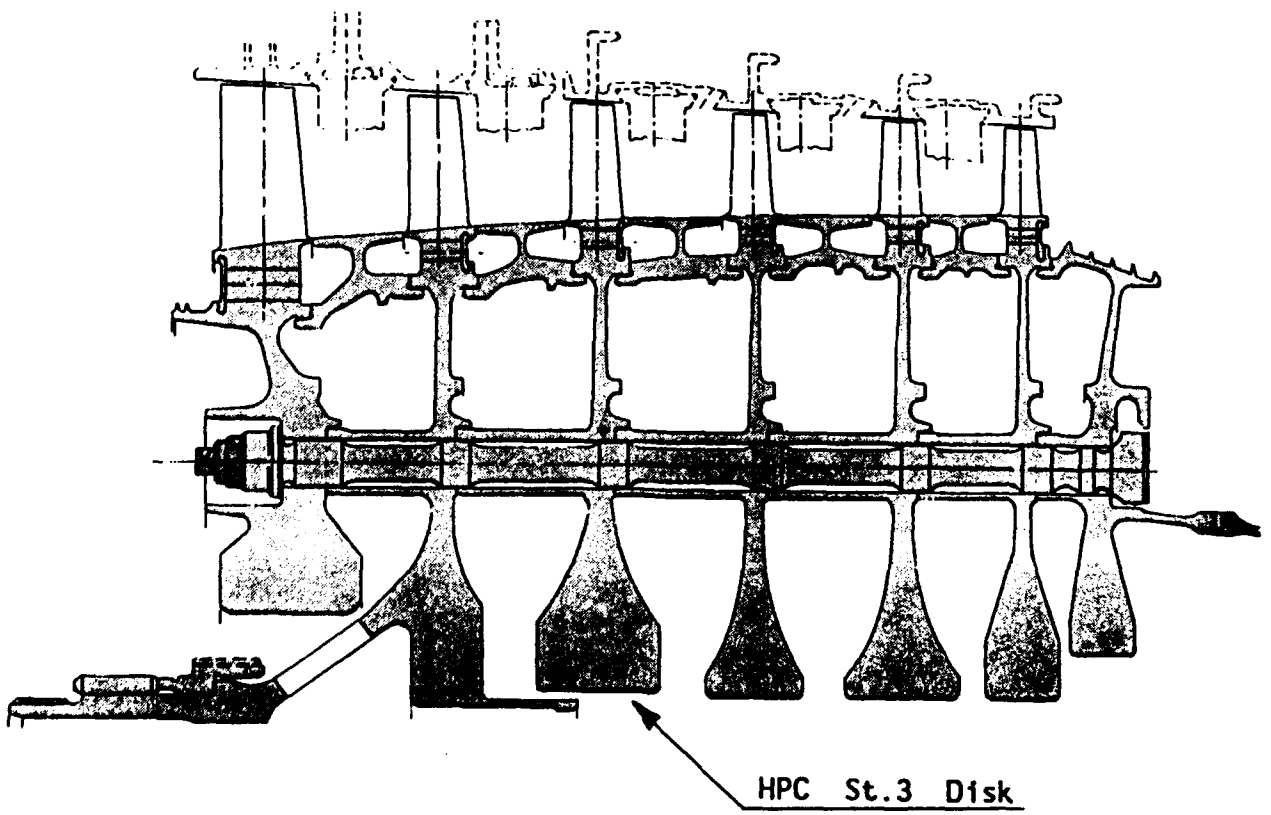

Fig. 3.1 : General Arrangement for Bolt Hole Testing

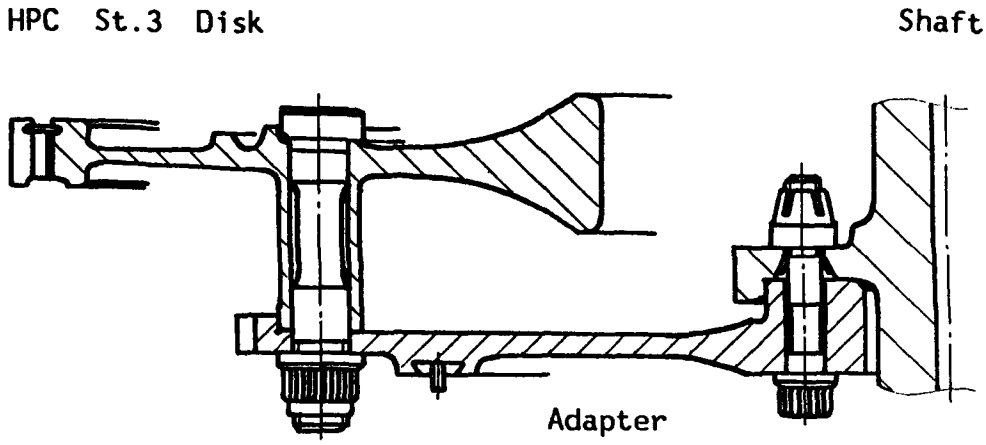

Fig. 3.2 : General Arrangement for Rim Slot Testing

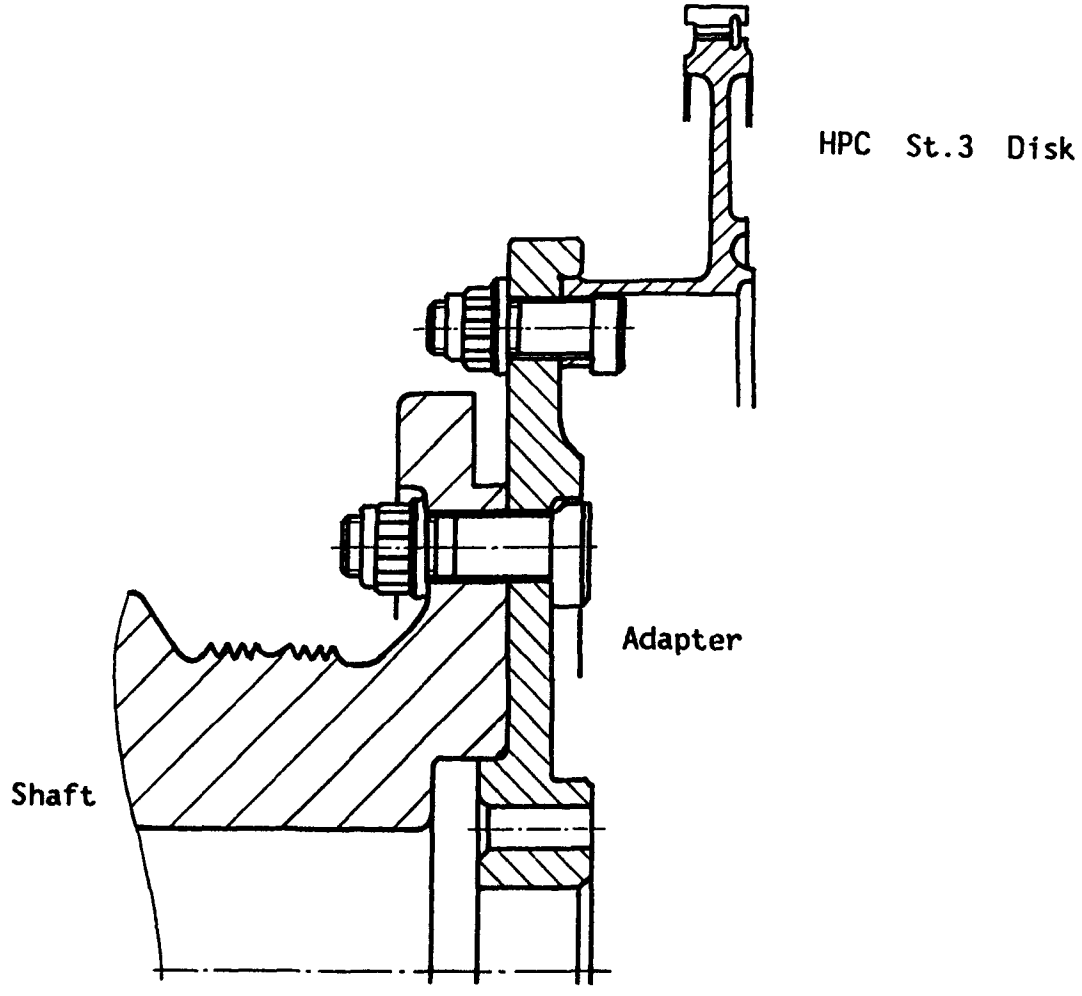

Fig. 4.1 : Disk; Cross Section

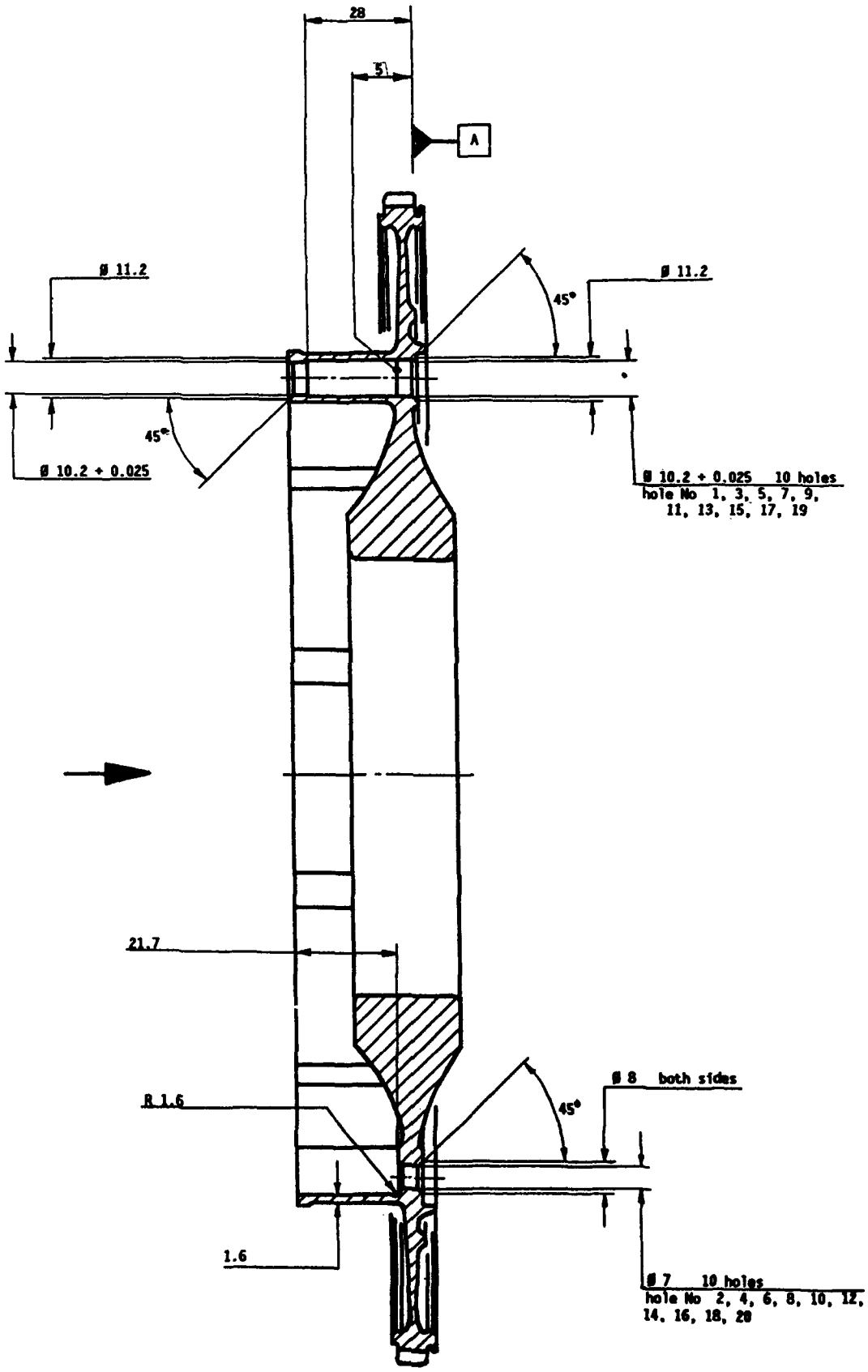

Fig. 4.2 : Disk; View to the Front

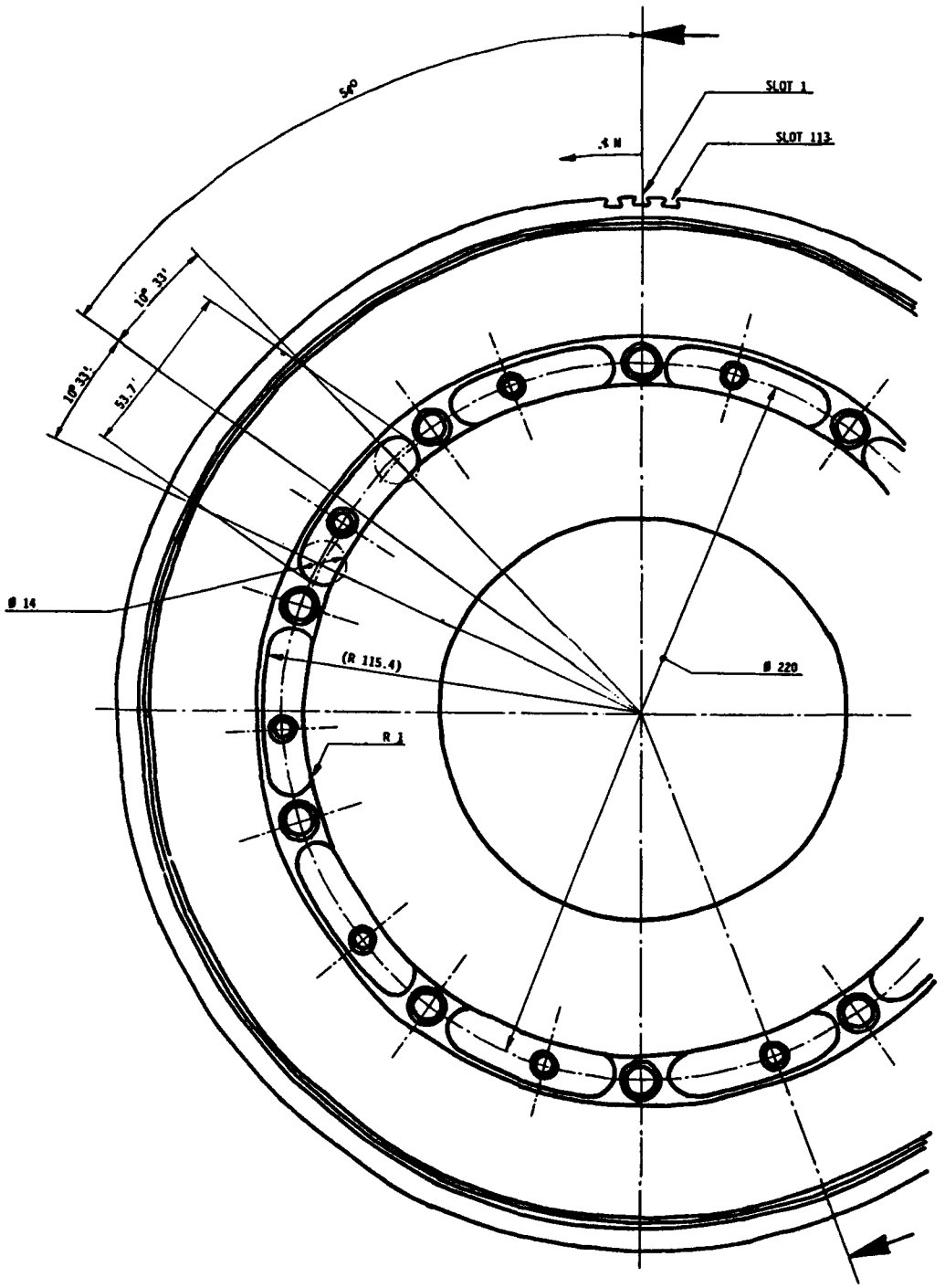

Hole No	Pitch Circle	∢ N	Hole No	Pitch Circle	∢ N
1	Ø 220	0°	11	Ø 220	180°
2	Ø 220	21°	12	Ø 220	201°
3	Ø 220	36°	13	Ø 220	216°
4	Ø 220	57°	14	Ø 220	237°
5	Ø 220	72°	15	Ø 220	252°
6	Ø 220	93°	16	Ø 220	273°
7	Ø 220	108°	17	Ø 220	288°
8	Ø ?0	129°	18	Ø 220	309°
9	Ø 220	144°	19	Ø 220	324°
10	Ø 220	165°	20	Ø 220	345°

Fig. 4.3 : Disk; Enlarged Cross Section

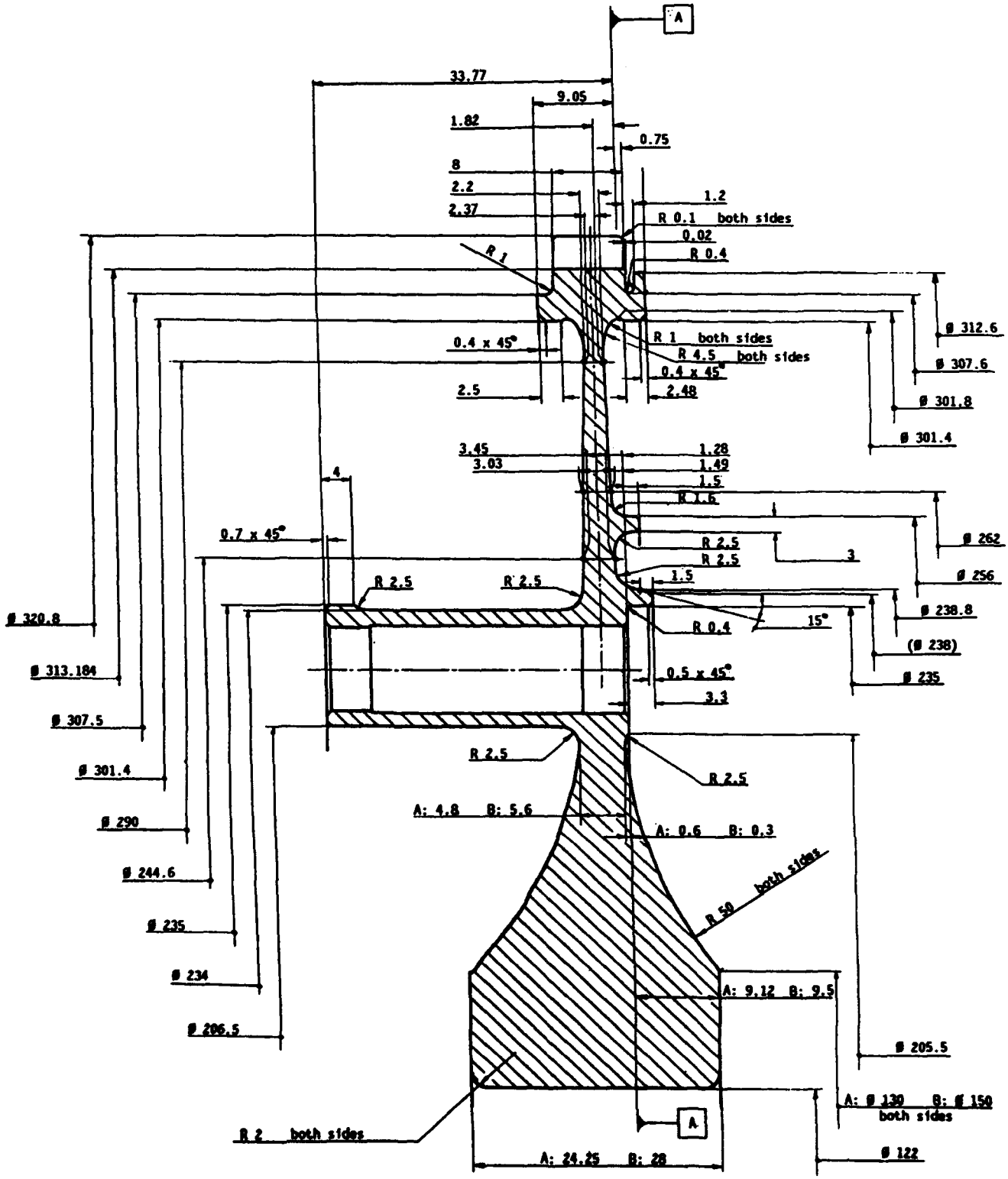

Fig. 4.4 : Disk; Enlarged Rim Slot

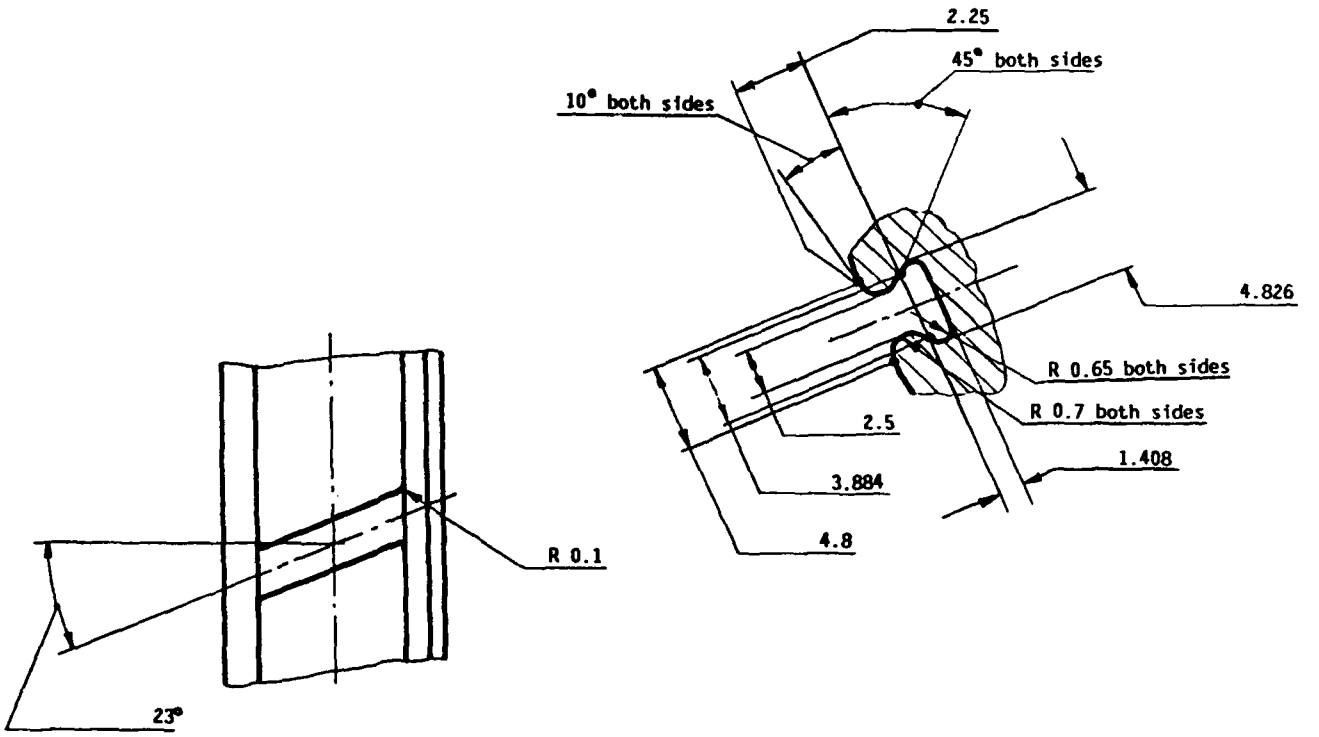

Fig. 4.6 : Disk; Modifications for Rim Slot Testing

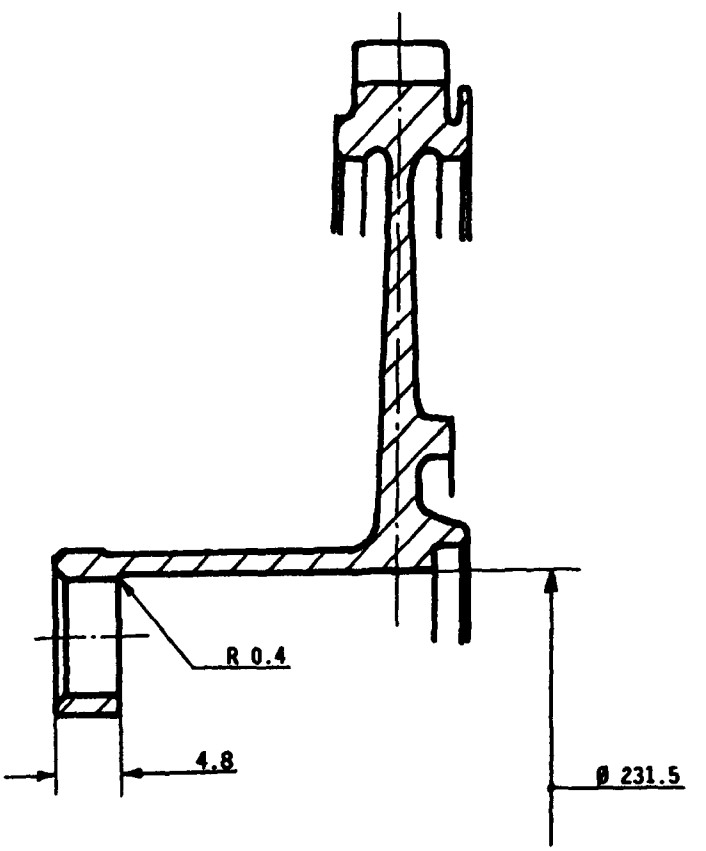

Fig. 4.5 : Disk; Modifications for Bolt Hole Testing

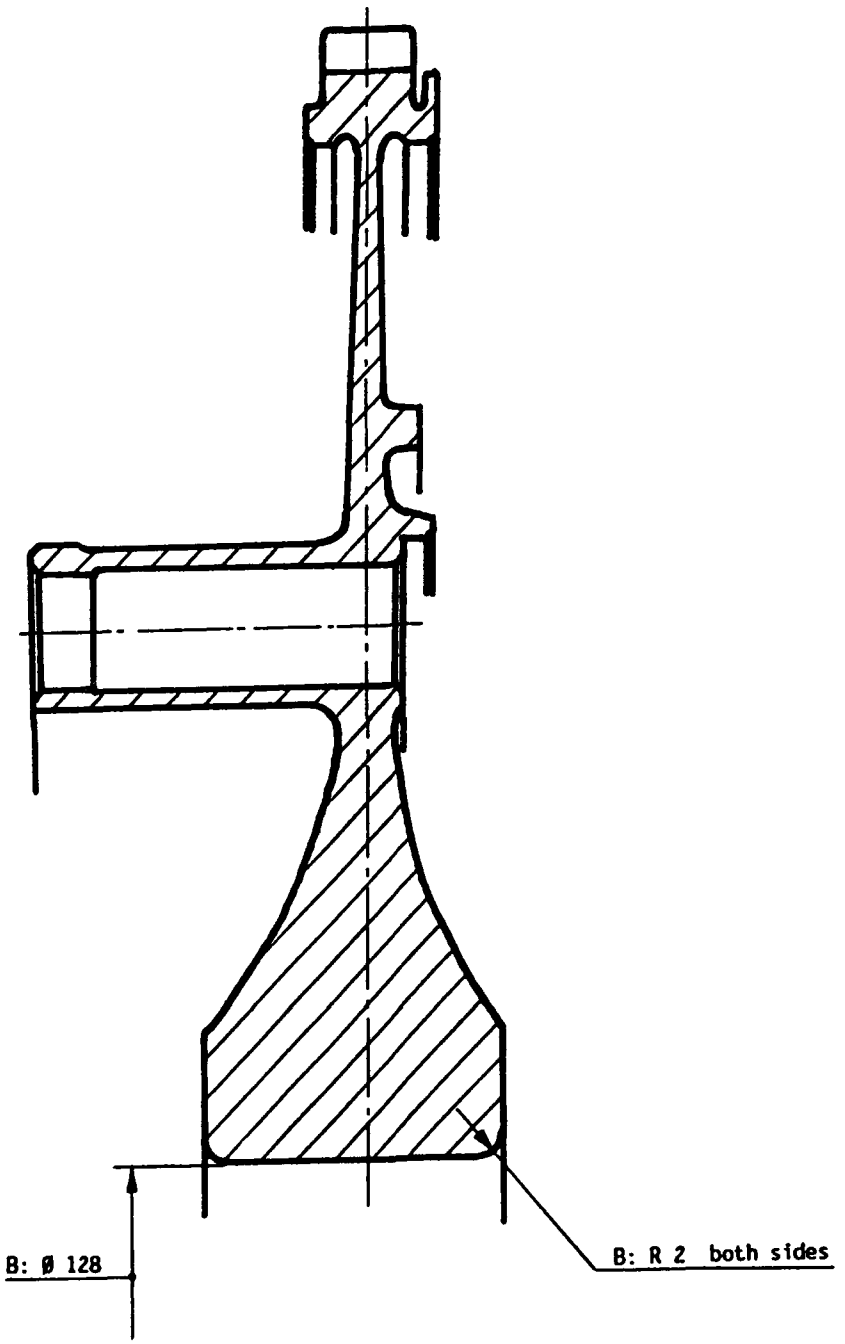

Fig. 5.1 : Adapter for Bolt Hole Testing

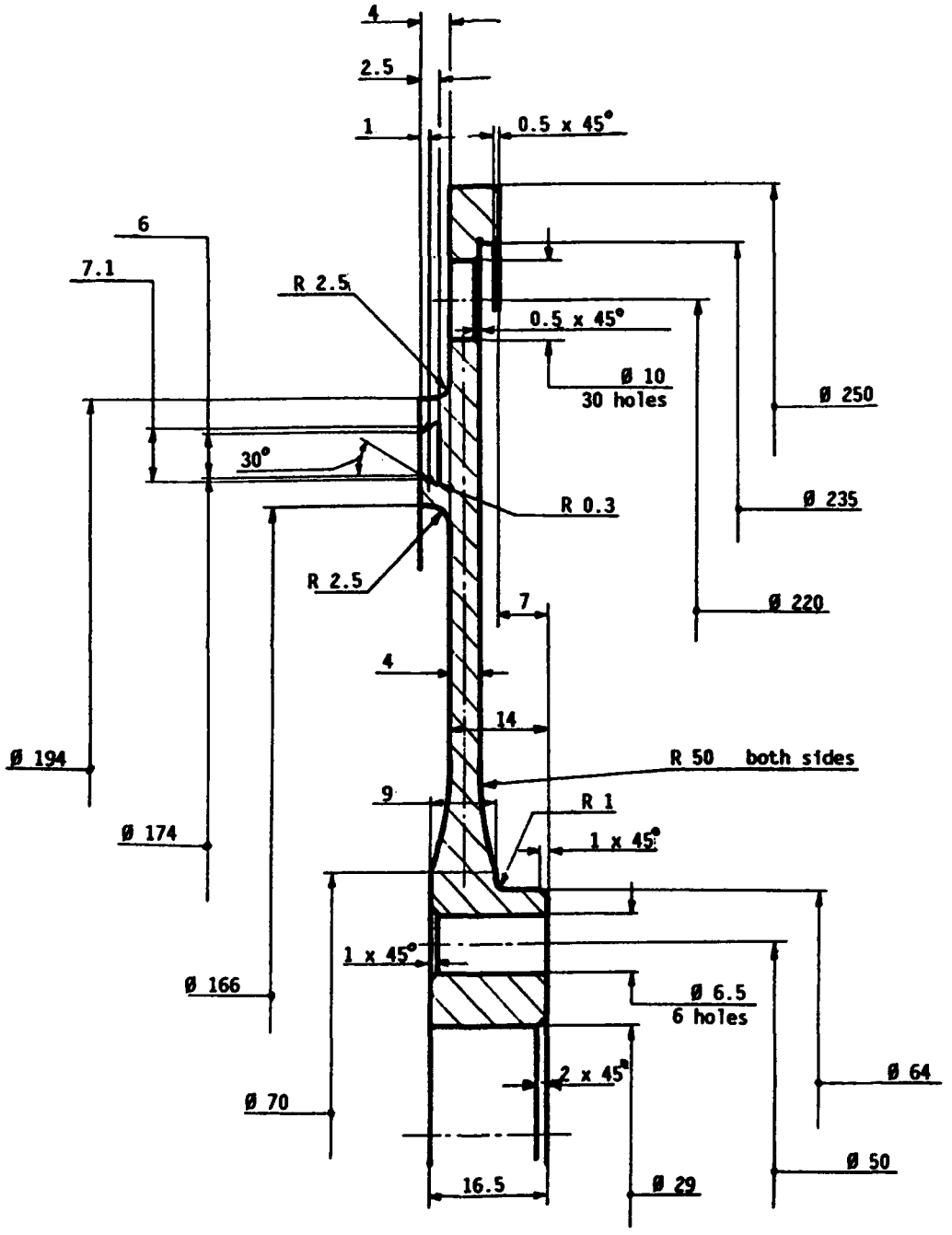

Fig. 5.2 : Adapter for Rim Slot Testing

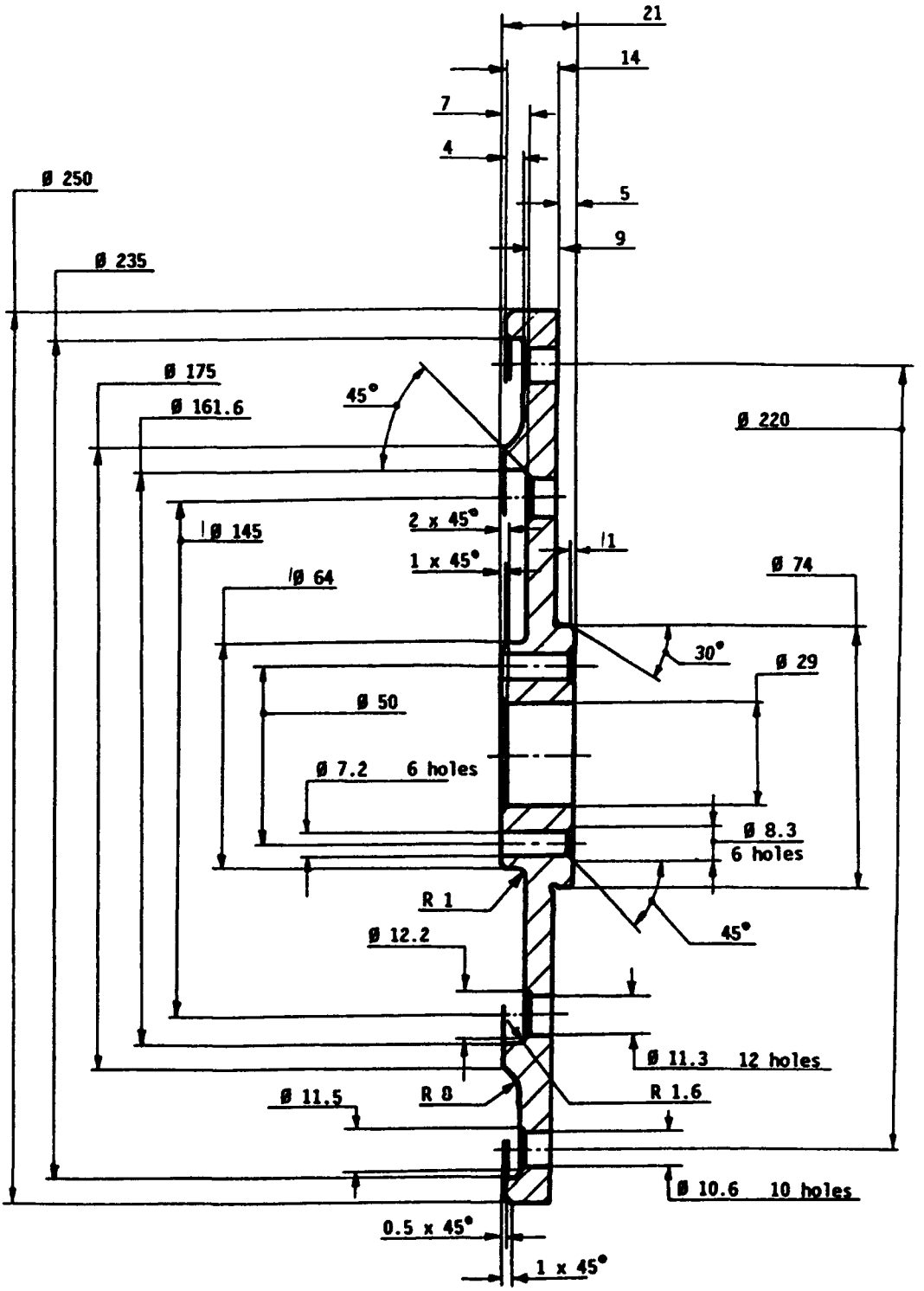

Fig. 5.3 : Shaft (partly) for Bolt Hole Testing

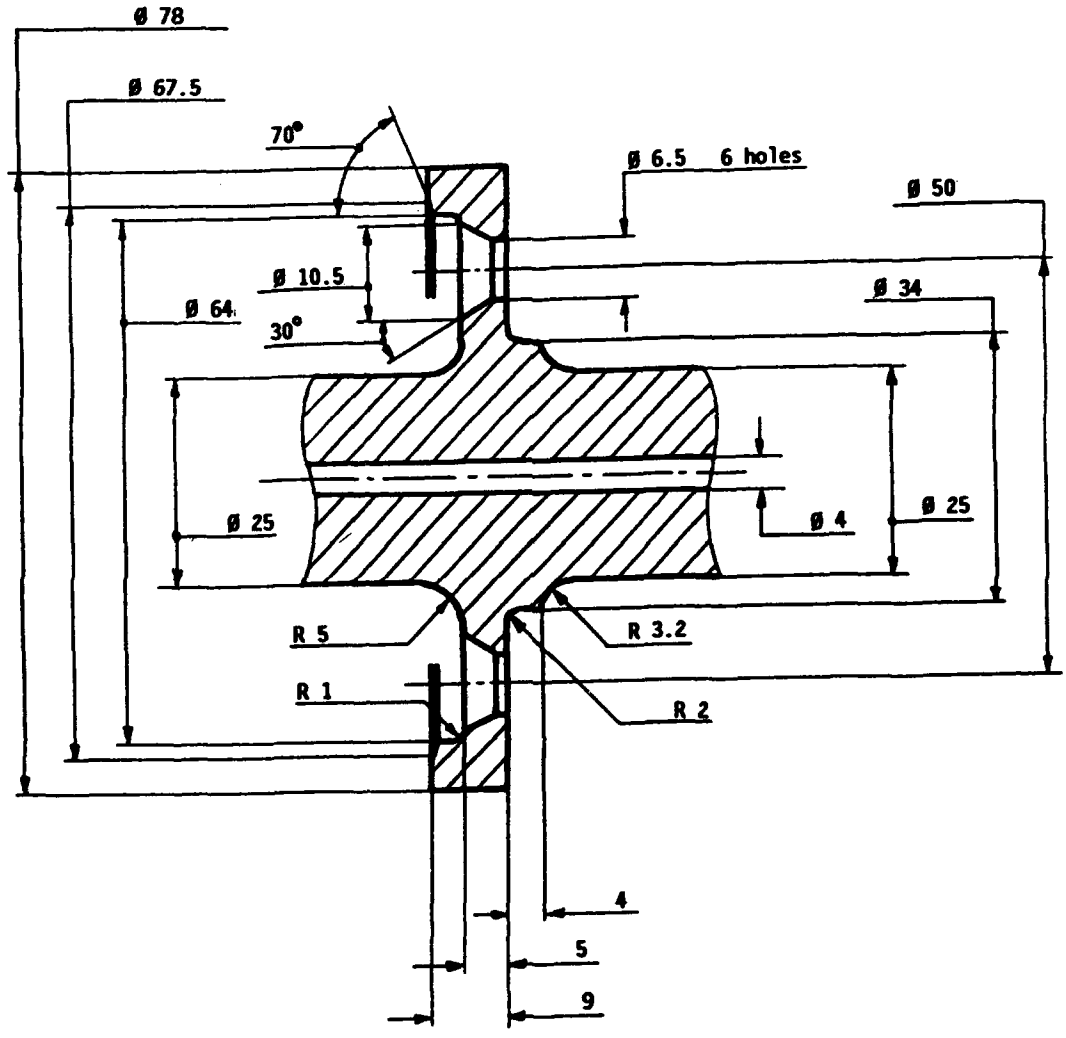

Fig. 5.4 : Shaft (partly) for Rim Slot Testing

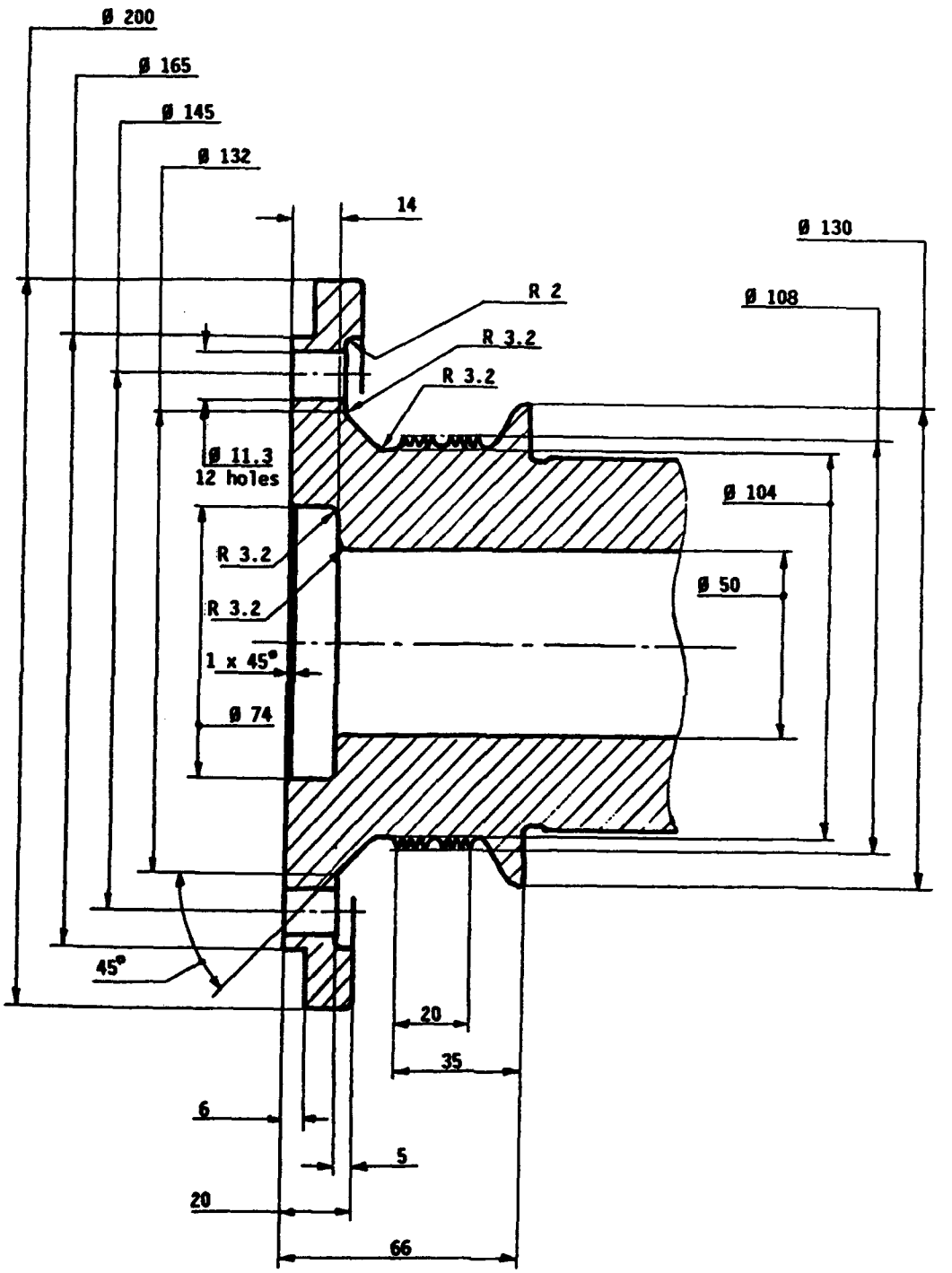

Fig. 6 : Temperature Distribution for Rim Testing

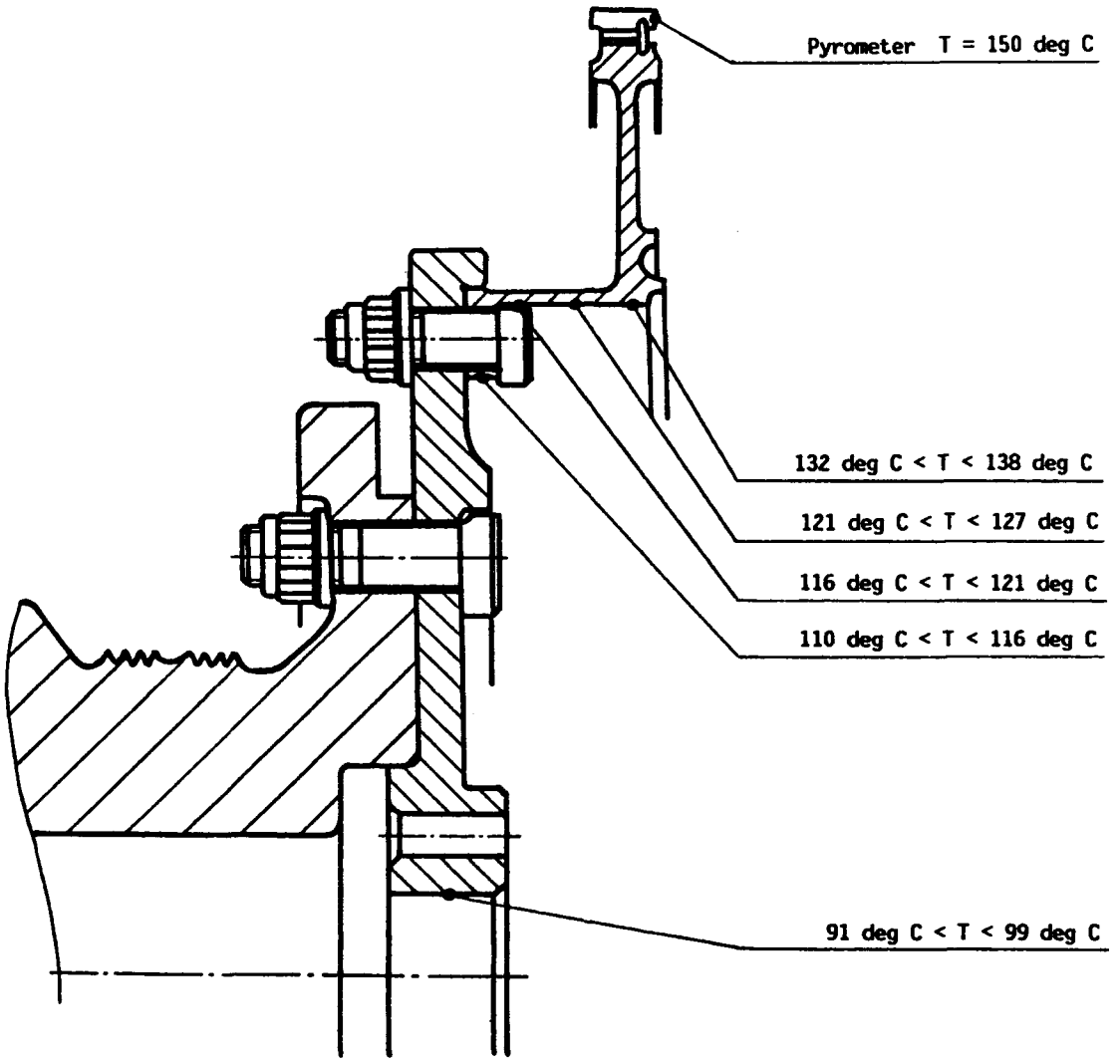

Fig. 7 : Part Specific LCF Data

Notched specimen, plain

LCF stress controlled

Stress concentration factor	Kt	=	2.1
Stress ratio	R	=	0
Test frequency	f	=	0.3 Hz
Test temperature	T	=	300 deg C

Specimen taken from disk, tangential direction

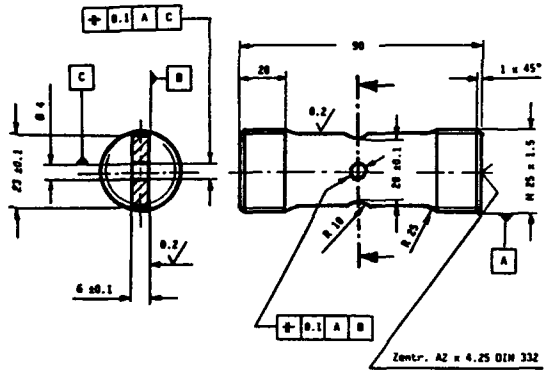

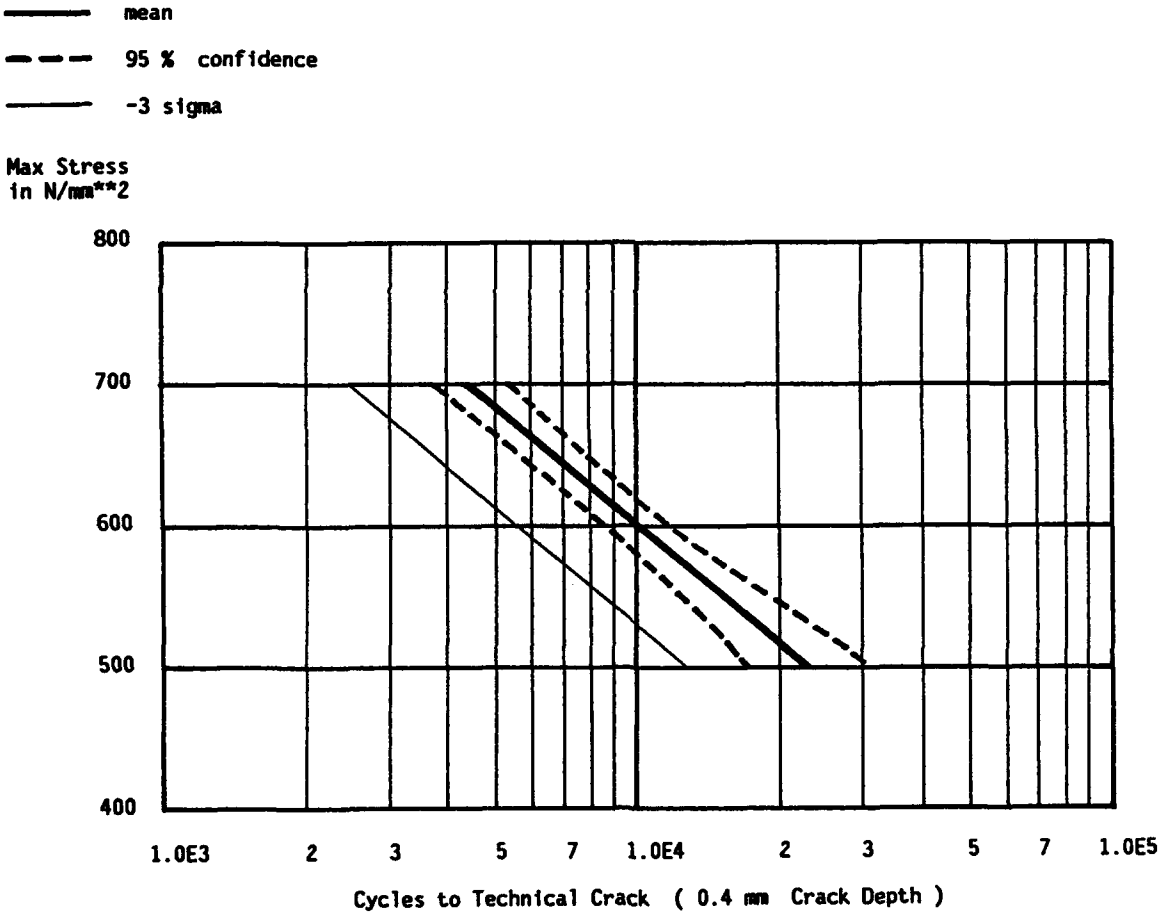

Fig. 8 : Load Sequence

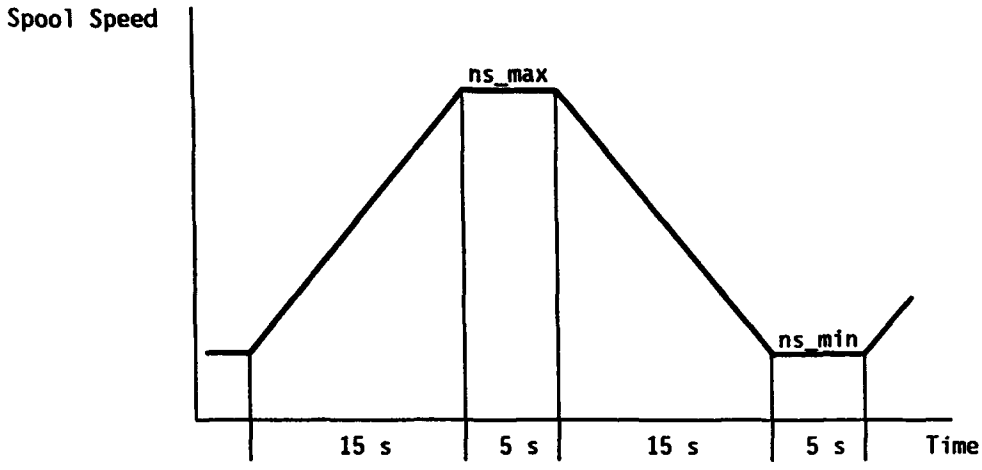

Fig. 9.1 : Crack Shape Overview for Bolt Hole Testing

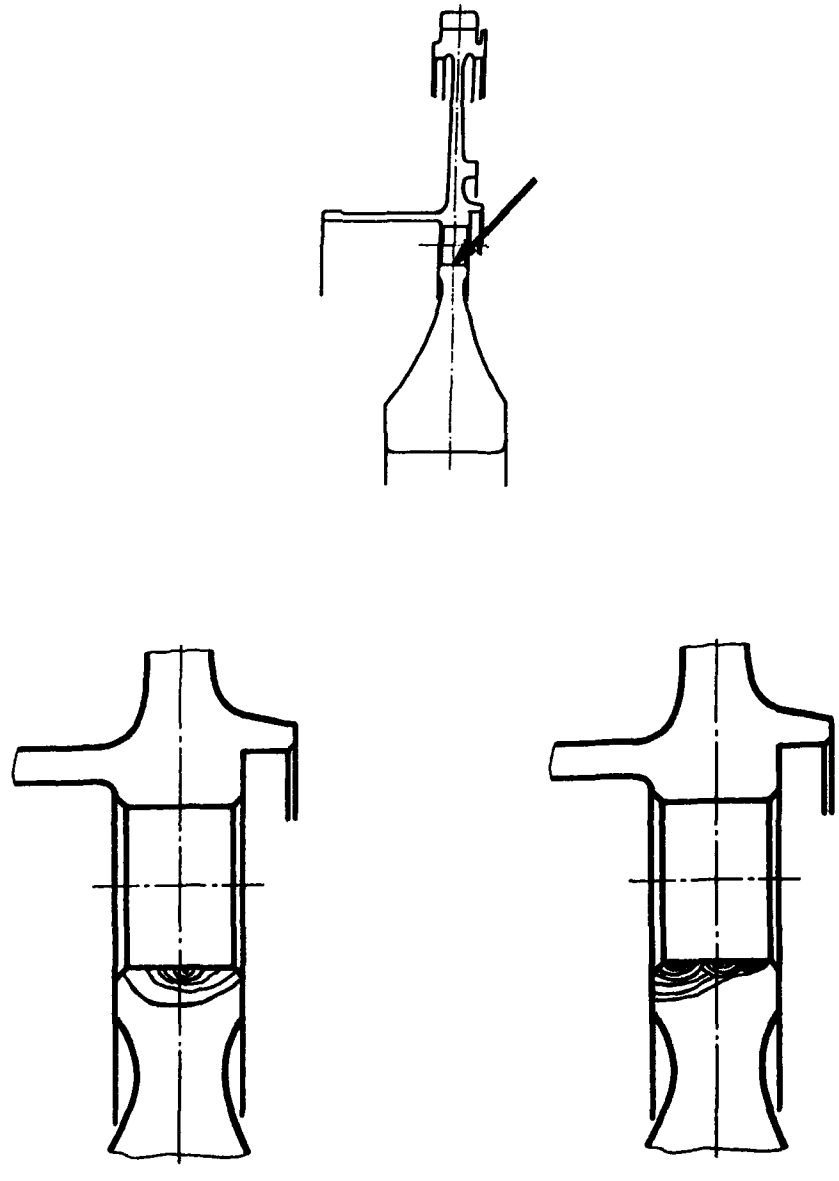

Fig. 9.2 : Crack Shape Overview for Rim Slot Testing

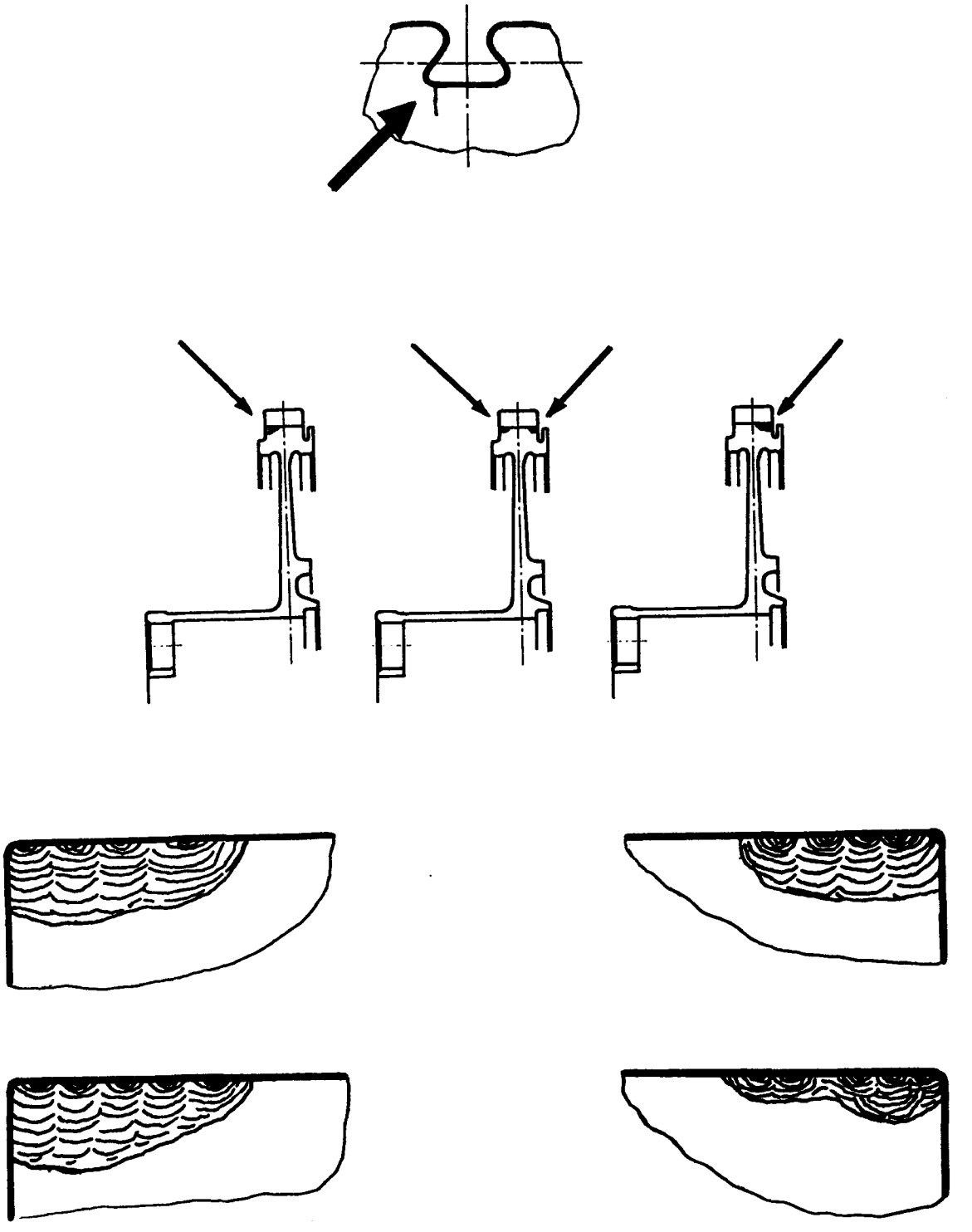

Chapter 4

CF6-6 HIGH PRESSURE COMPRESSOR STAGE 5 LOCKING SLOT CRACK PROPAGATION SPIN PIT TEST

P.A. Domas
GE Aircraft Engines
General Electric Company
P.O. Box 156301, One Neumann Way, M/Z Q105
Cincinnati, OH 45215-6301, USA

1. INTRODUCTION

The CF6-6 High Pressure Compressor Stage 5 Locking Slot Crack Propagation Spin Pit test case provides the opportunity for validation of stress analysis and crack propagation life prediction methodologies for a complex geometry, titanium material, gas turbine aircraft engine component.

The case addresses crack growth from an artificial crack starter notch under isothermal, constant amplitude, continuous (no dwell period), cyclic testing in a partially evacuated spin pit test facility. The most outstanding attribute of the case is the comprehensive crack growth measurement data available in 200 cycle increments throughout the 7355 cycle test duration.

Desirable complexities of the case include:

- Use of actual hardware (field returned, titanium material, engine part),
- Complex local part geometry involving a decaying stress gradient,
- An elastic-plastic stress level (local area yielding),
- Realistic surface conditions (milled and shot peened surface), and
- Assessment of a significant failure mode.

Limitations of the case include:

- Isothermal, constant amplitude (non-mission), continuous (no dwell), partially evacuated, spin pit test,
- Artificial crack starter notch introduced at predetermined location,
- Comprehensive stress analysis required to obtain local crack driving stress, and
- Presence of shot peened surface that potentially complicates assessment.

ASSESSMENT ANALYSIS

To evaluate this test case, Rolls-Royce completed a two-dimensional axisymmetric finite element stress analysis of the compressor spool followed by a two-dimensional finite element analysis of the concentration effect of the loading slot. These results were used to calculate the crack propagation behavior from the crack starter notches introduced at the loading slots. Factors to account for the effect of shot peening were derived empirically from the results given for the notched bend specimen. These factors were used in the component life calculation which resulted in a prediction within 13% of the observed life. The assessment carried out by Rolls-Royce confirmed the suitability of this test case.

2. COMPONENT GEOMETRY

This section provides an overall description of the basic part geometry and the specific feature to be analyzed (the stage 5 blade locking slots). A photograph of the spin pit test rig and a drawing providing dimensions and tolerances is also included.

Figure 1 shows the CF6-6 engine cross section including the high pressure compressor. The specific component to be analyzed is the stage 3-9 spool illustrated in Figure 2. Compressor blades are held by the spool in circumferential dovetails as shown in Figure 3. The blades are inserted through load slots cut into each dovetail. To secure the blades, a locking lug is inserted into each of two locking slots on either side of the load slot. The feature of interest is the fillet radius at the bottom of the stage 5 lock slots.

Figure 4 is a photograph of the overall spin pit test configuration. The test rig consisted of a modified Stage 2 disk (with no blades) and forward shaft, the bladed 3-9 spool (with crack starter notches electro-discharge machined (EDM) into two of the stage 5 lock slots), Stage 10 disk (with no blades), Stage 11-13 spool (with no blades),modified stage 14-16 spool bolt flange, compressor aft shaft, and facility adapters.

The EDM notches were in each of two of the four Stage 5 lock slots. Figure 14 shows the slot locations designated as 5B2 and 5C1. They were in the center of the stress concentrating fillet radius at the location calculated to have the maximum hoop stress.

3. PART PROCESSING INFORMATION

Included in this section is general machining and processing information and information related to surface enhancements.

The load and lock slots are cut into the dovetail using a numerically controlled end mill. Following the cutting operation the edges of the slots are hand benched to remove burrs. The entire spool is then shot peened to an intensity of 5 - 7A with S110 steel shot with 125% coverage.

Because of the steep stress gradient away from the slot it was anticipated that surface residual stress could significantly influence the crack propagation behavior. To assess the influence of the shot peen induced surface compressive stress, a crack growth test on a shot peened Ti 6-4 plate was conducted.

The test is described in Figure 6. The 0.270 inch (6.86mm) thick rectangular plate was surface ground and shot peened on one half. Three nominally identical crack starter notch pairs (six total notches) were placed on one surface of the plate to permit back-to-back comparison of the crack growth from the same notch in a peened and unpeened surface. A mixture of rectangular and semi-circular notches was used. The plate was continuously, elastically, cycled under constant amplitude (R = 0.03), in four point bending, at room temperature.

The crack growth behavior of the notches is shown schematically in Figure 6 generated from fractographs of the various cracks following plate failure. Figure 7 shows the fracture surface appearance of some of the cracks. Crack growth rates for the peened and unpeened cracks are compared in Figure 8.

These results suggest that the surface crack growth rate is significantly retarded by the presence of the shot peening. Recognition of this behavior (perhaps through empirical or theoretical model adjustments) may be important in obtaining correlation with the results of this test case.

4. OPERATING CONDITIONS

A description of the spin pit test cycle and environment is provided in this section.

The CF6-6 spin pit vehicle was cycled from 1,000 (± 50) Rpm to 12,000 (± 50) Rpm to 1,000 Rpm with acetate replication and eddy current inspection of the lock slots at 200 cycle increments. Stage 3,4, and 5 blades were removed for each inspection and reinstalled prior to resuming test.

The cycle was triangular with no dwell at maximum or minimum speed and approximately 2 minutes in duration.

The test facility was an evacuated vertical spin pit driven by a steam turbine. The drive turbine was attached to the lid of the spin pit and the drive shaft inserted through a small opening in the center of the lid. The test rotor was attached to the drive shaft by means of facility adapters and suspended from the turbine drive shaft under the pit lid. A pedestal anchored at the floor of the pit supported the lower damper bearing.

The compressor rotor was adapted to the steam turbine drive system by means of facility aft shaft adapter, spline adapter, retainer ring, and nut retainer. The drive shaft supported the weight of the rotor and transmitted driving torque from the steam turbine to the rotor. The forward shaft of the rotor was adapted to the lower catcher bearing assembly by facility damper, shaft adapter, and bottom shaft spindle.

Thermocouples were located in the upper and lower bearings, near the stage 5 blade tips and in pit ambient air. The average spool operating temperature was 150F (66C).

Vibration sensors at the forward and aft ends of the rotor were incorporated in the control system to keep vibration levels within set limits. No excessive vibration was recorded during the test.

5. BOUNDARY CONDITIONS FOR STRESS ANALYSIS

The boundary conditions required for stress analysis of the compressor rotor are discussed in this section.

Because the area of interest (High Pressure Compressor Rotor stage 5 lock slot) is far removed from the spool end flanges the stress analysis can be significantly simplified. It is recommended that only the spool itself and not the adjacent hardware be modeled in the stress analysis. Axially fixed end conditions at the forward flange and unrestrained end conditions at the aft flange are suggested.

Blades and locking lugs contribute radial load to the rim of the spool. Blade loads (including the lug weights) and relative centers of gravity are provided in Figure 9.

6. HEAT TRANSFER INFORMATION

No heat transfer analysis was conducted for the test rig. Temperature should be assumed constant at 150F (66C).

7. MATERIALS DATA

Physical and mechanical properties for the Titanium material are summarized in Figure 10.

Cyclic crack growth rate data (Figure 11) were obtained at 150F (66C), R = 0.05 from surface flaw test bars machined from low stress areas of the spin pit tested spool.

Cyclic Stress-Strain Data (Figures 12, 13) at 200F (93C) were obtained from longitudinal, smooth bar, strain control tests. Half life alternating stress versus alternating strain data are shown in Figure 12. To assist in developing the "complete" stress-strain curve, mean stress as a function of total (elastic plus plastic) strain range is shown in Figure 13. In the formula: alt. Stress = A * (alt. plastic strain)^n, A = 140 Ksi (965 Mpa), and n = 0.0512.

8. OPERATION HISTORY

PRIOR HISTORY

The tested 3-9 spool had 4,167 cycles of normal field usage prior to installation in the spin pit.

The test vehicle completed 7,000 cycles of spin pit endurance testing, consisting of a speed excursion from 1,000 to 12,500 to 1,000 Rpm at 150F (66C) prior to being run in the crack propagation test. Inspection of the spool after this phase of testing revealed no fatigue cracks. No significant fatigue damage was predicted to occur during this testing.

Notches, simulating cracks, were machined into the center of a corner radius of each of two of the four stage 5 lock slots following the fatigue test, Figure 14.

The crack propagation test was run using a cycle between 1,000 Rpm and 12,000 Rpm. The test rotor failed (complete separation) at 7,355 cycles near maximum speed.

DATA ACQUIRED DURING TEST

The spin pit test results are presented in this section and consist of tabulated measurements of the crack length as measured by acetate replicas at 200 cycle intervals throughout the test. Crack propagation data are presented in Figure 15 for crack growth from both starter notches. Figure 14 is a graph of the tabulated data.

FAILURE ANALYSIS DATA

The results of fractographic examination of the stage 5 lock slot region following rotor separation are presented in this section.

Two fractographs of the stage 5 lock slot region are shown in Figure 16. The arrows define the extent of stable crack propagation just prior to unstable growth and failure. Figure 17 shows the location of the EDM crack starter notch. Figure 18 shows a typical replica of the EDM notch and propagating crack and another fractograph.

9. SUMMARY

The CF6-6 compressor spool spin pit test case provides a challenging opportunity for validation of fracture mechanics life prediction methodology. Successful correlation with observed crack growth behavior will provide confidence in the supporting material behavior, stress analysis, and life analysis technologies.

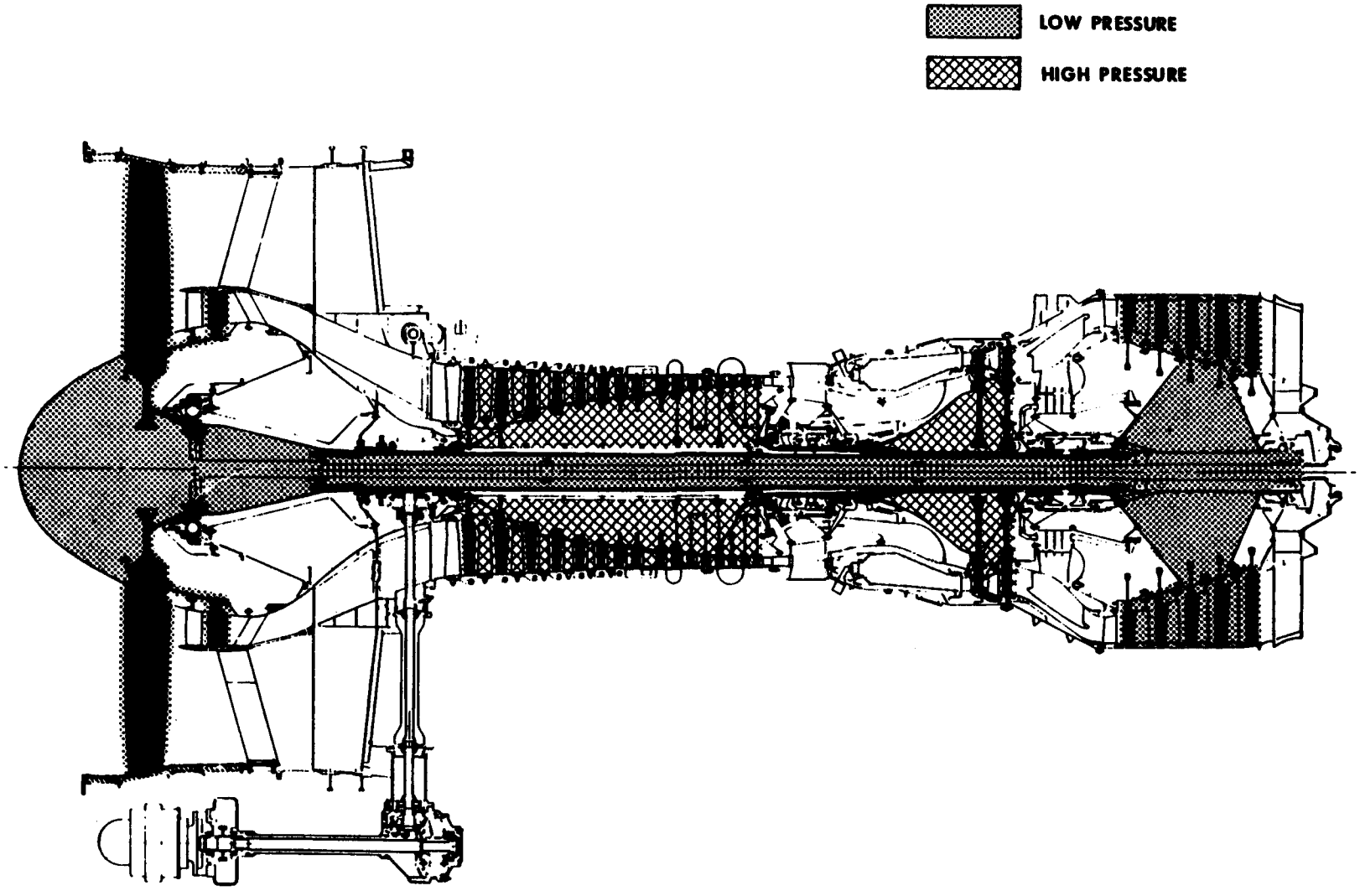

Figure 1 CF6-6 rotating assemblies.

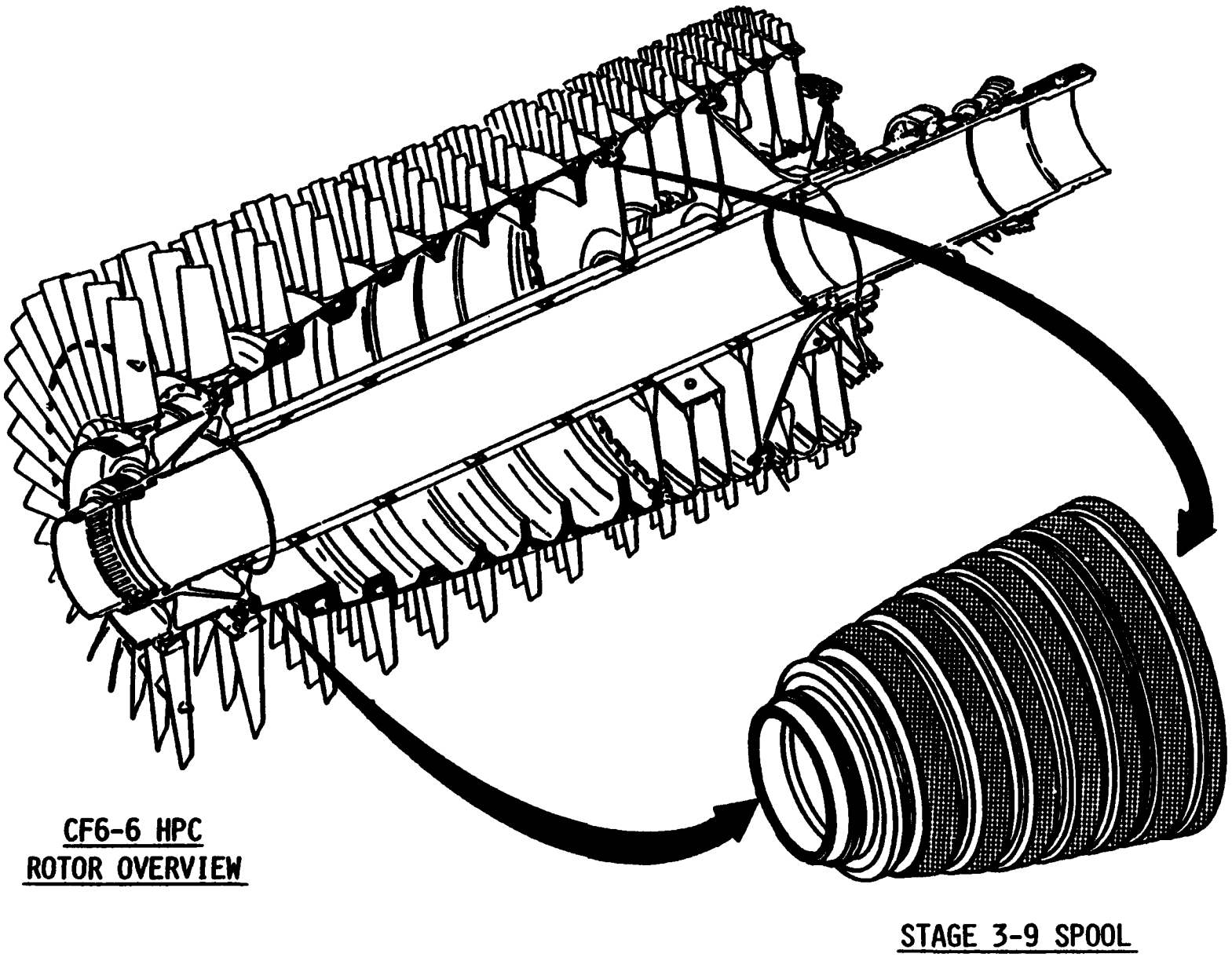

Figure 2 Component overview (Stage 3-9 Spool).

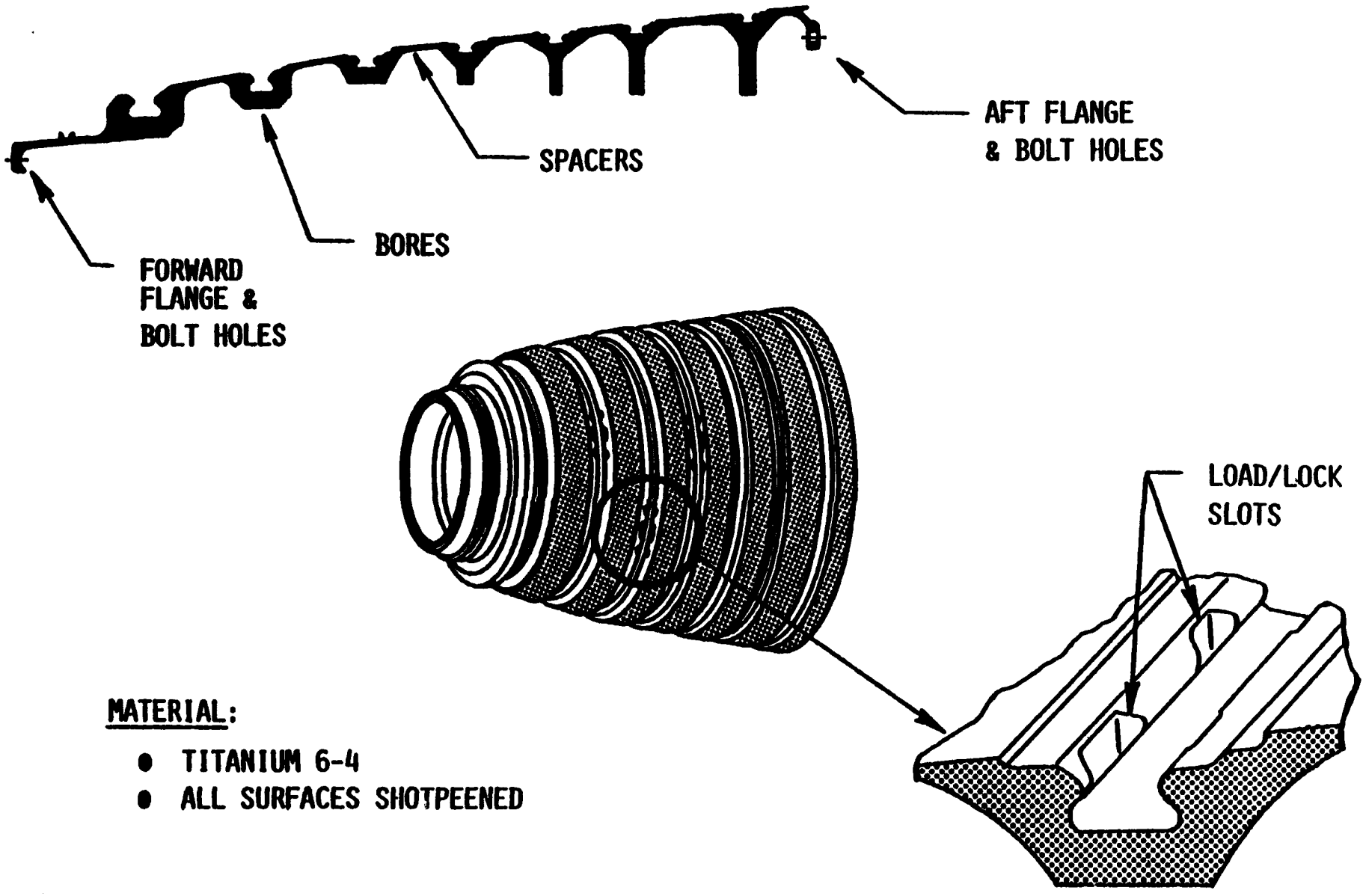

Figure 3 Component overview (load/lock slots).

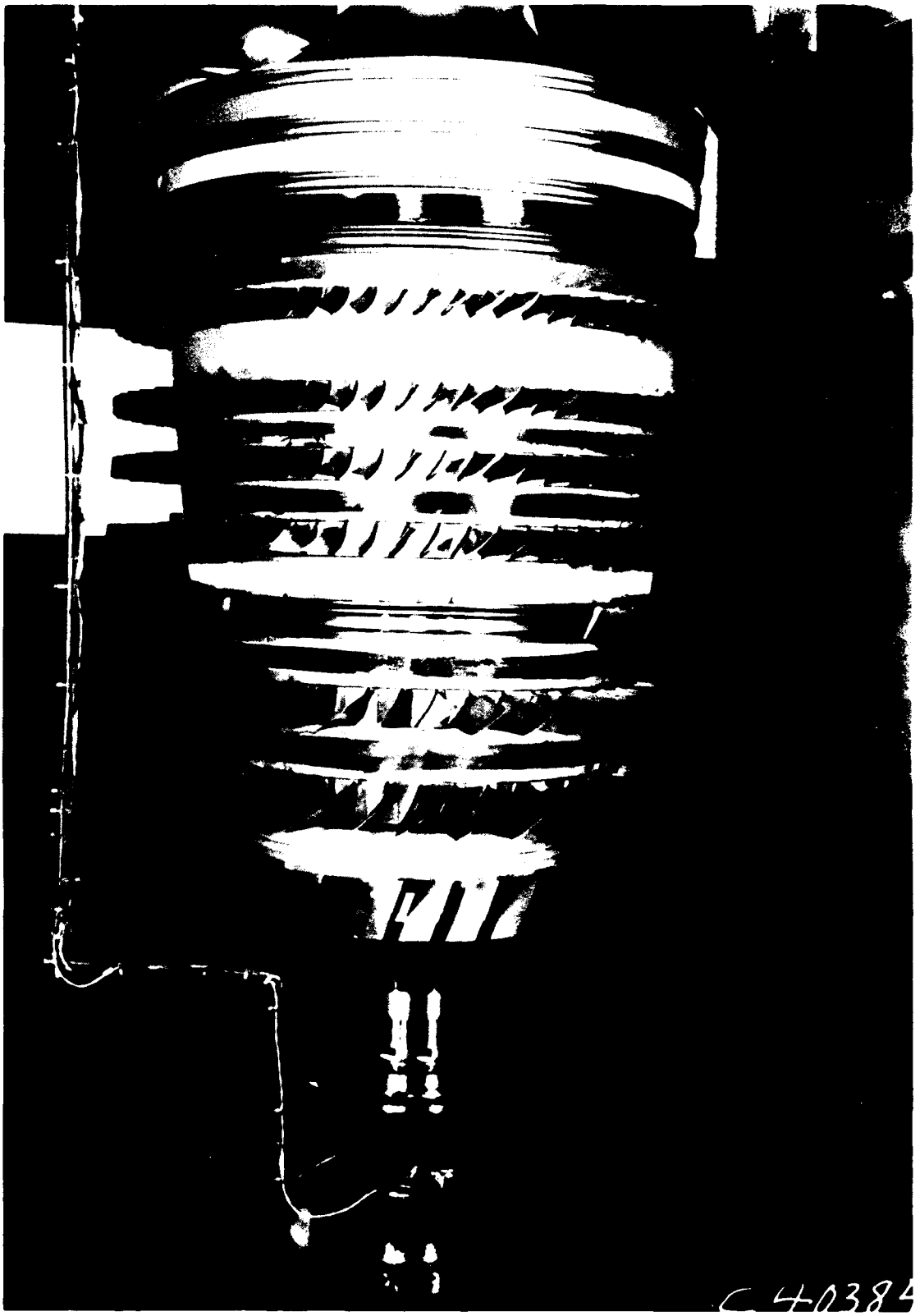

Figure 4 Photograph of overall test set-up.

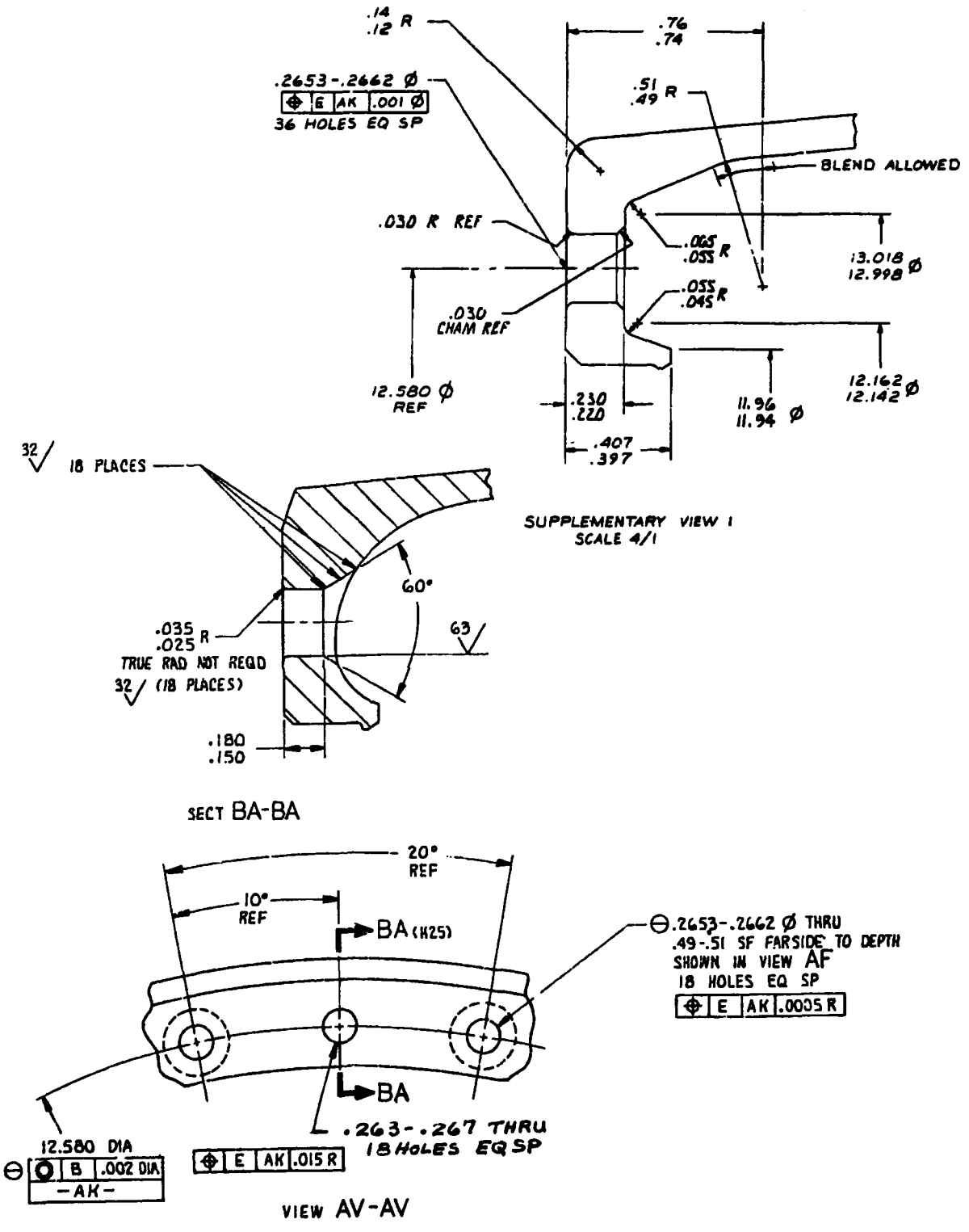

Figure 5 CF6-6 High Pressure Compressor 3-9 Spool.

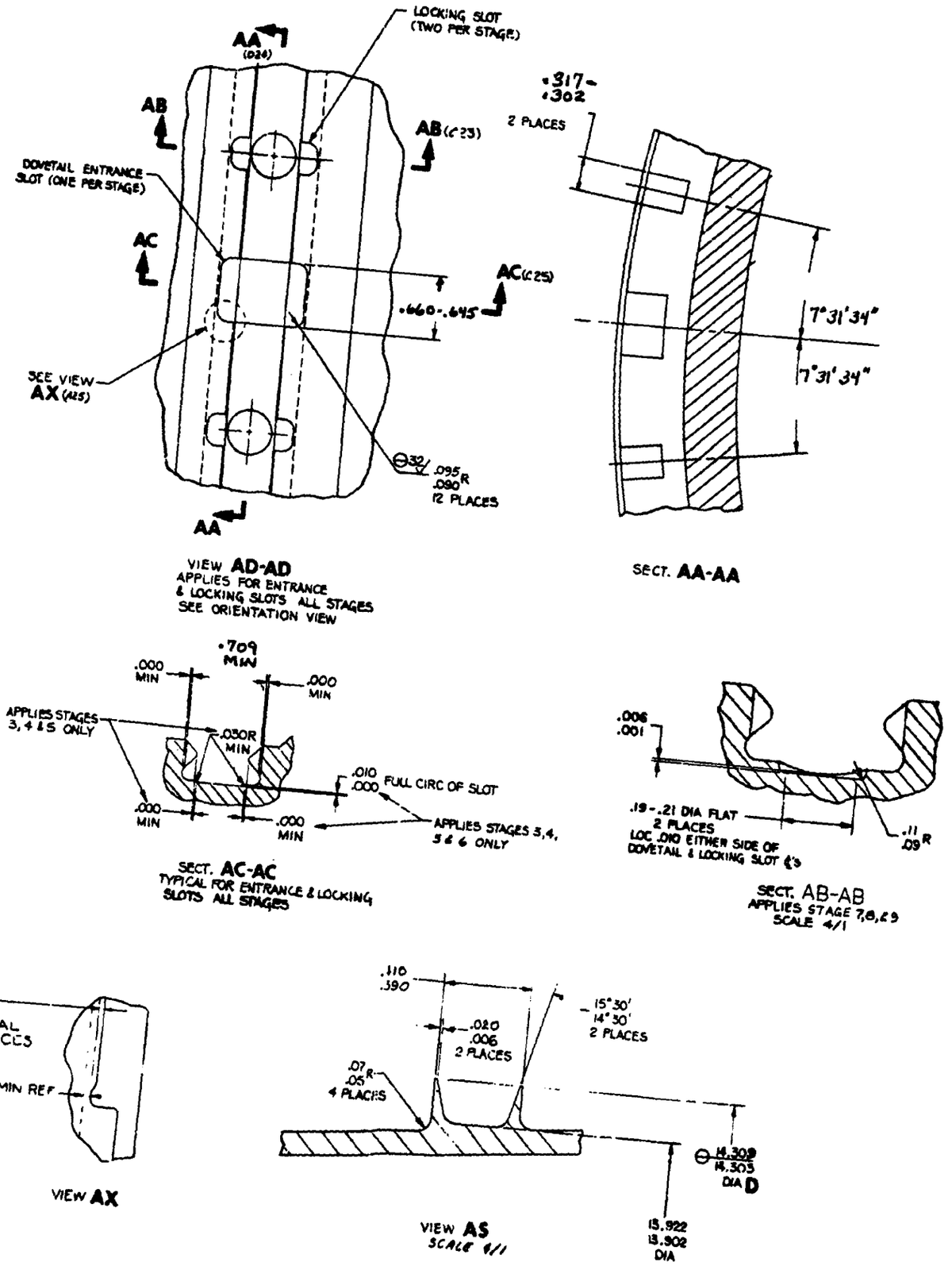

Figure 5 CF6-6 High Pressure Compressor 3-9 Spool. *(continued)*

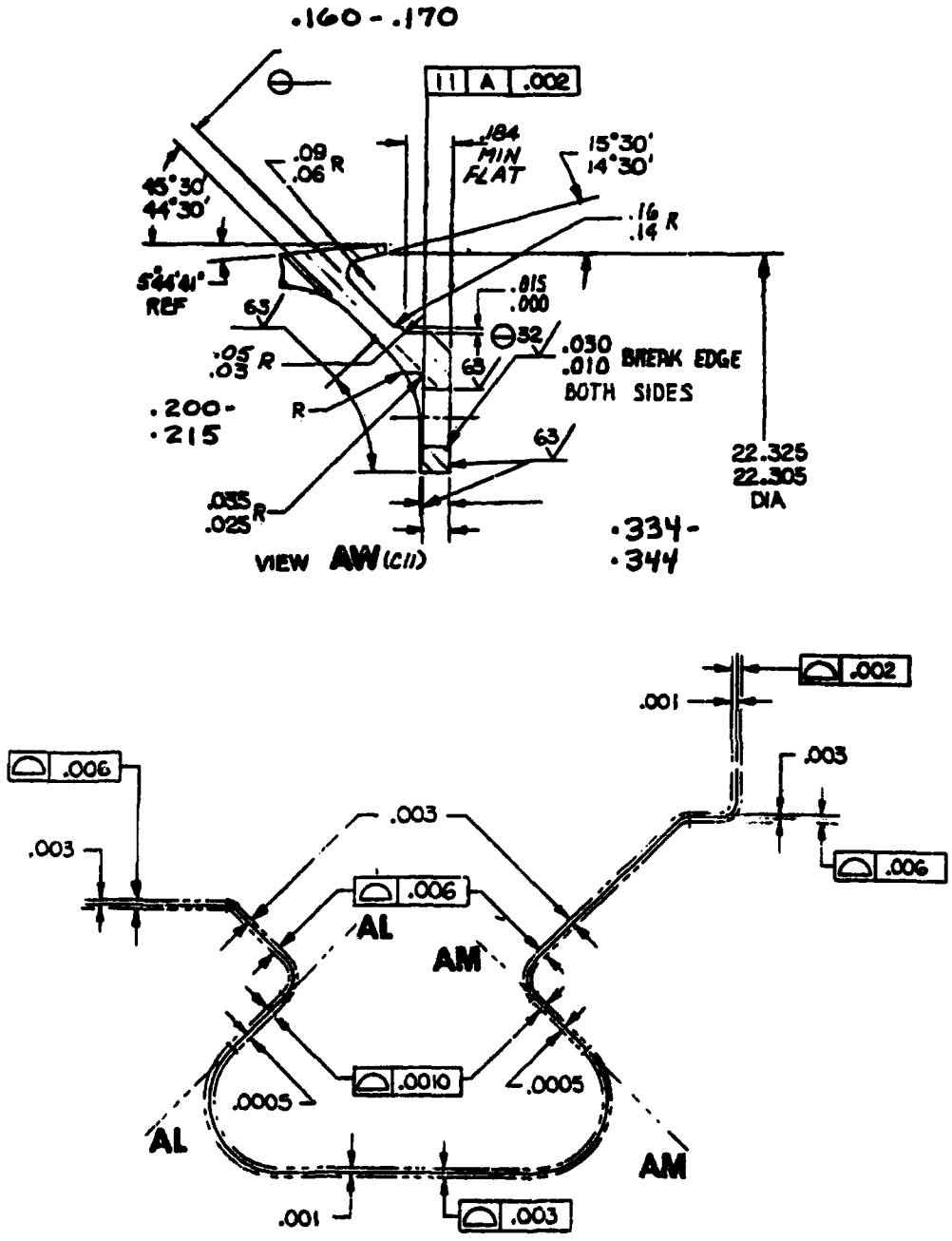

CONTOUR LIMITS FOR DOVETAIL SLOT
STAGE 3 SEE VIEWS AT (H21) & AU (F20)
SCALE 4/1

Figure 5 CF6-6 High Pressure Compressor 3-9 Spool. *(continued)*

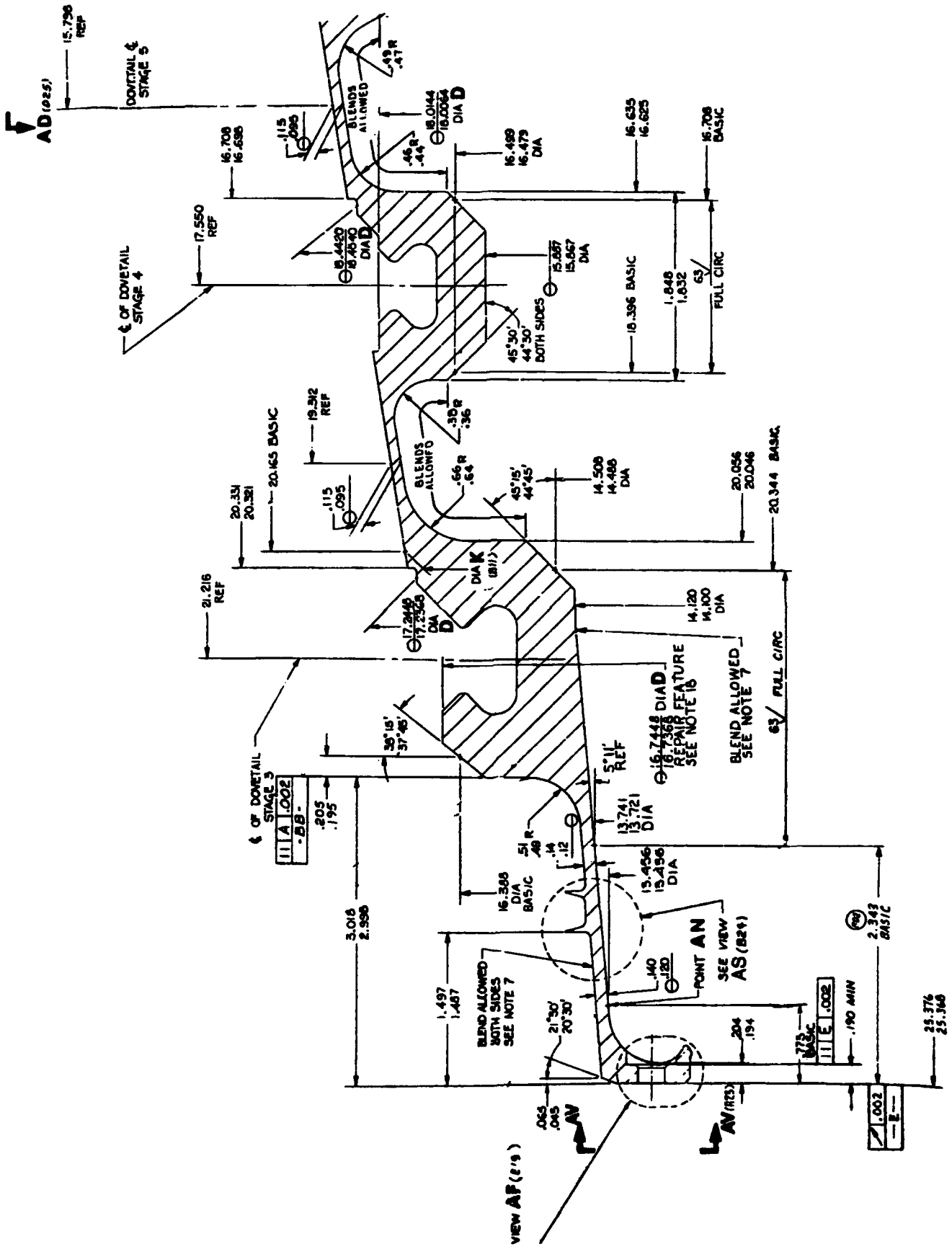

Figure 5 CF6-6 High Pressure Compressor 3-9 Spool. *(continued)*

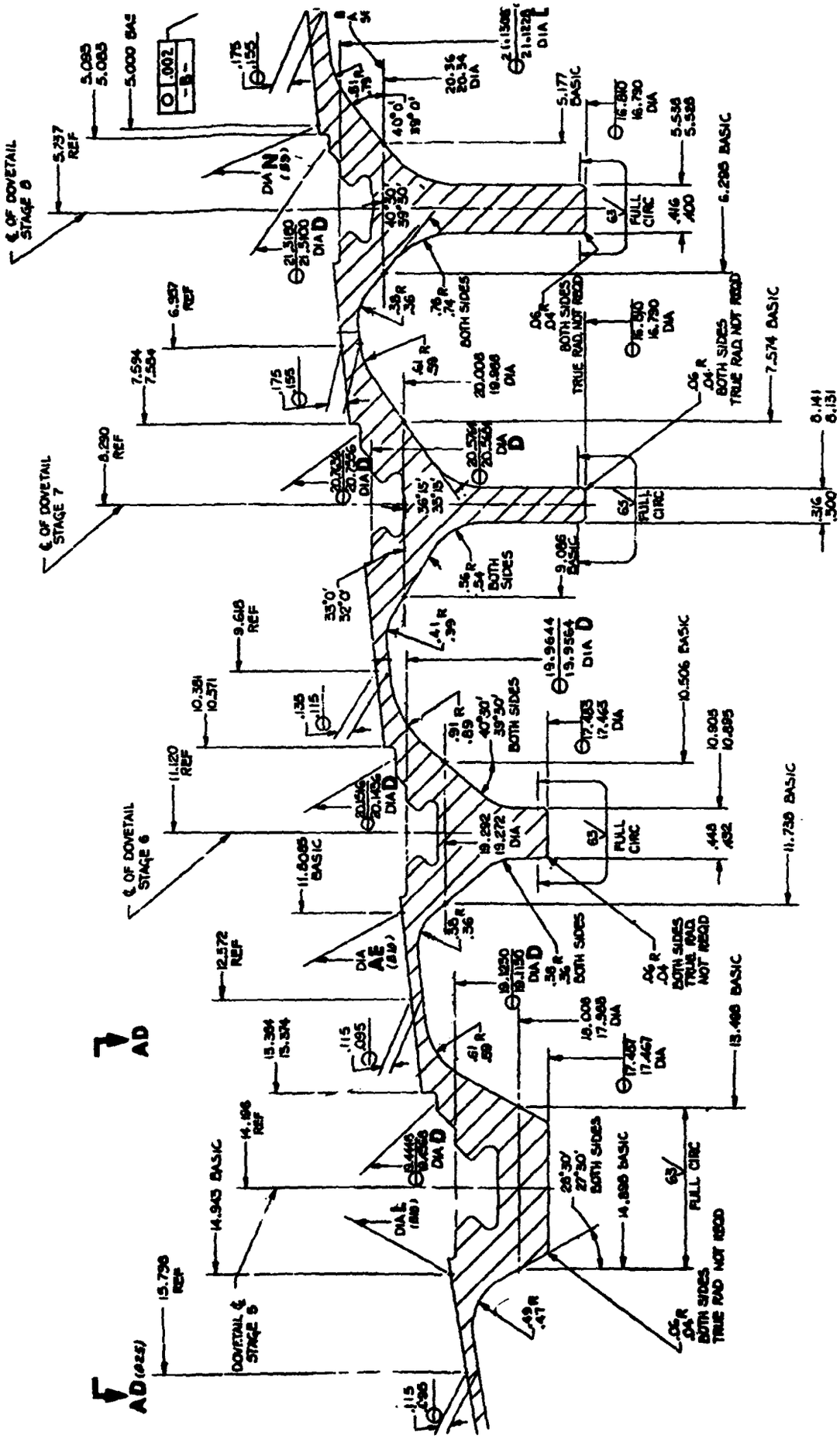

Figure 5 CF6-6 High Pressure Compressor 3-9 Spool. *(continued)*

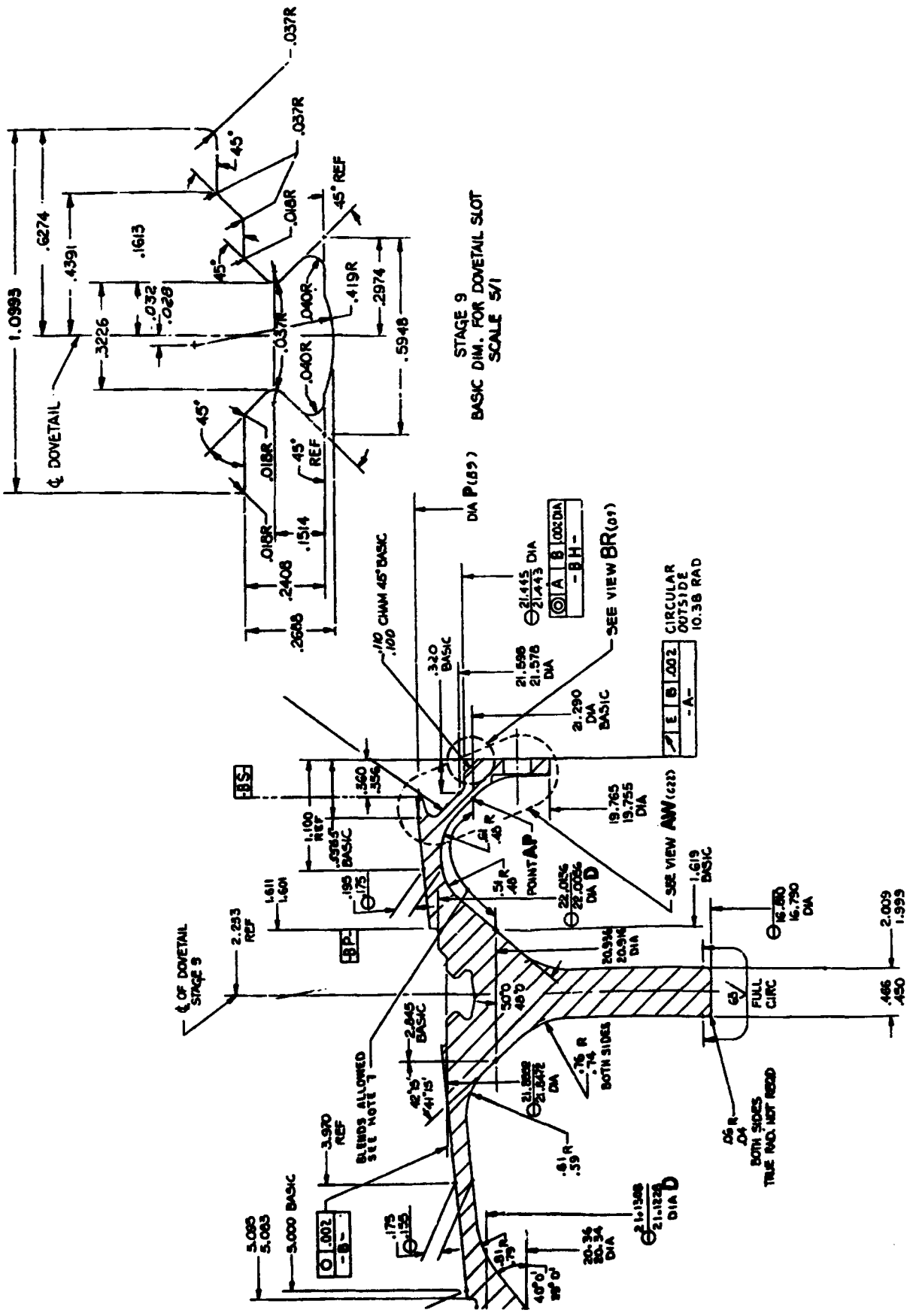

Figure 5 CF6-6 High Pressure Compressor 3-9 Spool. *(continued)*

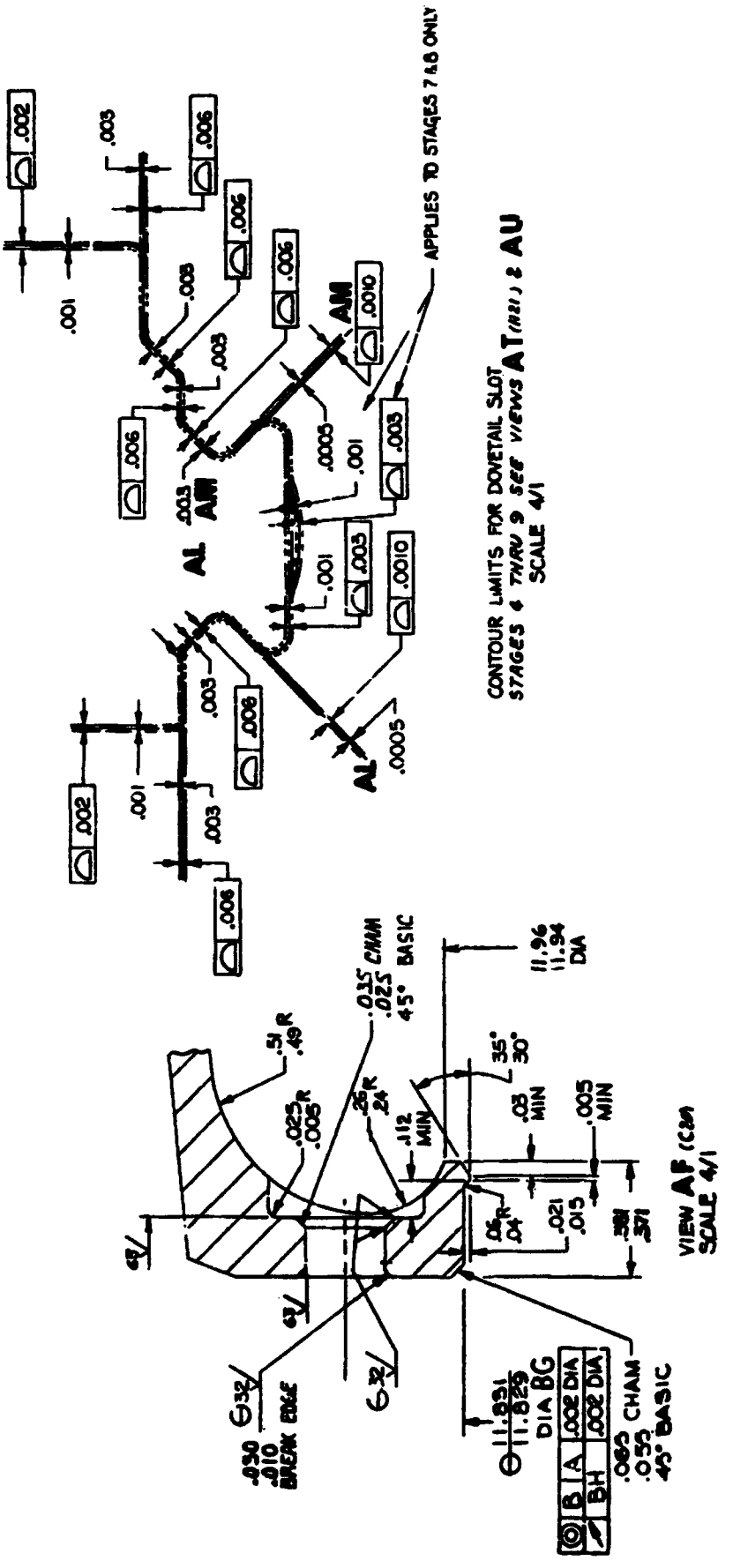

Figure 5 CF6-6 High Pressure Compressor 3-9 Spool. *(continued)*

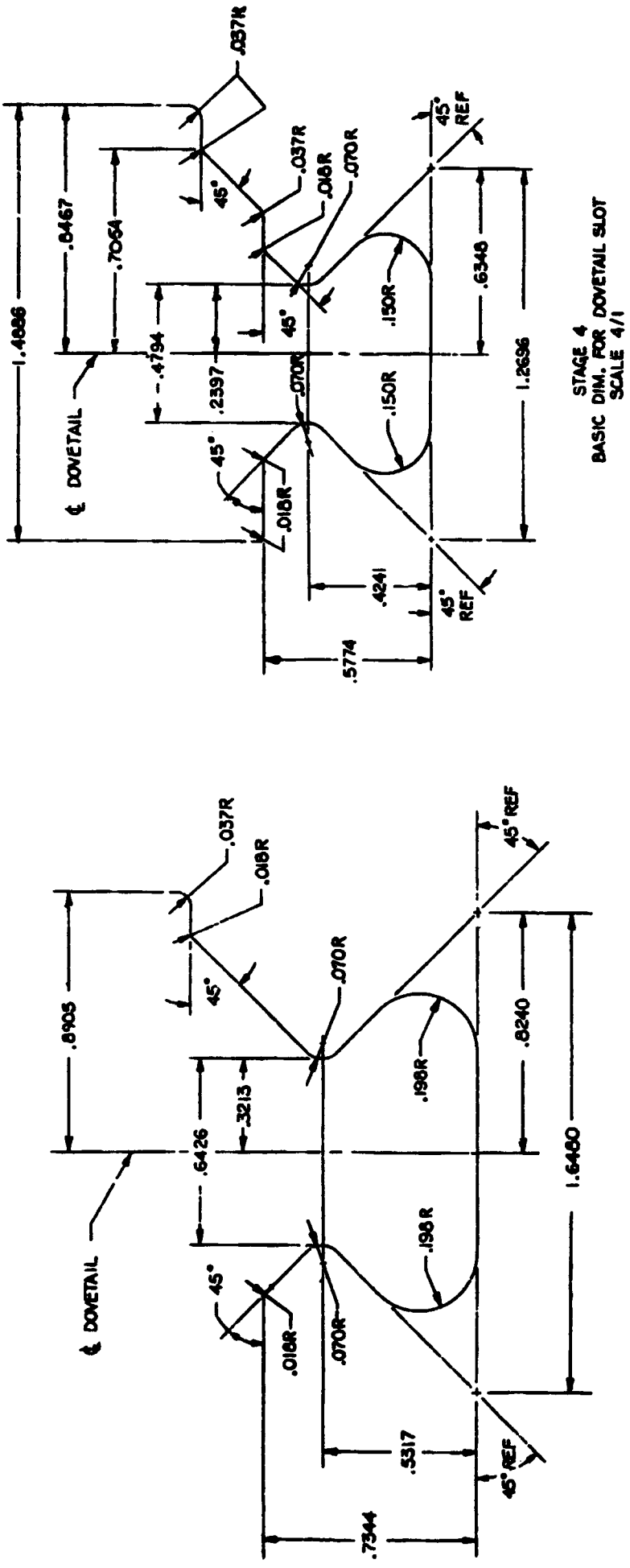

Figure 5 CF6-6 High Pressure Compressor 3-9 Spool. *(continued)*

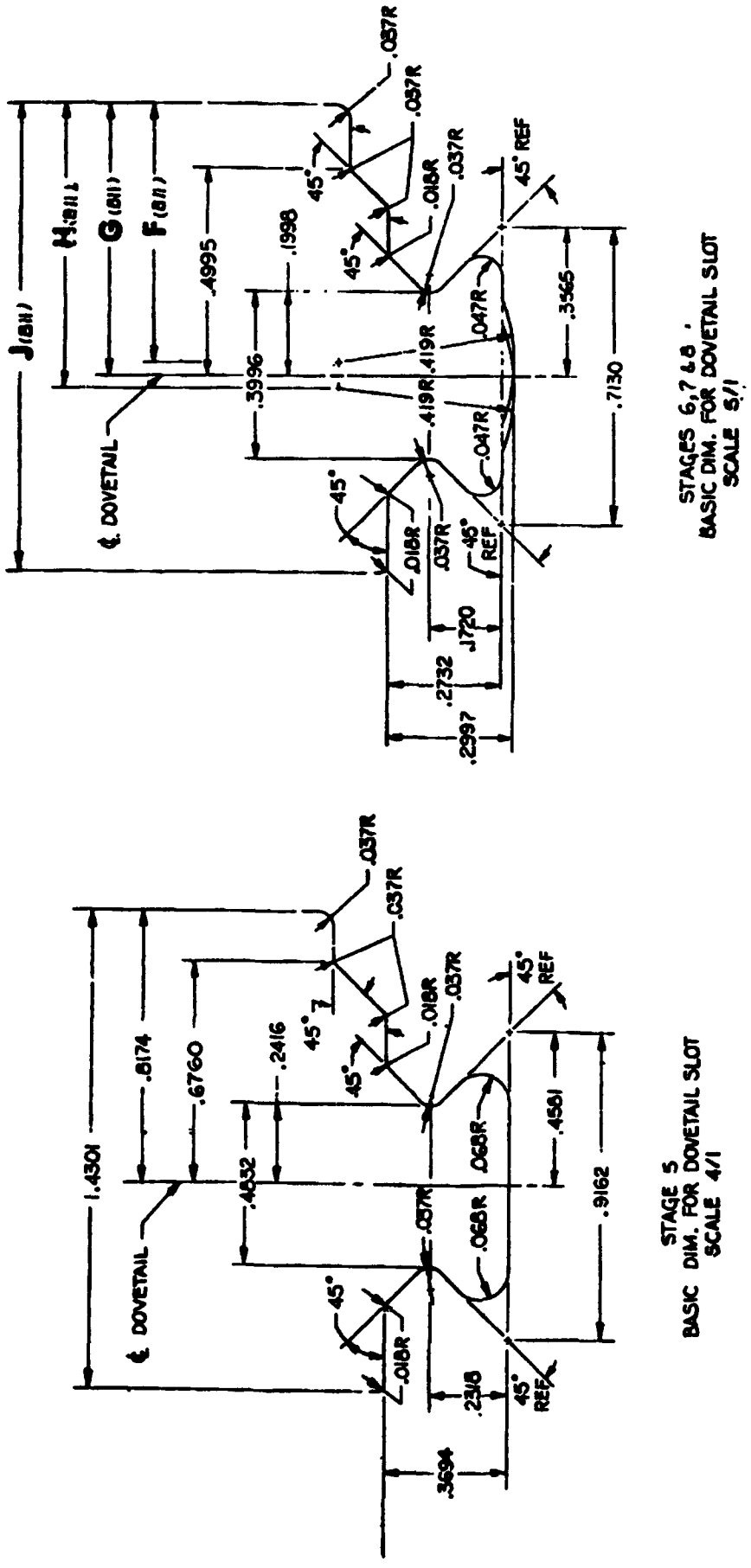

Figure 5 CF6-6 High Pressure Compressor 3-9 Spool. *(continued)*

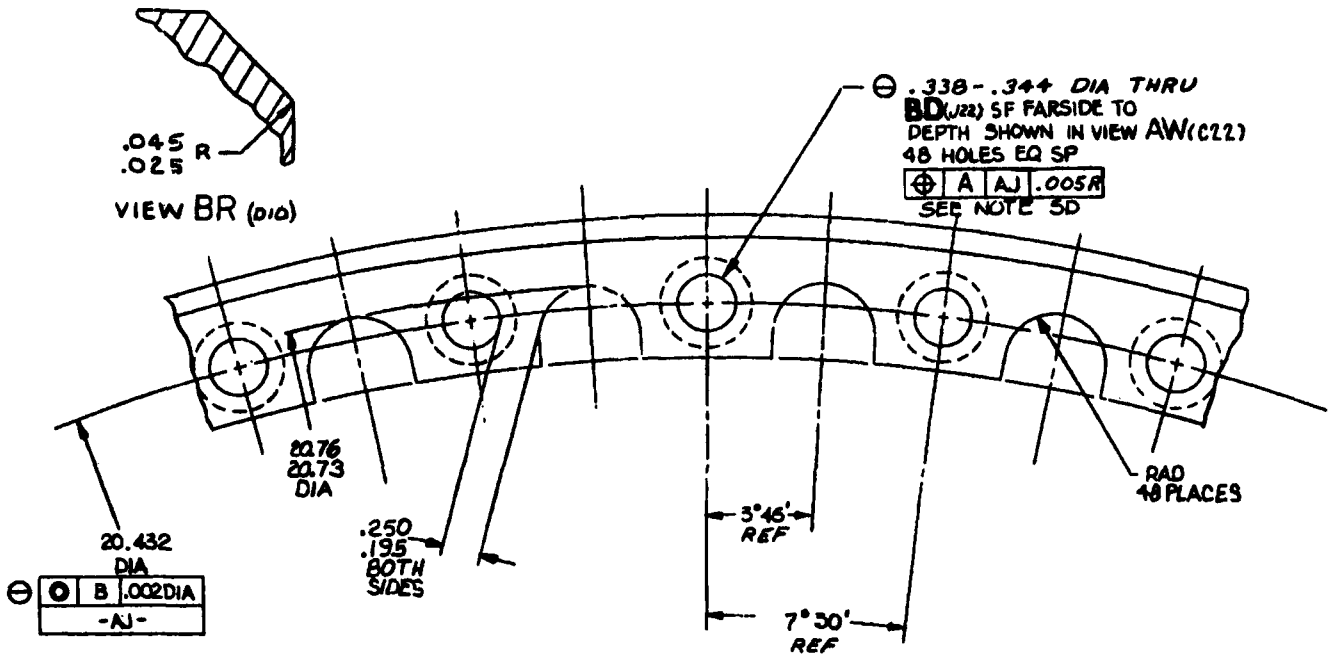

UNDIMENSIONED DWG NO	STAGE NO REF	F (J9)	G (J9)	H (J9)	J (J9)	K (C18)		L (D16)		AE (D15)		N (E13)		P (D10)	
						BEFORE COATING	AFTER COATING	BEFORE COATING	AFTER COATING	BEFORE COATING	AFTER COATING	BEFORE COATING	AFTER COATING	BEFORE COATING	AFTER COATING
964SM72	3	—	—	—	—	17.449 17.441	17.475 17.467	—	—	—	—	—	—	—	—
964SM73	4	—	—	—	—	—	—	19.173 19.165	19.199 19.191	—	—	—	—	—	—
964SM74	5	—	—	—	—	—	—	—	—	20.017 20.009	20.043 20.035	—	—	—	—
964SM75	6	—	.7443	—	1.2986	—	—	—	—	—	—	—	—	—	—
964SM75	7	—	.7007	.7327 .7287	1.2111	—	—	—	—	—	—	—	—	—	—
964SM75	8	.6213 .6179	.6493	—	1.1230	—	—	—	—	—	—	21.467 21.459	21.493 21.485	—	—
618E743	9	—	—	—	—	—	—	—	—	—	—	—	—	22.361 22.353	22.387 22.379

Figure 5 CF6-6 High Pressure Compressor 3-9 Spool. *(concluded)*

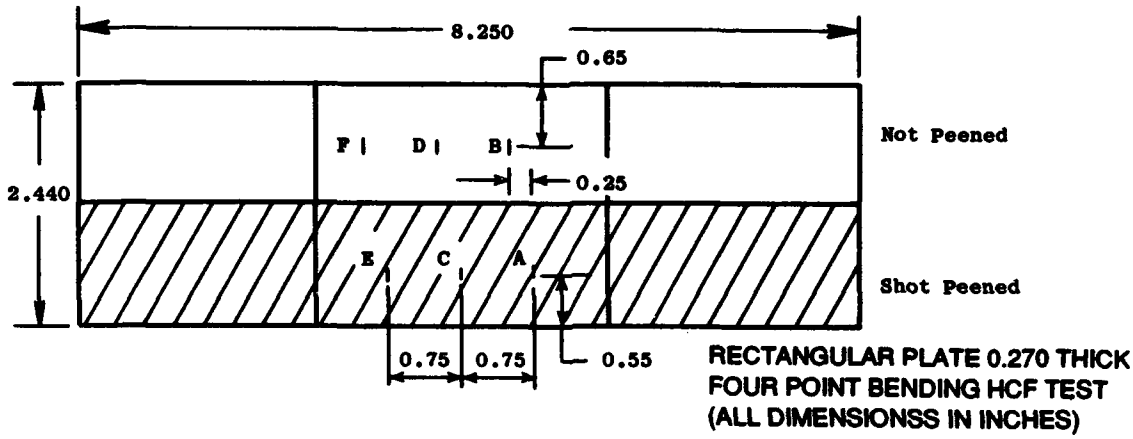

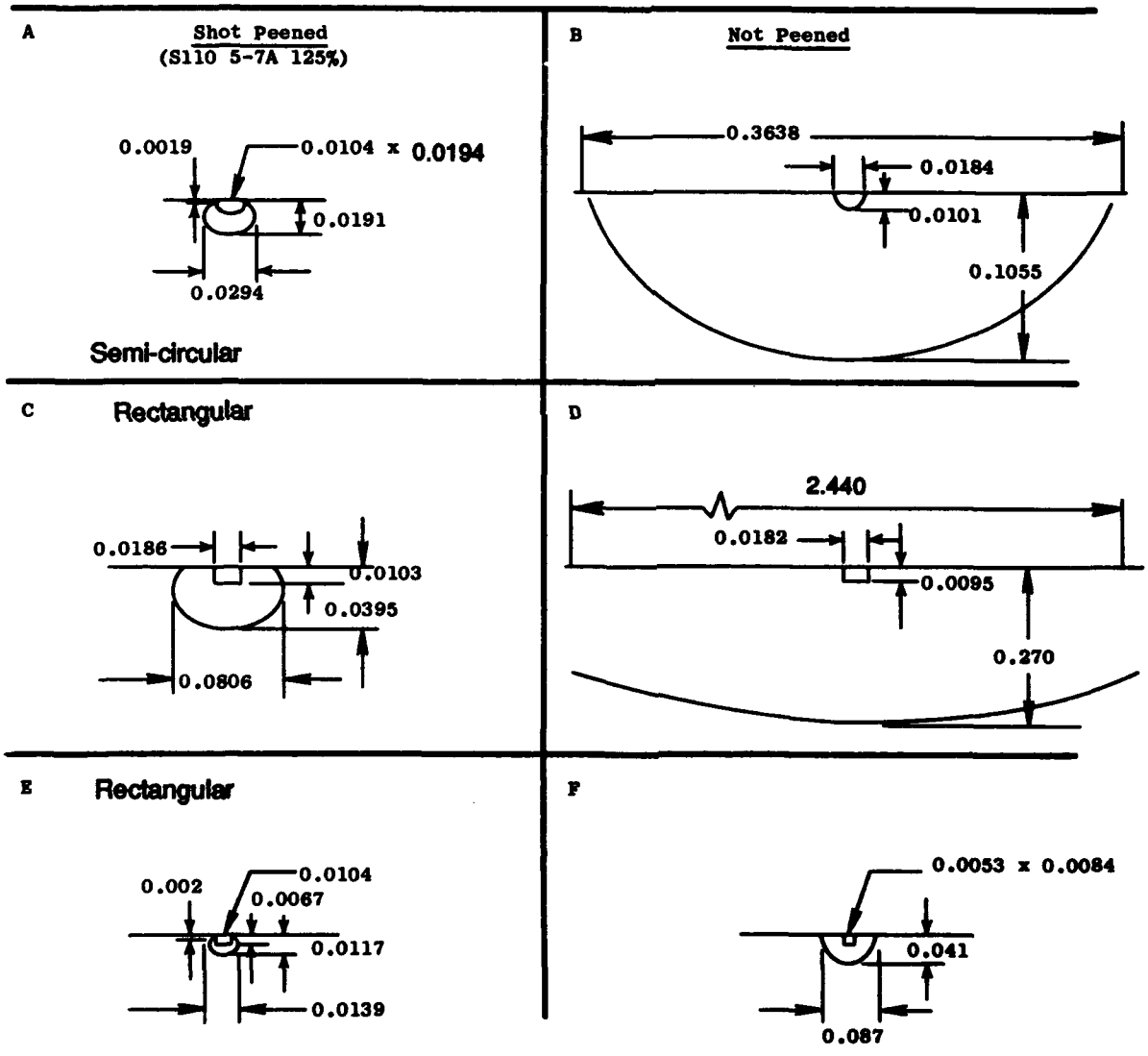

Figure 6 Specimen and schematic results. Ti-6-4 plate shot peening study.

(a) 0.010 x 0.020 Semicircular (10X)
Shot Peened

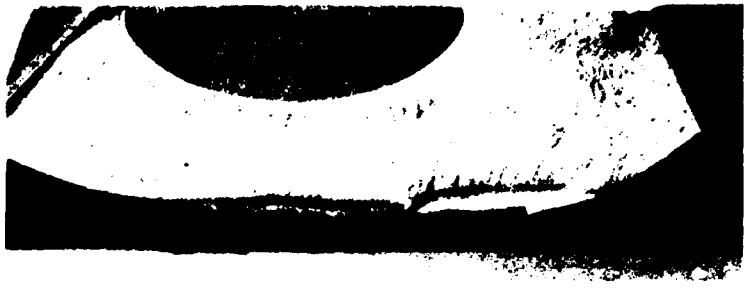

(b) 0.010 x 0.020 Semicircular (5X)
Not Peened

Material: Ti 6-4 Plate
70F (21C), R = 0.03, 30 Hz
Dimensions in inches

(c) 0.010 x 0.020 Rectangular (10X)
Shot Peened

(d) 0.010 x 0.020 Rectangular (10X)
Not Peened

Figure 7 Shot peen plate fracture surface appearance.

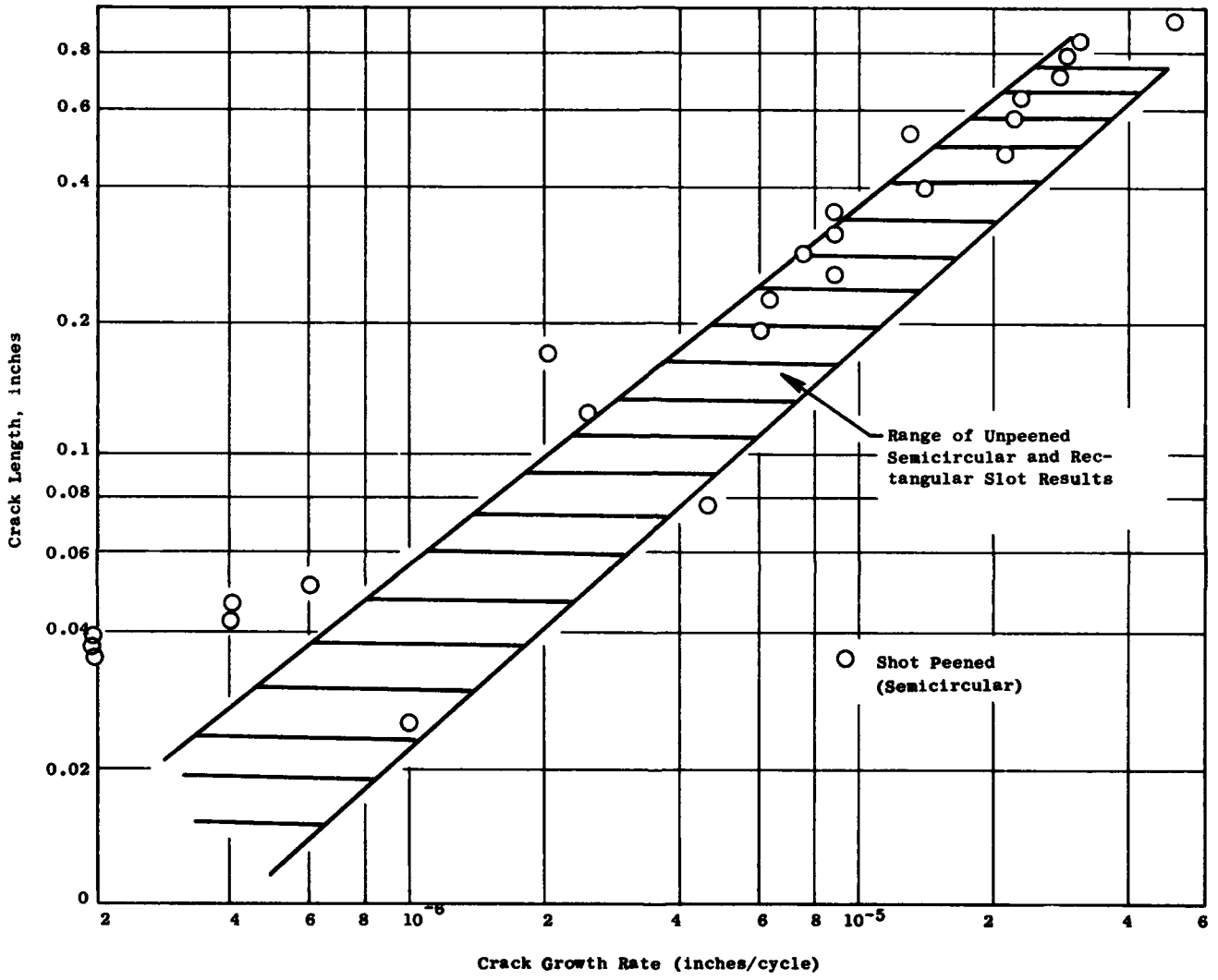

Figure 8 Shot peen plate crack growth rate comparison.

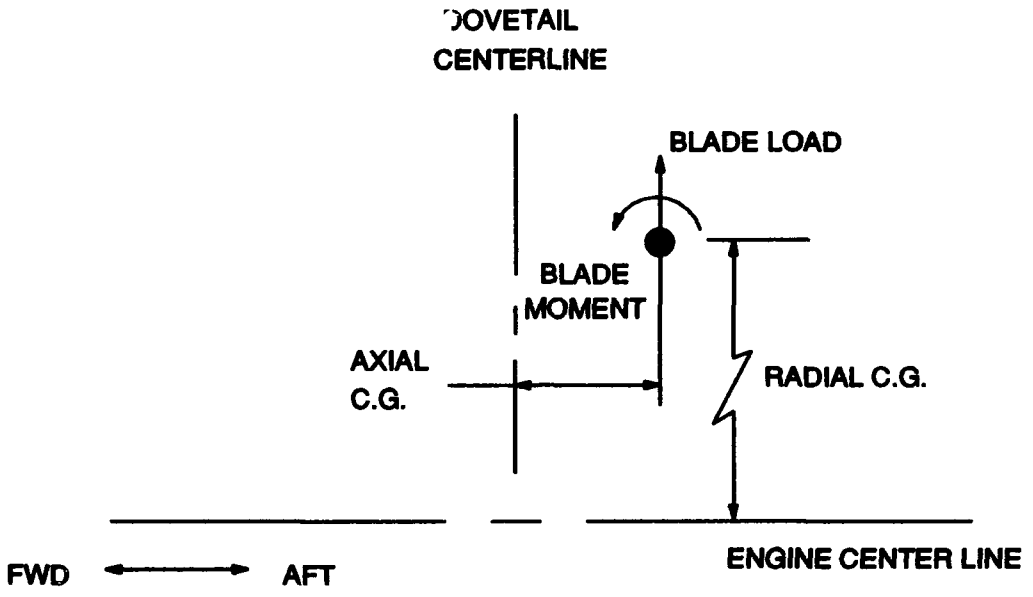

STG NO.	NO. OF BLADES	AVG. WEIGHT PER BLADE (1)		RADIAL C.G.		AXIAL C.G.		SAMPLE CALC. RIM LOAD @ 12500 RPM	
		(GRMS)	(LBS)	(CM)	(INS)	(CM)	(INS)	(GRMS/RAD)	(LBS/RAD)
3	42	92.957	0.2050	24.719	9.732	0.0073	0.0029	2.68E7	59170
4	45	58.544	0.1291	25.852	10.178	0.0549	0.0216	1.89E7	41757
5	48	46.340	0.1022	27.092	10.666	0.9462	0.0373	1.68E7	36945
6	54	28.461	0.0628	27.727	10.916	0.1286	0.0506	1.19E7	26126
7	56	25.588	0.0564	28.250	11.122	0.1365	0.0538	1.13E7	24818
8	64	21.647	0.0477	28.517	11.227	0.1018	0.0401	1.10E7	24222
9	66	17.270	0.0381	29.248	11.515	0.0644	0.0253	9.27E6	20439

(1) Includes weight of blades and lock lugs.

Figure 9 Blade load summary.

Density:	0.161 $lb.in^{-3}$ (4456 $Kg.m^{-3}$)
Modulus of Elasticity (E)	16.4E6 $lb.in^{-2}$ (113.1 GPa)
Shear Modulus (G)	6.17E6 $lb.in^{-2}$ (42.54 GPa)
Poisson's Ratio	0.285

	Average	Minimum*
0.02% Yield Strength	119 Ksi (820 MPa)	99 Ksi (683 MPa)
0.2% Yield Strength	128 Ksi (883 MPa)	105 Ksi (724 MPa)
Ultimate Strength	137 Ksi (945 Mpa)	125 Ksi (862 MPa)
Elongation	12.4 percent	6.2 percent
Reduction of Area	41.9 percent	21.6 percent

(* Minimum is 95% confidence of 99% exceedence)

Coeff. of Thermal Expansion = 4.72 E-6 $in.in^{-1}.F^{-1}$ (8.4E-6 $m.m^{-1}.C^{-1}$

Figure 10 Ti 6-4 material properties at 150F (66C).

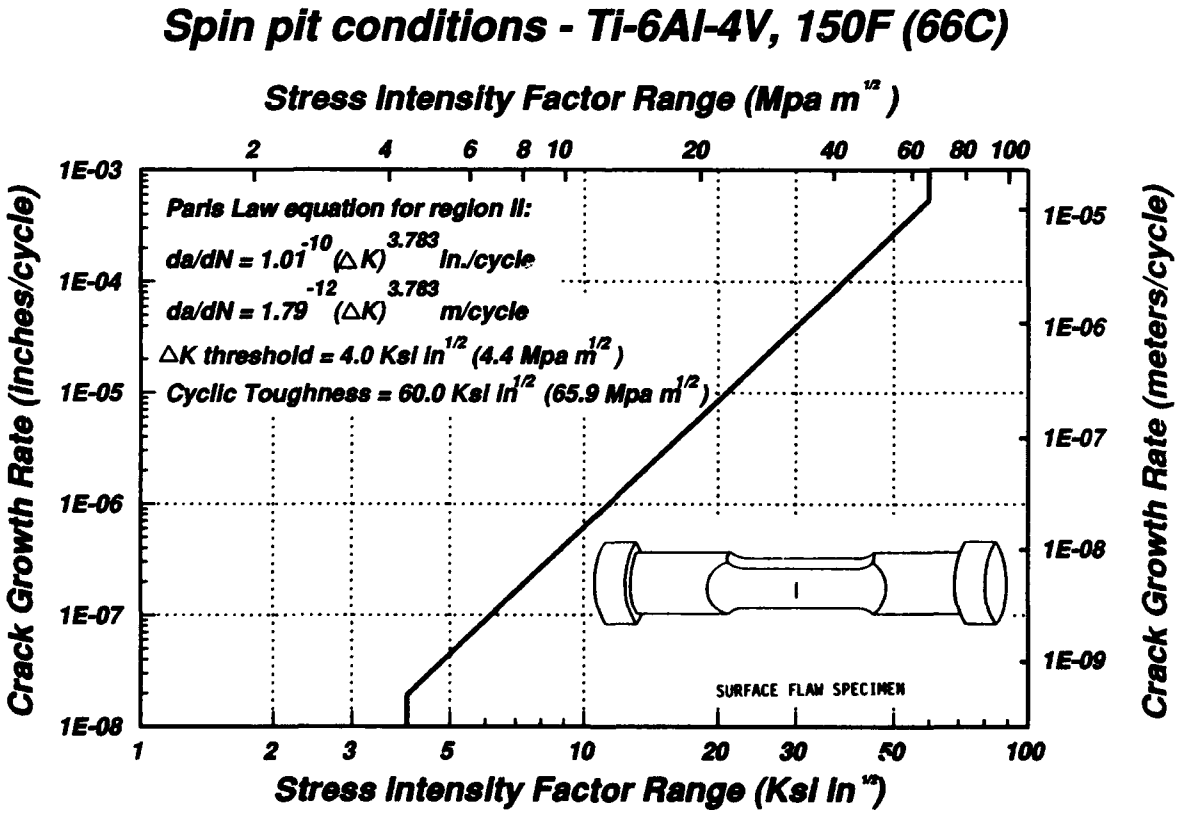

Figure 11 Cyclic crack growth rate data.

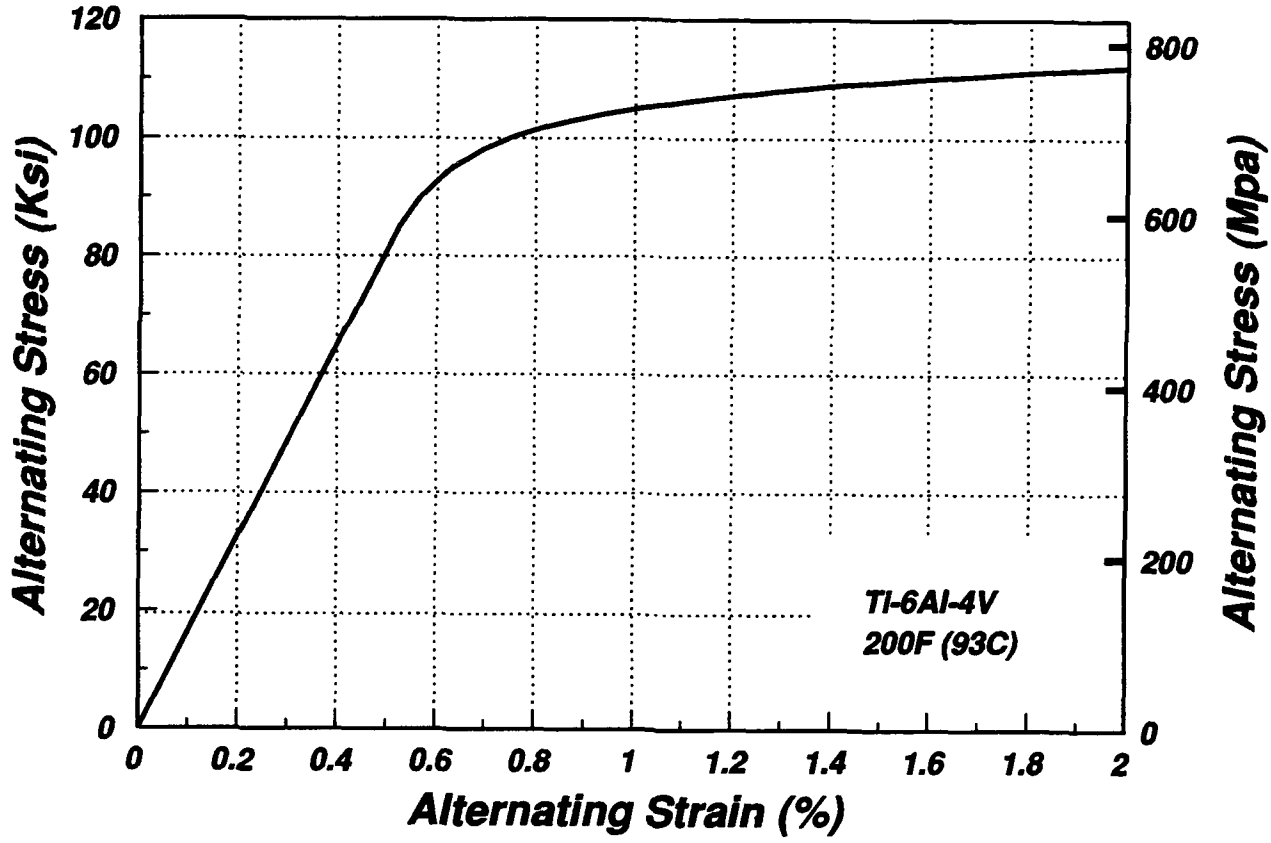

Figure 12 Ti 6-4 Cyclic stress-strain curve (at Nf/2).

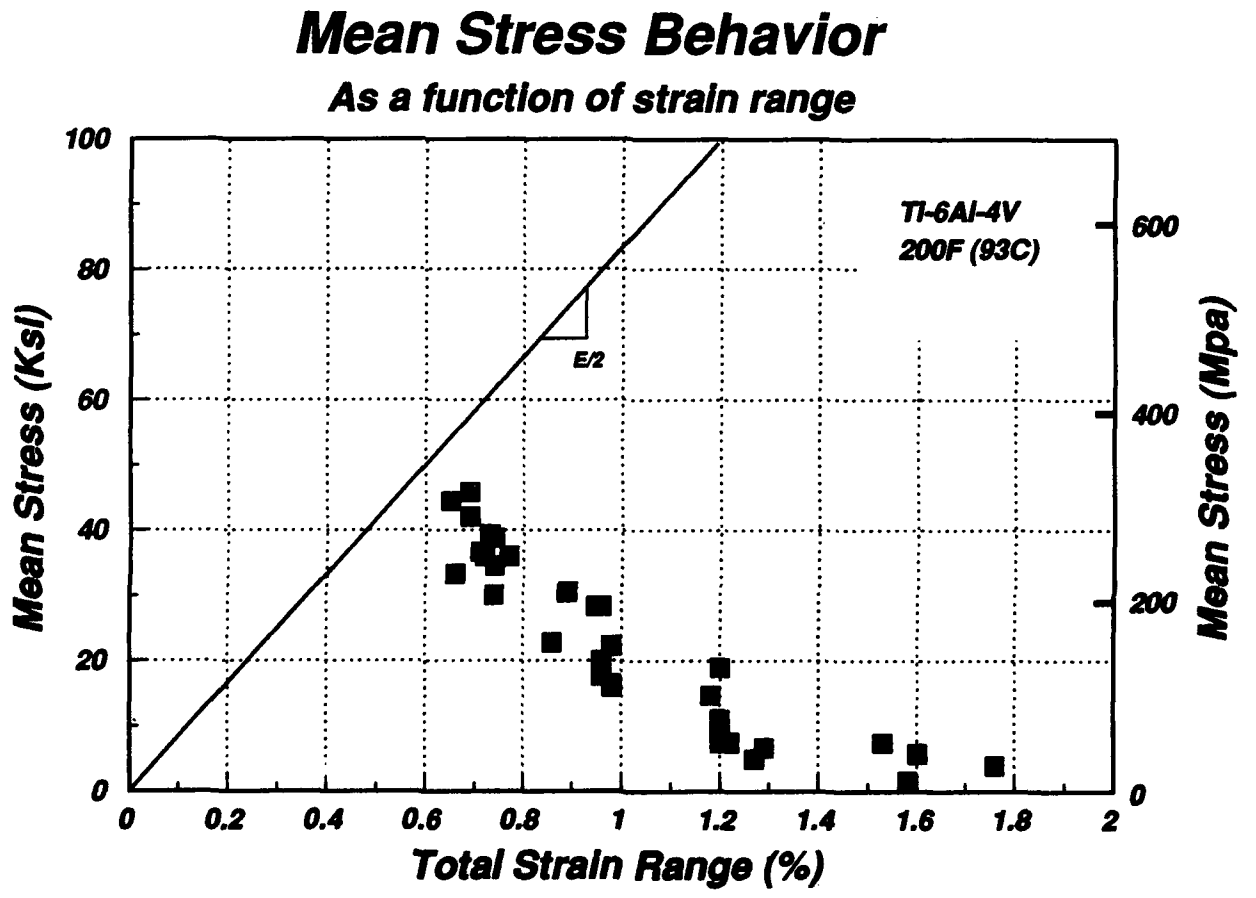

Figure 13 Ti 6-4 Mean stress relaxation versus Total strain range.

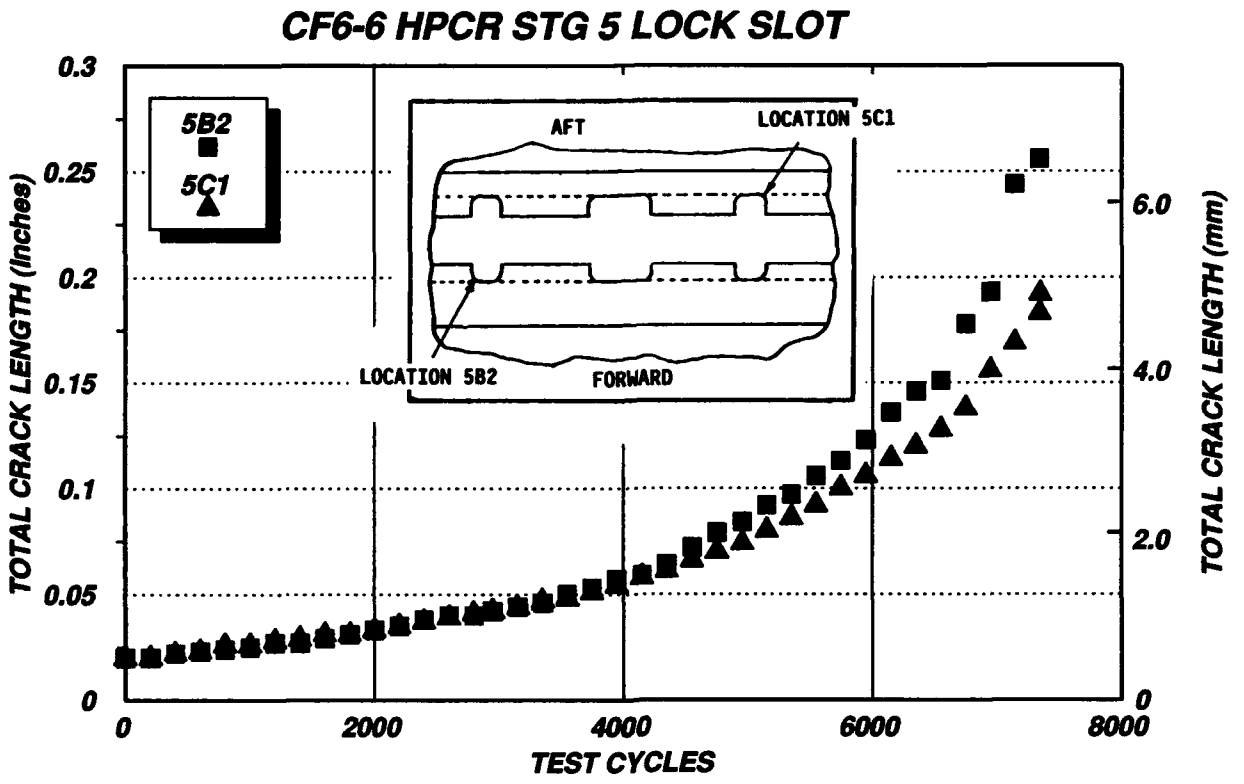

Figure 14 Spin pit crack propagation results.

Cycles	Slot 5B2 Length		Slot 5C1 Length	
	(inches)	(mm)	(inches)	(mm)
0	0.020	0.508	0.020	0.508
200	0.020	0.508	0.020	0.508
400	0.022	0.559	0.022	0.559
600	0.023	0.584	0.023	0.584
800	0.024	0.610	0.026	0.660
1,000	0.025	0.635	0.026	0.660
1,200	0.027	0.686	0.028	0.711
1,400	0.027	0.686	0.029	0.737
1,600	0.029	0.737	0.031	0.787
1,800	0.031	0.787	0.031	0.787
2,000	0.033	0.838	0.033	0.838
2,200	0.035	0.889	0.035	0.889
2,400	0.038	0.965	0.037	0.940
2,600	0.040	1.016	0.039	0.991
2,800	0.040	1.016	0.041	1.041
2,950	0.042	1.067	0.042	1.067
3,150	0.044	1.118	0.044	1.118
3,350	0.046	1.168	0.047	1.194
3,550	0.050	1.270	0.048	1.219
3,750	0.053	1.346	0.051	1.295

Cycles	Slot 5B2 Length		Slot 5C1 Length	
	(inches)	(mm)	(inches)	(mm)
3,950	0.057	1.448	0.054	1.372
4,150	0.059	1.499	0.058	1.473
4,350	0.064	1.626	0.061	1.549
4,550	0.072	1.829	0.066	1.676
4,750	0.079	2.007	0.070	1.778
4,950	0.084	2.134	0.074	1.880
5,150	0.092	2.337	0.080	2.032
5,350	0.097	2.464	0.086	2.184
5,550	0.106	2.692	0.092	2.337
5,750	0.113	2.870	0.100	2.540
5,950	0.123	3.124	0.106	2.692
6,150	0.136	3.454	0.114	2.896
6,350	0.146	3.708	0.120	3.048
6,550	0.151	3.835	0.128	3.251
6,750	0.178	4.521	0.138	3.505
6,950	0.193	4.902	0.156	3.962
7,150	0.244	6.198	0.169	4.293
7,350	0.256	6.502	0.183	4.648
7,355			0.192	4.877

Figure 15 Test crack propagation data.

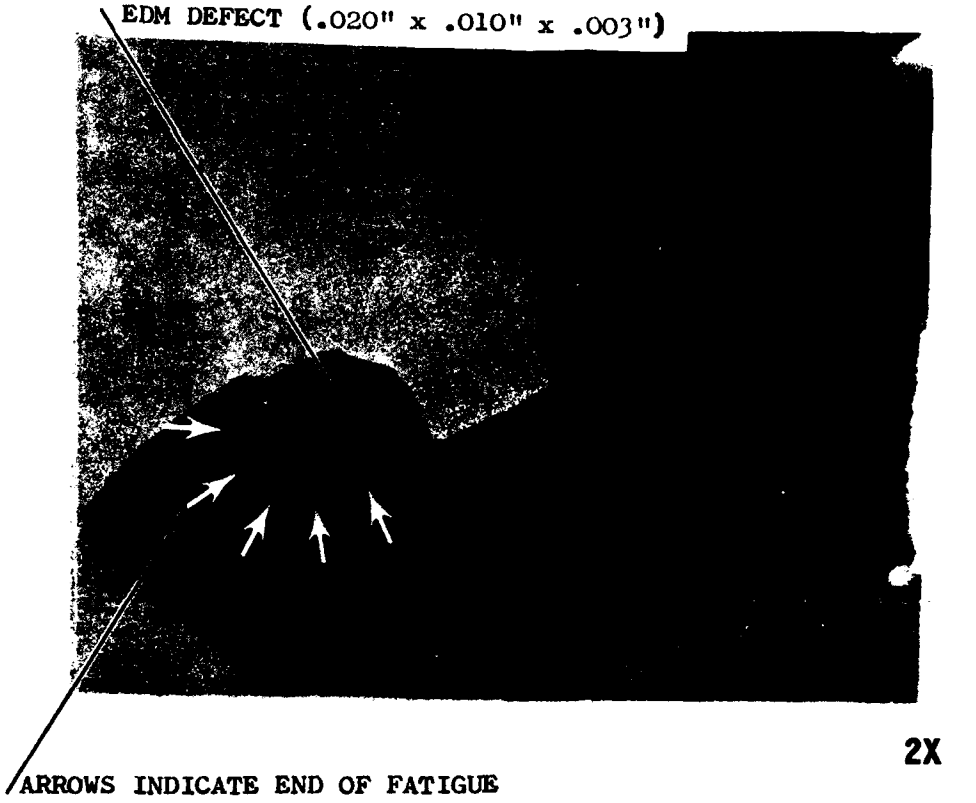

Figure 16 Stage 5 locking slot fracture surface.

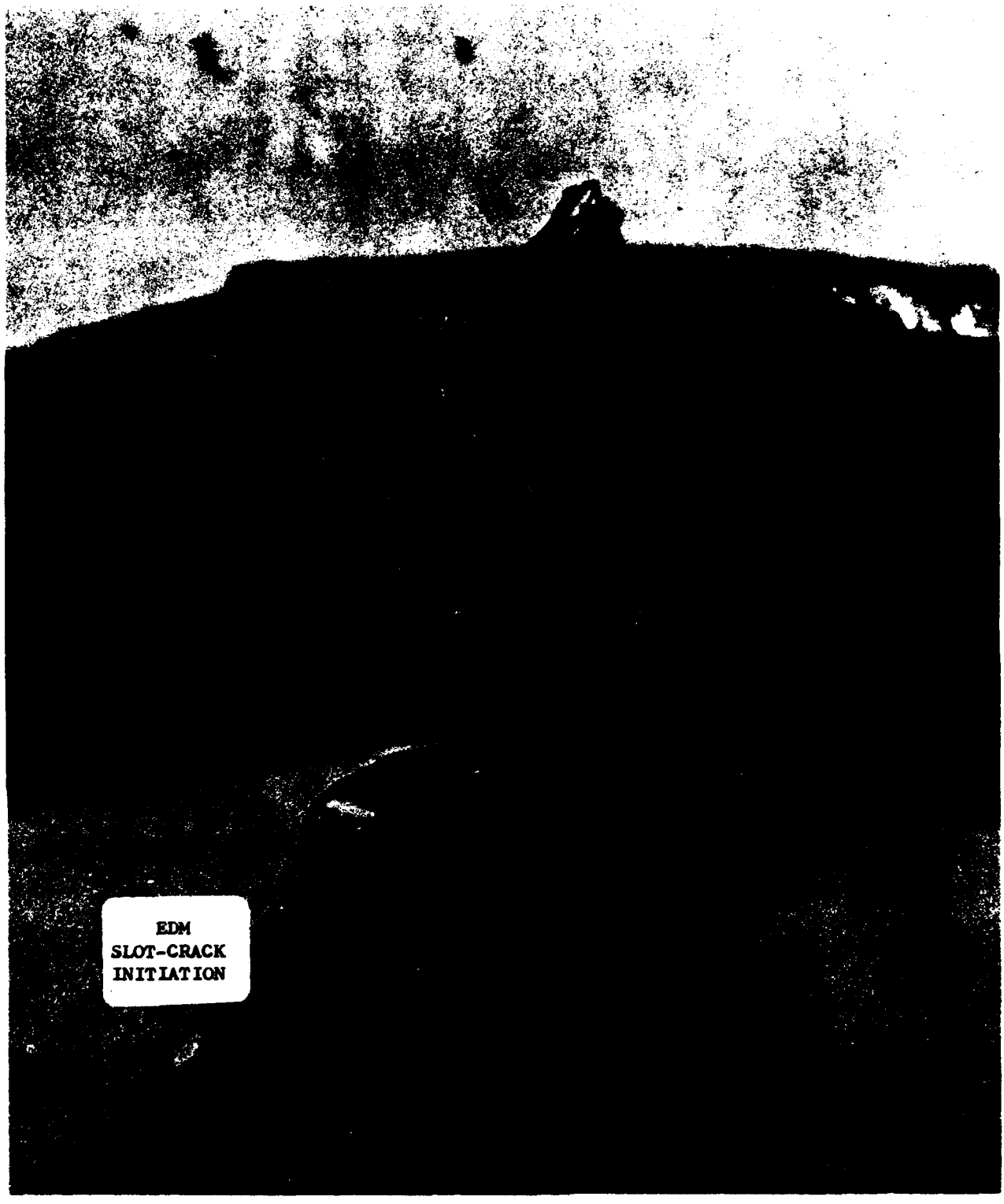

Figure 17 Stage 5 locking slot fracture surface.

CRACK PROPAGATION TEST
FAILURE ANALYSIS

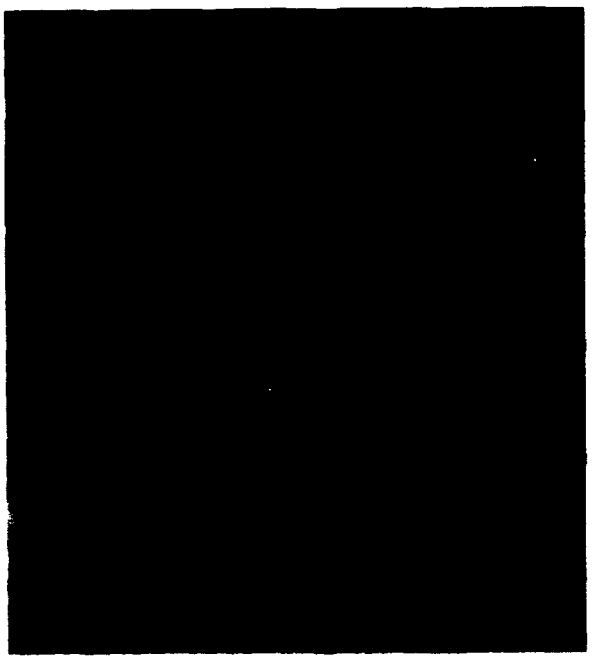

ACETATE REPLICATION OF
EDM SLOT AND CRACK
200X

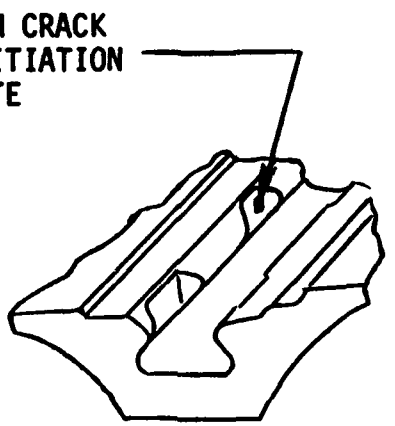

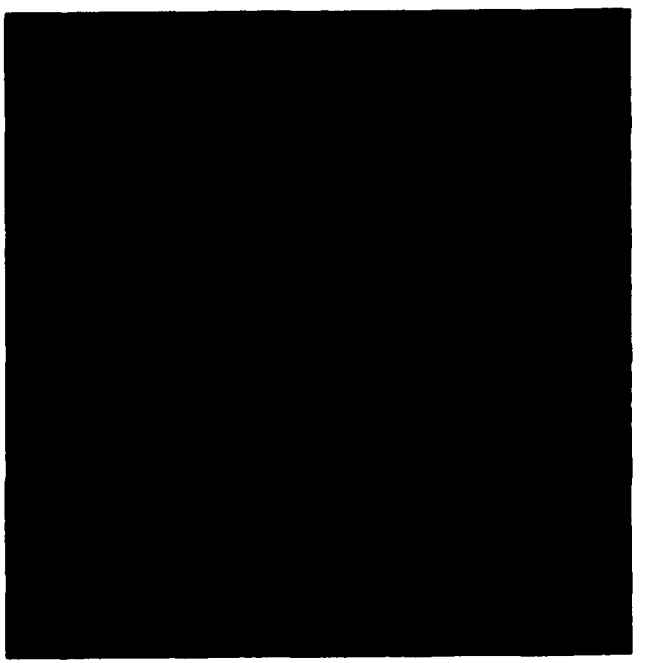

MICROSCOPIC VIEW OF EDM
SLOT AND FRACTURE SURFACE
8X

Figure 18 Crack growth from Stage 5 locking slot.

Chapter 5

RB211-524B DISC AND DRIVE CONES
HOT CYCLIC SPINNING TEST

by

L M Jenkins and S E Crow
Rolls-Royce plc
PO Box 3
Filton
Bristol
BS12 7QE

1. INTRODUCTION

This data package presents the RB211-524 HPT Disc and Drive Cones as a test case for life assessment. The package is the contribution of Rolls-Royce plc to a set of test cases which will be used by AGARD participants to compare lifing predictive tools. The testing was carried out over the period 10th to 22nd November 1975 to establish stress levels and to model the effect of sub-surface inclusions in a Nickel based superalloy using fracture mechanics analysis techniques. Presented are the details of component dimensions, loads, material properties and general arrangement required to perform a stress analysis.

A linear elastic finite element analysis of the assembly was performed by personnel from the authors' Company. The bolt holes and rim slots were modelled as non-hoop continuous material. The blade loads were modelled as a uniformly distributed pressure loading along the length of the disc slot. The behaviour of the sub-surface inclusion was modelled using linear elastic fracture mechanics. A reasonable prediction of crack growth rate was achieved.

2. COMPONENT GEOMETRY

This section consists of the basic part geometry and includes a general arrangement of the parts and details of each part including dimensions. All units are mm.

The assembly chosen for the exercise was the HPT Disc and Drive Cones of the RB211-524. The parts used in the exercise were a modification of the engine parts in that the Engine Rear Seal Panel was replaced by a Bolt Trap Ring.
See Figures 1-22.

3. PART PROCESSING INFORMATION

Included in this section is the general machining and processing information and any other information relating to surface enhancements.

DETAILS OF TEST DISC

Material	-	Waspaloy
No. of remelts	-	2 (Triple melt) (VIM/DEVR)
Forging Process	-	Extruded
Quench Medium	-	Oil
Manufacturer	-	Rolls-Royce Barnoldswick and Derby

HEAT TREATMENT

The specification heat treatment for Waspaloy material is as follows :

4 hours at 995°C to 1035°C, oil quench
4 hours at 850°C, air cool
16 hours at 760°C, air cool

MACHINING DETAILS

The alloy from which the disc was produced is susceptible to high straining of the surface layers in varying degrees during machining. Adverse machining conditions can produce high strains, and in some cases these can lead to surface cracking.

Because of these restrictions, all machined surfaces must be generated by single point tools of specified maximum radius, with the final cut restricted to 0.13 mm minimum. Broaching, grinding, boring and honing operations, however, are planned to remove metal in cuts of less than 0.13 mm, and these restrictions do not then apply.

The disc component used in this exercise was produced under the above restrictions, with a max tool radius of 3.0 mm, a machining speed of 0.4 m/sec, and a feed of 0.2 mm per revolution, to a surface finish of 0.05 mm.

After machining the disc was vapour blasted as shown in Figure 23.

4. OPERATING CONDITIONS

This section presents the test schedule.

TEST PROGRAMME

The required temperature for the test was 500°C. A radial load was applied by the use of dummy blade weights rather than engine blades.

Test speeds were 500 - 12000 - 500 rpm.

A drawing of the test arrangement including instrumentation is shown in Figure 24.

DESCRIPTION OF TEST

1. On receipt of the major engine components from the pre-test laboratory inspection they were assembled with the remaining engine and rig parts, dummy blades being fitted to the disc.

2. A dynamic balance was carried out at each stage of assembly, final dynamic balance being carried out in the planes of the Rig Drive Adaptor and the Engine Disc by adding weights to the former and by blade manipulation in the latter.

3. With the test assembly in position on the flexible drive shaft of the vertical cyclic spinning facility, rigging of the test equipment commenced.

4. A framework was built around the test assembly, off which were mounted banks of 1 KW domestic firebars, and thermocouples for measuring proximity temperatures.

5. Actual temperatures of the test disc and associated engine components were measured using Retractable Contact Thermocouples (RCT), reading out through a pen recorder.

6. The completed test assembly was then shrouded and lagged to form an oven.

7. With the test assembly in position the test chamber was evacuated to a pressure of 25 mm Hg absolute, the rig started, heaters switched on, and the assembly soaked for 3.5 hours at 9600 rpm.

8. Actual disc temperatures were obtained by carrying out RCT temperature checks, analysing the pen recorder charts and applying known temperature factors. Temperatures were then raised or lowered until the correct temperature for the test assembly had been obtained. Actual RCT temperatures were then correlated to proximity thermocouple temperatures and these then used to monitor disc temperatures throughout the test.

9. When test conditions were satisfactory the assembly was cycled over a speed range of 500 - 12000 - 500 rpm. The cycle included a dwell time of 5 seconds at maximum rpm, and the time for a cycle was 154 seconds.

10. On completion of the test the assembly was stripped and the major components subjected to a laboratory inspection as follows :

Penetrant	- all over
Binocular	- all over
Ultrasonic (disc only)	- Bore Cob
Eddy current (disc only)	- Bore Cob and Diaphragm

DETAILS OF DRIVE

The test assembly was driven by a 500 hp motor through a primary gearbox, a bevel gearbox and a secondary gearbox. The max motor speed is 2100 rpm, and the max speed of the output shaft from the secondary gearbox is 29970 rpm. The secondary gearbox drives a shaft 3 ft. long x 1 3/4" diam through two bearings and a damper. The shaft is flared up to a 5.8" diam spigot to which is bolted a backing plate and then the test assembly.

5. BOUNDARY CONDITIONS FOR STRESS ANALYSIS

The dummy blade weight used for the test was 124.85 KN/slot at 12000 rpm. (102 slots).

Residual hoop stresses of -120 MPa in the bore, falling to -60 MPa 30.48 mm into the bore were assumed, based on the measurements from similar discs.

Thermocouple measurements gave temperatures of 501°C at the rim and 494°C at the bore.

6. HEAT TRANSFER INFORMATION

No heat transfer analysis was performed on this test configuration. As stated in the previous section close to isothermal conditions of 500°C were achieved and validated by temperature measurement.

7. MATERIAL DATA

All components were produced in Waspaloy material.

This section contains details of the physical, plastic and elastic properties in addition to the part specific crack propagation data, see Figure 25. The fracture toughness of the material is included in the crack propagation data, although it is not needed as a failure criterion since the disc failed from another feature rather than the embedded defect. It does however form part of the Forman equation used to define the crack growth data.

Part specific mechanical properties obtained from the test ring are also contained in this section.

The specification material properties at 500°C are as follows :

Density	8221 $Kg.m^{-3}$
E	192.8 GPa
Alpha	13.7E-6 C^{-1}
Poisson's Ratio	0.3

UTS	1166.04 MPa typical 1088 MPa minimum spec
Yield strength	830.9 MPa typical 772 MPa minimum spec

The actual properties achieved on the disc material were

UTS	at 20°C	1300 Mpa
	at 535°C	1156 Mpa
0.2% P.S.	at 20°C	892 Mpa
	at 535°C	788 Mpa
Elongation	at 20°C	25%
	at 535°C	20%
Reduction of area		
	at 20°C	27%
	at 535°C	24%

8. OPERATING HISTORY

This section contains the cyclic life achieved, crack inspection data and crack fractography.

The test was halted after 3734 rig cycles. The disc had failed due to LCF cracking at the runout of the bolt hole boss blend radius to the rear face diaphragm. A large bore crack 3.81 mm long and 15.24 mm in from the rear corner when sectioned revealed a crack originating from a non-metallic (alumina) inclusion approximately 1.73 mm x 1.85 mm just below the bore surface; the crack had propagated to a depth of 2.92 mm.

Investigations into the bore defect revealed a -11 dB ultrasonic indication reported by the forging supplier.

The initial defect size was 1.73 mm axially by 1.85 mm radially in the bore surface, and the final crack size was 3.81 mm axially by 2.92 mm radially. The achieved cyclic life was 3734 cycles.

Details of the inclusion and the final fracture surface are shown in Figure 26.

9. SUMMARY

The details of component dimensions, loading, material properties and general arrangement required to perform a stress analysis on the RB211-524 HPT Disc and Drive Cones are presented.

The experimental assembly was modelled using finite element stressing techniques at a temperature of 500°C, with the radial load being applied for the dummy blade weights.

The test was halted after 3734 rig cycles due to LCF cracking at the runout of the bolt hole boss blend radius to the rear face diaphragm of the disc.

DRA ASSESSMENT OF ROLLS-ROYCE RB211-524B WASPALOY DISC TEST CASE

From the information supplied, DRA was able to complete a 2-D axisymmetric elastic stress analysis. After DRA had finished the analyses, Rolls-Royce stress analyses were made available for comparison only since these data are not part of the test case. Predicted stresses were in close agreement, peak stress levels being within 2%.

With respect to life assessment, DRA has carried out a LEFM analysis of the disc using the modified Forman crack growth data supplied. The crack was modelled as a semi-elliptical surface crack. The residual stress data supplied by Rolls-Royce was incorporated into the stress field into which the crack grew. The RAE predicted life is within 25% of the test result.

General arrangement

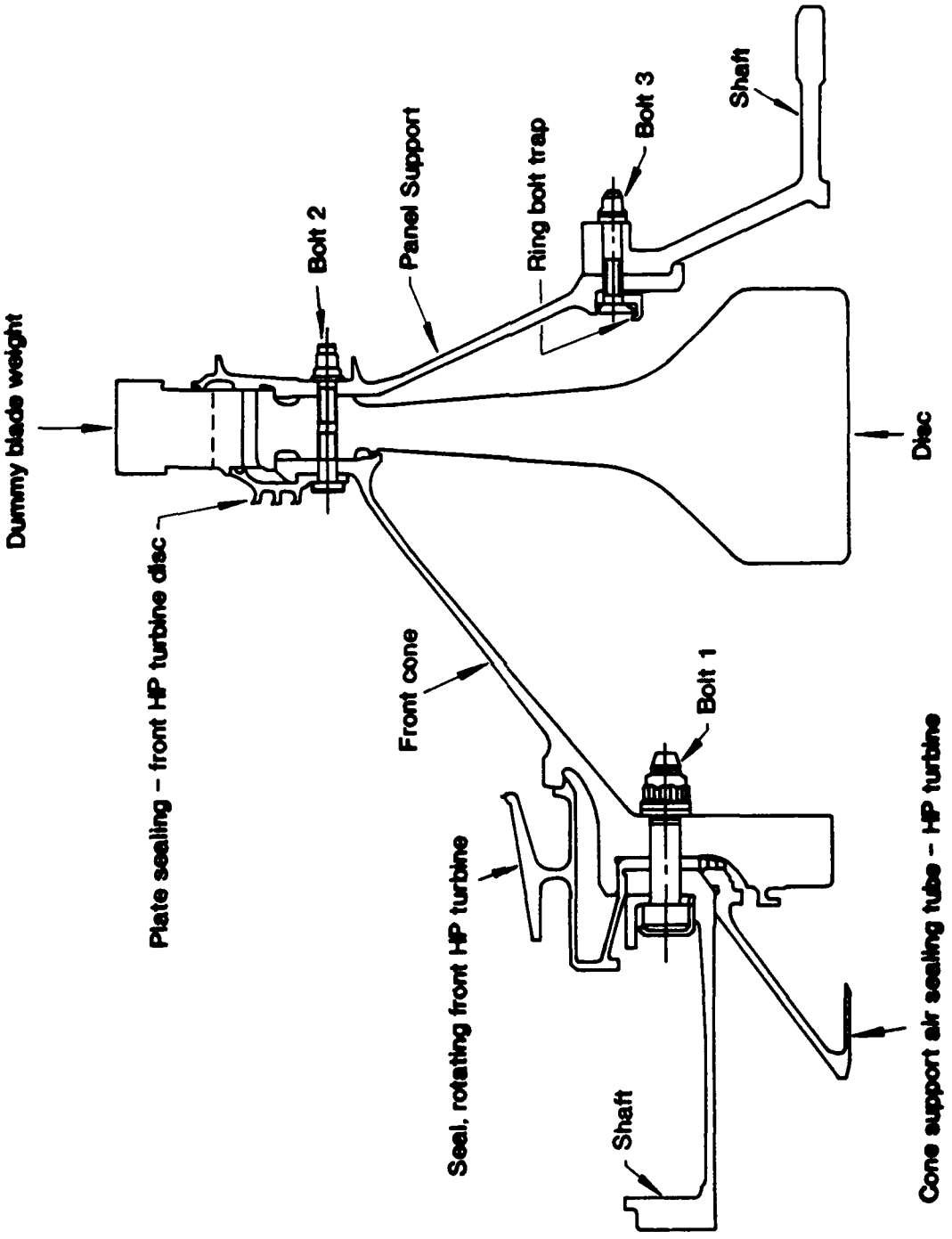

Figure 1

Disc

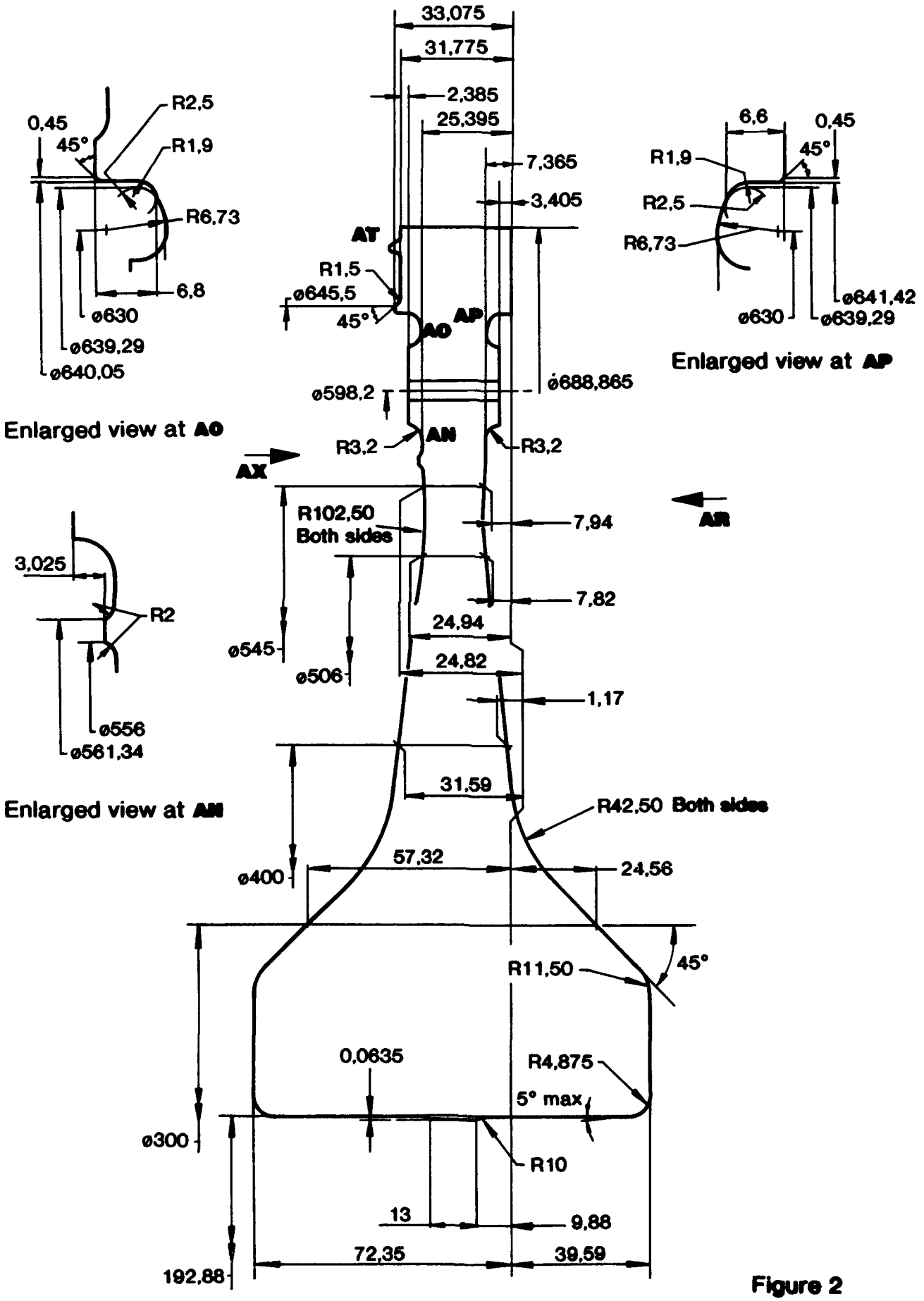

Figure 2

D.sc

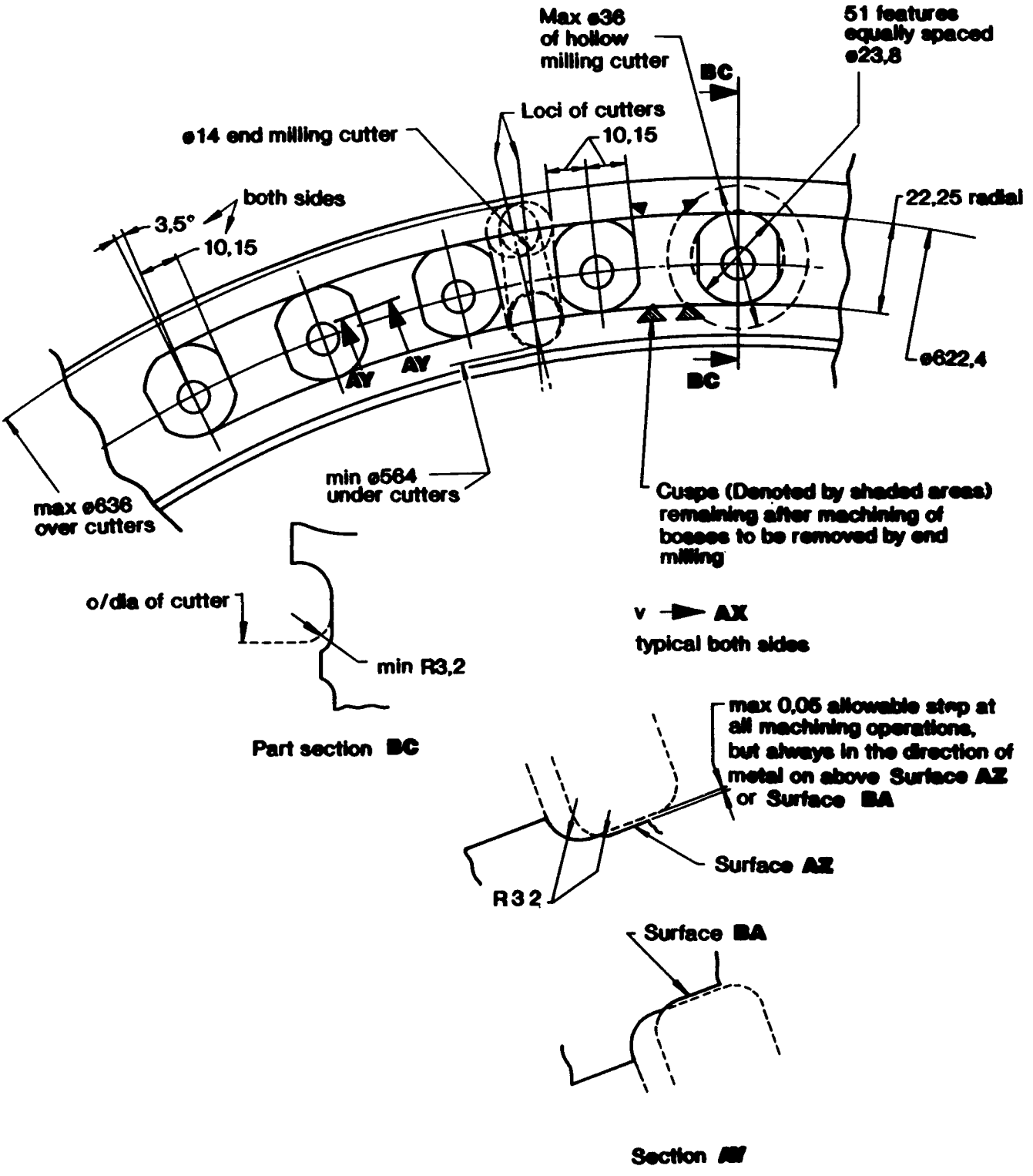
Max ø36
of hollow
milling cutter
51 features
equally spaced
ø23,8
BC
Loci of cutters
10,15
ø14 end milling cutter
both sides
3,5°
10,15
22,25 radial
AY
AY
BC
ø622,4
min ø564
under cutters
max ø636
over cutters
Cusps (Denoted by shaded areas)
remaining after machining of
bosses to be removed by end
milling
o/dia of cutter
min R3,2
v → AX
typical both sides
Part section BC
max 0,05 allowable step at
all machining operations,
but always in the direction of
metal on above Surface AZ
or Surface BA
Surface AZ
R3 2
Surface BA
Section AY

Figure 3

Disc

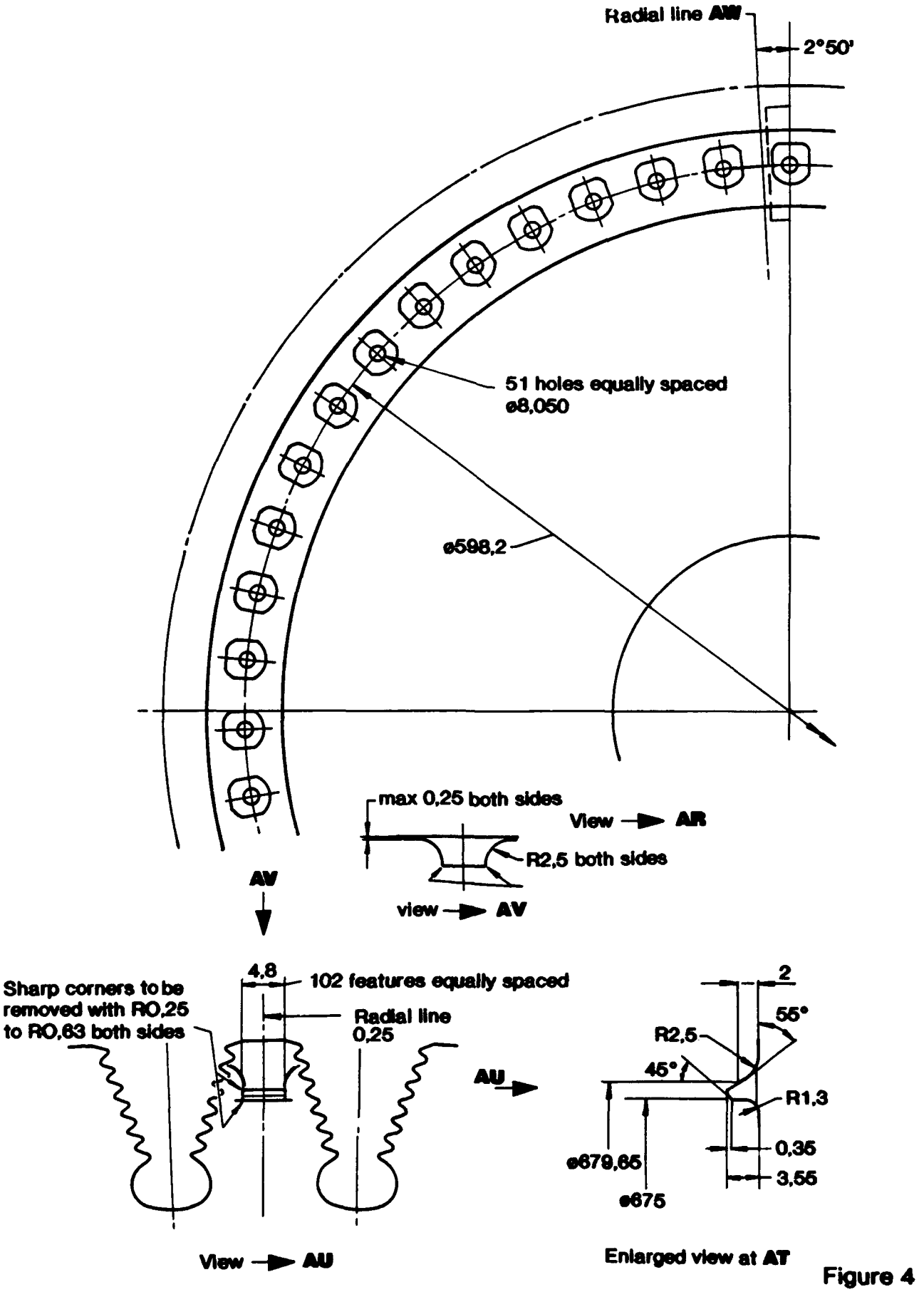

Figure 4

Root slot

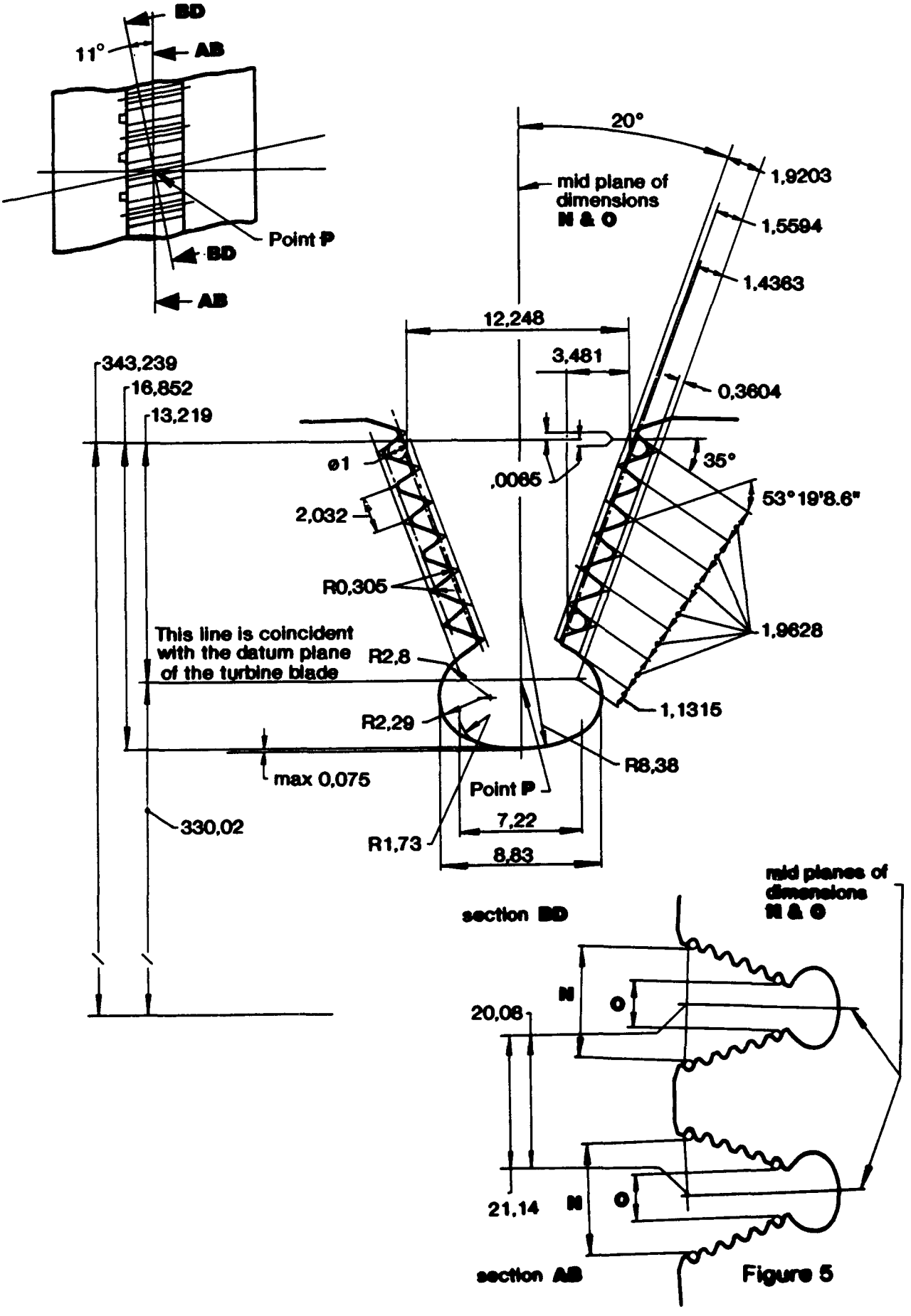

Figure 5

Shaft

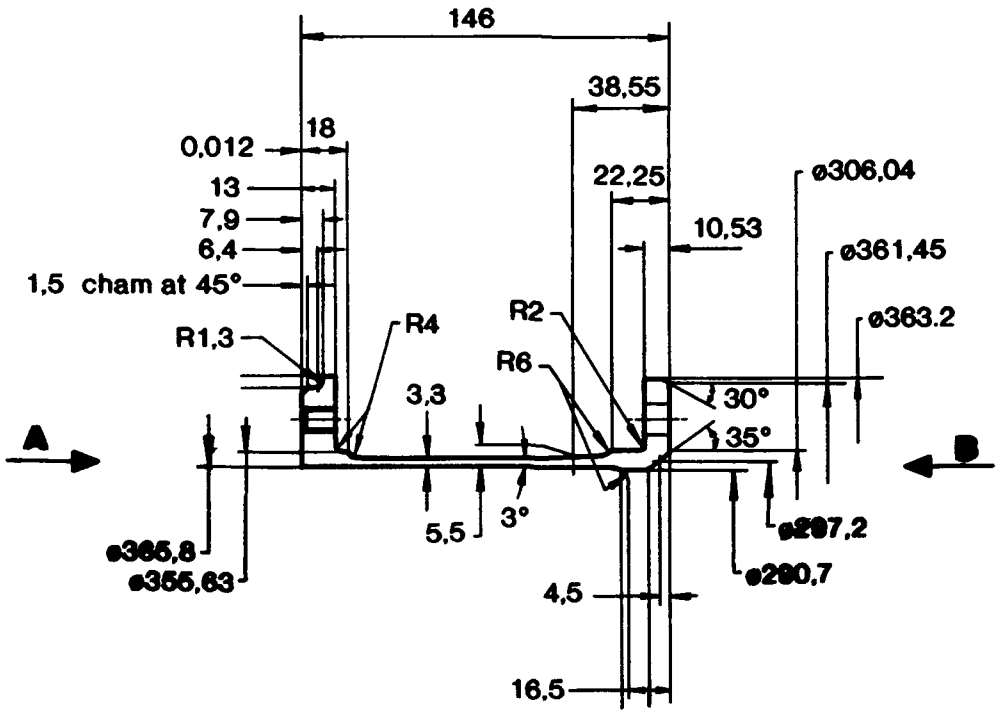

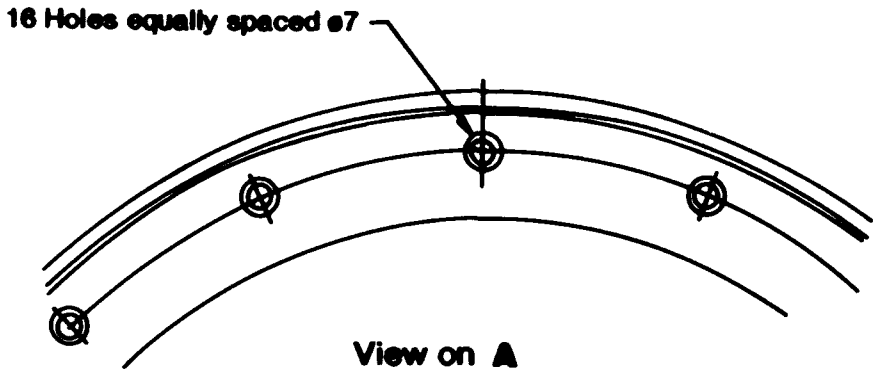

View on **A**

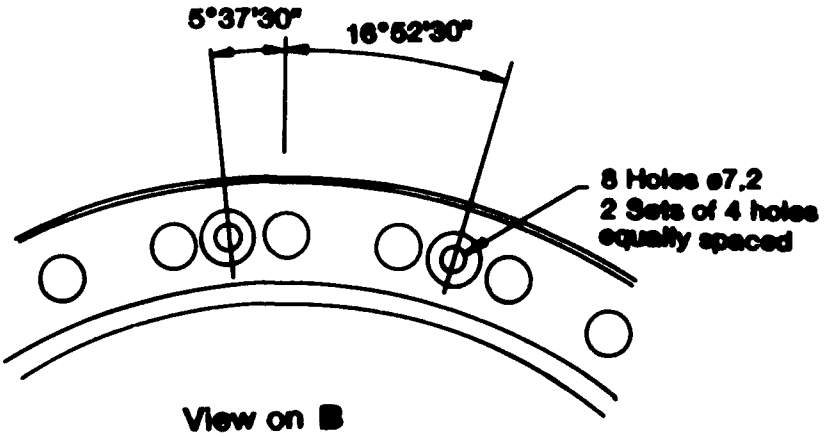

View on **B**

Figure 6

Cone support air sealing tube - HP turbine

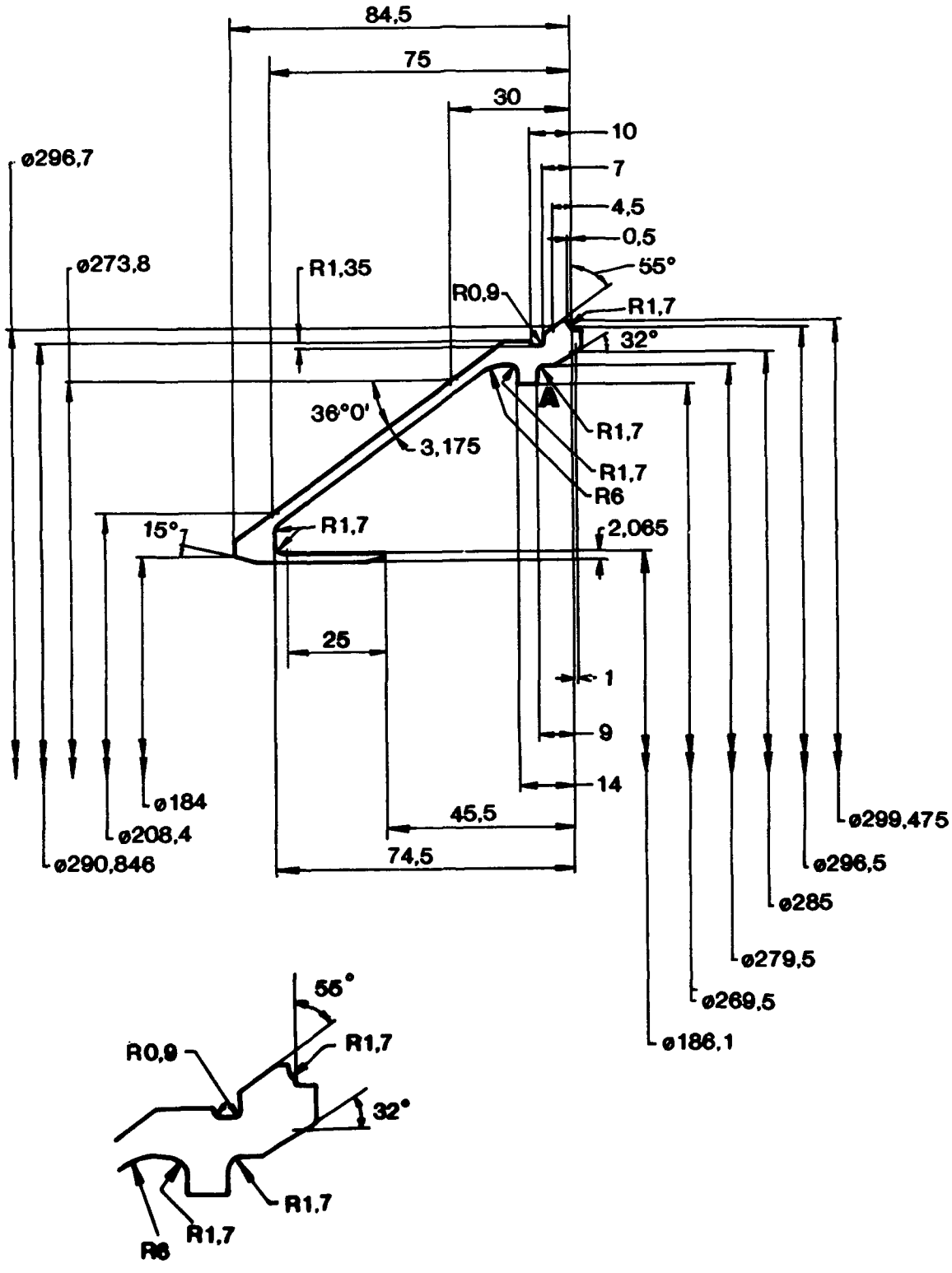

Enlarged view at A

Figure 7

Seal, rotating front HP turbine

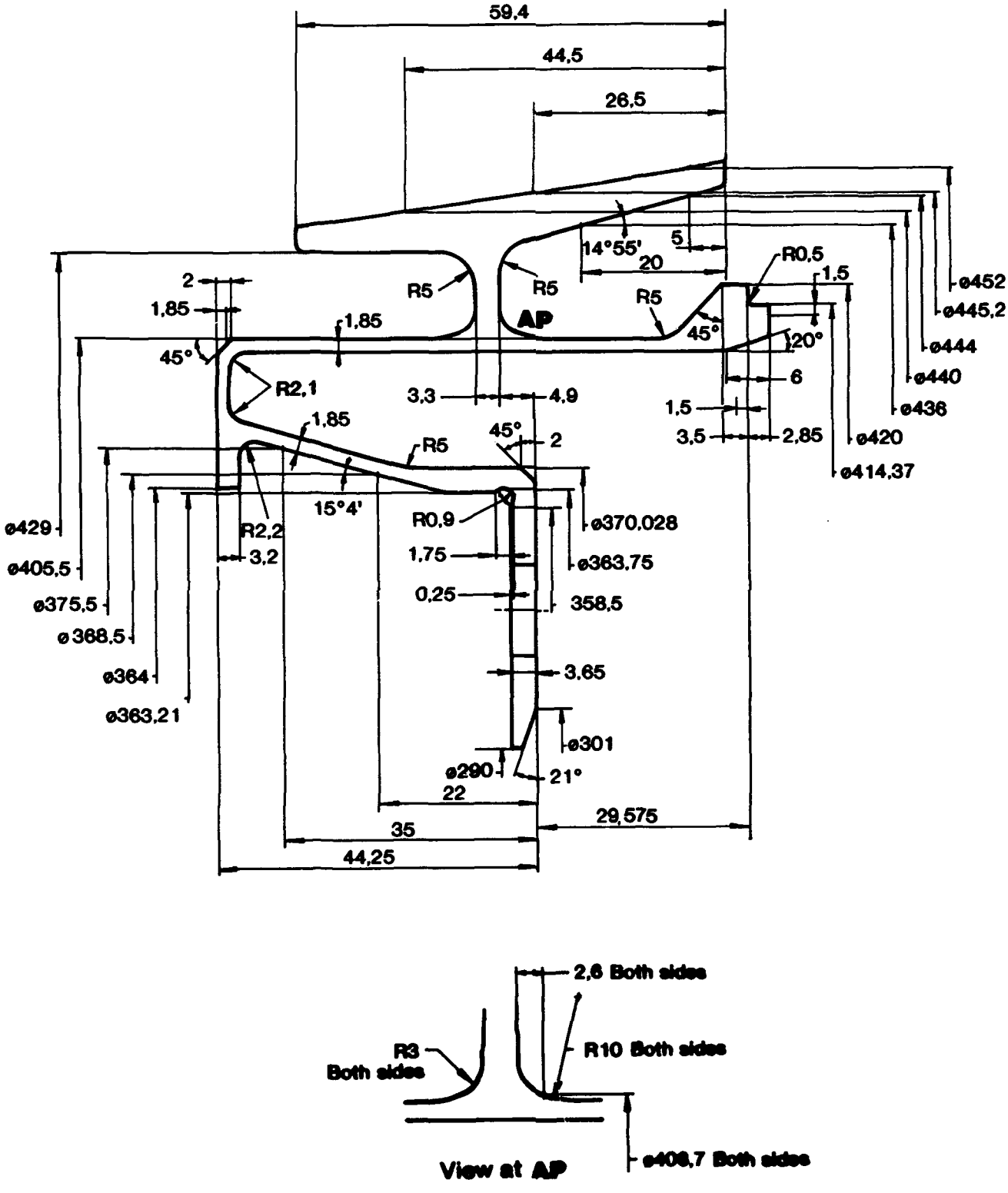

Figure 8

Front cone (Sheet 1 of 3 sheets)

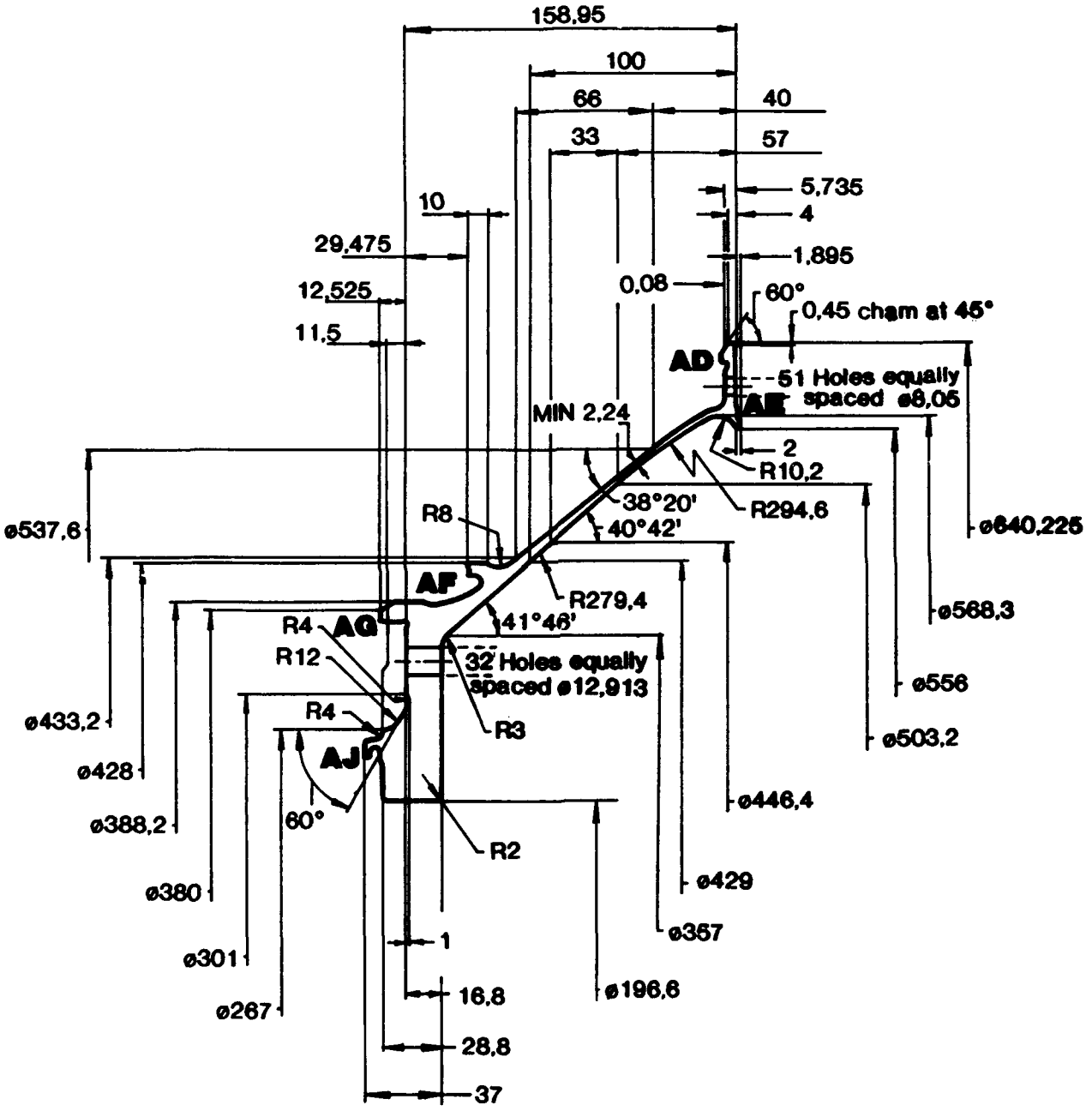

Figure 9

Front cone (Sheet 2 of 3 sheets)

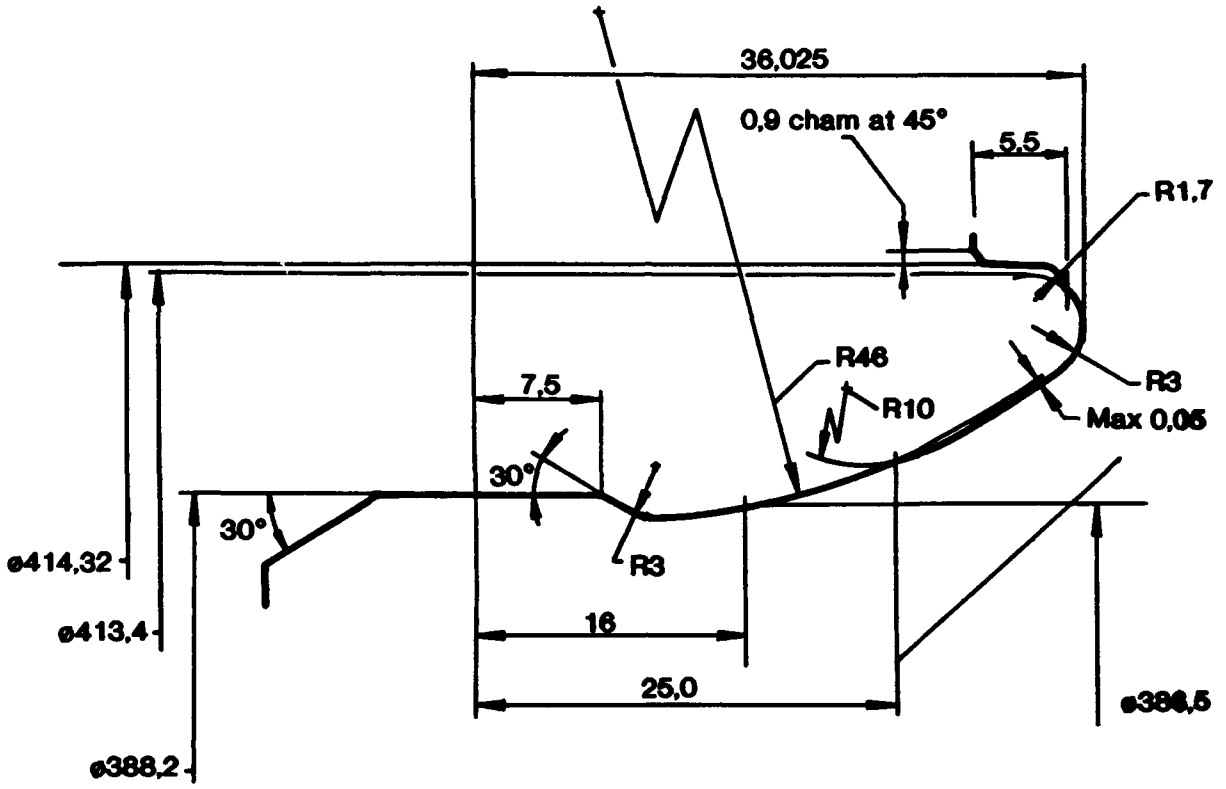

Section AF

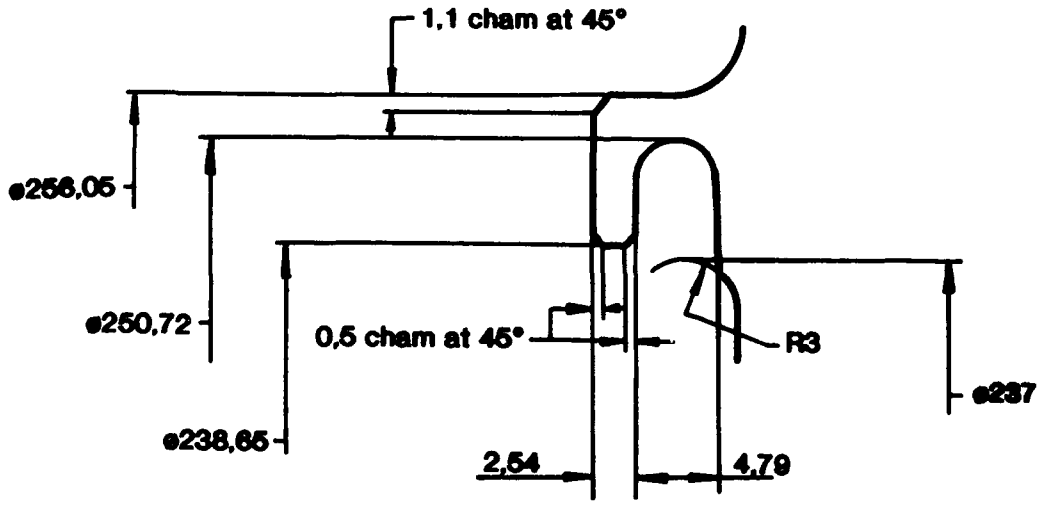

View at AJ

Figure 10

Front cone (Sheet 3 of 3 sheets)

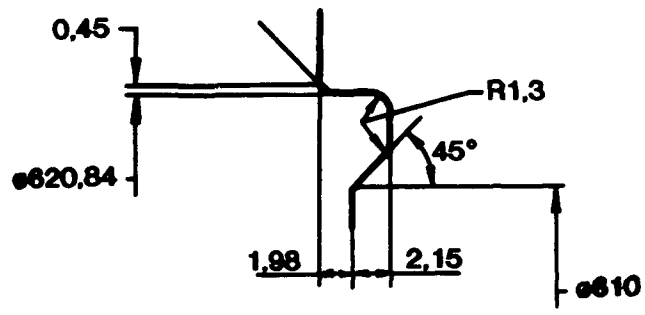

View at **AD**

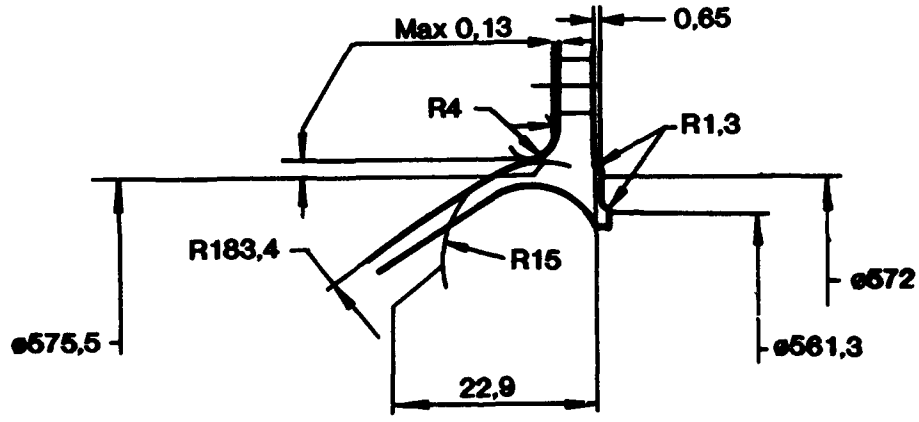

View at **AE**

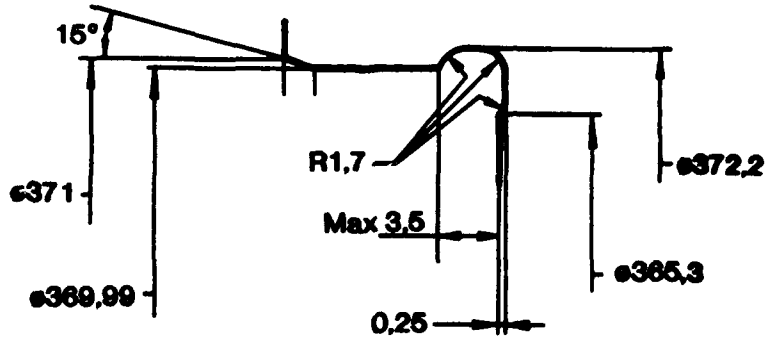

View at **AG**

Figure 11

Plate sealing – front HP turbine disc

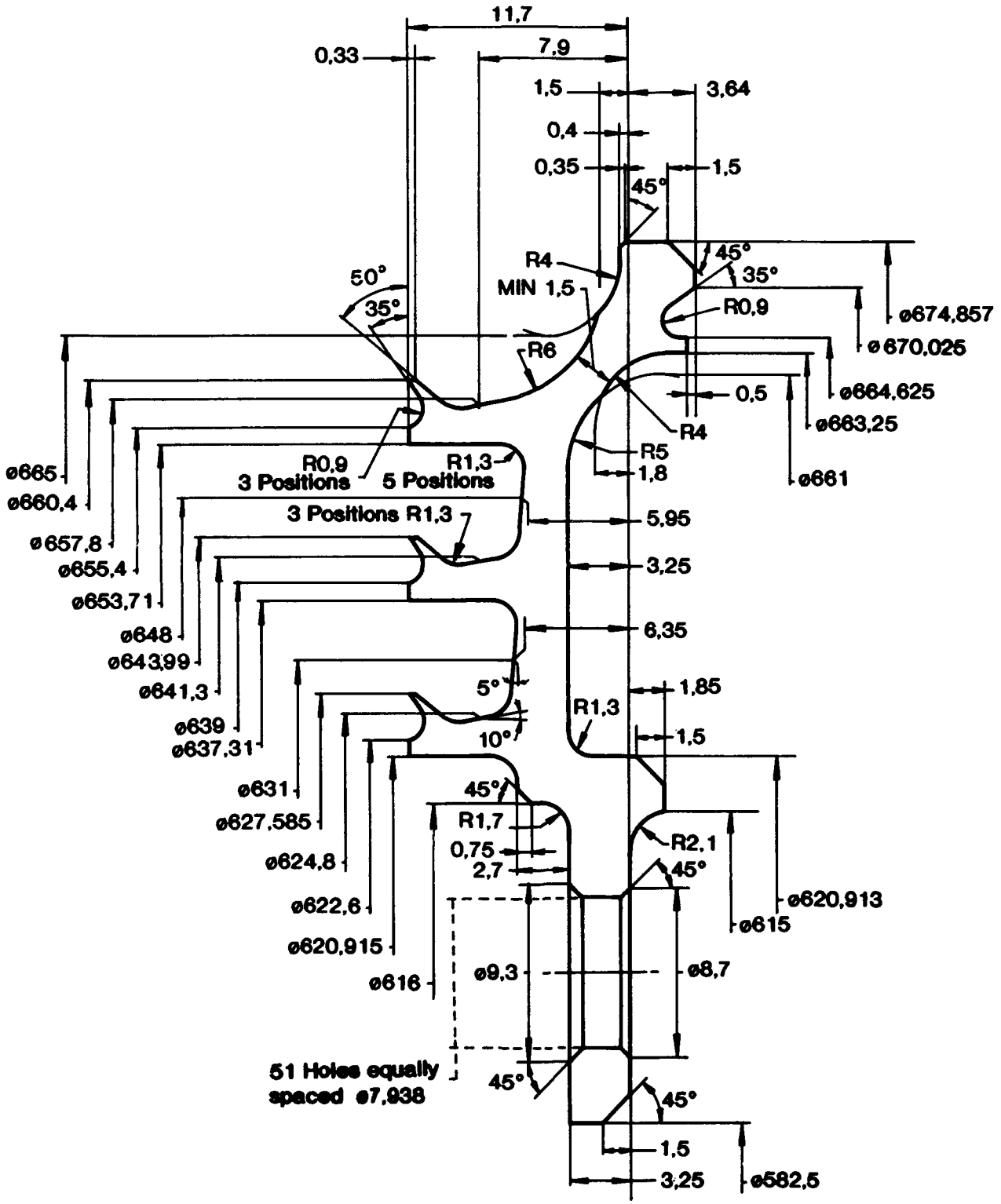

Figure 12

Panel support (Sheet 1)

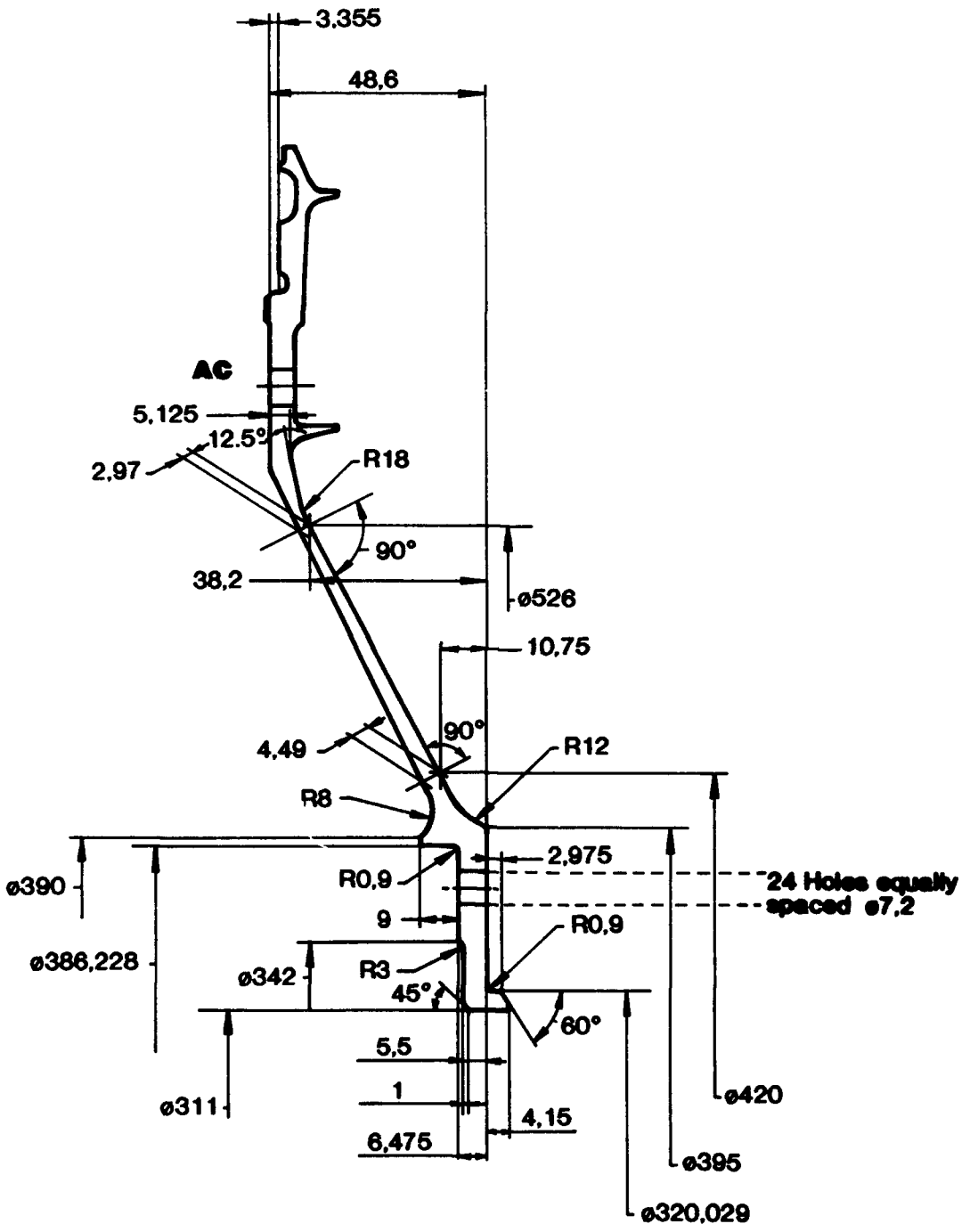

See sheet 2

Figure 13

Panel support (Sheet 2)

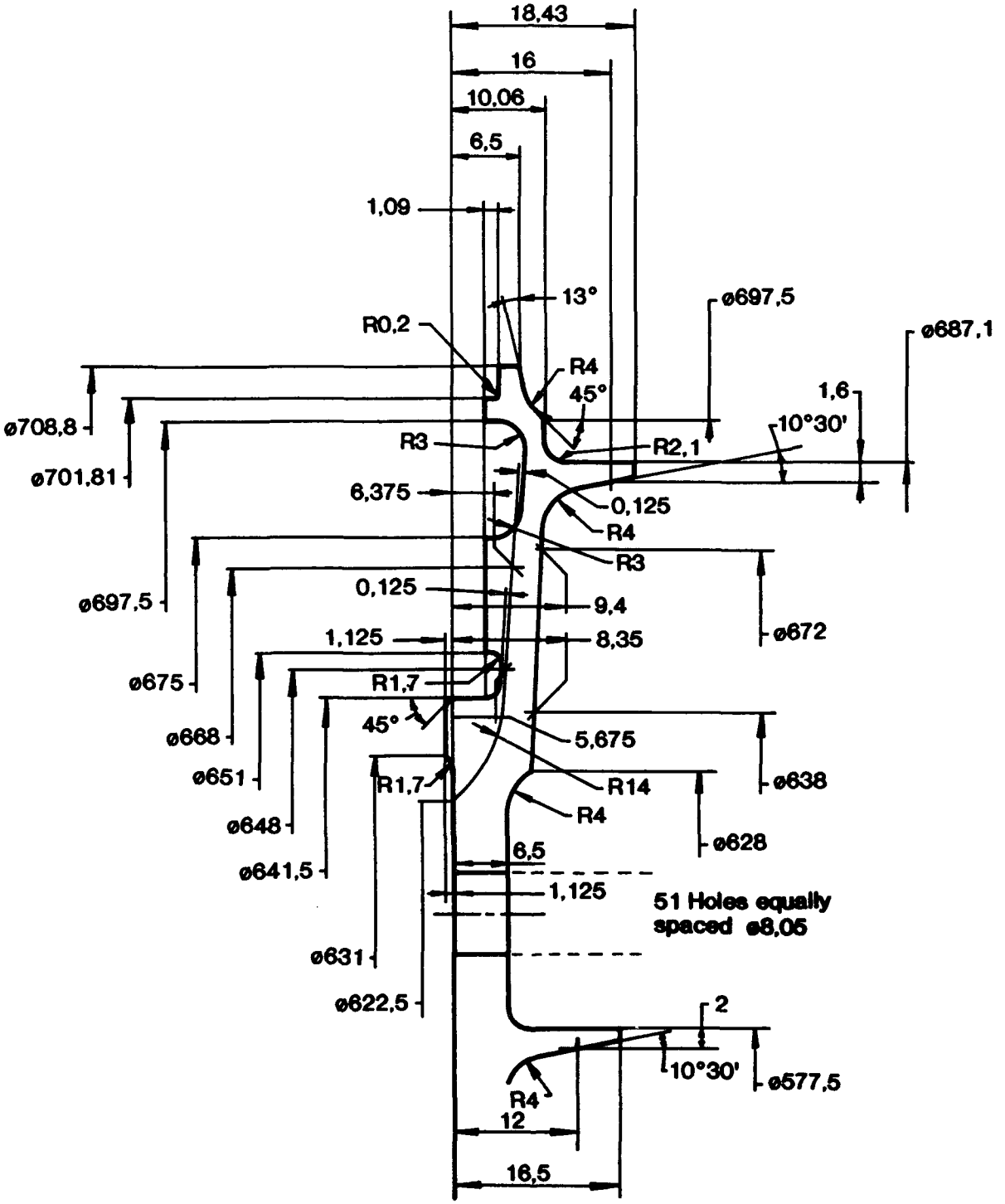

Enlarged view at **AG**

Figure 14

Ring, bolt trap

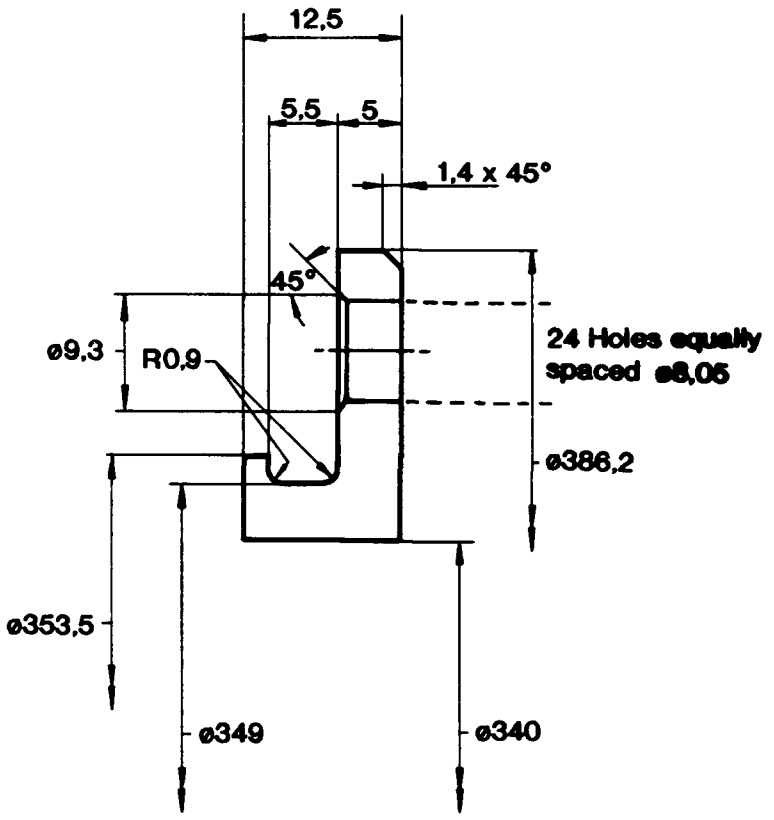

Figure 15

Shaft

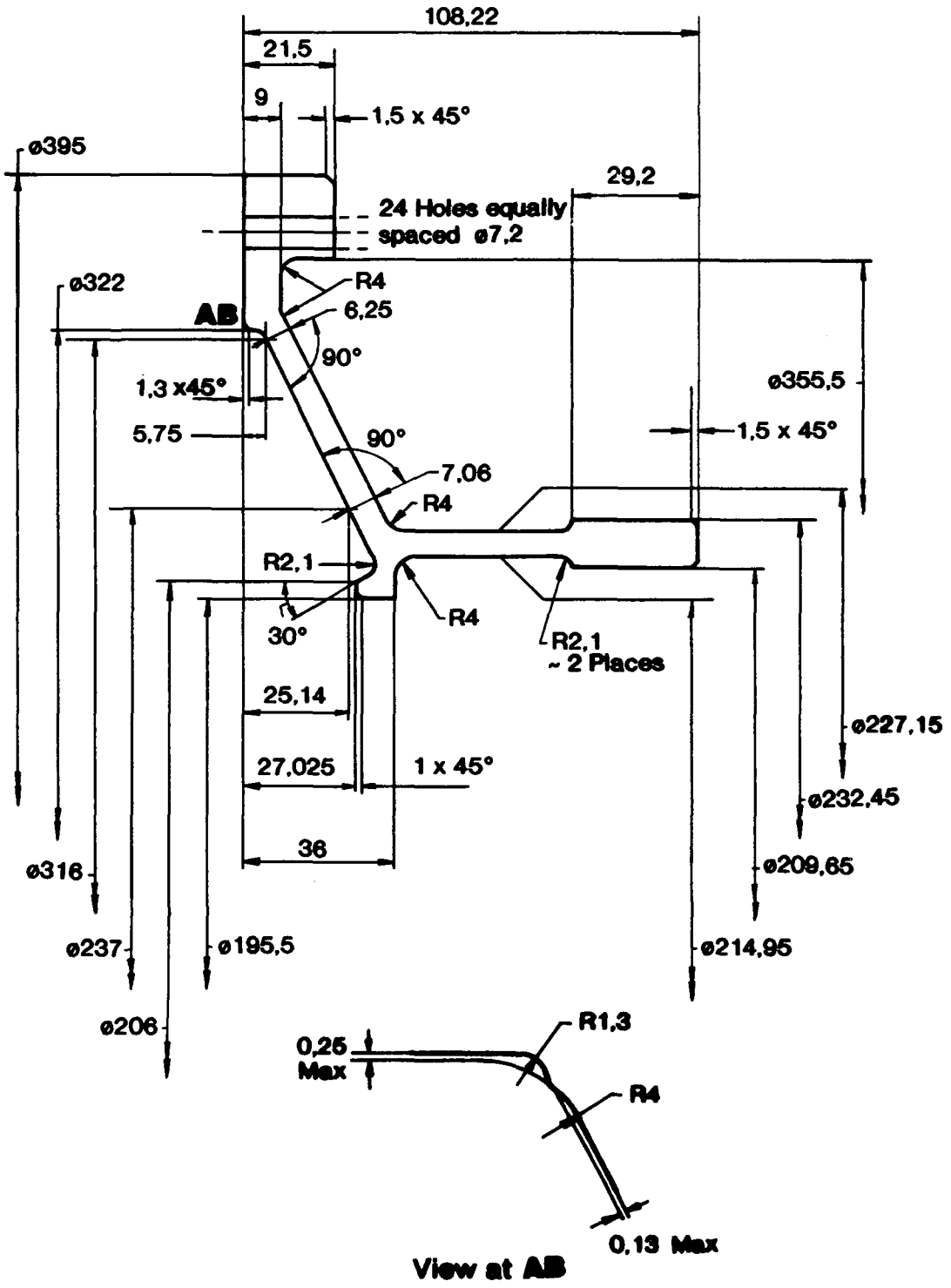

Figure 16

Dummy blade

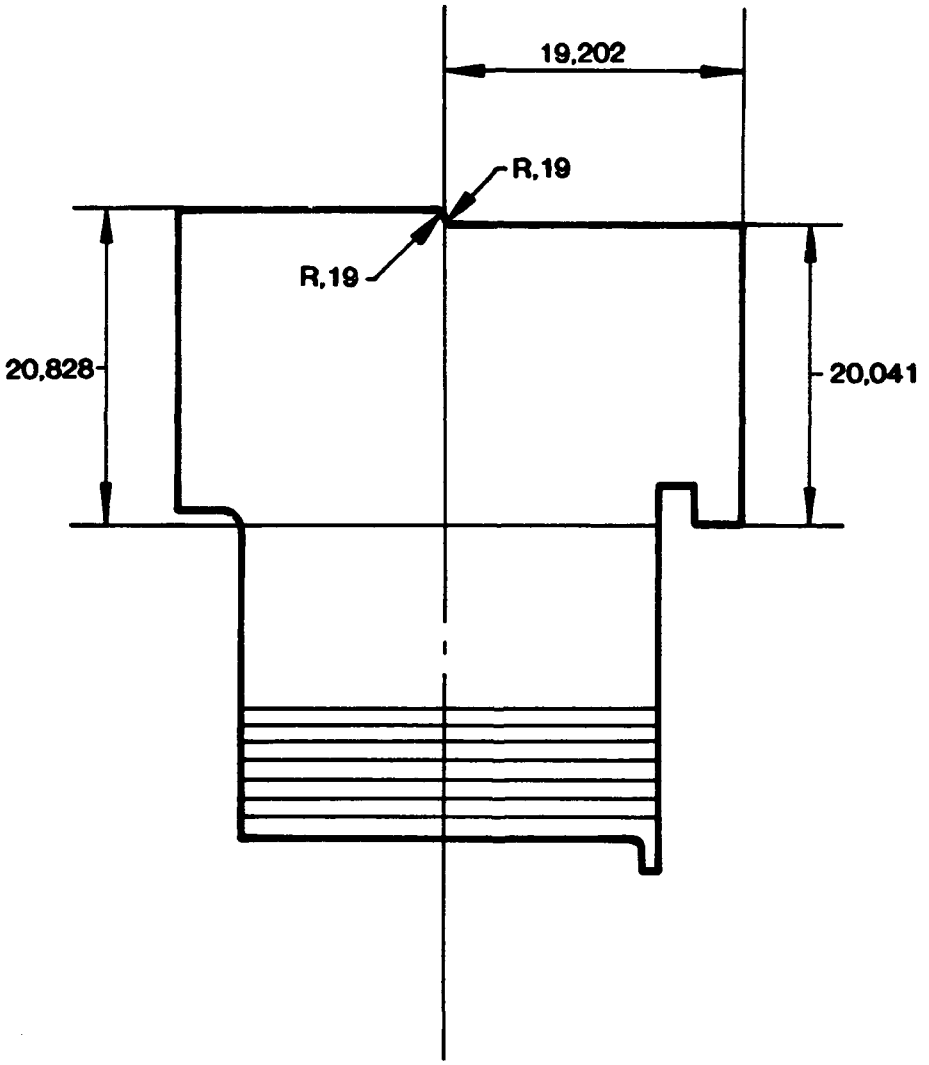

Figure 17

Bolt 1

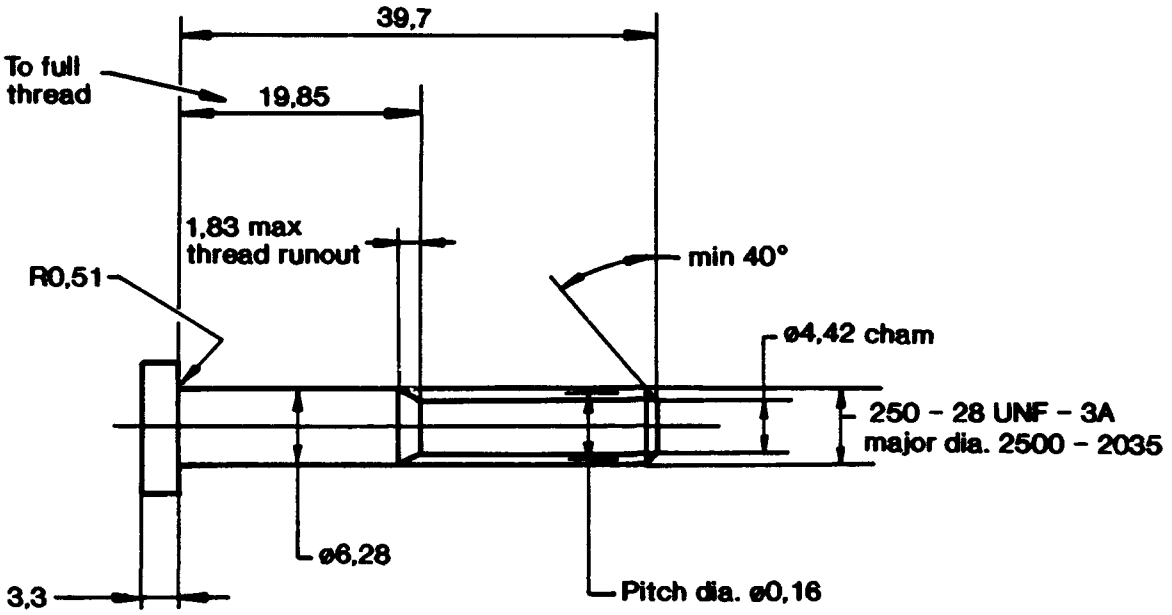

Weight = 12.5 gm

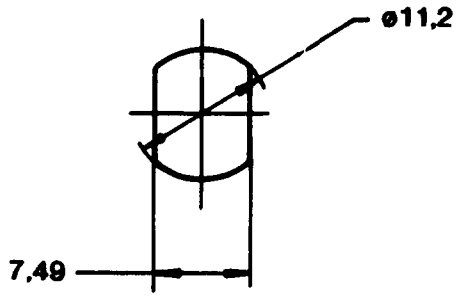

Material Nimonic 80A

Figure 18

Bolt 2

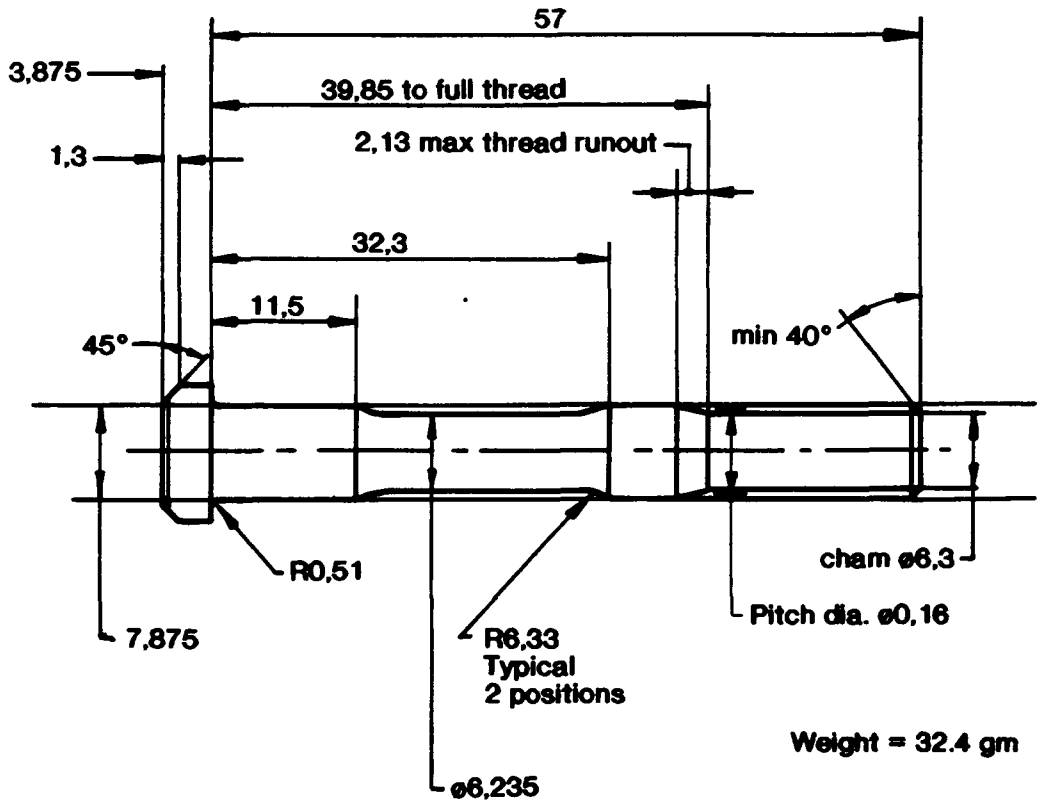

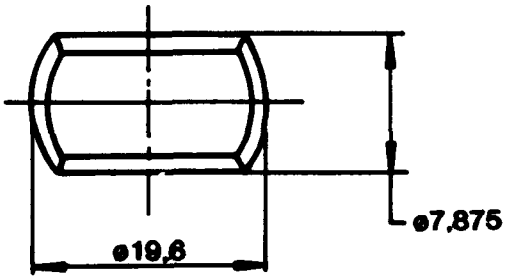

Material Waspaloy

Figure 19

Bolt 3

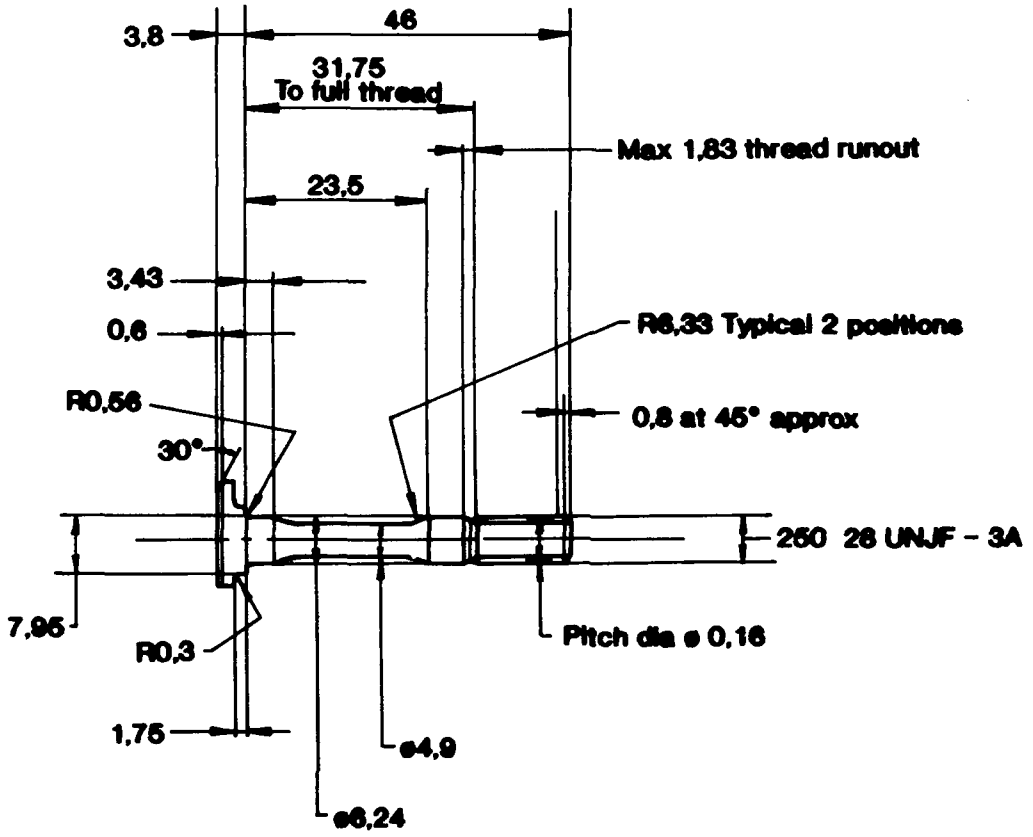

Weight = 3 gm

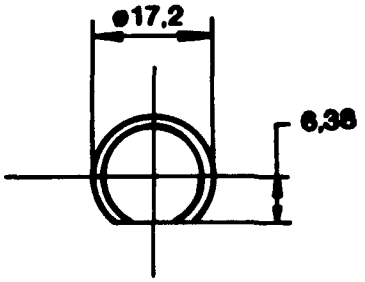

Material BSHR801

Figure 20

Nut

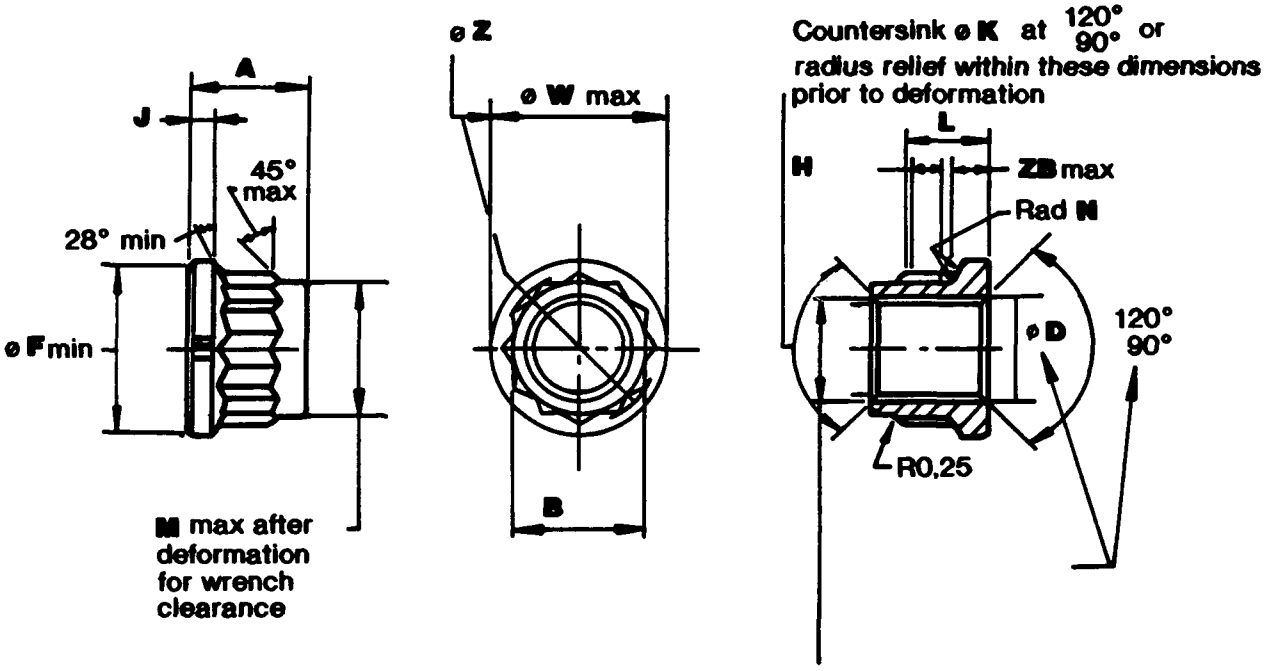

Material BSHR850

Figure 21

The dimensions of the nuts are as follows :

NUT	A	B	D	F	H	J	K
1	8.075	7.92	6.73	10.41	2.41	1.33	6.35
2	8.89	9.52	8.305	12.57	2.74	1.71	7.94
3	8.075	7.92	6.73	10.41	2.41	1.33	6.35

NUT	L	M	N	S	W	X	Z	ZB
1	5.4	8.28	0.445	0.13	11.18	0.036	0.18	2.79
2	6.225	9.96	0.445	0.13	13.34	0.04	0.2	3.3
3	5.4	8.28	0.445	0.13	11.18	0.036	0.18	2.79

Weights: Nuts 1 and 3 0.2 kg/100
Nut 2 0.3 kg/100

Tensile strengths: Nuts 1 and 3 23220 N
Nut 2 37276 N

Figure 22

3RD ANGLE PROJECTION

REASON FOR ISSUE:- TO INCORPORATE VAPOUR BLASTING ON THE R.I.G SPECIAL HPT DISC IN LINE WITH THE PRESENT PRODUCTION STANDARD.

Hwp/RAB 15th OCT 75

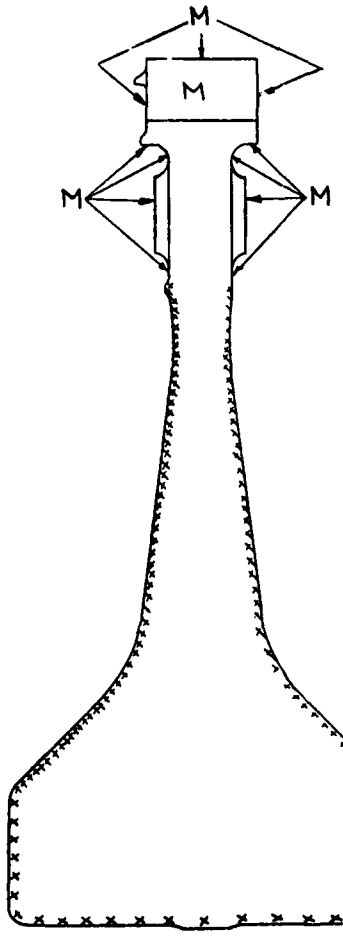

VAPOUR BLAST DETAILS:-

REMOVE 0·0011 (0,03) TO 0·0051 (0,13) BY MECHANICAL VAPOUR BLASTING. AREAS SHOWN xxxxxxxx TO BE TO RPS 386 WITH DATA CARD CONTROL

FIRTREE GROOVES, JOINT AND LOCATION FACES BOSSES SPIGOT DIAMETERS AND BOLT HOLES ETC (MARKED 'M') ARE TO BE MASKED PRIOR TO BLASTING.

ALT'n No.	Change Letter	ALTERATION	DATE

SCALE: N.T.S		MATL. CODE	QDY	DRAWN	R.S Barnett	ENGINE	RB 211-524
		SPEC. No.	M38R 7934	CHECKED		SECTION	HP Turbine Lamp
MACHINE ALL OVER OR WHERE MARKED ✓		HARDNESS		DATE	15th Oct 75	No. OFF	
ALL DIMENSIONS AND TOLERANCES ARE IN INCHES (mm)		HEAT TREAT		APPROVAL	Hwp/RAB		
Scheme Ref RTS 59374	ROLLS-ROYCE (1971) LIMITED			SHEET 1 OF 1 SHEETS			

VAPOUR BLASTING OF RB 211-524 SPECIAL HP TURBINE DISC RY 87802

DR 32536

Figure 23

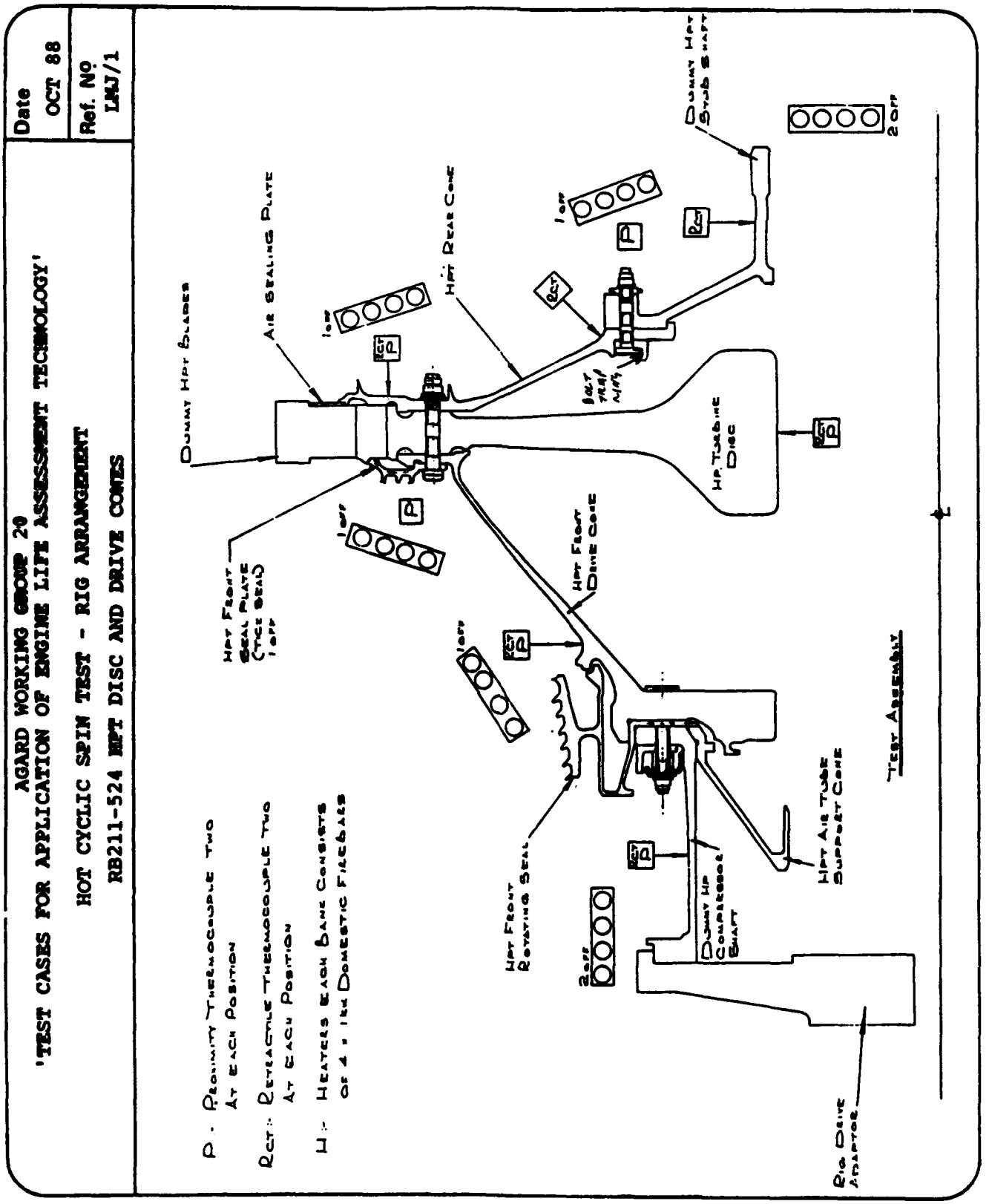
AGARD WORKING GROUP 20
'TEST CASES FOR APPLICATION OF ENGINE LIFE ASSESSMENT TECHNOLOGY'
HOT CYCLIC SPIN TEST - RIG ARRANGEMENT
RB211-524 HPT DISC AND DRIVE CONES
Date OCT 88
Ref. No LMJ/1
P - Proximity Thermocouple Two At Each Position
RCT - Retractile Thermocouple Two At Each Position
H - Heaters Each Bank Consists of 4 + 1kW Domestic FireBars
Dummy Hpt Blades
Air Sealing Plate
Hpt Rear Cone
Dummy Hpt Stub Shaft
Hpt Front Seal Plate (Cyce Seal) 1 off
Hpt Front Drive Cone
Hp Turbine Disc
Hpt Front Rotating Seal
Dummy Hp Compressor Shaft
Hpt Air Tube Support Cone
Rig Drive Adaptor
Test Assembly

Figure 24

Part specific crack propogation data

Modified forman fit

$$\frac{da}{dn} = \frac{C\ (\Delta K - \Delta K_{th})^n}{(1-R)K_c - \Delta K}$$

C = 1,569e-8 m/cycle

n = 2,109

K_{th} = 0

K_c = 150,61 MPa $\sqrt{m}$

$\frac{da}{dn}$ = m/cycle

K = MPa $\sqrt{m}$

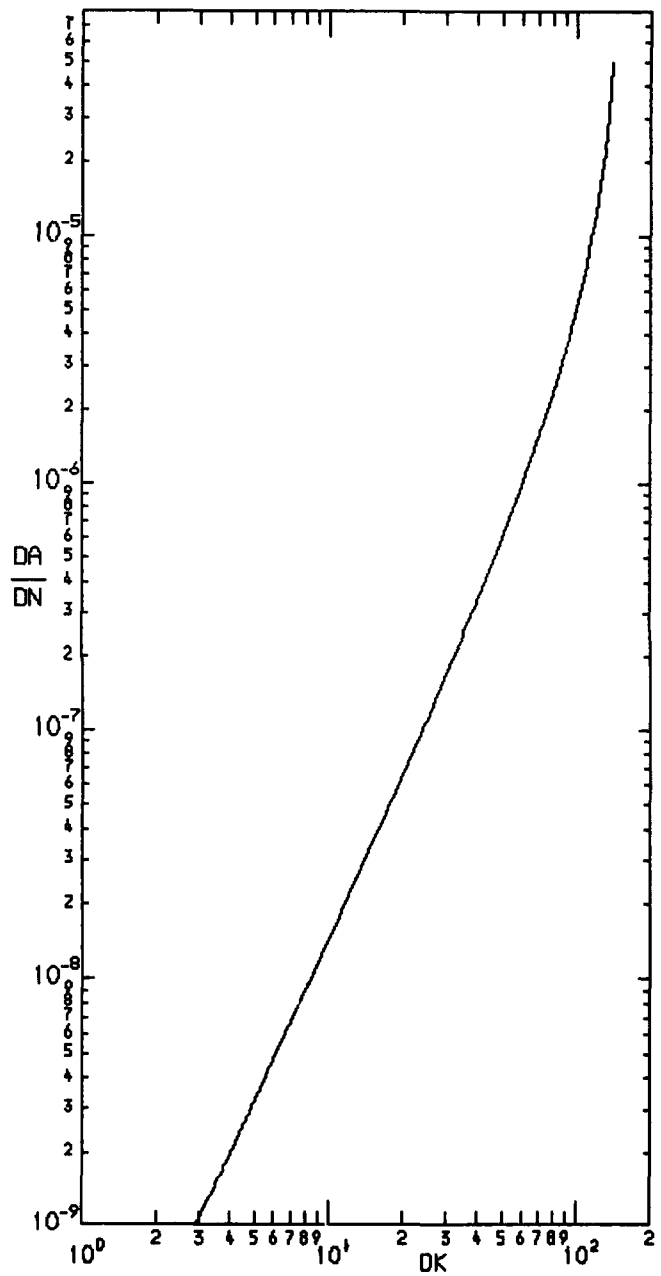

Figure 25

Rig test — Waspaloy disc test
Fatigue cracking initiating at an inclusion

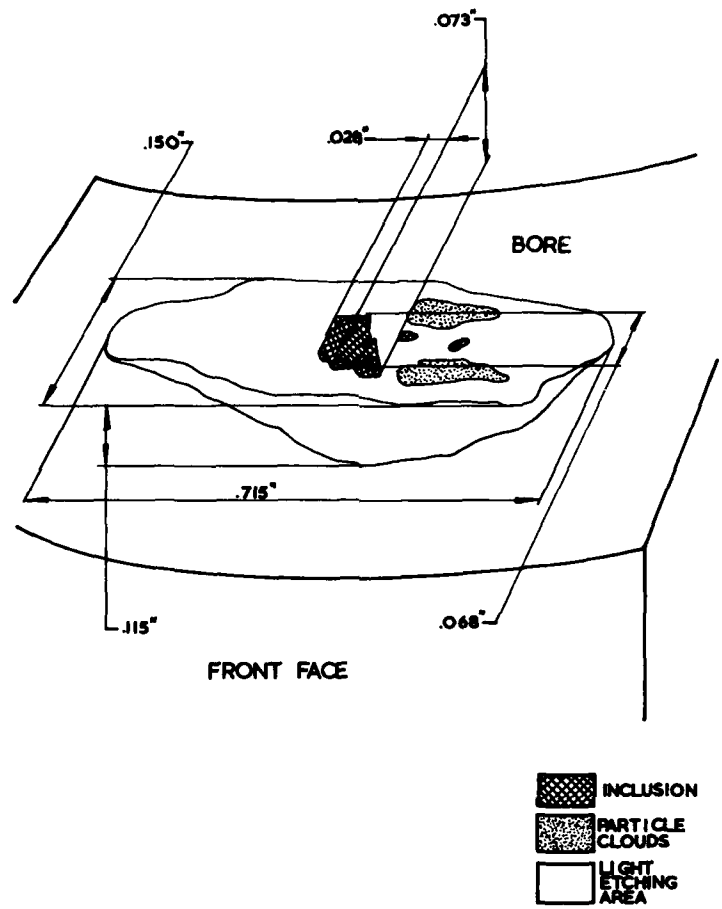

Figure 26

Chapter 6

ENGINE LIFE ASSESSMENT TEST CASE

TF41 LP COMPRESSOR SHAFT TORSIONAL FATIGUE

W. H. Parker
Allison Gas Turbine Division
General Motors Corporation
P. O. Box 420, M/S T10B
Indianapolis, Indiana 46206-0420 USA

1. INTRODUCTION

In this paper the TF41 low pressure (LP) compressor shaft torsional fatigue is presented as a test case for life assessment. This is Allison's contribution to a set of test cases which may be used by AGARD participants to ground individual life predictive tools.

The TF41-A-1B, a product of Allison and Rolls-Royce, is a two-spool nonaugmented turbofan engine which produces 14,500 pounds of thrust and powers the Vought A-7D for the United States Navy and Air Force. The engine's specifications are the following[1]:

- No. compressor stages: 3,2,11
- No. turbine stages: 2,2
- Max. power at sea level: 14,500 lb
- Max. power specific fuel consumption (SFC): 0.65
- Max. power pressure ratio: 21.1
- Max. diameter: 39.5 in
- Max. length: 114.2 in

During the late 1970s, plans were formulated to initiate a program to extend the life of critical rotor components. The Engine Life Extension Program, sponsored by the United States Air Force, started in January 1980 and was deferred in September 1986. One of the components studied was the LP compressor shaft. The technical approach was to:

- develop the shaft material fatigue characteristics
- perform in-depth finite element modeling and life analyses
- conduct controlled environment torsional fatigue testing
- compare results of test and life prediction

The TF41 LP compressor shaft was tested at Allison between 1982 and 1987 as part of the Engine Life Extension Program. The content of that testing forms the basis for this test case. Presented are details of the shaft dimensions, loads, material properties and test results required to perform and verify a life analysis.

Four production shafts were tested, each of which had experienced partial field service. The load spectrum used for testing was zero-maximum major torque cycles with steady axial load and ±10% high cycle torque superimposed. Testing was conducted until a 1/8th inch crack was initiated and continued until the total crack length measured along the crack reached approximately 1.5 inches in length. In all instances the crack was initiated in the forward oil holes. For the two specimens where fractography information was available, the failure had multiple initiation sites in corrosion pits on the inner diameter (I.D.) of the forward oil hole on one and single fatigue origin sites associated with the forward oil hole surface imperfections on the other. Fractography information is not available for the other two specimens.

The test case was independently reviewed and found to provide sufficient information to conduct the required stress analysis,

[1] "Specifications - U.S. Gas Turbine Engines", Aviation Week & Space Technology, March 18, 1991, p. 134.

predict the crack propagation of the fatigue cracks originating at the shaft front oil feed hole location, and compare the predictions to the actual test results.

The component geometry description was used to generate a NASTRAN 3-D analysis of the forward region of the shaft which contains the oil feed holes of concern. A 60 degree segment of the shaft from the forward spline to an equal distance aft of the oil hole was modelled and solved for the defined load conditions using the dihedral symmetry solution option. This analysis provided the stress gradient utilized in prediction of the fatigue crack progression. The crack propagation analysis was based on mode I stress intensity solution and the provided fatigue crack growth rate data was assumed to be mode I generated data. The stress gradient normal to the plane of the crack path progression (mode I opening stress) was determined and utilized in the crack propagation analysis. Predictions were based on LEFM techniques. Only the major cycle was assumed to cause significant fatigue crack growth and the predictions were based on R=0.05, Kth=5.7, Kc=120. data. The provided FCGR data was refit to permit direct use of existing fracture mechanics code. Results of the crack propagation analysis compared reasonably with the actual test results. No attempt was made to predict initiation at the oil feed holes, since the stated goal of the test case is crack growth prediction from fatigue cracks.

2. COMPONENT GEOMETRY

This section presents the basic part geometry, dimensions and tolerances, of the TF41 LP compressor drive shaft along with a description of the test setup. Details of the shaft definition are presented in Figure 2-1[2]. The finished helical splines at each end of the shaft are nitrided to a case depth of 0.013-0.019 for wear resistance and stress relieved after grinding.

[2] All figures appear at the end of this paper.

The test setup is shown in Figure 2-2. Torque is applied by a hydraulic actuator. The system is fully automated and permits unattended 24 hr/day operation. The desired shaft torque is maintained through a closed loop servo control system coupled to a torque transducer (strain gage full torsion bridge installed on the coupling fixture). The system was calibrated with a torque sensor traceable to the U.S. Bureau of Standards. The results were checked against a strain gage torsion bridge cemented to the first test shaft run.

The control system provides protection against overtorque which is independent of the servo control system. Continuous recording of torque and windup with an intermittent record of temperature is used to document the test parameters. The ability of the rig to maintain satisfactory shaft alignment was verified through deflection measurements recorded during the static and dynamic application of the test torques and axial loads as shown in Figure 2-3.

Shaft heating was provided by quartz lamps and two individual controllers. The temperature gradient was monitored by three thermocouples positioned 120 degrees apart at each of the five planes shown in Figure 2-4. They were held against the shaft by multiple wraps of stainless steel wire. Control thermocouples were welded to the compressor and turbine spanner nuts.

As can be seen from the test arrangement used and realizing that the failures occurred at the front oil holes, it is not necessary to define the adjacent hardware. No processing, machining or handling anomalies were noted prior to testing. No assembly loads or fits should affect the life of the shaft at the oil holes.

3. PART PROCESSING INFORMATION

Included in this section is the general machining and processing information and any other information related to surface enhancements. The TF41 LP compressor shaft is coated with a black oxide after processing. The oil holes, location of the test

failures, are initially drilled with rounded breaks. They are jig ground to a 32 finish, although the drawing specifies a 63 finish. There are no surface enhancements such as peening or ball burnishing. However, the four shafts tested were used parts and had approximately 3400 hours of use. The fractography information available showed that one failure initiated in corrosion pit imperfections while another initiated from surface imperfections. These imperfections were not quantified. No fractography information is available for the other two failed shafts.

4. OPERATING CONDITIONS

The test cycle used to evaluate the LP compressor shaft torsional fatigue life, shown in Figure 4-1, is composed of a major and minor torque application with a steady axial load. The major torque cycle of 172,400 in-lbs represents the intermediate power condition. The minor torque cycle of 8620 in-lbs applied at 4-1/2 Hz represents high cycle torques measured during engine operation. The 20,000 pound tensile axial load represents separation forces seen by the shafting during normal gas loading.

5. BOUNDARY CONDITIONS FOR STRESS ANALYSIS

The boundary condition data necessary to perform a proper stress analysis of the shaft is shown as Figure 5-1. It shows a free body diagram of the LP main shaft which includes the LP compressor shaft as an element. Shown are the loads and torques applied in the test case. As the figure indicates, this test was a simulation of a -19°F day, 0.6 Mn at sea level condition.

6. HEAT TRANSFER INFORMATION

Because of the relatively low temperature environment in the neighborhood of the oil holes (crack origin), there was no heat transfer analysis performed on this test configuration. A linear temperature distribution using the data presented in Figure 2-4 was used in the analysis.

7. MATERIALS DATA

Shaft material of the TF41 LP compressor is Allison material EMS64500. It has a density of 0.283 lb/in^3 and Poisson's ratio of 0.281. A complete definition of this material sufficient to perform a fatigue analysis is presented in Figures 7-1 through 7-35. Included is the material specification and plots of the fundamental properties such as modulus, density, yield and ultimate strengths. LCF data, summarized in Figures 7-15 to 7-29, are based on load drop critera under strain-controlled test conditions. Also attached is a description of the specimen processing informa-tion.

8. OPERATION HISTORY

This section contains the cycles to cracking for each of the four test shafts, crack inspection data and crack fractography for two of the cracked shafts. These data are presented in the Appendix, and the results for the four shafts tested are summarized in Table 8-1. Each shaft tested had about 3400 engine cycles prior to bench testing.

The summary combines the service time and test cycles to form a total for crack initiation cycles based on 3.2 cycles per hour, an average conversion number for the A-7D mission. Average initiation life for the four shafts tested was 60,000 cycles with a standard deviation of 15,000 cycles.

Fractography data were available for only two of the four shafts tested. It showed one shaft had multiple initiation sites from corrosion pits while the other had a single initiation site at a surface irregularity. The surface imperfections were not quantified.

9. SUMMARY

The test case presented here provides an example for crack initiation and crack growth of a shaft loaded with major, zero to maximum, torsional cycles with steady axial load and high cycle minor torsional cycles superimposed. The TF41 LP compressor drive shaft was tested as part of a U.S. Air Force Life Extension Program in the early to

mid 1980s. This test program provided a controlled set of fatigue testing information and material characterization data which form the basis of the test case.

Details of the engine shaft are presented along with pertinent processing information. The test setup and program are described in sufficient detail to permit users to model the component and predict the state of stress. Material data are presented with enough detail so that fatigue life models can be used to predict the shafting life and comparisons with test results can be made.

Table 8-I.
Summary of TF41 LPC shafts tested.

P/N	S/N	Service time (hr)	Crack init. cycles	Failure cycles (major)	Failure cycles (minor)
6860005 million	DN0092	3,434	48,000	75,540	18.3
6860005 million	DP10356	3,410	40,000	43,457	10.6
6860005 million*	DN10033	3,760	31,000	64,896	15.5
6860005 million*	DN10273	3,378	73,000	112,000	26.9

Conversion: 3.2 cycles/hour

* No fractography report avail.

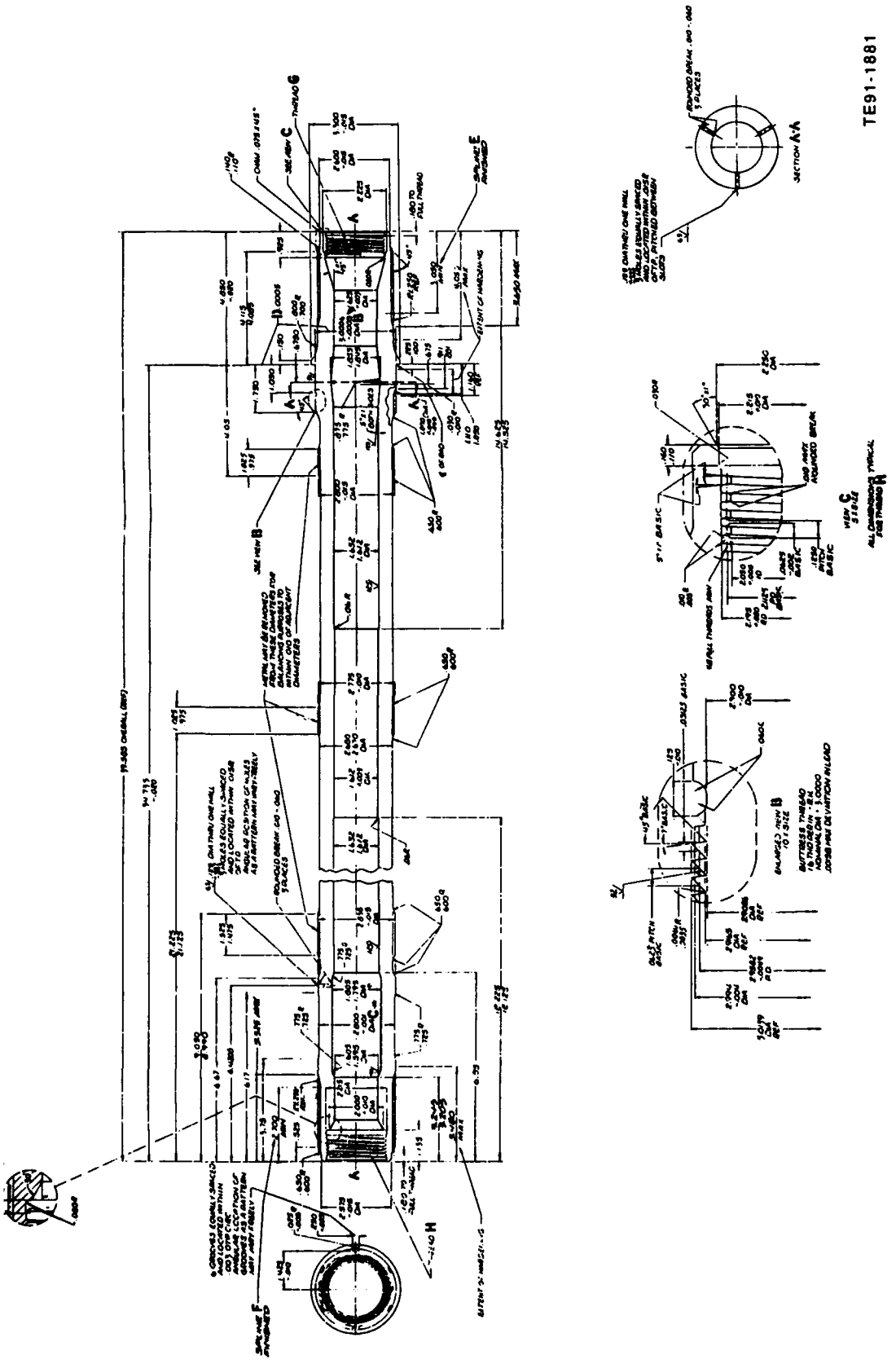

Fig. 2-1. TF41 LP compressor shaft geometry.

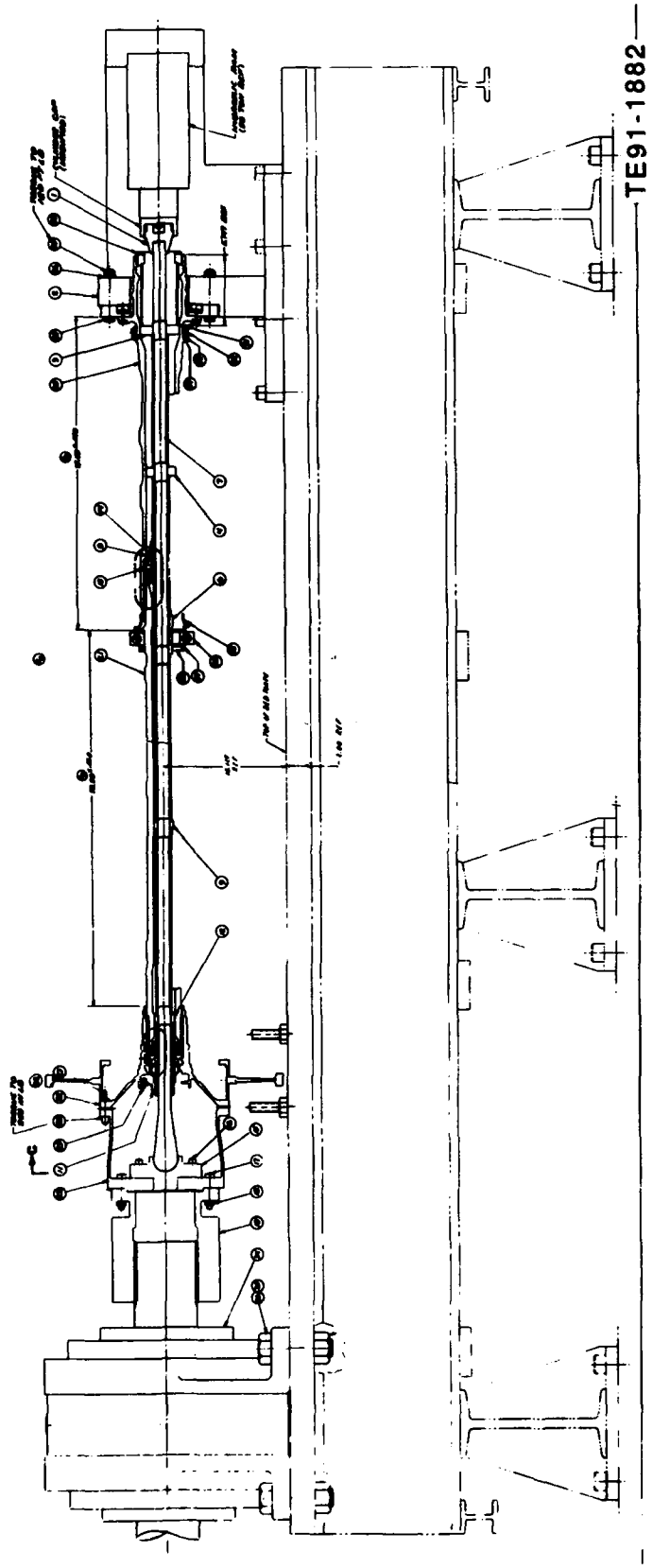

Fig. 2-2. TR41 LP compressor drive shaft test setup.

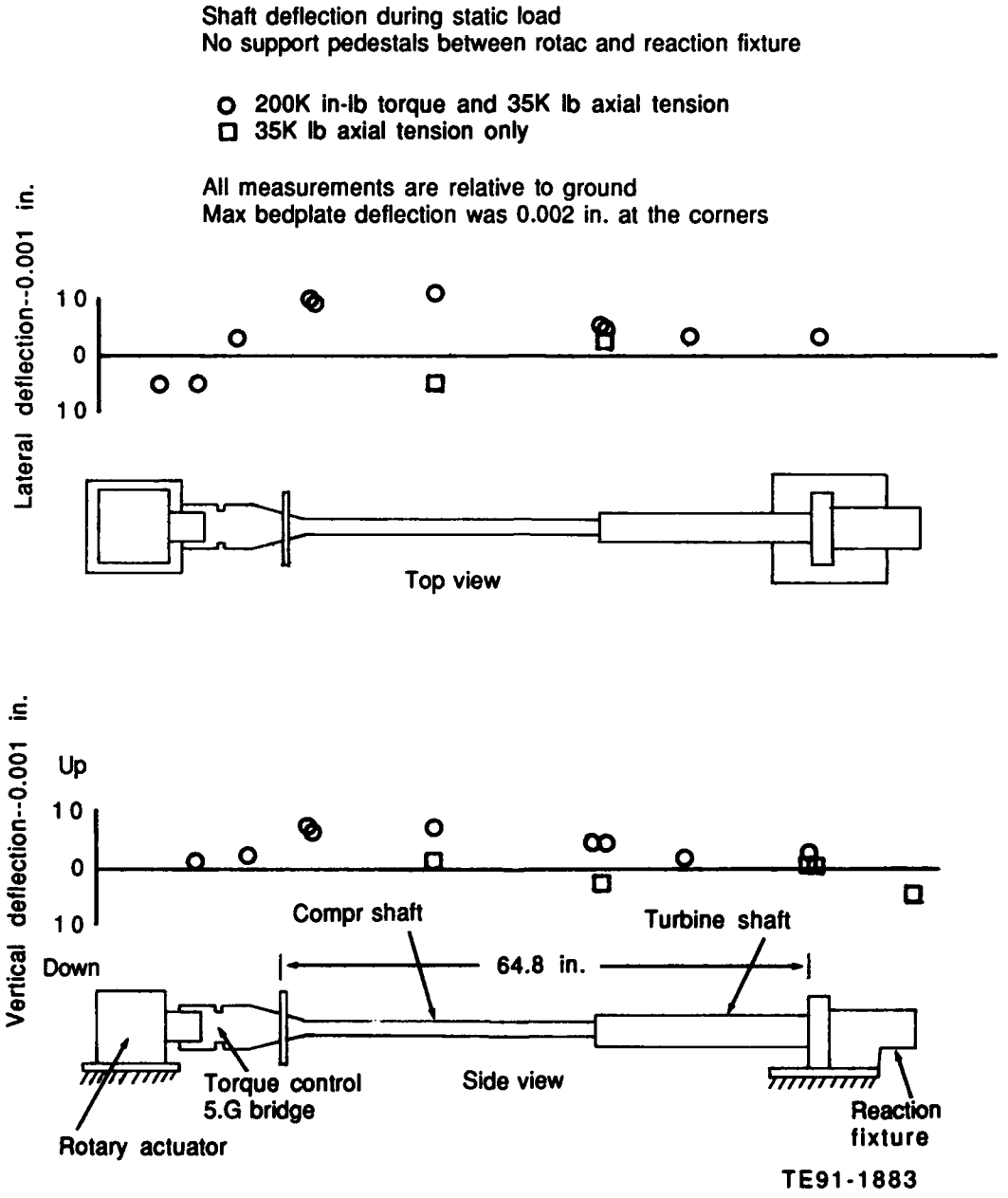

Fig. 2-3. Shaft deflection during static load.

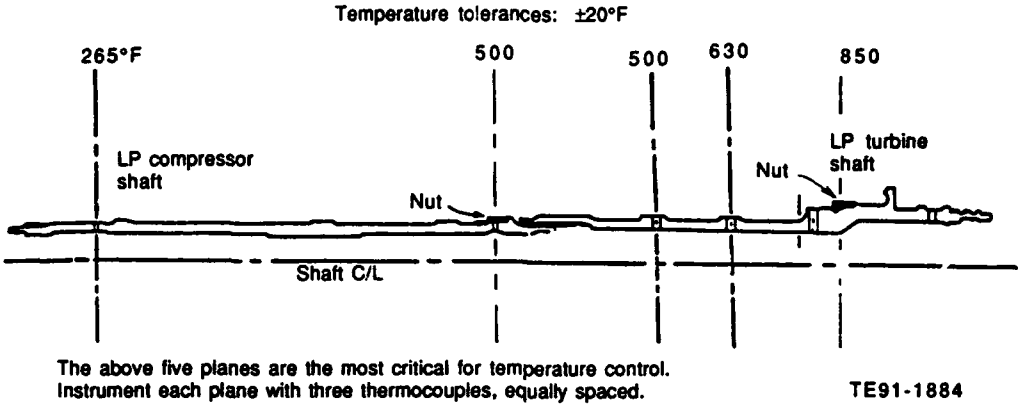

Fig. 2-4. Temperature profile of LP shaft system.

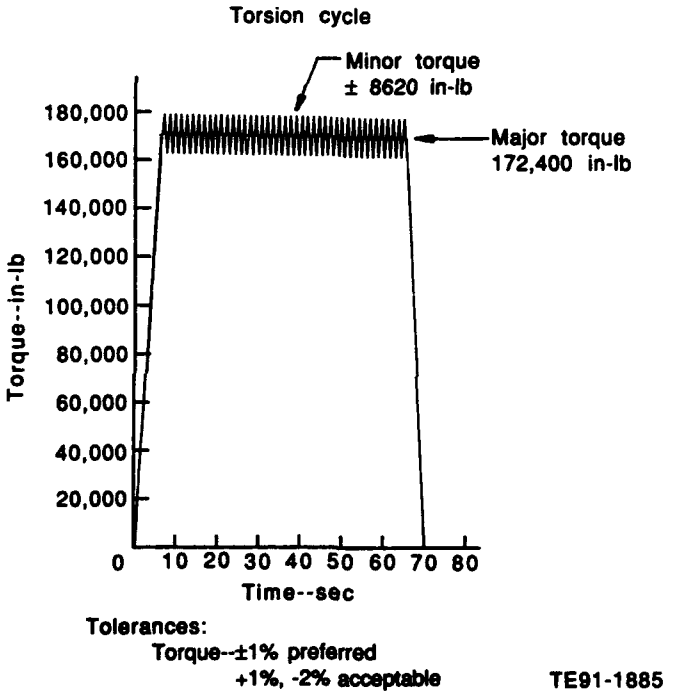

Fig. 4-1. Load cycle fatigue for fatigue testing.

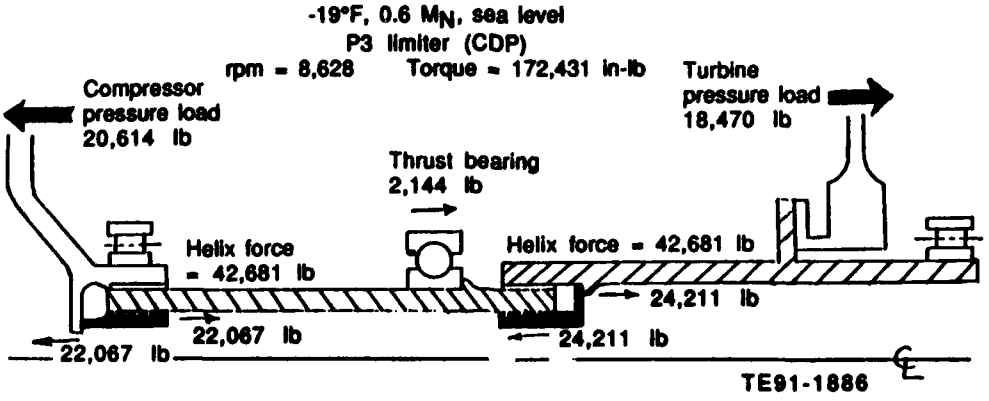

Fig. 5-1. LP drive shafting free body diagram.

SECTION IX SHEET 1 OF 5

ISSUED 5-04-60 REVISED 3-16-82 CODE NUMBER 73342	ENGINEERING MATERIAL SPECIFICATION E11	EMS 64500D AEROSPACE

STEEL, LOW HEAT RESISTANT
3.25Cr - 0.95Mo - 0.20V (0.35 - 0.45C)

1. ACKNOWLEDGMENT: A supplier shall mention this specification number and its revision letter in all quotations and when acknowledging purchase orders.

2. FORM: Bars, forgings, and forging stock.

3. APPLICATION: Primarily for turbine and compressor rotor shafts, requiring high strength up to 1000°F (538°C).

4. COMPOSITION:

		min		max
	Carbon	0.35	-	0.45
	Silicon	0.10	-	0.35
	Manganese	0.45	-	0.70
	Nickel	--		0.3
	Chromium	3.0	-	3.5
	Molybdenum	0.8	-	1.1
	Vanadium	0.15	-	0.25
	Phosphorus	--		0.020
ø	Tin	--		0.025
ø	Phosphorus + Tin, Total	--		0.025
	Sulfur	--		0.020

5. CONDITION:

5.1 Bars: In a machinable condition having hardness not higher than 241 HB or equivalent, except that, if cold finished, hardness may be as high as 248 HB or equivalent.

5.2 ø Forgings: Normalized and tempered, having hardness not higher than 277 HB.

5.3 Forging Stock: As ordered by the forging manufacturer.

Fig. 7-1. Engineering Material Specification for TF41 LP compressor shaft material - EMS 64500. (Part 1 of 5)

EMS 64500D

6. TECHNICAL REQUIREMENTS: When ASTM methods are specified for determining conformance to the following requirements, tests shall be conducted in accordance with the issue of the ASTM method listed in the latest issue of AMS 2350.

6.1 Bars and Forgings: Test specimens shall be capable of meeting the following requirements:

6.1.1 Heat Treatment: Heat parts to a temperature between 1690°F (921°C) and 1780°F (971°C), hold at heat for not less than 30 minutes and quench in oil. Temper by heating to a suitable temperature between 1060°F (571°C) and 1200°F (649°C), holding at the selected temperature for not less than two hours and cool in air.

6.1.1.1 It is optional to double temper with an oil quench after the first temper, but each temper operation shall be in the 1060°F (571°C) - 1200°F (649°C) range.

6.1.2 Hardness: Hardness shall be within the range 388-429 HB.

6.1.3 Tensile Properties:

Ultimate Tensile Strength, psi (MPa)	190,400 (1306) min 212,800 (1467) max
Yield Strength, 0.1% Offset, psi (MPa)	156,800 (1081) min
Elongation, % in 4D	12 min

6.1.4 Impact Strength: A standard Izod impact specimen shall, after being heat treated in accordance with paragraph 6.1.1, be heated at a temperature between 895°F (479°C) and 970°F (466°C) for not less than 48 hours. Impact strength when tested at room temperature shall be not less than 20 foot pounds.

6.2 Grain Size: Predominantly 5 or finer with occasional grains as large as 3 permissible, determined in accordance with ASTM E112.

6.3 Decarburization:

6.3.1 Bars ordered ground, turned, or polished shall be free from decarburization on the ground, turned, or polished surface.

6.3.2 Allowable decarburization on bars ordered for redrawing or forging, or to definite microstructural requirements, shall be as agreed upon by purchaser and supplier.

6.3.3 Decarburization of bars to which 6.3.1 or 6.3.2 is not applicable shall be not greater than the following:

Fig. 7-1. Engineering Material Specification for TF41 LP compressor shaft material - EMS 64500. (Part 2 of 5)

Nominal Diameter or Distance Between Parallel Sides				Depth of Decarburization	
	Inches		Millimetres	Inch	Millimetres
	0.375 and under		(9.39 and under)	0.010	(0.25)
Over	0.375 to 0.500, incl	(Over 9.39 to 12.70, incl)		0.015	(0.38)
Over	0.500 to 0.625, incl	(Over 12.70 to 15.88, incl)		0.020	(0.51)
Over	0.625 to 1.000, incl	(Over 15.88 to 25.40, incl)		0.025	(0.64)
Over	1.000 to 1.500, incl	(Over 25.40 to 38.10, incl)		0.030	(0.76)
Over	1.500 to 2.000, incl	(Over 38.10 to 50.80, incl)		0.035	(0.89)
Over	2.000 to 2.500, incl	(Over 50.80 to 63.50, incl)		0.040	(1.02)
Over	2.500 to 3.000, incl	(Over 63.50 to 76.20, incl)		0.048	(1.22)
Over	3.000 to 4.000, incl	(Over 76.20 to 101.60, incl)		0.062	(1.57)
Over	4.000 to 5.000, incl	(Over 101.60 to 127.00, incl)		0.094	(2.39)
Over	5.000	(Over 127.00)		0.125	(3.18)

6.3.4 Unless otherwise agreed upon by purchaser and supplier, decarburization shall be measured by the microscopic method, or by Rockwell Superficial 30-N scale hardness method, or equivalent hardness testing method, on hardened specimens. Depth of decarburization, when measured by a hardness method, is defined as the distance measured from the nearest original surface to the point at which no increase in hardness is found.

6.3.4.1 When determining the depth of decarburization, it is permissible to disregard local areas provided the depth of decarburization of such areas does not exceed the limits above by more than 0.005 inch (0.13mm) and the width is 0.065 (1.65mm) or less.

7. QUALITY: Steel shall be premium quality and shall conform to the requirements of the latest issue of AMS 2300; it shall be multiple melted using vacuum consumable electrode process in the remelt cycle, unless otherwise permitted. Material shall be uniform in quality and condition, sound, free from foreign materials, and from internal and external imperfections detrimental to fabrication or to usage of product.

8. TOLERANCES: Unless otherwise specified, tolerances shall conform to the following:

8.1 Bars: The latest issue of AMS 2251 as applicable. Diameter or thickness tolerances for cold finished bars and all hexagons shall conform to Table I, column headed "over 0.28 to 0.55 inch".

9. REPORTS:

9.1 Unless otherwise specified, the supplier of the product shall furnish with each shipment three copies of a report of the results of tests for chemical composition, hardness, tensile properties, impact strength, grain size and cleanliness rating of each heat in the shipment. Results

Fig. 7-1. Engineering Material Specification for TF41 LP compressor shaft material - EMS 64500. (Part 3 of 5)

of tests on billets shall be furnished for 2 samples each taken from the top and bottom of the first and last billet of each heat of material supplied. If forgings are supplied, the part number and size of stock used to make the forgings shall also be included.

9.2 Unless otherwise specified, the supplier of finished or semi-finished parts shall furnish with each shipment three copies of a report showing the purchase order number, EMS 6450OD,, contractor or other direct supplier of material, part number, and quantity. When material for making parts is produced or purchased by the parts supplier, that supplier shall inspect each lot of material to determine conformance to the requirements of this specification, and shall include in the report a statement that the material conforms, or shall include copies of laboratory reports showing the results of tests to determine conformance.

10. IDENTIFICATION:

10.1 Bars: Individual pieces or bundles shall have attached a metal or plastic tag embossed with the purchase order number, EMS 6450OD, nominal size, and heat number, or shall be boxed and the box marked with the same information. In addition to the above identification, flats 2 inches (50 mm) and larger in both dimensions and other bars 2 inches (50mm) and over in diameter or distance between parallel sides shall be stamped with the heat number within 2 inches (50mm) of one end.

10.2 Forgings: Shall be identified in accordance with the latest issue of AMS 2808.

10.3 Forging Stock: Shall be identified as agreed upon by purchaser and supplier.

11. REJECTIONS: Material not conforming to the requirements of this specification, or to authorized modifications, shall be subject to rejection.

12. NOTES:

12.1 Marginal Indicia: The phi (Ø) symbol is used to indicate technical changes from the previous issue of this specification.

12.2 Referenced Specifications:

AMS 2251 - Tolerances - Low Alloy Steel Bars
AMS 2300 - Premium Aircraft - Quality Steel Cleanliness - Magnetic Carbide Inspection Procedure
AMS 2350 - Standards and Test Methods
AMS 2808 - Identification - Forgings
ASTM E112 - Estimating Average Grain Size of Metals

Fig. 7-1. Engineering Material Specification for TF41 LP compressor shaft material - EMS 64500. (Part 4 of 5)

FORM 2708 (REV. 4/71) SHEET 5 OF 5

EMS 64500D

12.3 Patent Liability: The above specification is given without considering whether patents may or may not be involved. In all cases, therefore, the supplier shall be required to assume patent liability.

12.3.1 This specification is issued by Detroit Diesel Allison, Division of General Motors Corporation, for use in its production operations; by suppliers making parts to DDA purchase orders when specified on DDA drawings; and by users of DDA products as applicable. The risk of compliance to the latest revision of this specification and of patent infringement shall be the responsibility of the user of this document.

12.3.2 When called out on a DDA drawing, this specification takes precedence over any government specification not specifically referenced herein.

12.4 Revision "D" authorized by AEM SC - 530.

Signed Marcus Herman
Chief
Materials Research and Engineering

Fig. 7-1. Engineering Material Specification for TF41 LP compressor shaft material - EMS 64500. (Part 5 of 5)

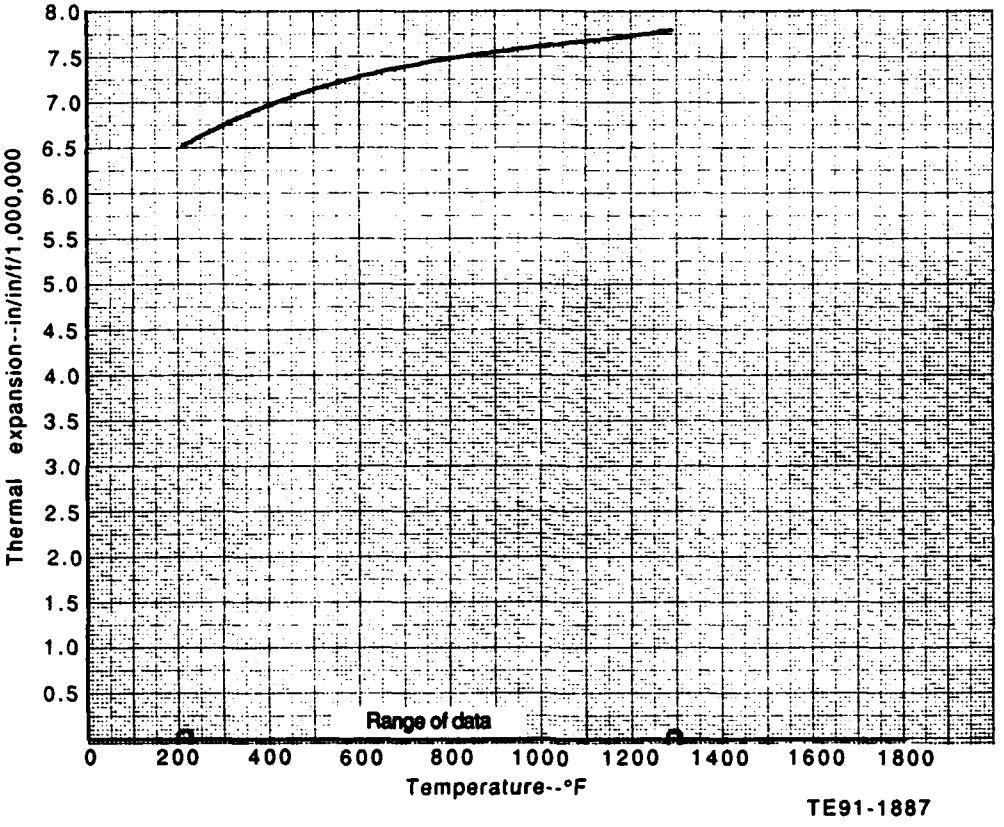

Fig. 7-2. Coefficient of thermal expansion - EMS 64500.

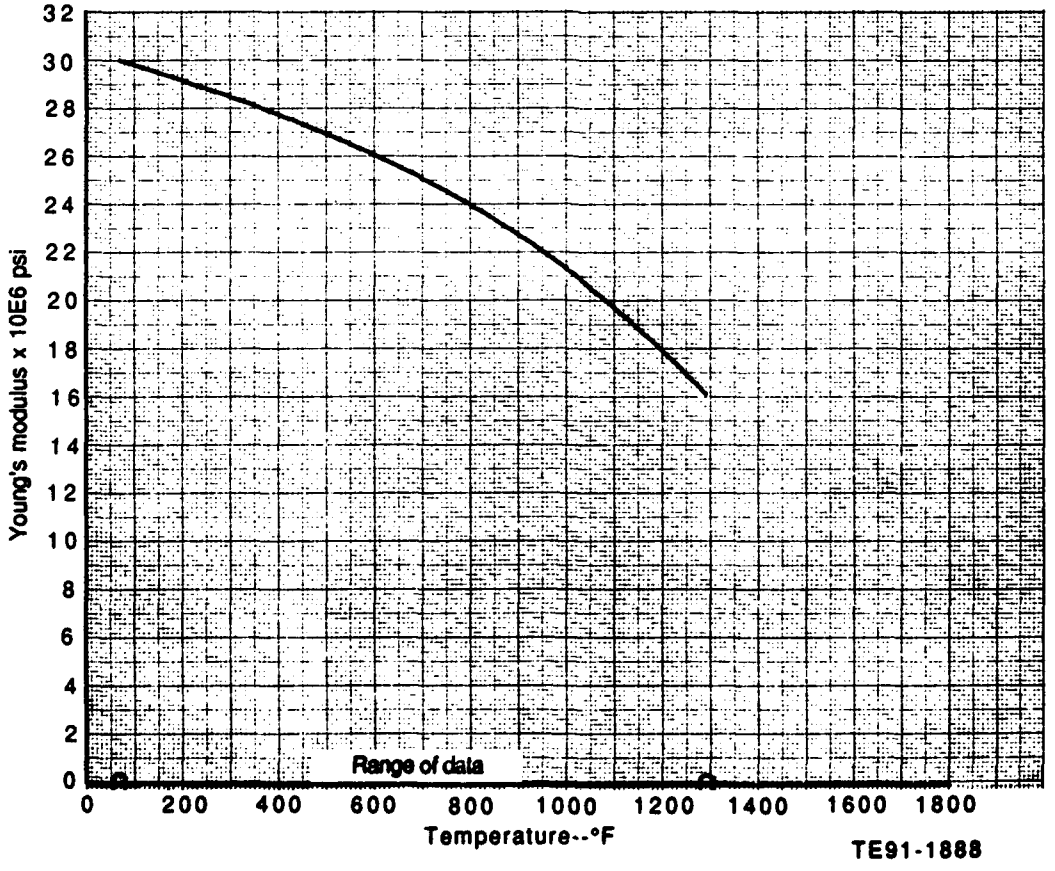

Fig. 7-3. Young's modulus - EMS 64500.

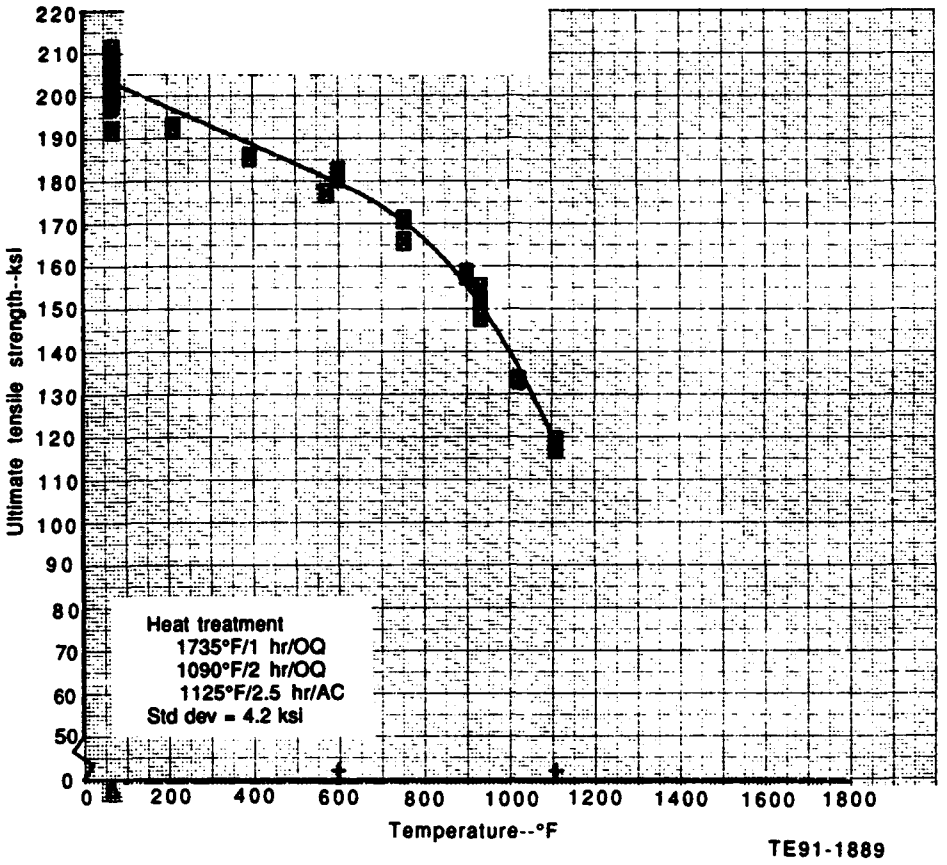

Fig. 7-4. Ultimate tensile strength - EMS 64500.

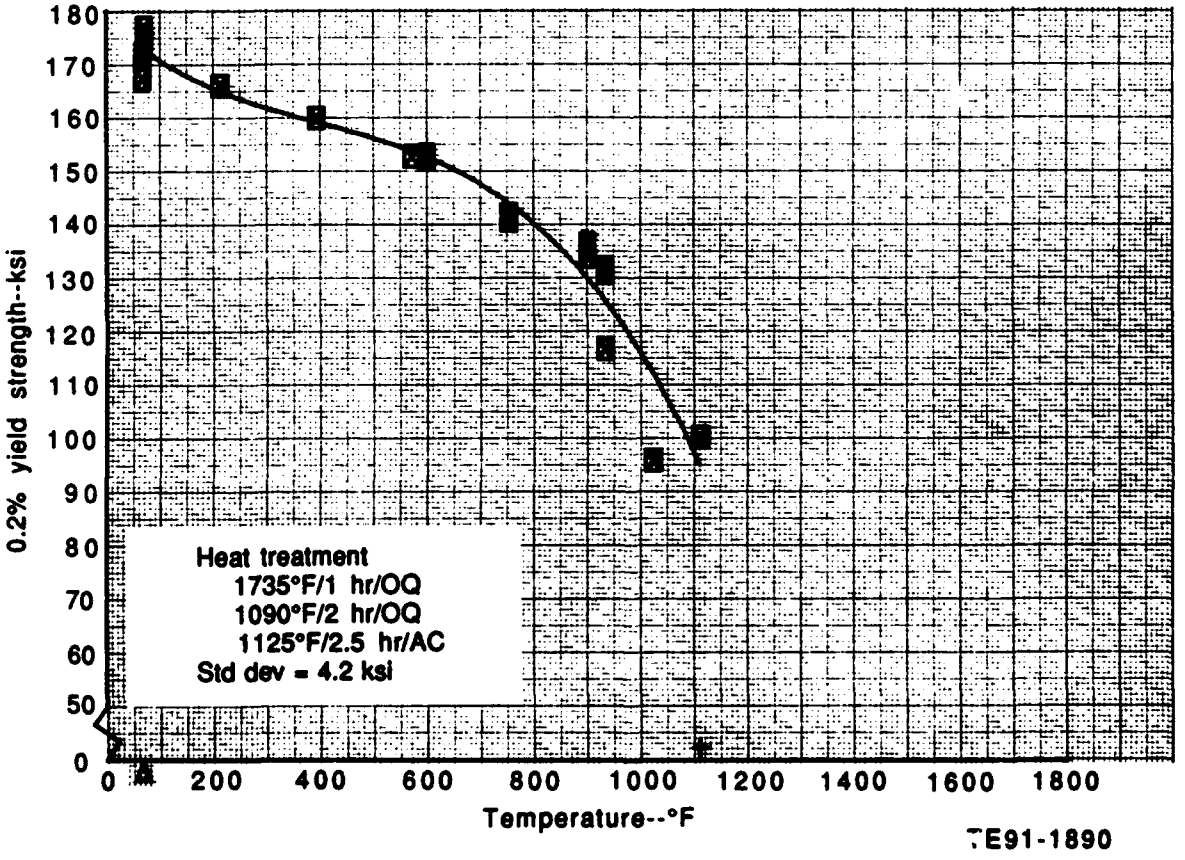

Fig. 7-5. 0.2% yield strength - EMS 64500.

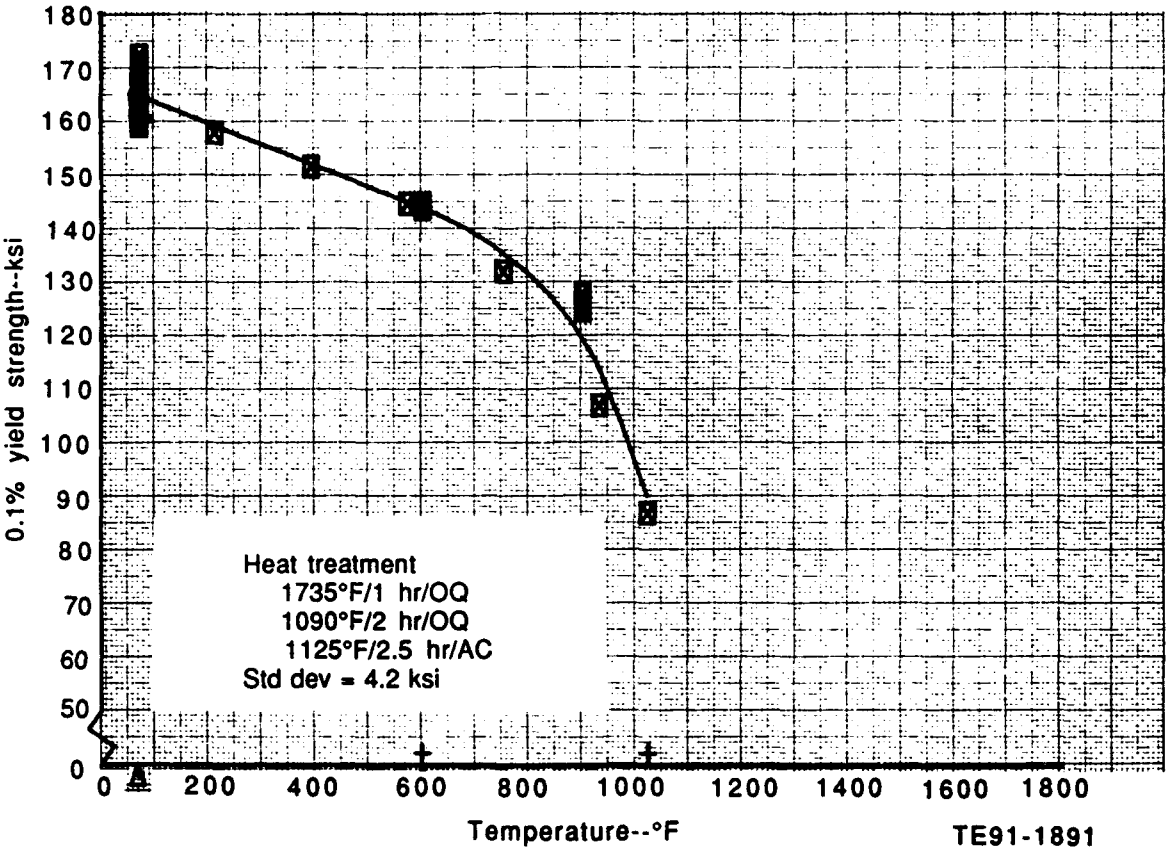

Fig. 7-6. 0.1% yield strength - EMS 64500.

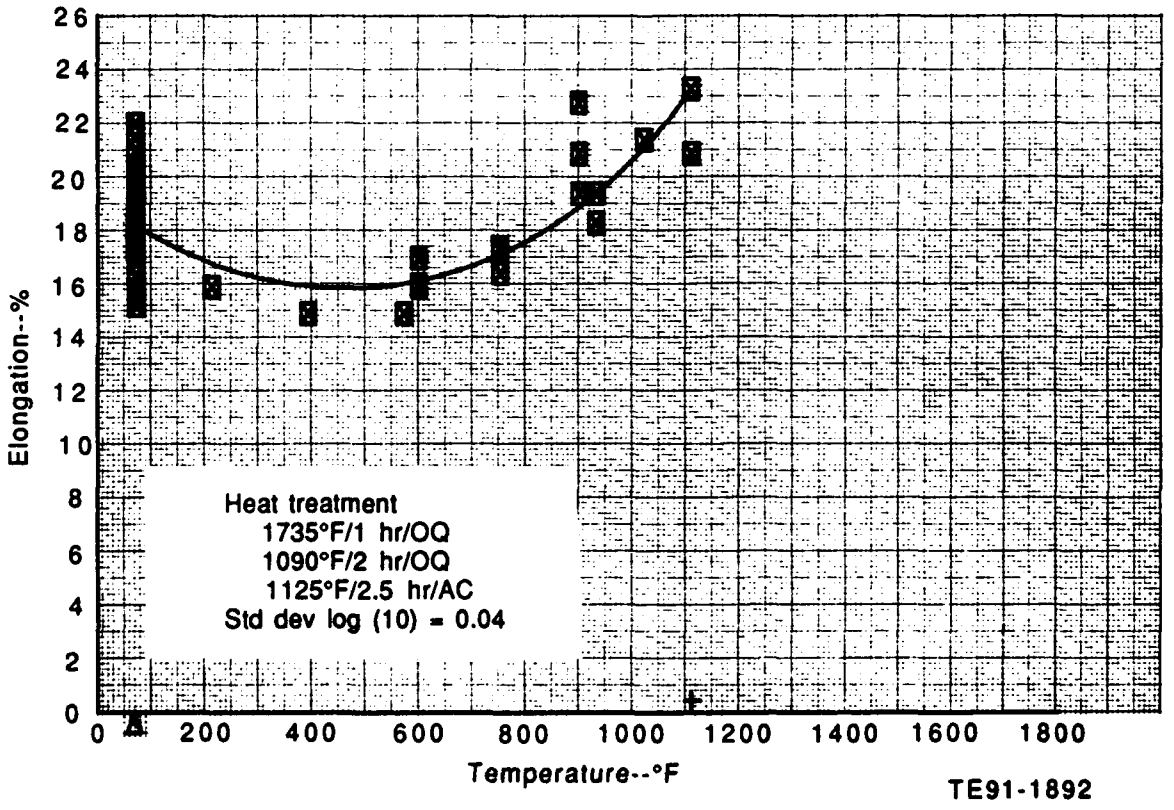

Fig. 7-7. Elongation - EMS 64500.

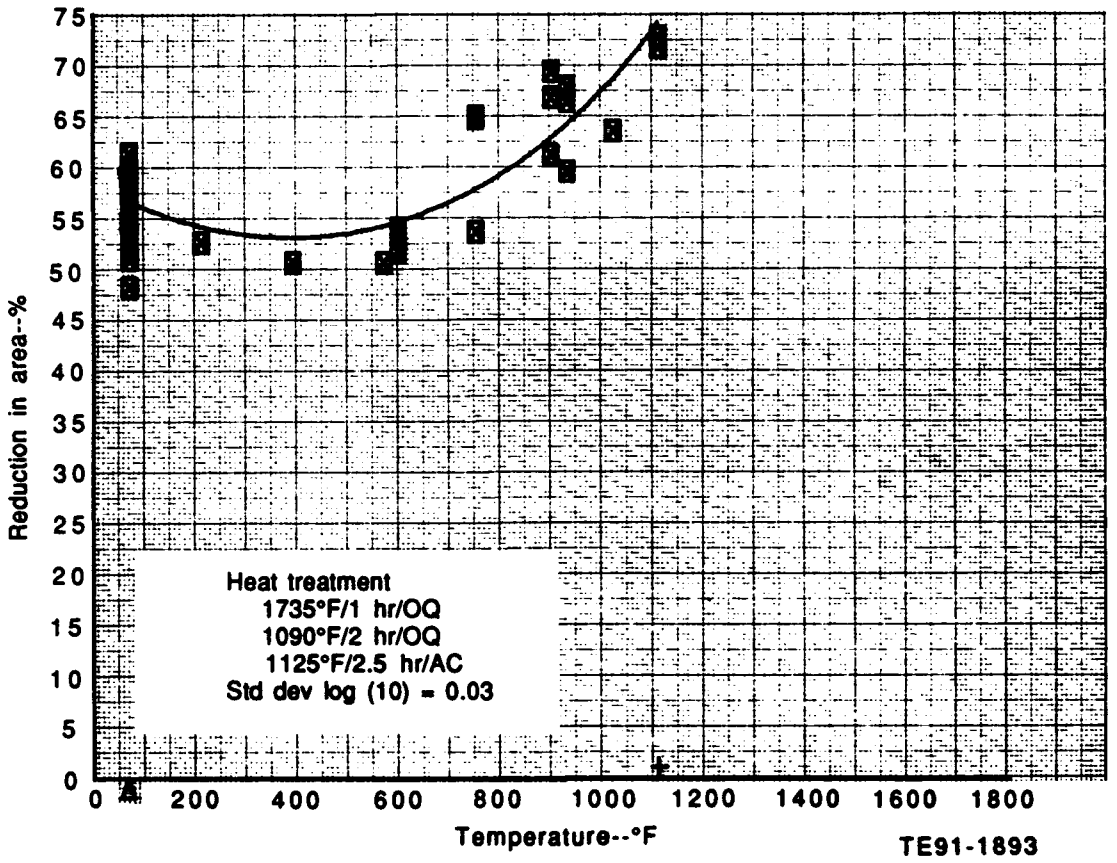

Fig. 7-8. Reduction in area - EMS 64500.

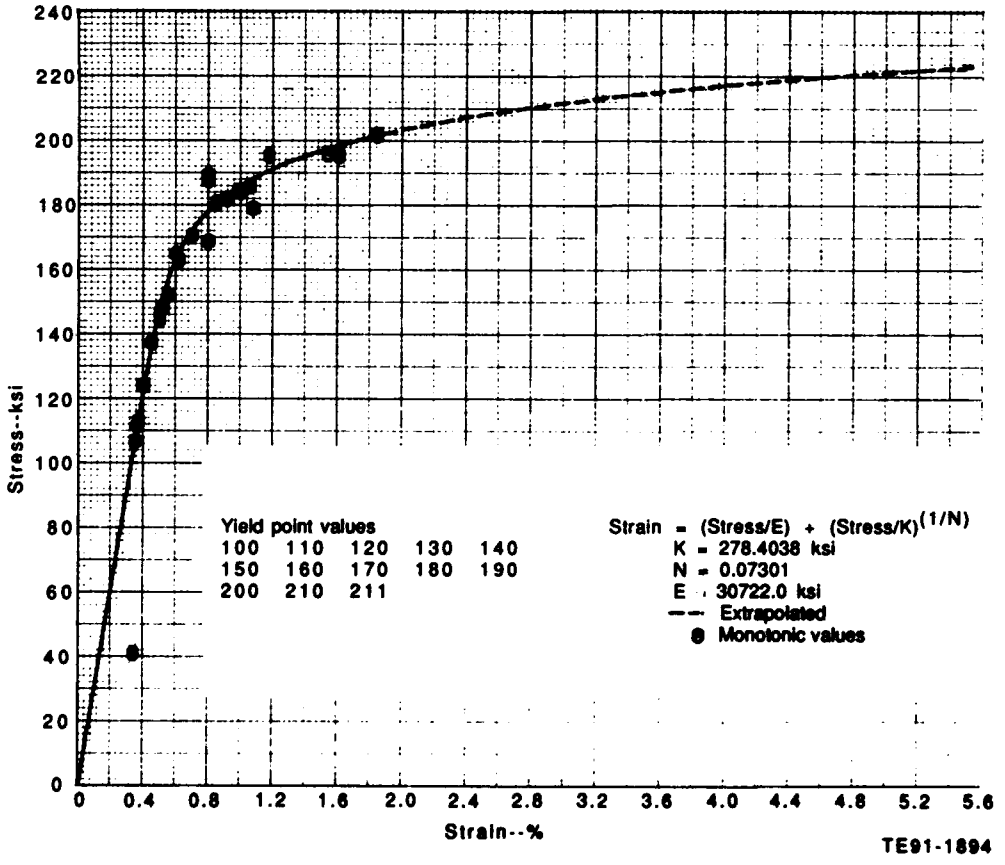

Fig. 7-9. Monotonic stress strain at 78°F - EMS 64500.

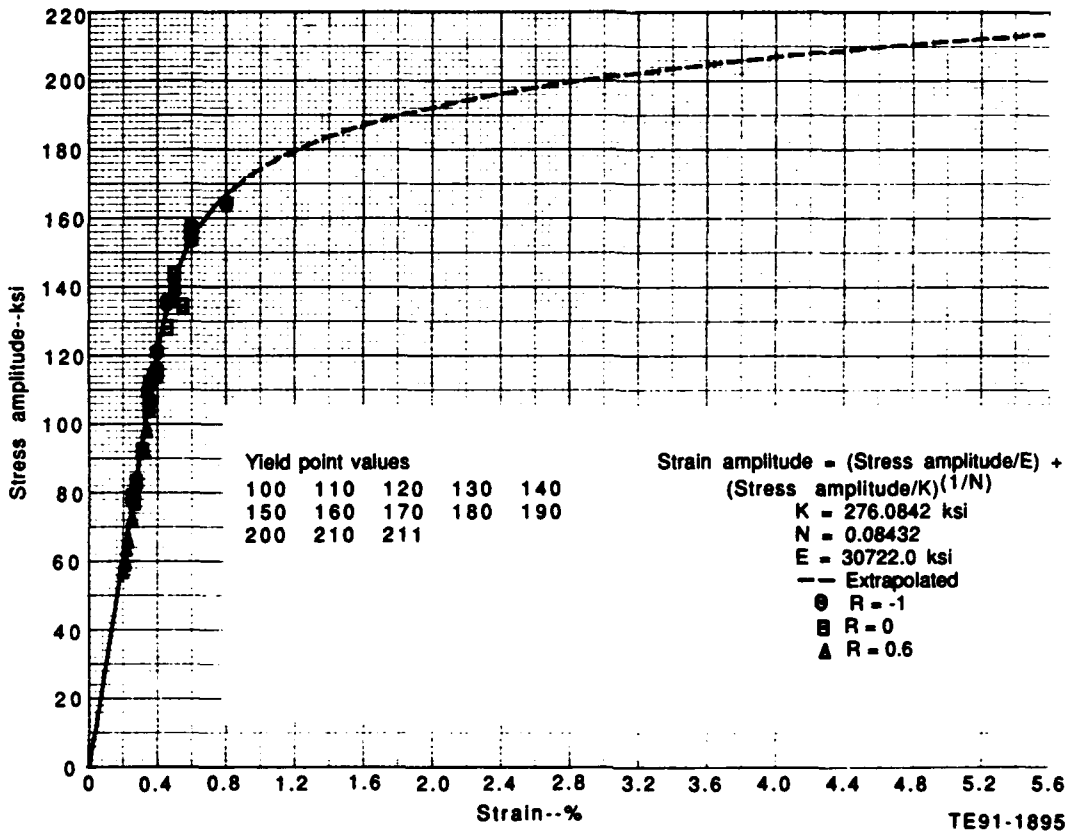

Fig. 7-10. Cyclic stress strain curve at 78°F - EMS 64500.

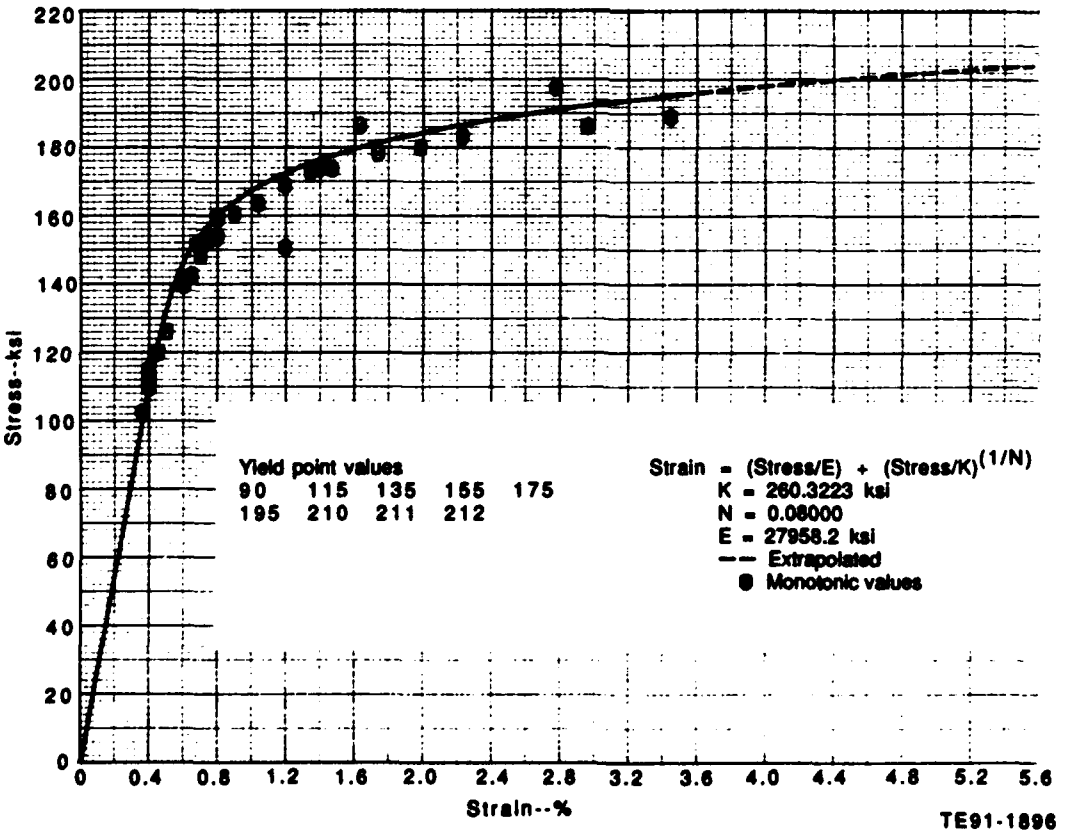

Fig. 7-11. Monotonic stress strain at 500°F - EMS 64500.

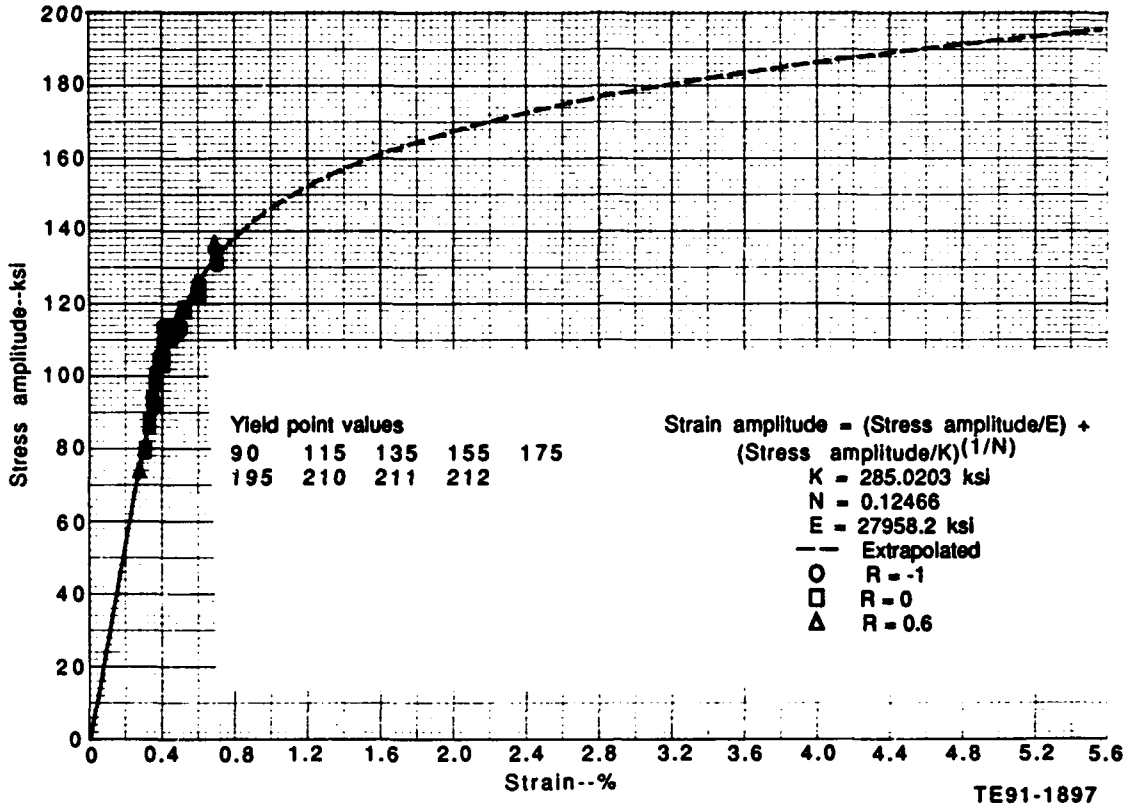

Fig. 7-12. Cyclic stress strain at 500°F - EMS 64500.

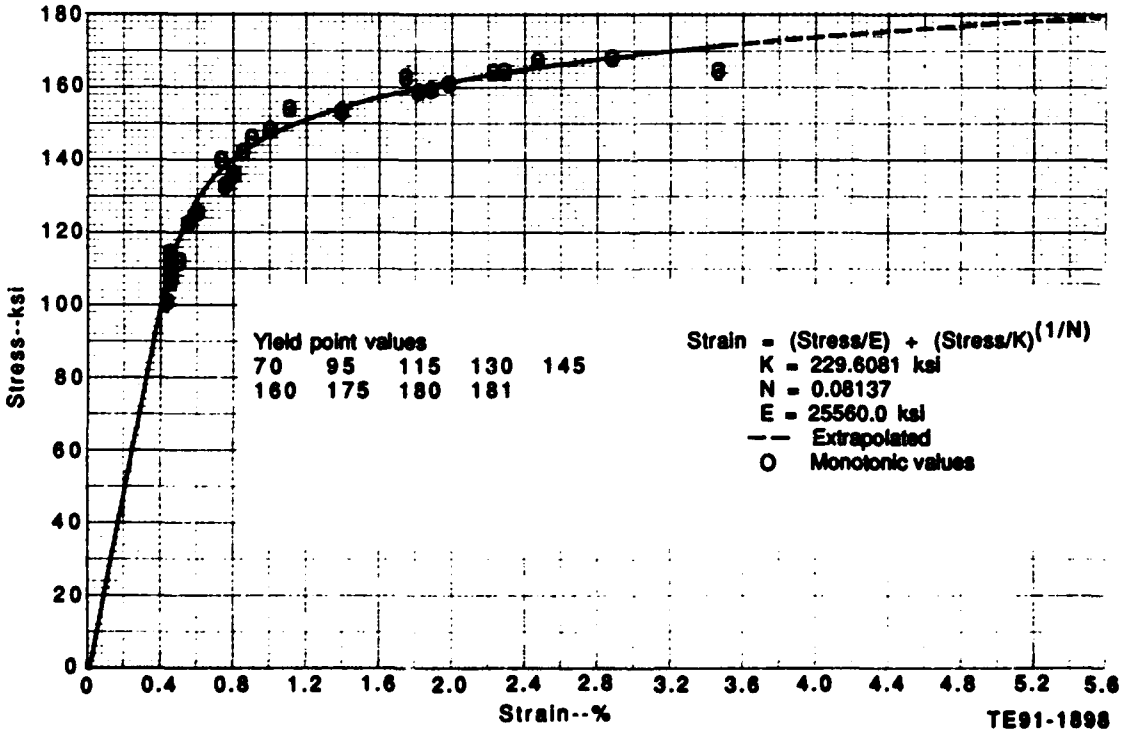

Fig. 7-13. Monotonic stress strain at 850°F - EMS 64500.

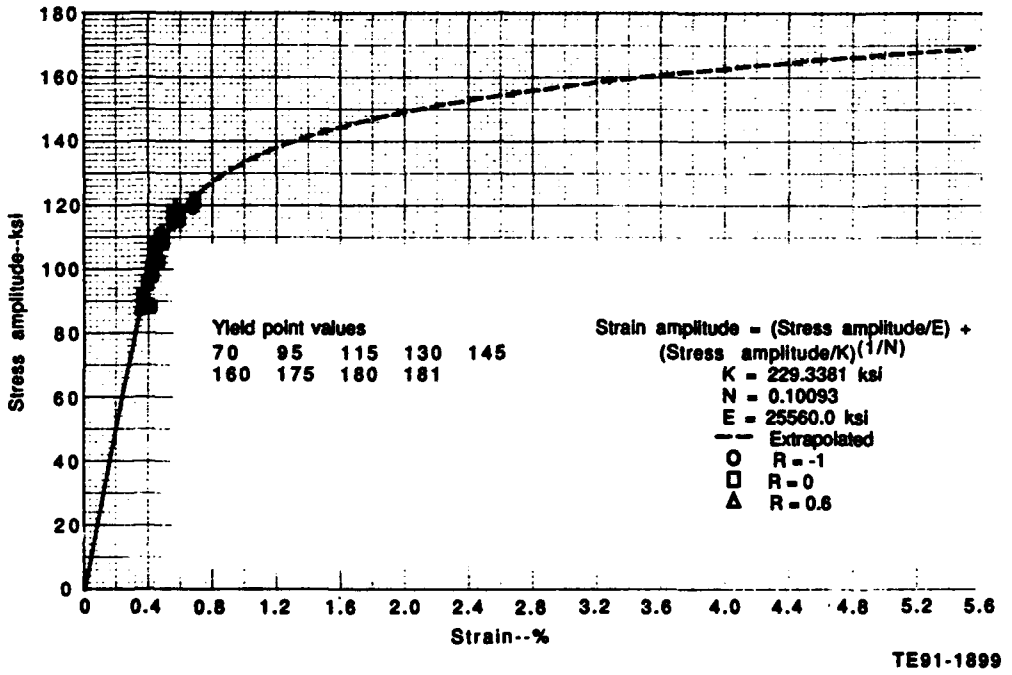

Fig. 7-14. Cyclic stress strain at 850°F - EMS 64500.

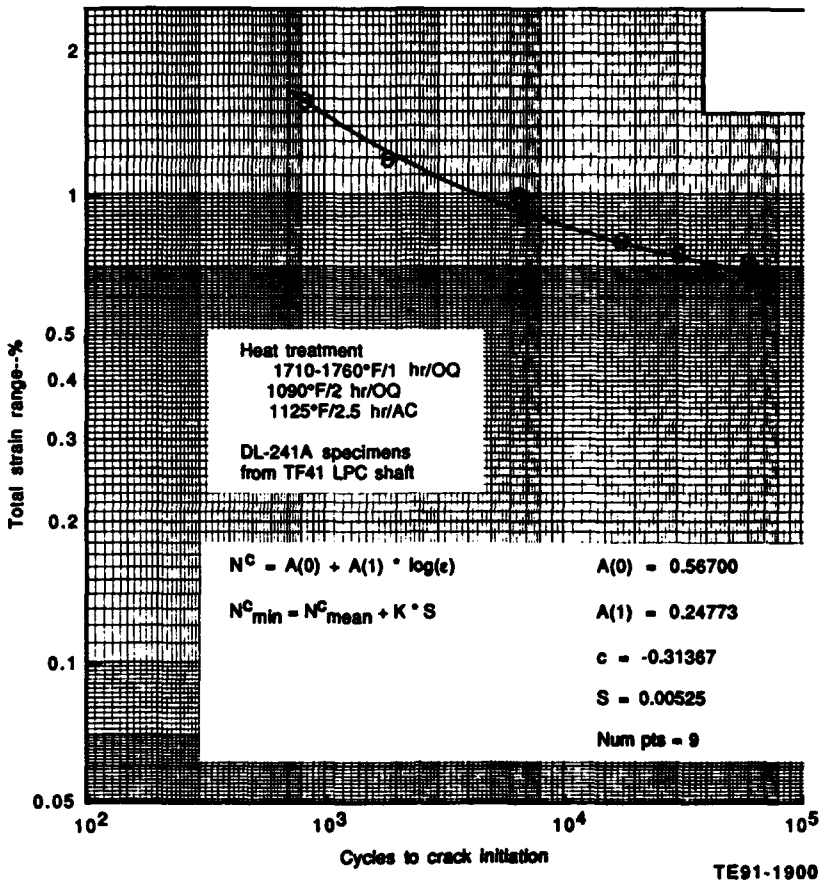

Fig. 7-15. EMS 64500 LCF data - 78°F, R=-1.0, KT=1.0.

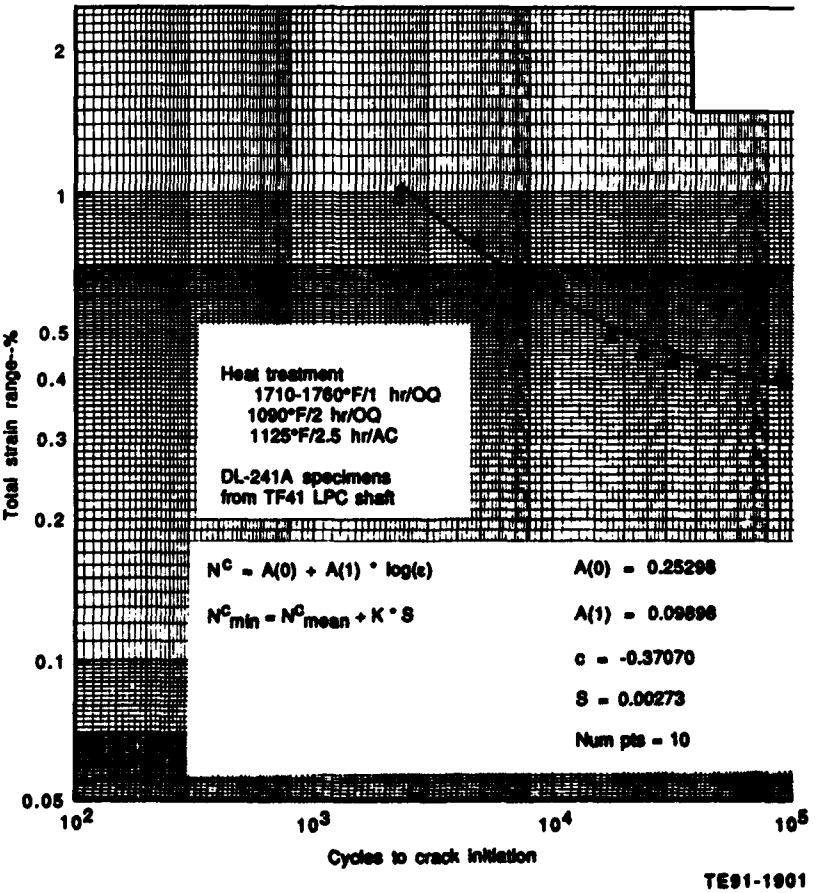

Fig. 7-16. EMS 64500 LCF data - 78°F, R = 0.6, KT = 1.0.

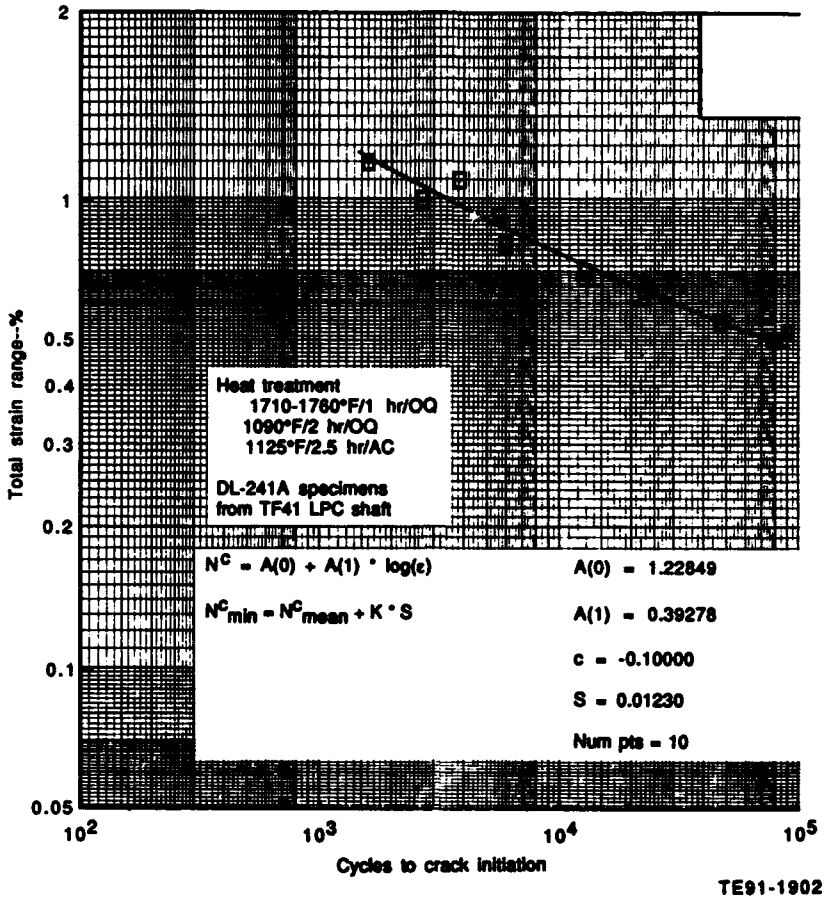

Fig. 7-17. EMS 64500 LCF data - 78°F, R= 0.0, KT = 1.0

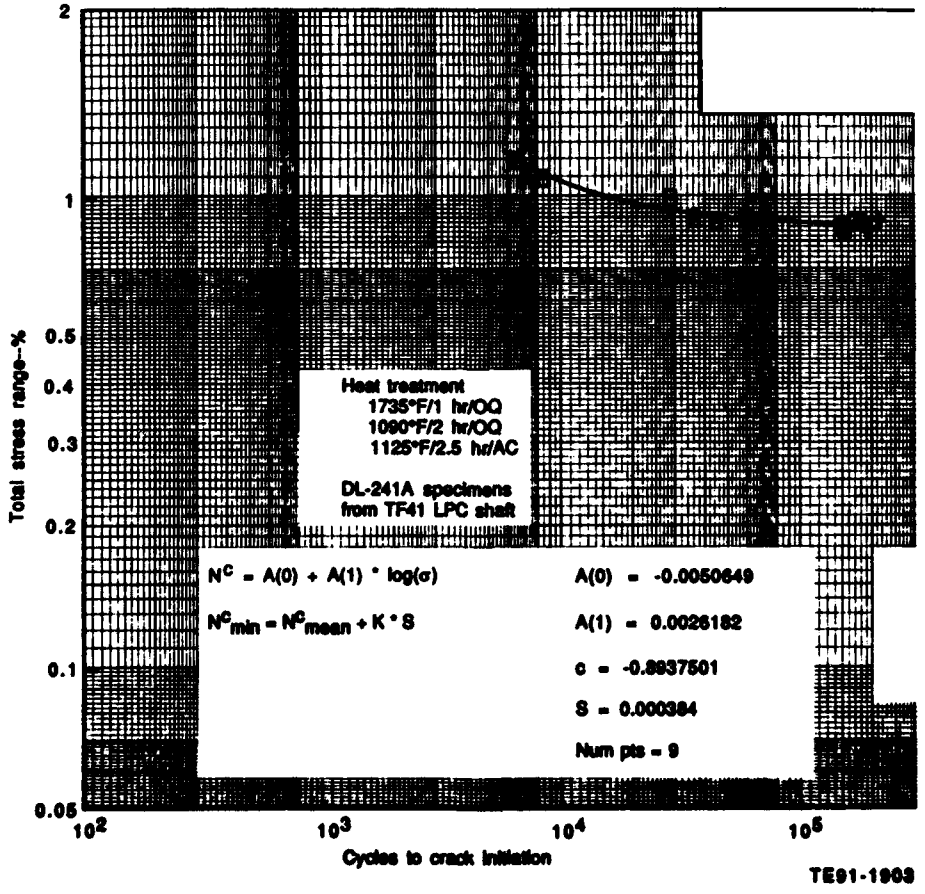

Fig. 7-18. EMS 64500 LCF data - 78°F, R = 0.0, KT = 2.0.

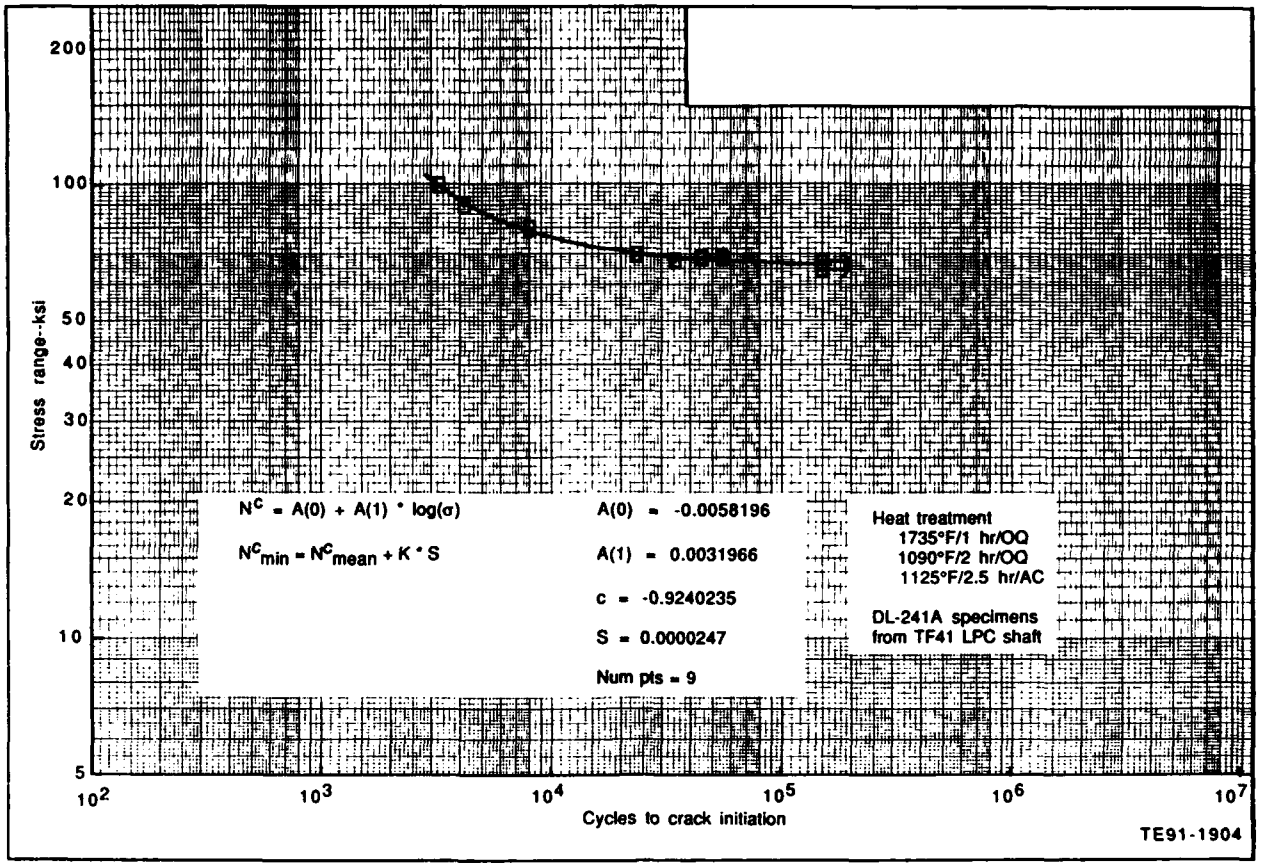

Fig. 7-19. EMS 64500 LCF data - 78°F, R = 0.0, KT = 3.0

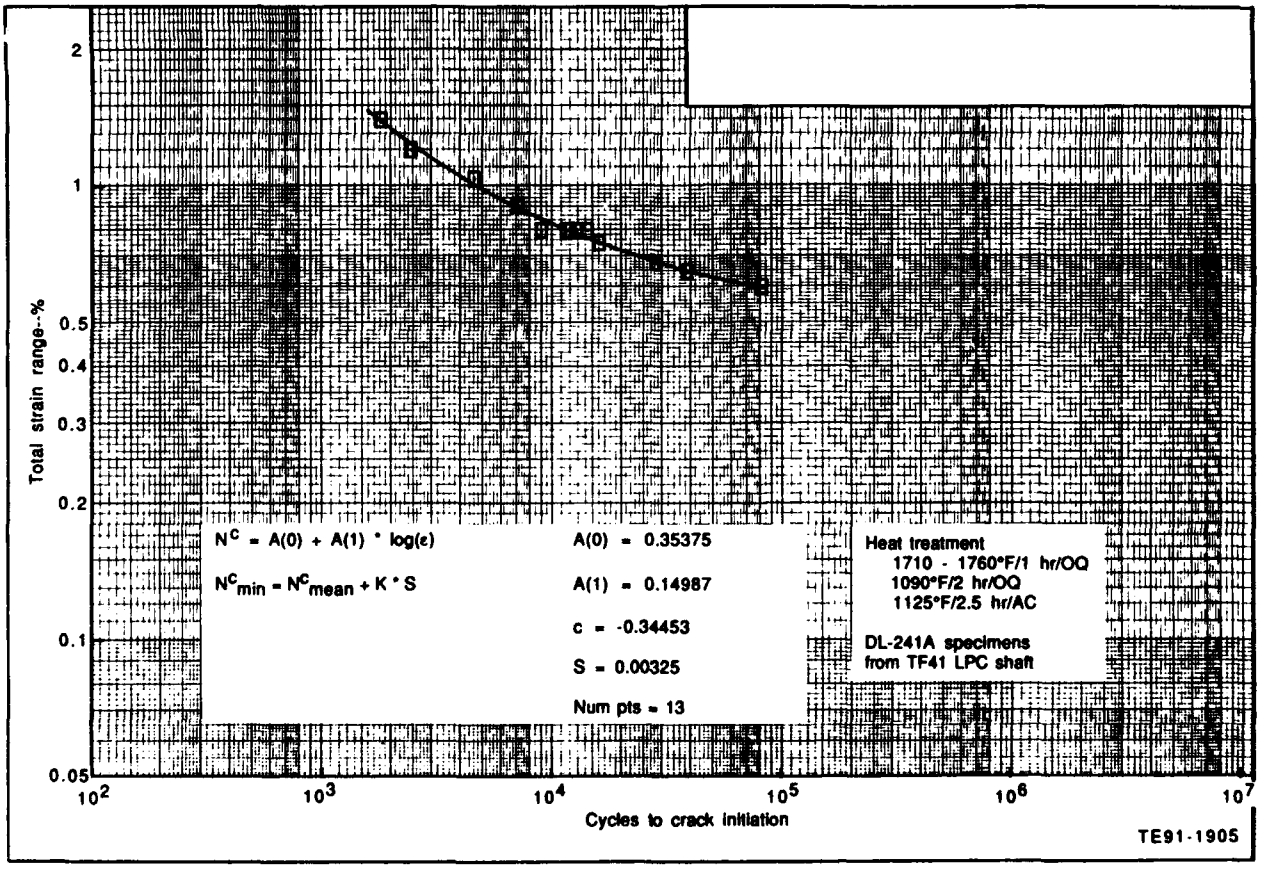

Fig. 7-20. EMS 64500 LCF data - 500°F, R= 0.0, KT = 1.0

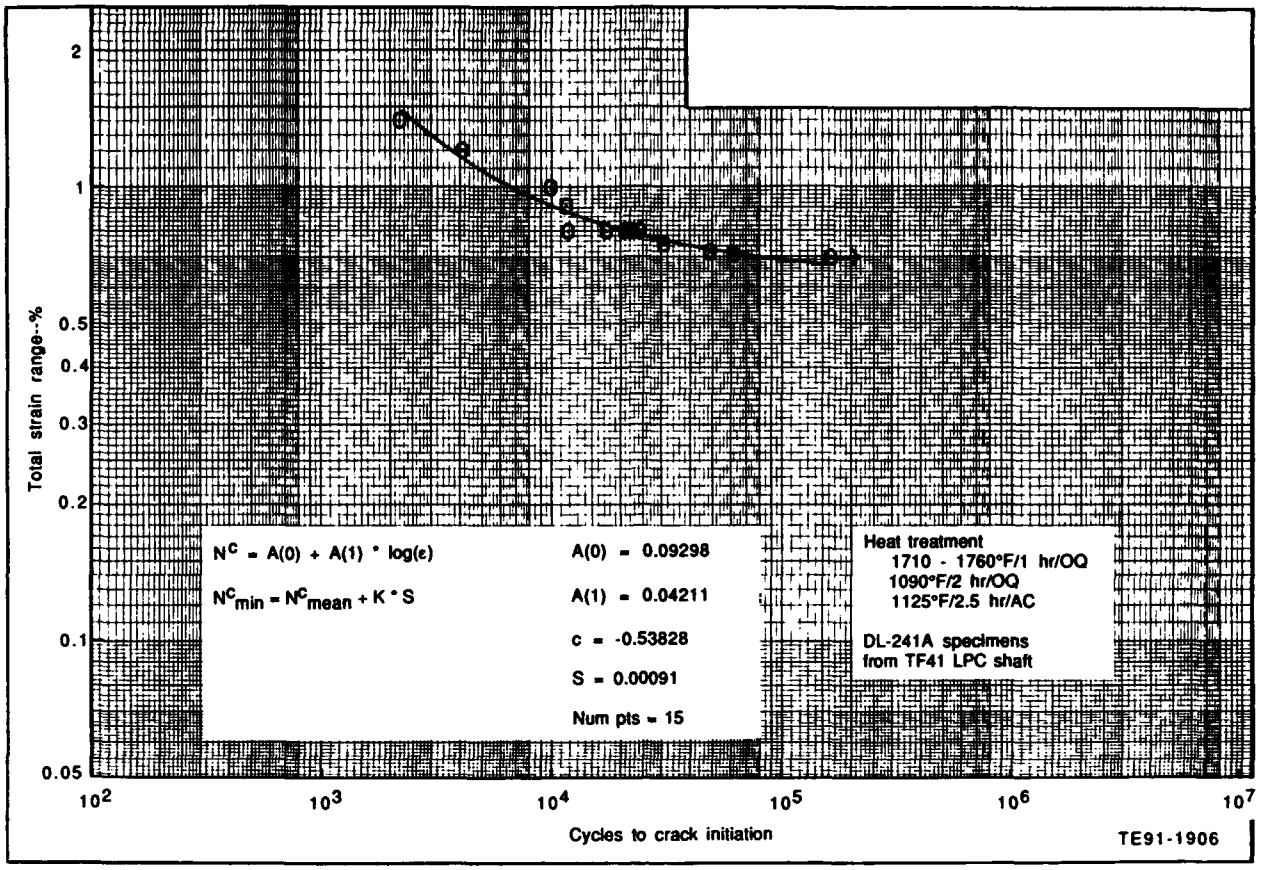

Fig. 7-21. EMS 64500 LCF data - 500°F, R = -1.0, KT = 1.0

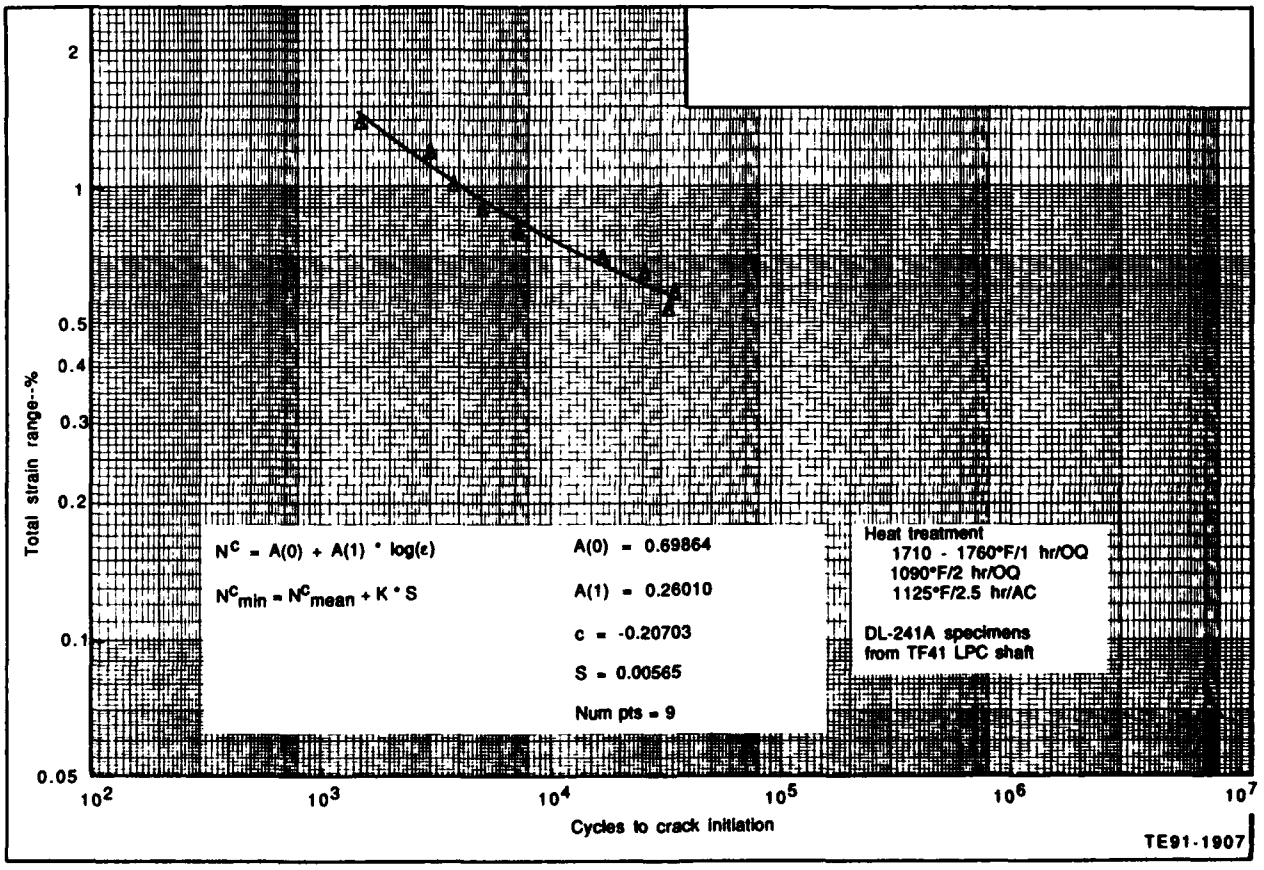

Fig. 7-22. EMS 64500 LCF data - 500°F, R = 0.6, KT = 1.0

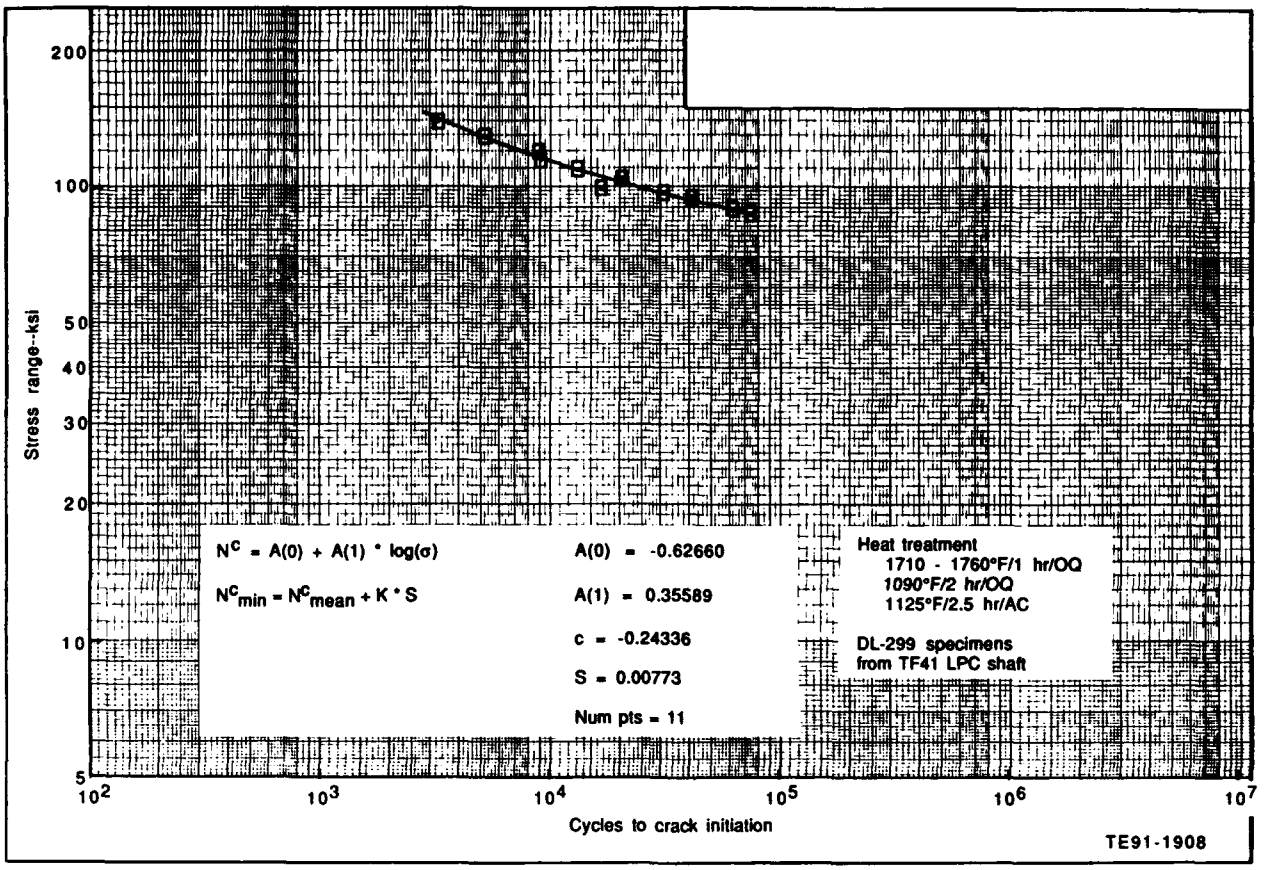

Fig. 7-23. EMS 64500 LCF data - 500°F, R = 0.0, KT = 2.0.

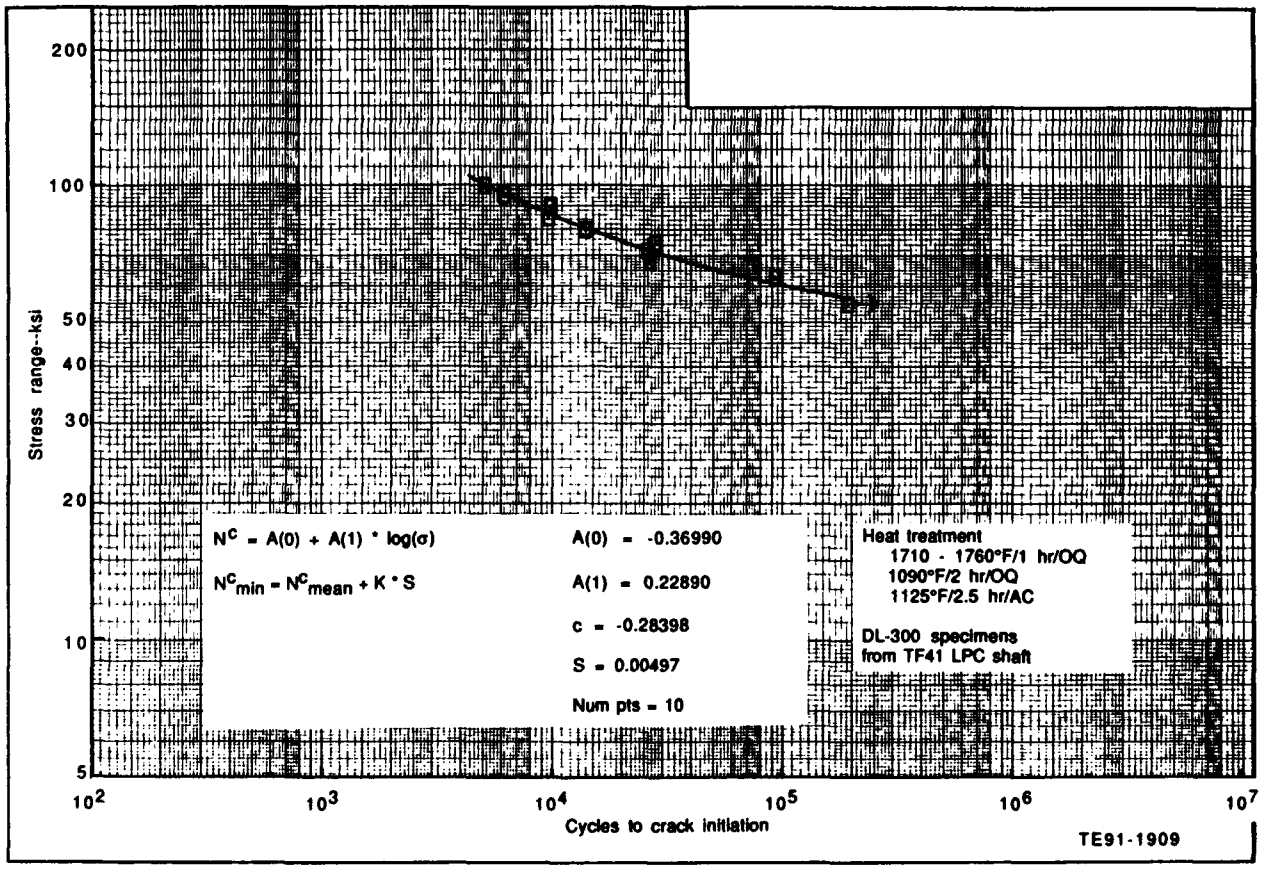

Fig. 7-24. EMS 64500 LCF data - 500°F, R = 0.0, KT = 3.0.

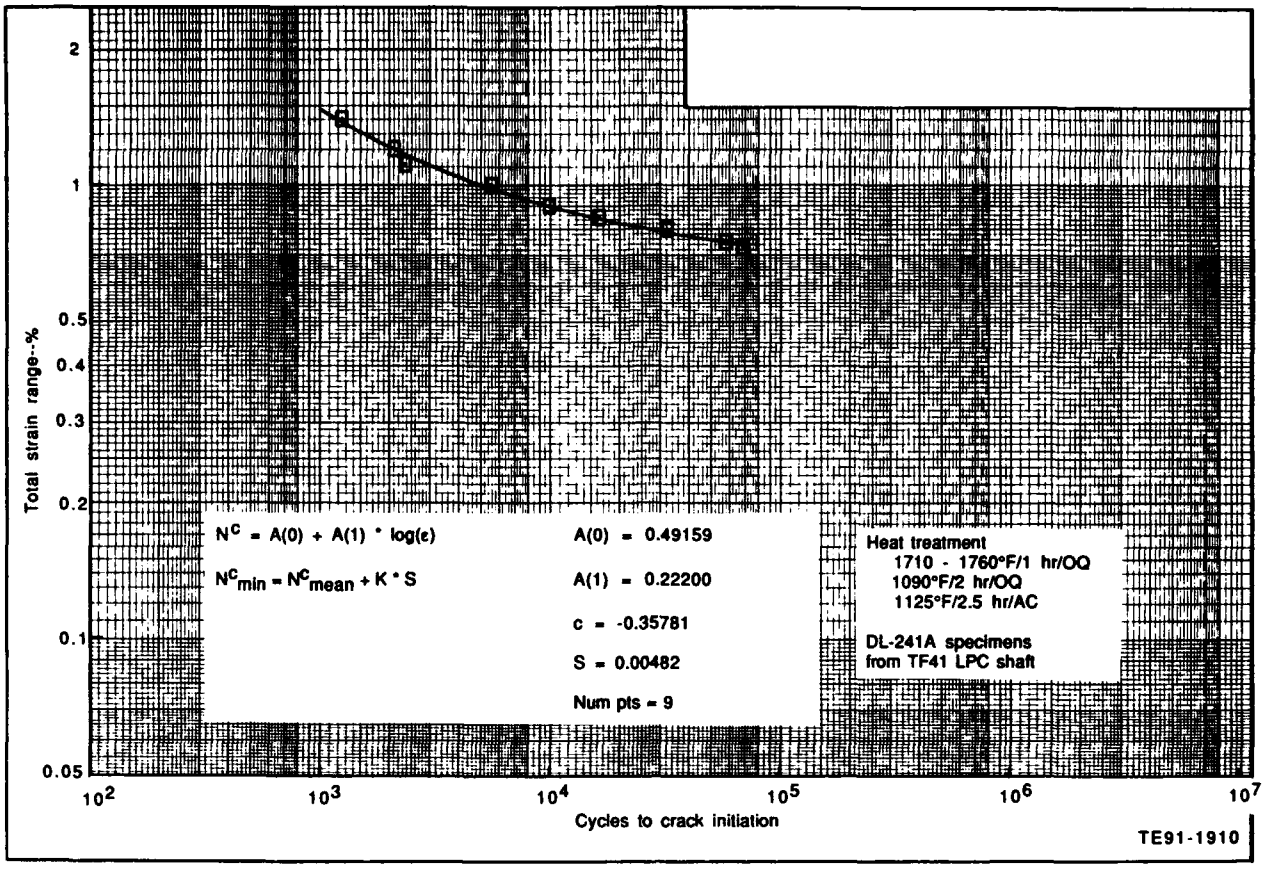

Fig. 7-25. EMS 64500 LCF data - 850°F, R = 0.0, KT = 1.0.

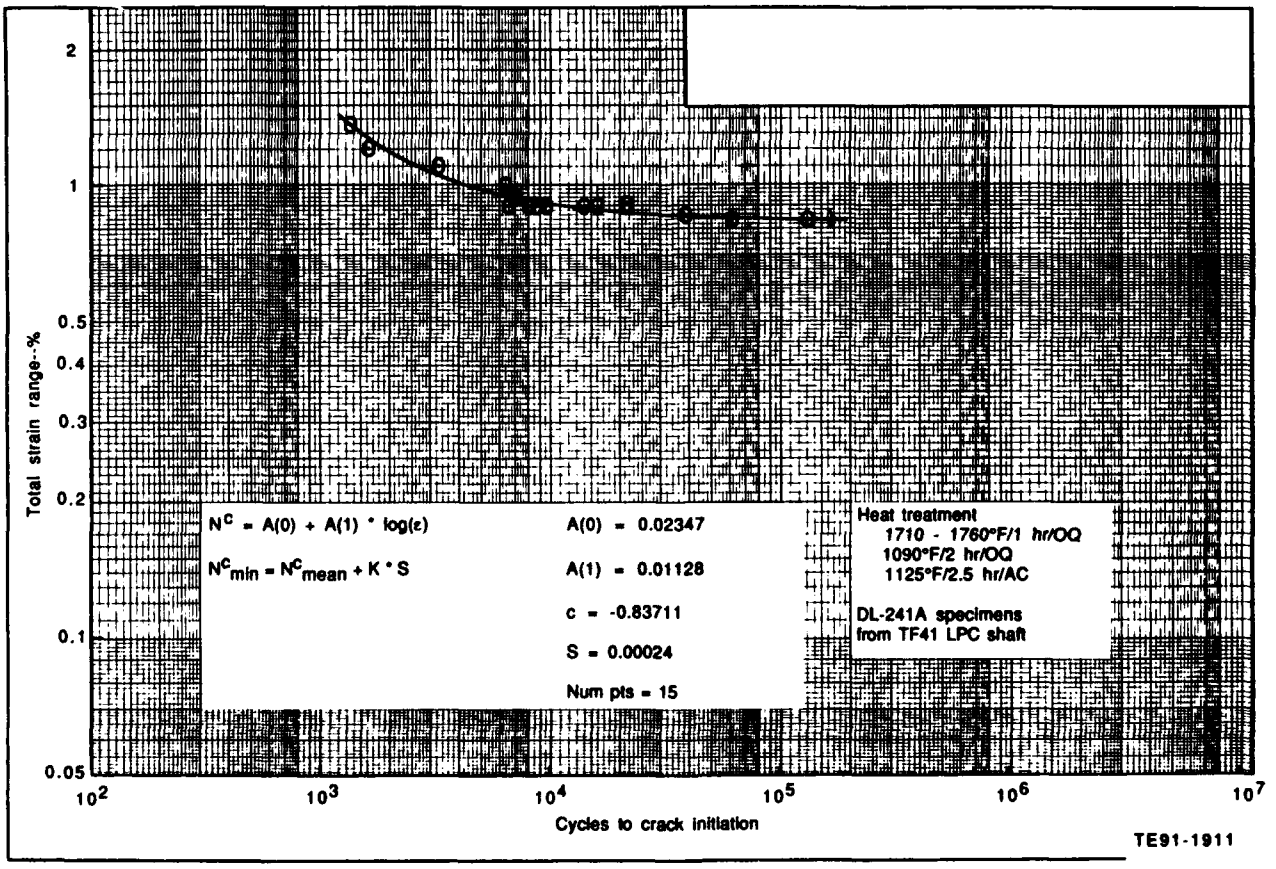

Fig. 7-26. EMS 64500 LCF data - 850°F, R = 1.0, KT = 1.0.

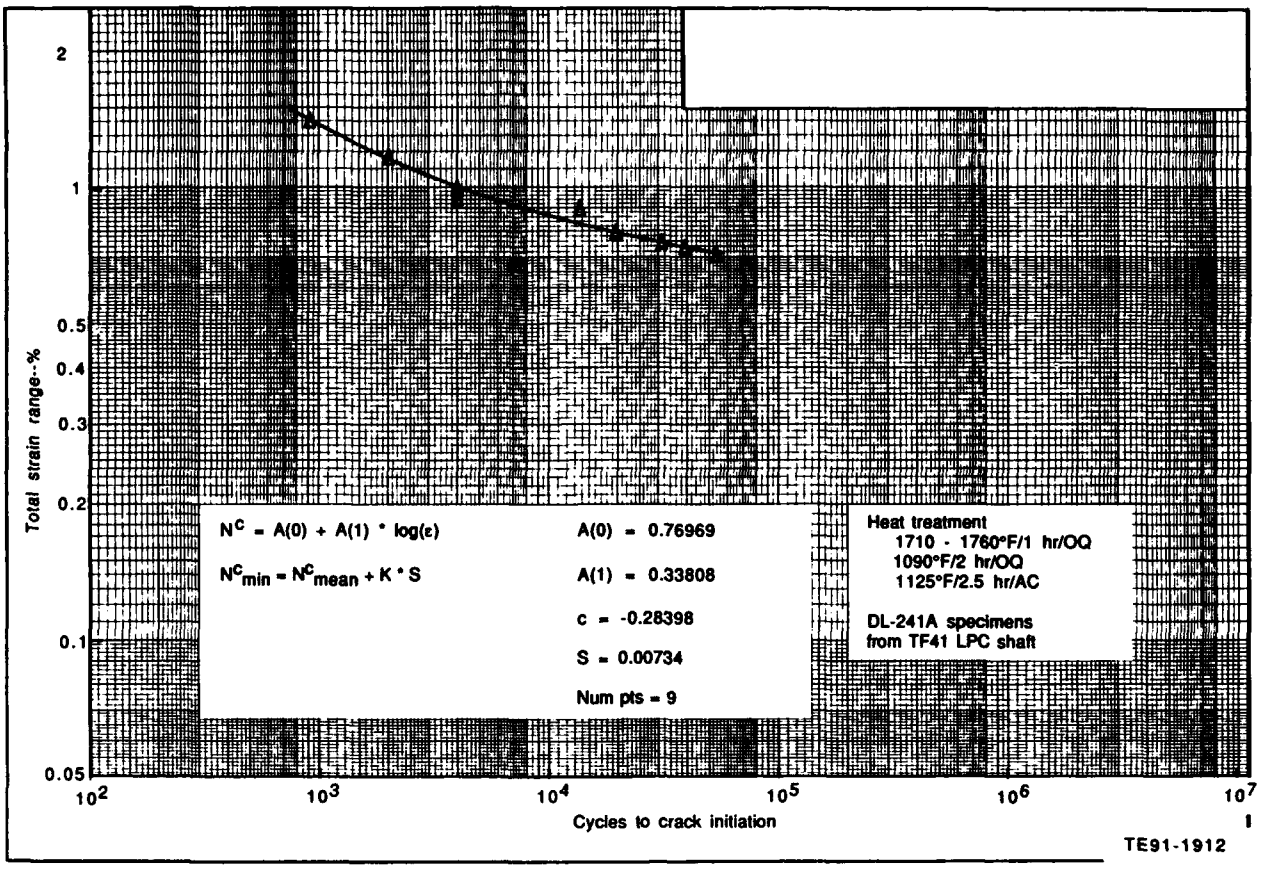

Fig. 7-27. EMS 64500 LCF data - 850°F, R = 0.6, KT = 1.0.

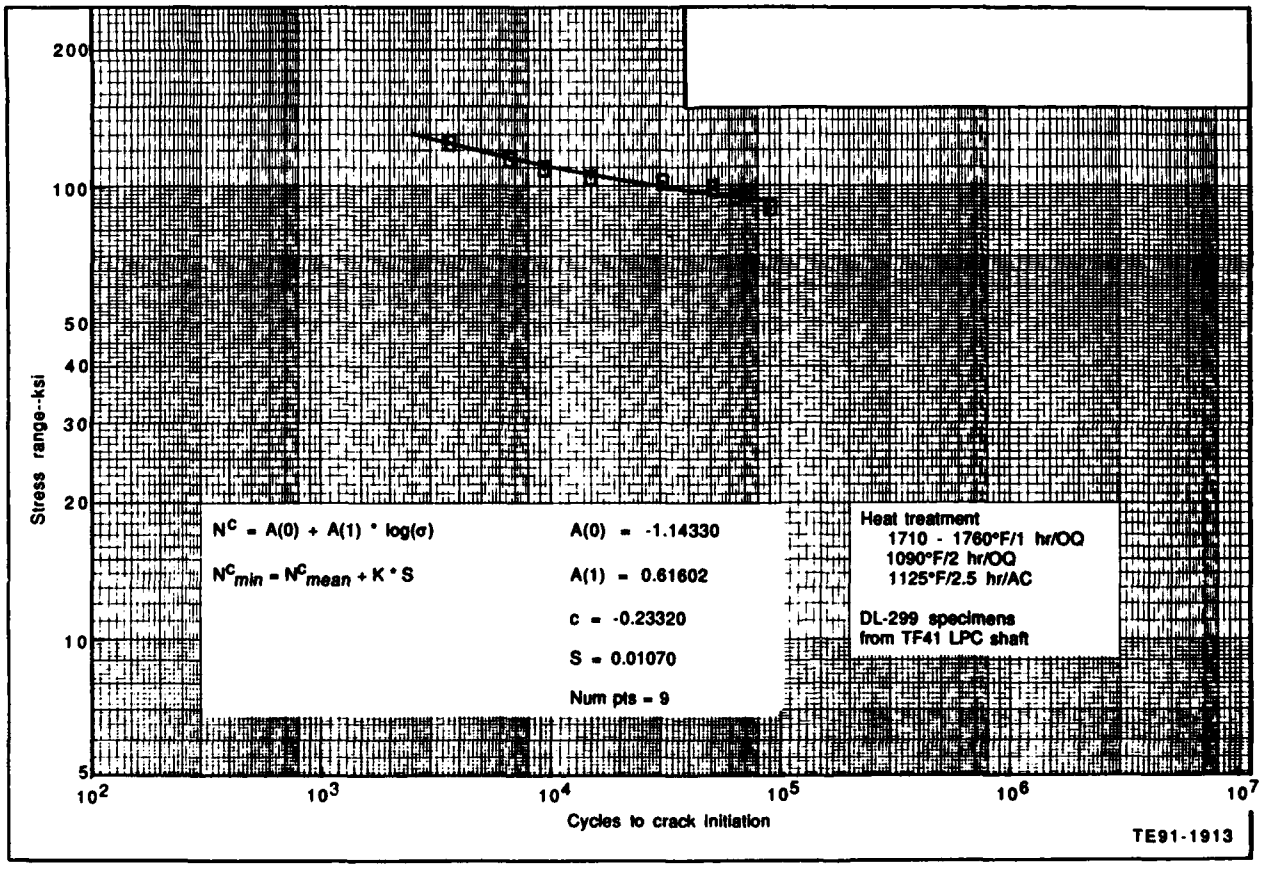

Fig. 7-28. EMS 64500 LCF data - 850°F, R = 0.0, KT = 2.0.

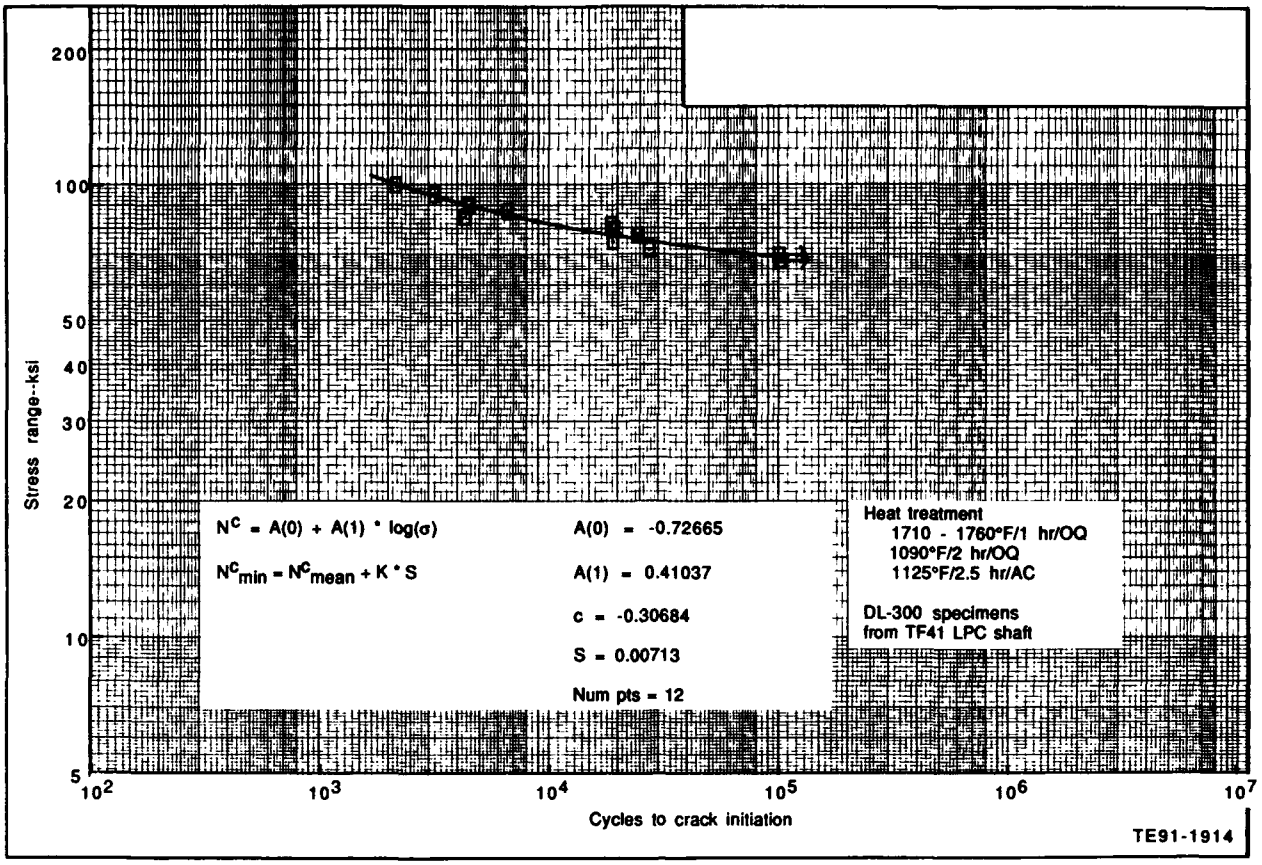

Fig. 7-29. EMS 64500 LCF data - 850°F, R = 0.0, KT = 3.0.

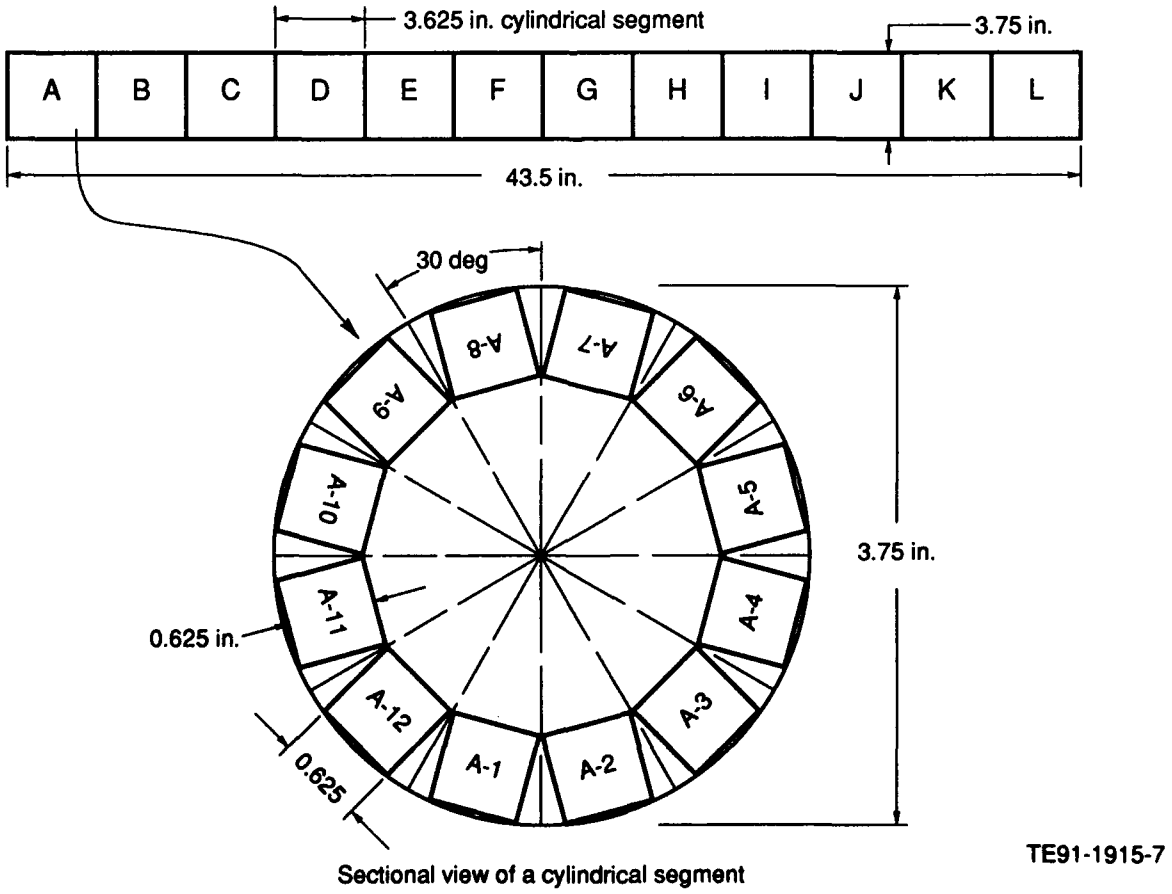

Fig. 7-30. Cut up diagram for EMS 64500 TF41 LPC shaft.

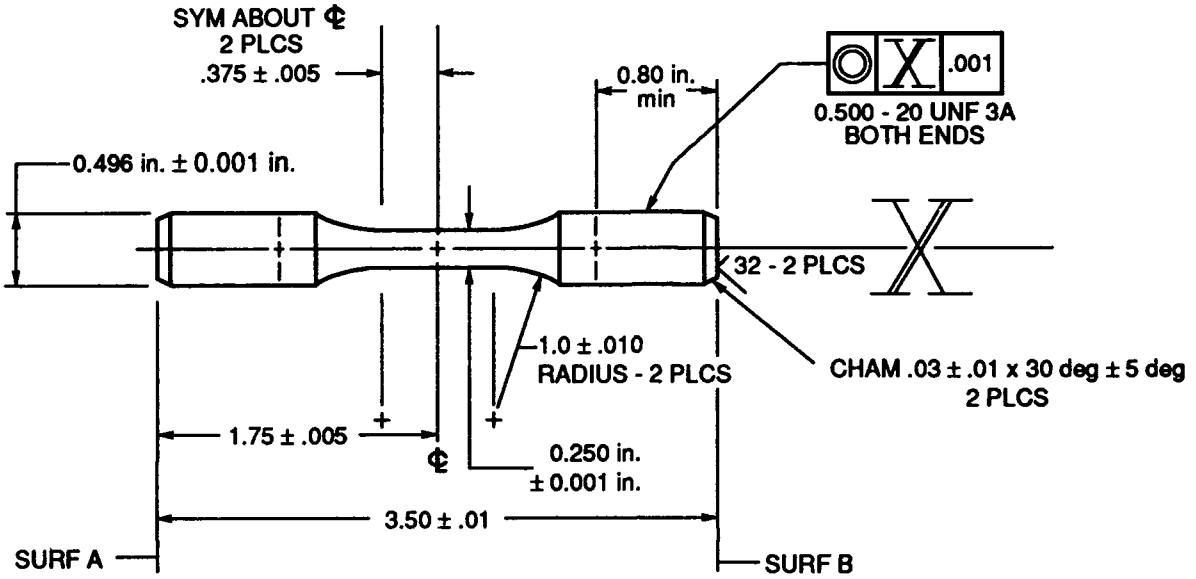

Notes:
1. Surfaces A & B to be ground parallel within 0.001 in.
2. Surfaces A & B to be flat and perpendicular to X within 0.0005 T.I.R.
3. Radius and gage section to blend smoothly without undercut
4. All diameters to be concentric within 0.001 T.I.R.
5. Radius and gage section to be finished as specified

TE91-1916-7

Fig. 7-31. LCF uniform machined test specimen.

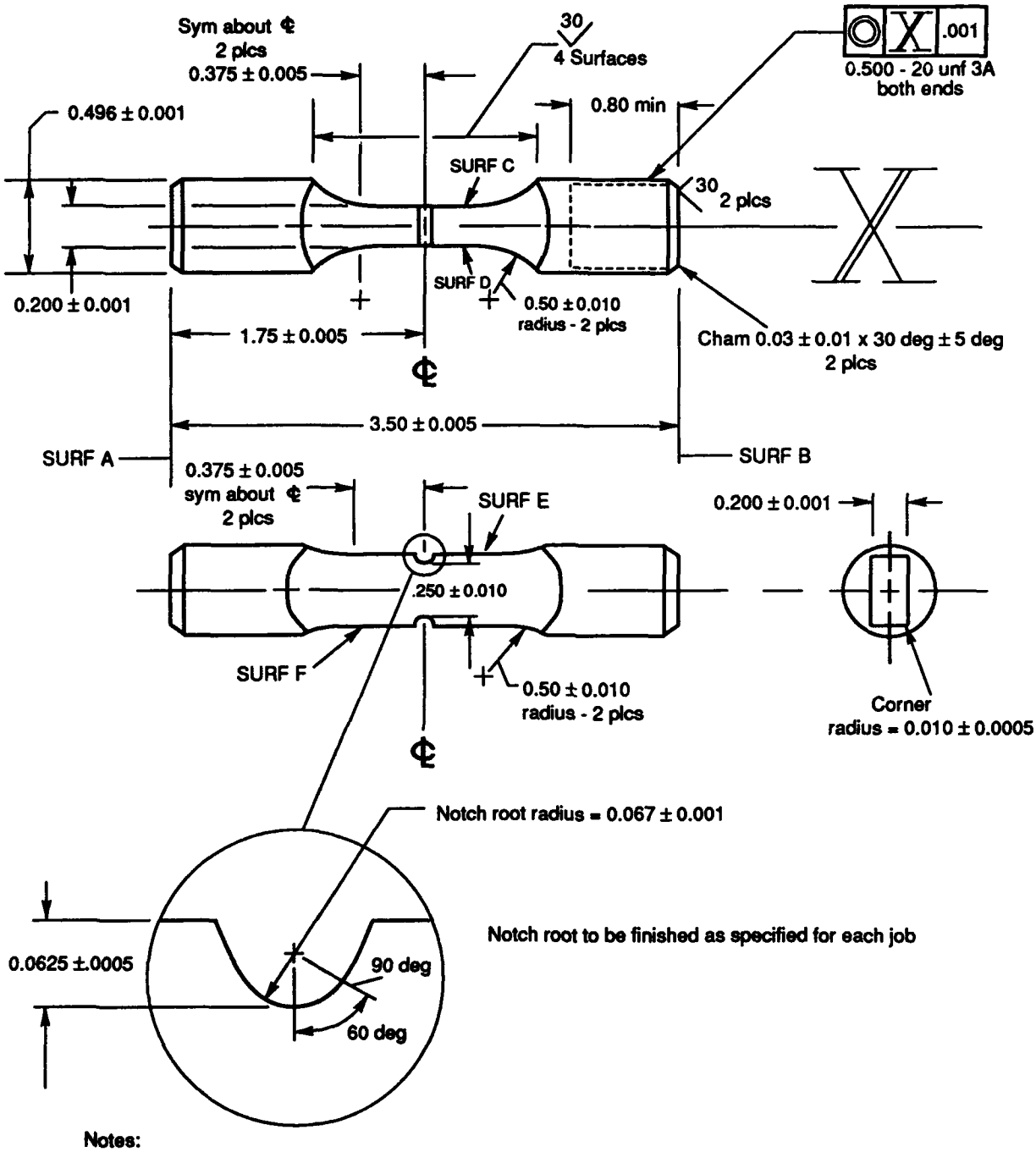

Notes:

1. Surfaces A & B parallel within 0.001 in.
2. Grind A & B flat and perpendicular to X within 0.0005 T.I.R.
3. C & D and E & F parallel to, and equidistant from X within 0.001in.
4. Radius and gage section to blend smoothly, no undercut
5. Centerline of notches on surfaces E & F are not to be axially displaced by more than 0.001 in. of each other

TE91-1917-7

Fig. 7-32. Notched flat LCF specimen - KT = 2.0.

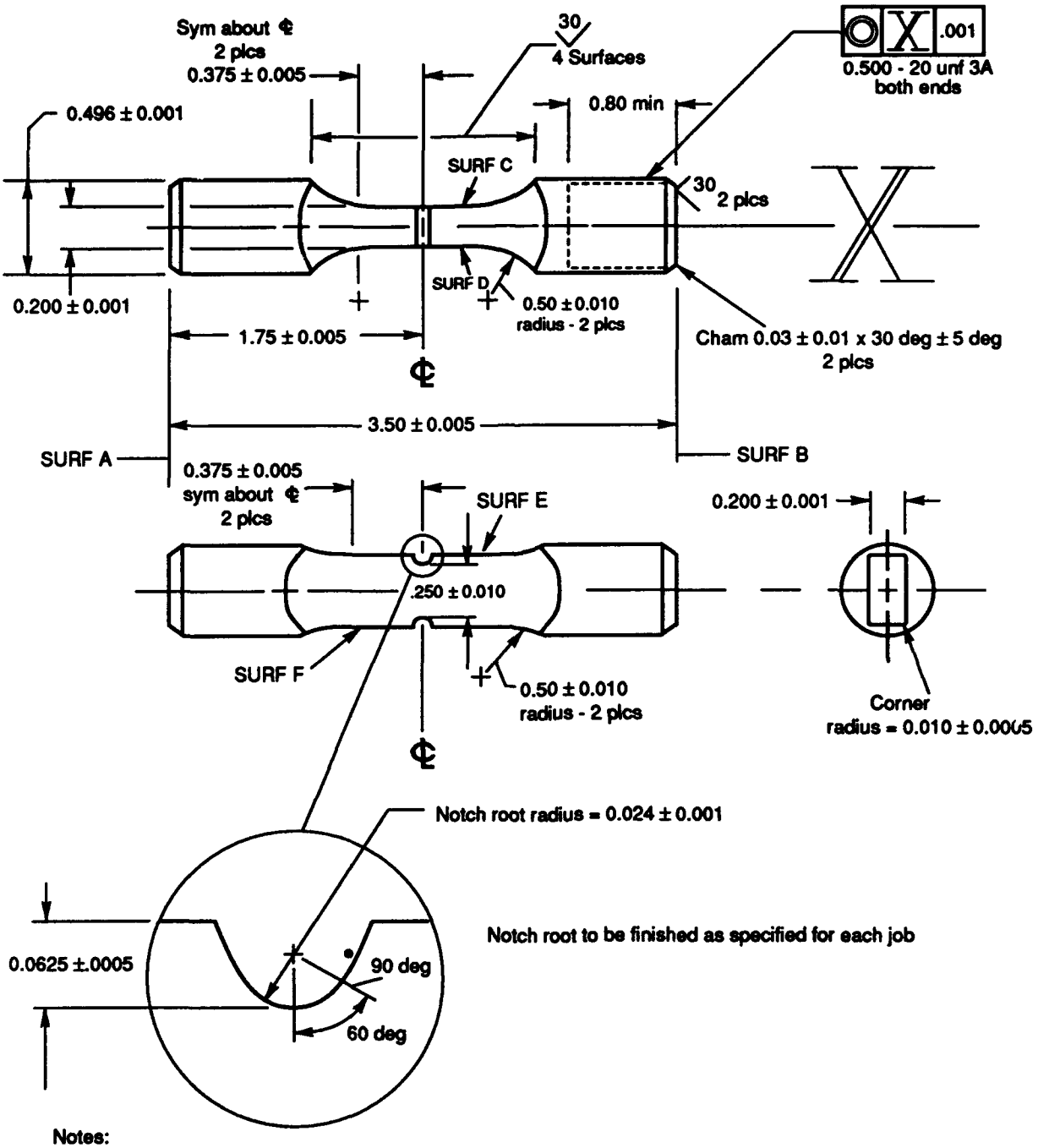

Notes:

1. Surfaces A & B parallel within 0.001 in.
2. Grind A & B flat and perpendicular to X within 0.0005 T.I.R.
3. C & D and E & F parallel to, and equidistant from X within 0.001in.
4. Radius and gage section to blend smoothly, no undercut
5. Centerline of notches on surfaces E & F are not to be axially displaced by more than 0.001 in. of each other

TE91-1918-7

Fig. 7-33. Notched flat LCF specimen - KT = 3.0.

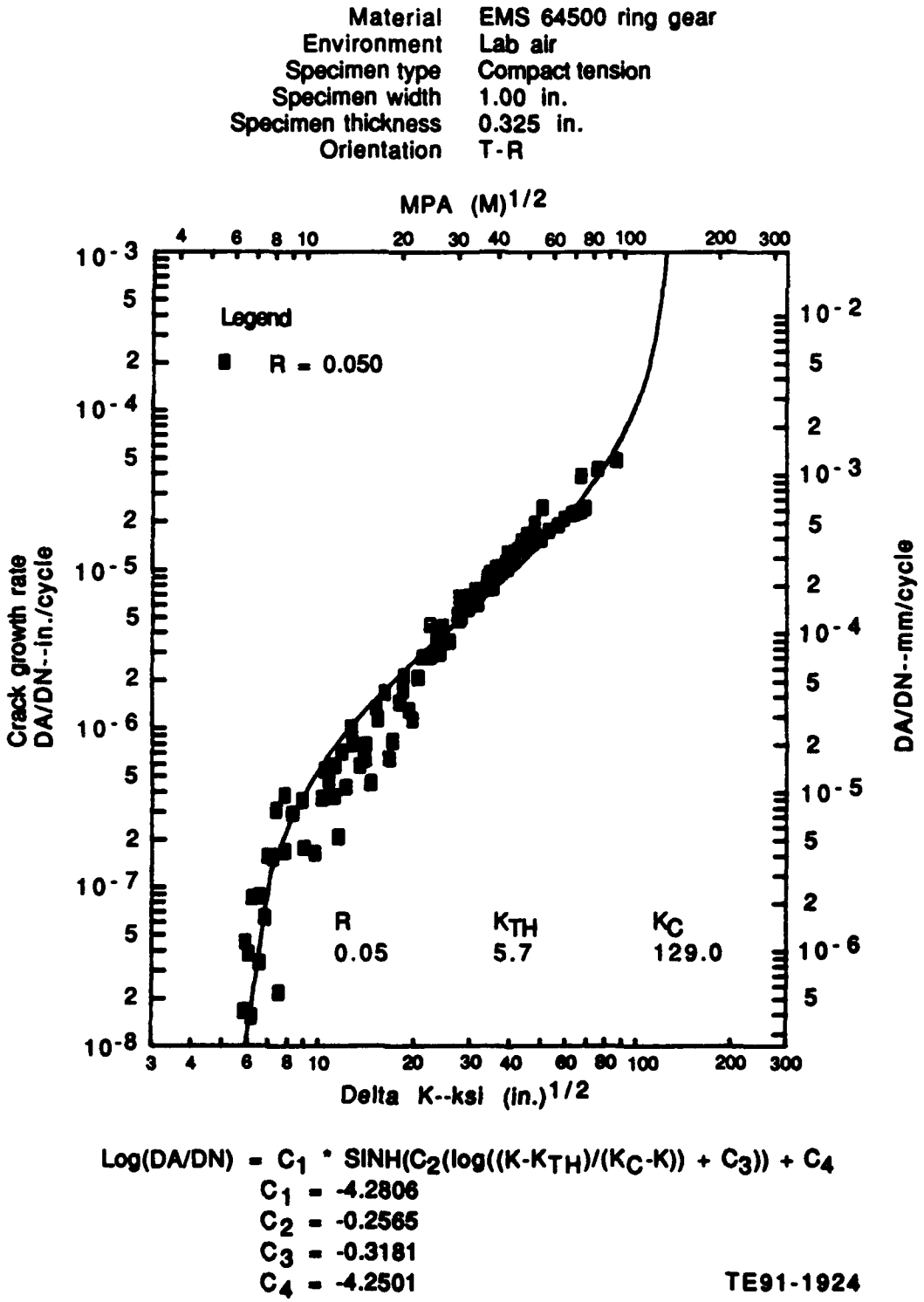

Fig. 7-34. Fatigue crack growth of EMS 64500 at 200°F - compact tension.

FCGR OF EMS 64500 AT 200F
FREQUENCY = 5 HZ

EMS 64500 RING GEAR
LAB AIR
COMPACT TENSION SPECIMEN
1.0" SPECIMEN WIDTH
0.325" SPECIMEN THICKNESS
T-R ORIENTATION

DA/DN	DELTA K	DA/DN	DELTA K
0.166000E-07	0.585000E+01	0.437000E-05	0.245000E+02
0.153000E-07	0.618000E+01	0.478000E-05	0.276000E+02
0.217000E-07	0.752000E+01	0.519^00E-05	0.272000E+02
0.332000E-07	0.653000E+01	0.590000E-05	0.277000E+02
0.378000E-07	0.604000E+01	0.670000E-05	0.275000E+02
0.449000E-07	0.591000E+01	0.676000E-05	0.298000E+02
0.645999E-07	0.680000E+01	0.564000E-05	0.294000E+02
0.856999E-07	0.621000E+01	0.505000E-05	0.280000E+02
0.872000E-07	0.653000E+01	0.585000E-05	0.280000E+02
0.156000E-06	0.692000E+01	0.601000E-05	0.313000E+02
0.158000E-06	0.712000E+01	0.617000E-05	0.315000E+02
0.152000E-06	0.718000E+01	0.721000E-05	0.310000E+02
0.168000E-06	0.783000E+01	0.664000E-05	0.297000E+02
0.177000E-06	0.897000E+01	0.741000E-05	0.310000E+02
0.163000E-06	0.969000E+01	0.768000E-05	0.335000E+02
0.207000E-06	0.115000E+02	0.761000E-05	0.351000E+02
0.378000E-06	0.779000E+01	0.864999E-05	0.348000E+02
0.306000E-06	0.735000E+01	0.954999E-05	0.345000E+02
0.290000E-06	0.827000E+01	0.102000E-04	0.359000E+02
0.351000E-06	0.885000E+01	0.110000E-04	0.388000E+02
0.364000E-06	0.102000E+02	0.104000E-04	0.391000E+02
0.466000E-06	0.107000E+02	0.101000E-04	0.391000E+02
0.544000E-06	0.104000E+02	0.896999E-05	0.359000E+02
0.579000E-06	0.112000E+02	0.810999E-05	0.346000E+02
0.371000E-06	0.111000E+02	0.904999E-05	0.338000E+02
0.425000E-06	0.121000E+02	0.100000E-04	0.376000E+02
0.453000E-06	0.145000E+02	0.111000E-04	0.404000E+02
0.579000E-06	0.134000E+02	0.126000E-04	0.391000E+02
0.640000E-06	0.139000E+02	0.129000E-04	0.411000E+02
0.708000E-06	0.118000E+02	0.133000E-04	0.423000E+02
0.797000E-06	0.127000E+02	0.151000E-04	0.433000E+02
0.101000E-05	0.126000E+02	0.156000E-04	0.459000E+02
0.782000E-06	0.140000E+02	0.155000E-04	0.465000E+02
0.646000E-06	0.166000E+02	0.163000E-04	0.478000E+02
0.833000E-06	0.170000E+02	0.165000E-04	0.449000E+02
0.114000E-05	0.153001E+02	0.141000E-04	0.451000E+02
0.133000E-05	0.151002E+02	0.196000E-04	0.476000E+02
0.168000E-05	0.161000E+02	0.246000E-04	0.503000E+02
0.145000E-05	0.179000E+02	0.156000E-04	0.500000E+02
0.173000E-05	0.184000E+02	0.176000E-04	0.528000E+02
0.130000E-05	0.192000E+02	0.191000E-04	0.563000E+02
0.113000E-05	0.197000E+02	0.209000E-04	0.589000E+02
0.213000E-05	0.185000E+02	0.225000E-04	0.622000E+02
0.209000E-05	0.206000E+02	0.227000E-04	0.639000E+02
0.282000E-05	0.212000E+02	0.233000E-04	0.663000E+02
0.282000E-05	0.225000E+02	0.244000E-04	0.688000E+02
0.295000E-05	0.240000E+02	0.385000E-04	0.666000E+02
0.348000E-05	0.234000E+02	0.429000E-04	0.753000E+02
0.378000E-05	0.234000E+02	0.487000E-04	0.863000E+02
0.445000E-05	0.223000E+02		
0.351000E-05	0.258000E+02		TE91-1925

Fig. 7-35. Tabulation of DA/DN versus delta K for EMS 64500.

Appendix A

TEST SUMMARY FOR TF41 LP COMPRESSOR SHAFT (P/N 6860005, S/N DN0092)

FOREWORD

Tests were conducted on a bench test facility in Test Cell (TC) 875 that is dedicated to the torsional evaluation of the TF41 LP mainshaft assembly. Static loading examined the stress distribution on the inside surface of the turbine shaft cooling air holes and splines, while hot fatigue tests provide experimental verification of the shaft lives.

SUMMARY

The LP mainshaft assembly BU 2 used P/N 6860005, S/N DN0092 LP compressor shaft. The shaft failed after 53,492 major and 12.9 million minor torsional fatigue cycles at elevated temperatures. The load cycle was 0 to 172.4K in-lb with ±8.6K in-lb superimposed at 4.5 Hz, and return to zero in a 69 sec period. The cracks originated in the compressor shaft's three forward cooling air holes and propagated along a line 45 deg from the shaft's axis or rotation.

DISCUSSION

Test Facility

Testing was conducted in TC 875 using the same load level, cycle, and temperature distribution as reported earlier. The test procedure and setup were identical to the previous tests.

Low Cycle, Hot Fatigue Testing

Elevated temperature fatigue testing of the LP mainshaft assembly was conducted according to the load cycle and temperature distribution previously described. The major torque level represents the intermediate power condition which the engine reportedly experiences during normal field service. The minor cycle torque was included to simulate the stresses resulting from the LP turbine shaft's torsional resonance. A frequency of 40 Hz was desired, but a 4.5 Hz was the maximum rate at which the test rig would provide the required level of torque. The minor cycle was held for 60 sec to allow for the effect of material creep. The 20K lb axial static tension load represents the separation forces seen by the shafting due to normal gas loading. The temperature distribution is based on the levels measured in test engines.

Test Results

Shaft fracture was visually detected with a magnifying glass at 53,492 major and 12.9 million minor cycles. The test was not stopped, however, until a total of 75,540 major and 18.3 million minor cycles were accumulated. Figures A-1, A-2, A-3, A-4 and A-5 describe the crack progression and change in system compliance. Magnaflux inspection indicated that the compressor shaft was cracked only in the forward oil feed holes. The helical splines of both parts, which had been lubricated with Molycote spray lubricant, were noticeably fretted.

During BU 9 there were three automatic shutdowns after 109.9 thousand major cycles, but all were within the 1% tolerance on torque.

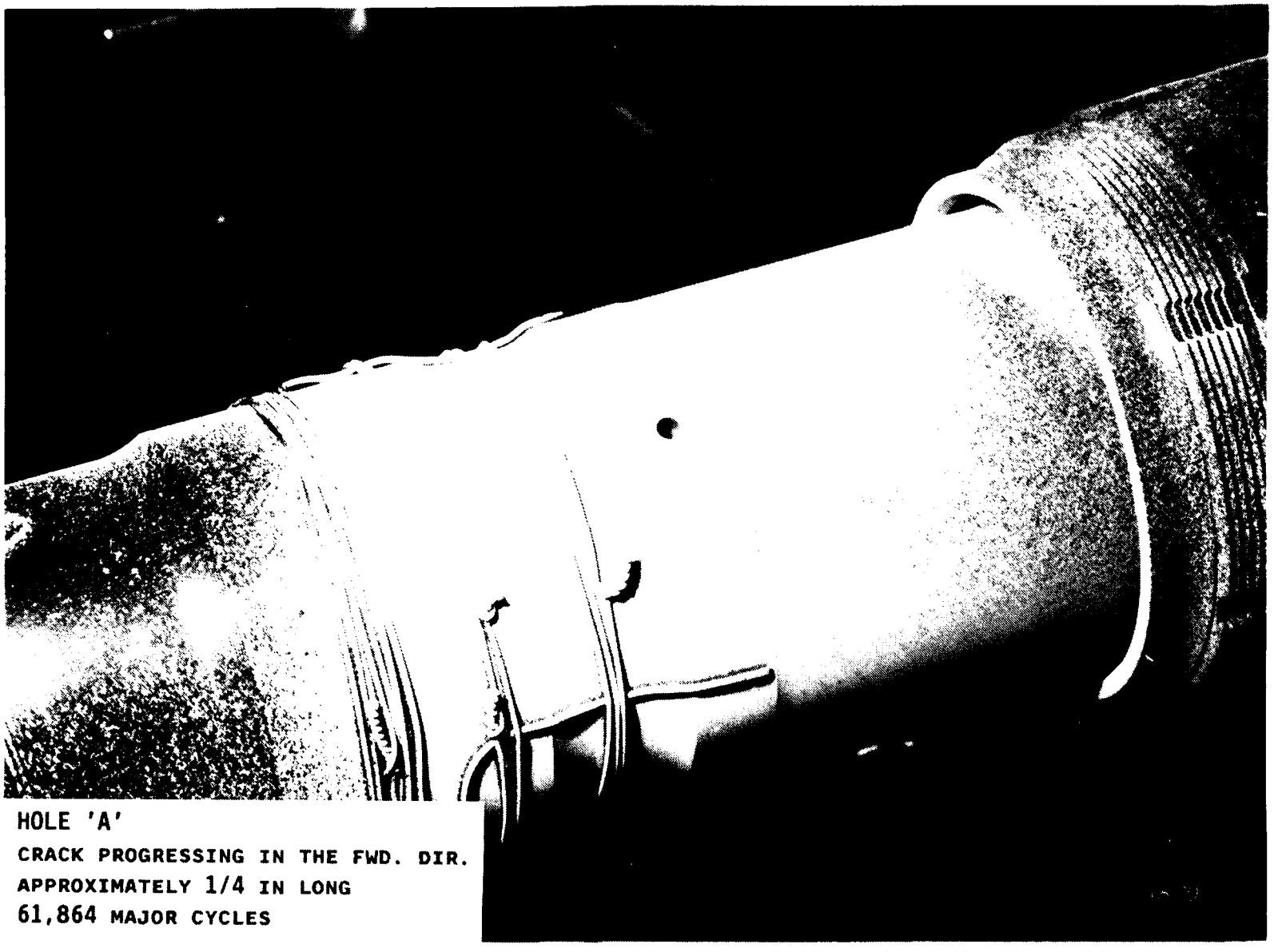

Fig. A-1. Hole 'A'--crack progressing in the forward direction; approximately 1/4 in. long, 61,864 major cycles. (Part 1 of 2)

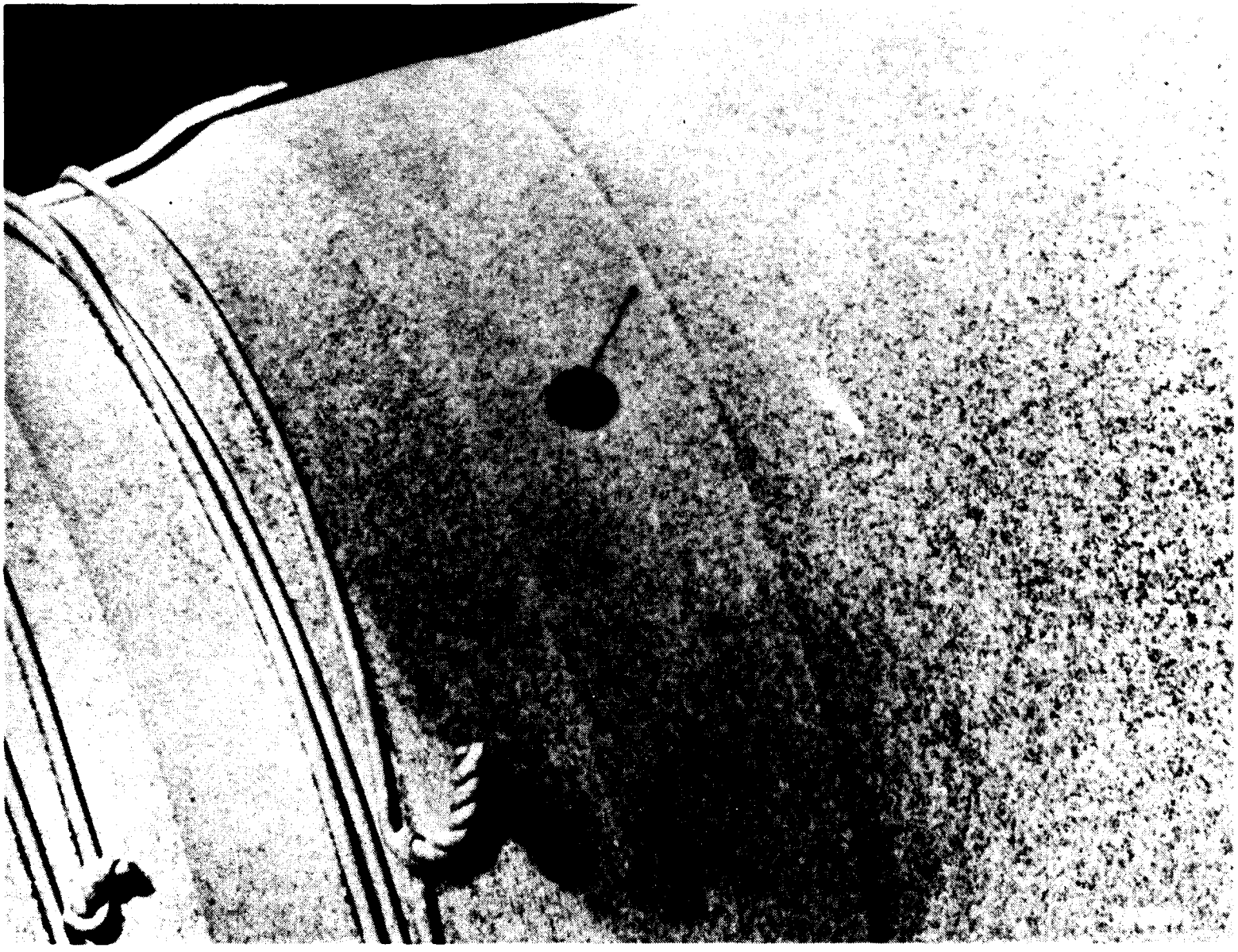

Fig. A-1. Hole 'A'--crack progressing in the forward direction; approximately 1/4 in. long, 61,864 major cycles. (Part 2 of 2)

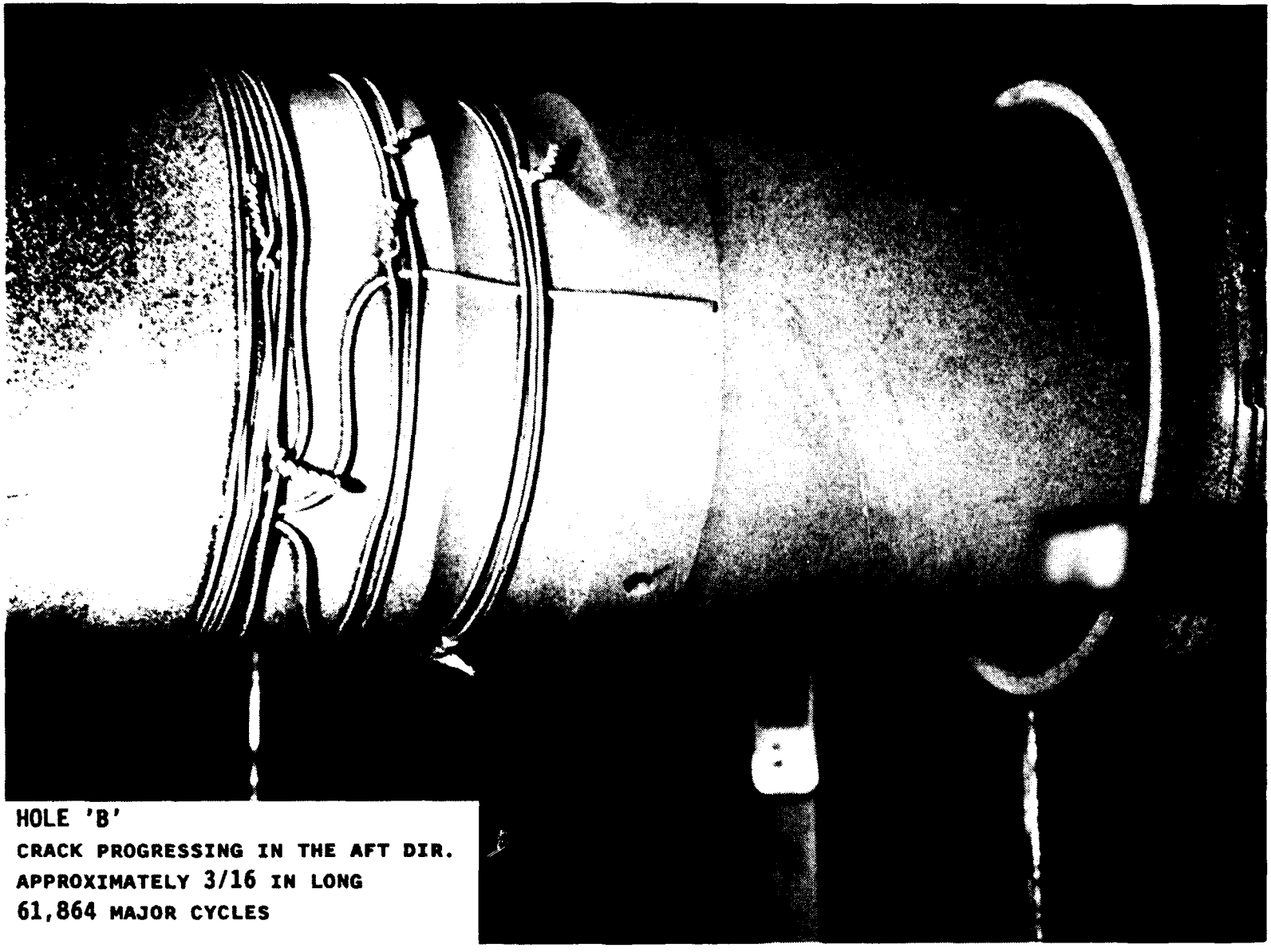

Fig. A-2. Hole 'B'--crack progressing in the aft direction; approximately 3/16 in. long, 61,864 major cycles. (Part 1 of 2)

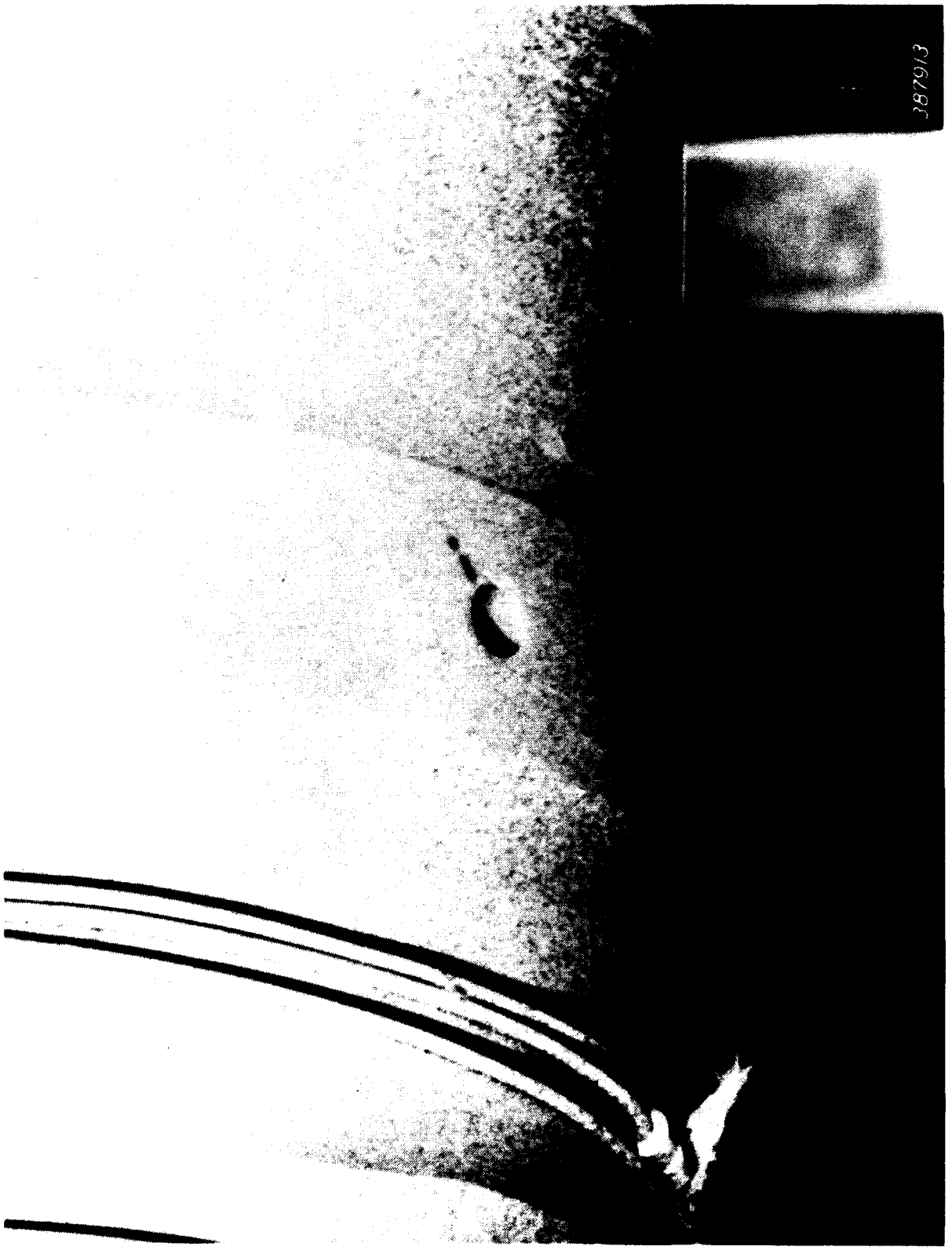

Fig. A-2. Hole 'B'--crack progressing in the aft direction; approximately 3/16 in. long, 61,864 major cycles. (Part 2 of 2)

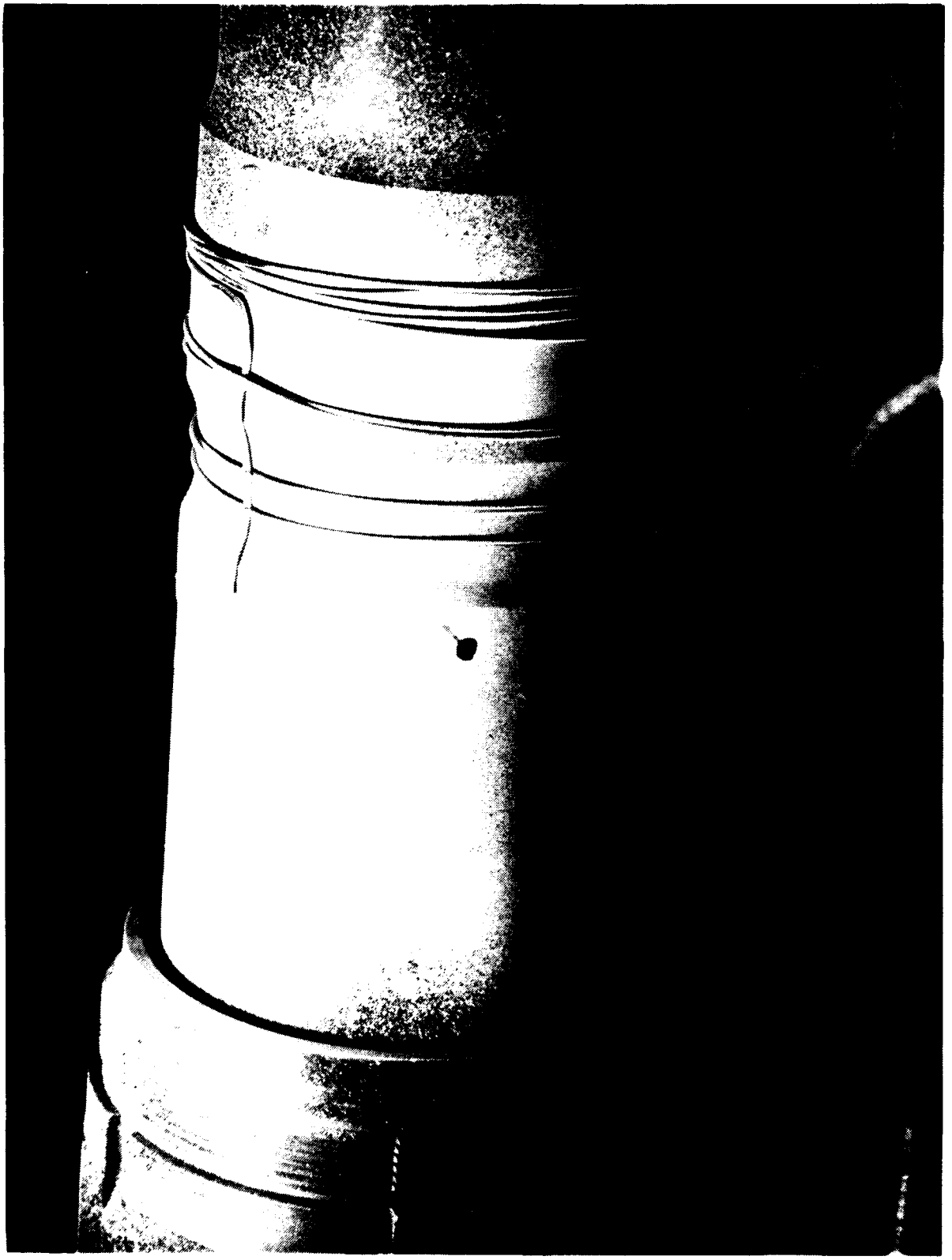

Fig. A-3. Hole 'C'--crack progressing in the aft direction; approximately 1/4 in. long, 61,864 major cycles. (Part 1 of 2)

Fig. A-3. Hole 'C'--crack progressing in the aft direction; approximately 1/4 in. long, 61,864 major cycles. (Part 2 of 2)

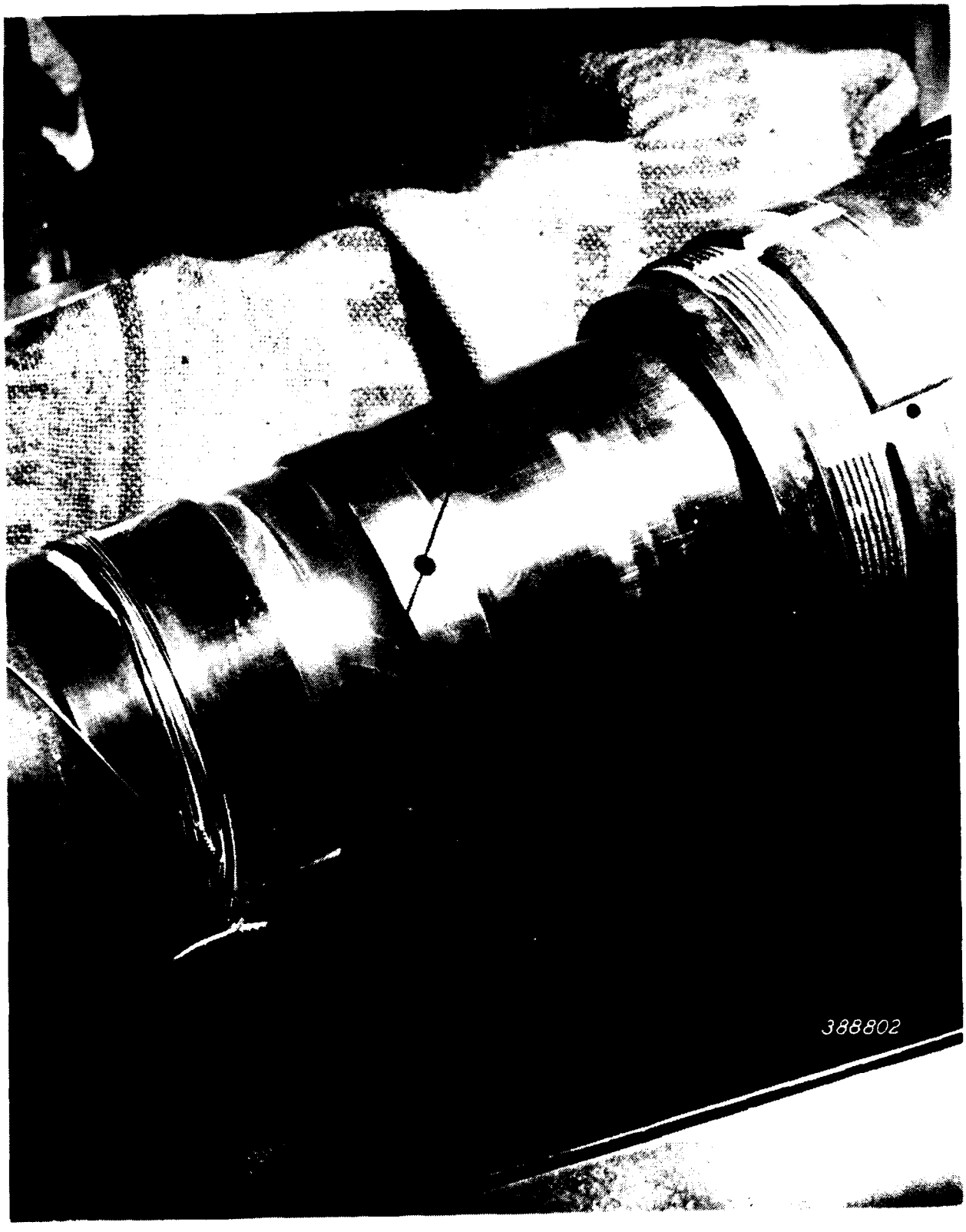

Fig. A-4. Hole 'A'--crack progressing fore and aft; 75,540 major cycles.

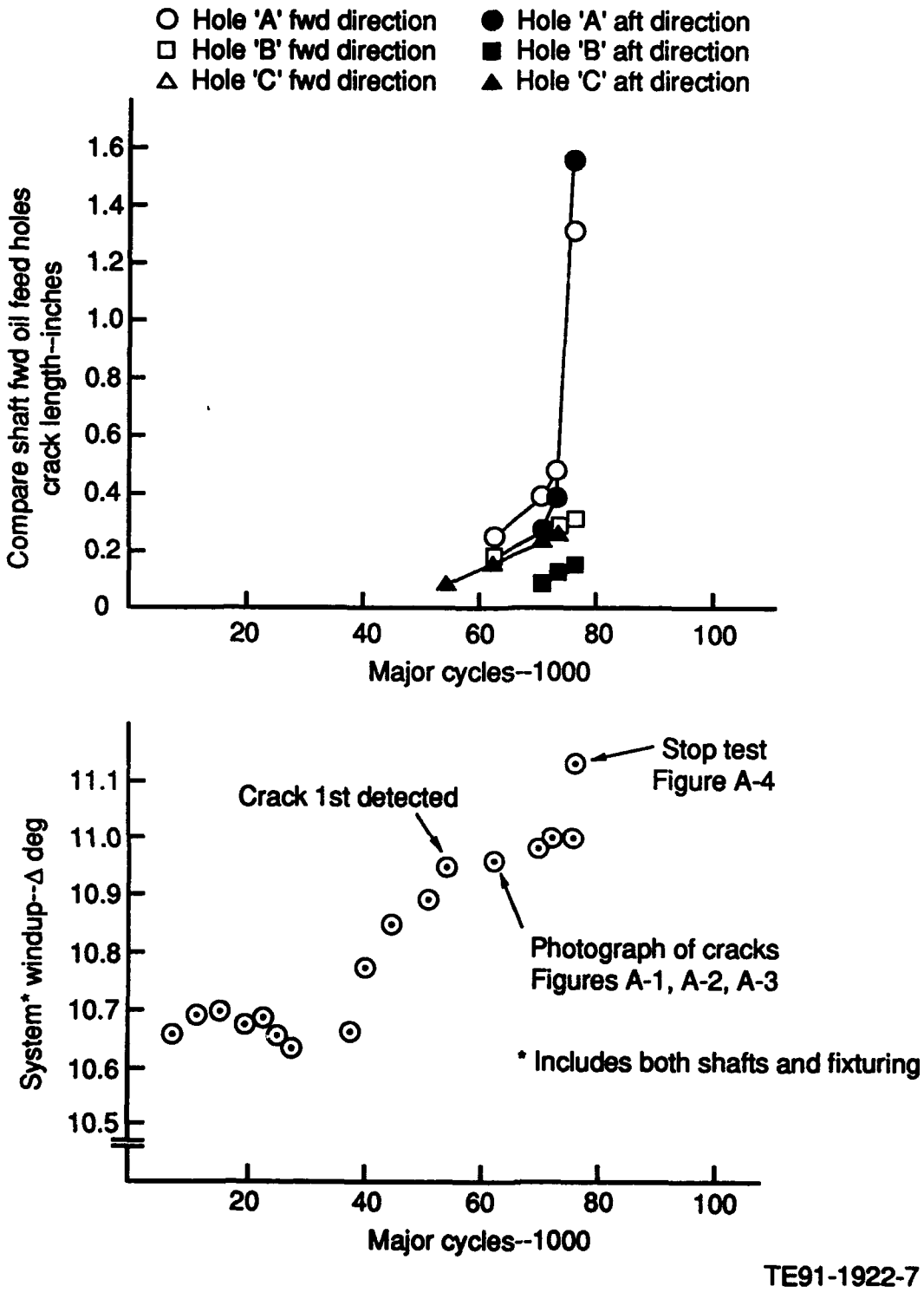

Fig. A-5. TF41 LP mainshaft LCF torsion (TC 875)--compressor shaft 686,006, DN0092, 3434 serv. hr. not B.B.; turbine shaft 6878261, KK11636, 2021 serv. hr, B.B.

The following summarizes the results of the testing:

BU	Shaft S/N	Service hours	Major cycles at 1/8 in crack	Major/minor cycles/ length at end of test
2	DN0092	3434	48K	75.5K/18.3M/1.6 in.

TEST SUMMARY FOR TF41 LP COMPRESSOR SHAFT (P/N 6860005, S/N DP10356)

This report contained results from four shaft configurations. Only one of the shafts had the configuration of interest for this lifing example. All reference to the other shafts has been removed.

FOREWORD

Low cycle torsional fatigue tests at elevated temperatures have been initiated to study the life of TF41 LP compressor shaft oil feed holes. The test facility and results of previous work were reported earlier. Testing of two additional assemblies is reported herein.

SUMMARY

The LP mainshaft assemblies failed at the compressor shaft forward oil feed holes.

- Compressor shaft 6860005, DP10356 demonstrated a shorter test life with more rapid crack propagation than that reported for shaft 6860005, DP0092. The shafts each had 3410 and 3434 service hours, respectively.

DISCUSSION

Test

Testing was conducted in TC 875 using the same load level, cycle, and temperature distribution as reported earlier.

Test Results

Failure of the test shaft resulted from cracks originating at the compressor oil feed holes and propagation fore and aft along a line 45 deg from the axis of shaft rotation. Crack growth was monitored until the maximum crack length reached approximately 1.5 in. Figure A-6 shows the cracks of greatest length for BU 5 at the conclusion of the test. Figure A-7 illustrates the crack progression. The following summarizes the results of the testing:

BU	Shaft S/N	Service hours	Major cycles at 1/8 in crack	Major/minor cycles/ length at end of test
5	DP10356	3410	40K	43.6K/10.6M/1.4 in.

Cracks were not detected until their length had reached 0.25 in.

Disassembly/measurement of test parts did not indicate a change in fit between the LP thrust bearing inner race and the shaft.

Fig. A-6. Longest cracks for BU 5 at conclusion of the test.

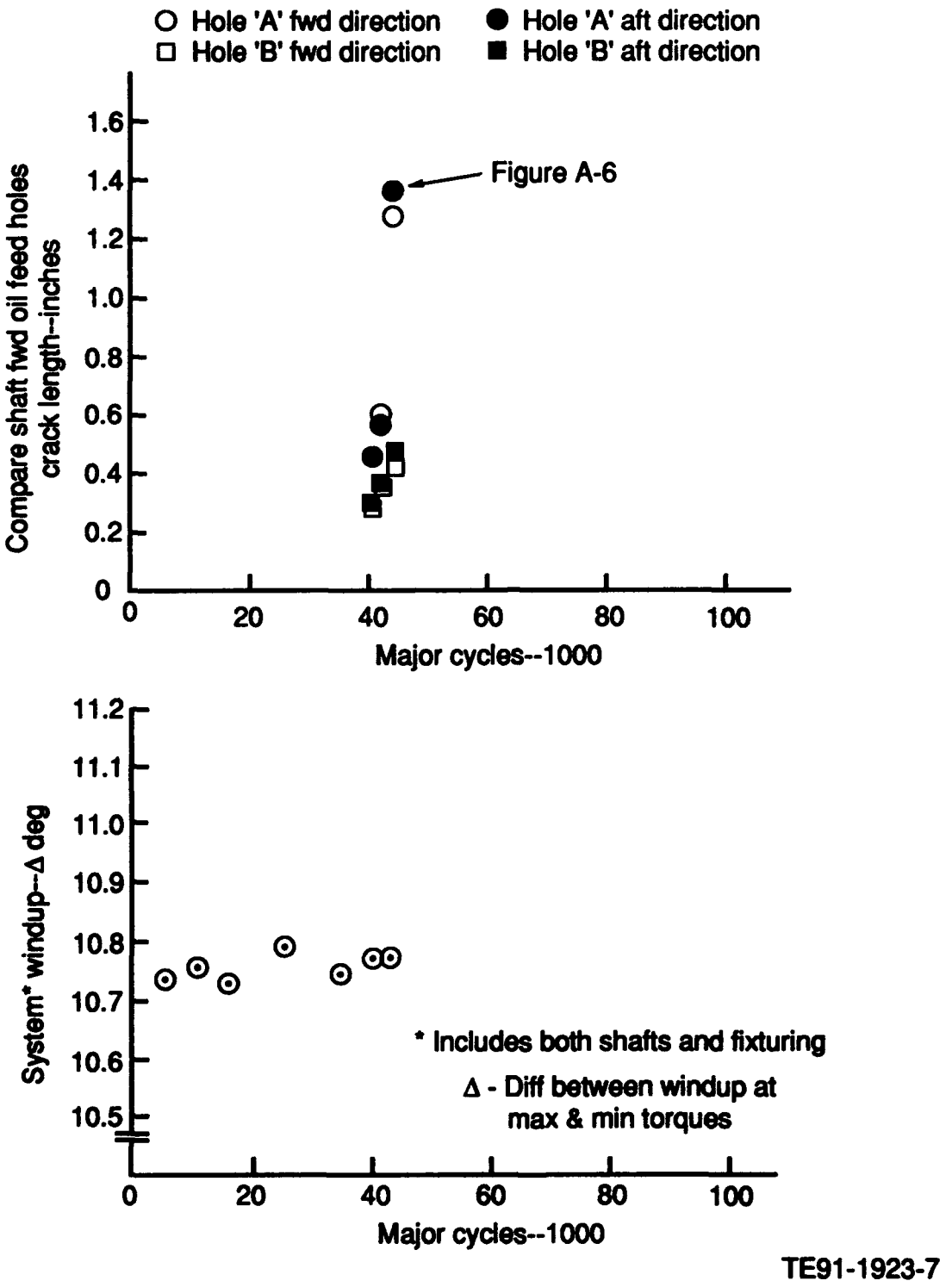

Fig. A-7. TF41 LP mainshaft LCF torsion (TC 875)--compressor shaft 6860005, DP 10356, N.B., 3410 hr; turbine shaft EX 142055, KK12846, B.B., 0 hr, XA18268, BU 5.

TEST SUMMARY FOR TF41 LP COMPRESSOR SHAFT (P/N 6860005, S/N DP10033)

Elevated temperature, low cycle, torsional fatigue tests are being conducted to document the test life of TF41 LP compressor shafts. The results for P/N 6860005, S/N DN10033 are reported herein to supplement information previously provided.

SUMMARY

The LP mainshaft assembly failed at the compressor shaft forward oil holes. The crack initiation and propagation characteristics were consistent with the results reported previously for shafts of a common configuration.

DISCUSSION

Test

Testing was conducted in TC 875 using the same load level, cycle, and temperature distribution as reported earlier. The test procedure and setup were identical to the previous tests except that a commercial torque sensor was added to the test system to expedite the periodic calibration procedure.

Strain gages placed on the compressor shaft in the region of the forward oil feed holes verified that no significant bending occurred during application of the axial or torsional loads.

One automatic shutdown occurred when the test torque level of 181.02K in-lb ±1% was exceeded. The displayed torque was 183.24K in-lb or 1.22% above the nominal level.

RESULTS

The fracture pattern of the test shaft was identical to that reported earlier and resulted from cracks originating at the compressor oil feed holes and propagation fore and aft along a line 45 deg from the axis of shaft rotation. Crack growth was monitored until the maximum crack length reached approximately 1.5 in. Figure A-8 describes the crack propagation rate for the shaft in BU 6.

The following summarizes the results of the testing:

BU	Shaft S/N	Service hours	Major cycles at 1/8 in crack	Major/minor cycles/ length at end of test
6	DN10033	3760	31K	64.9K/15.5M/1.4 in.

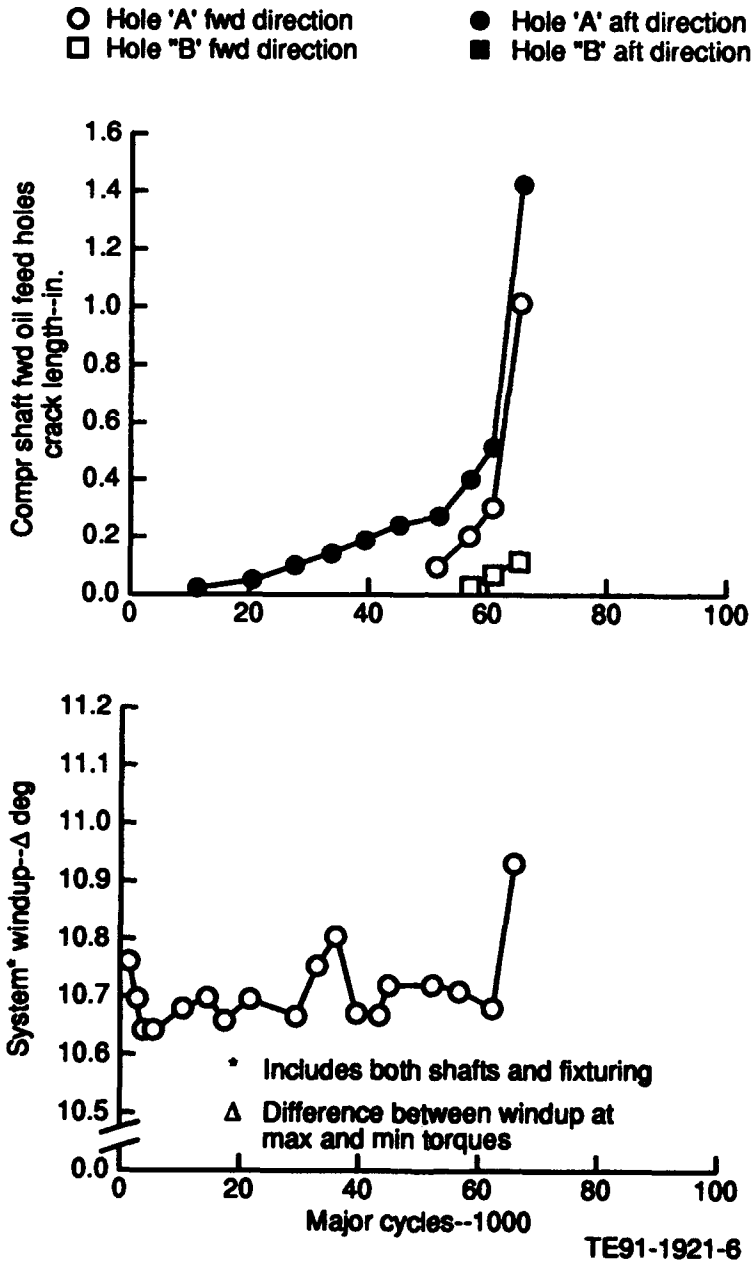

Fig. A-8. TF41 LP mainshaft LCF torsion (TC 875)—compressor shaft 6860005, DN 10033, N.B., 3760 hr; turbine shaft EX 147595, KK 13071, N.B., 0 hr, XA18268, BU 6.

TEST SUMMARY FOR TF41 LP COMPRESSOR SHAFT (P/N 6860005, S/N DP10273)

FOREWORD

Elevated temperature, low cycle, torsional fatigue tests are being conducted to document the test life of TF41 LP compressor shafts. The results for P/N 6860005, S/N DN10273 are reported.

SUMMARY

The LP mainshaft assembly for BU 9 failed at the compressor shaft forward oil holes after 112.1 thousand major cycles similar to the past compressor shaft test failures.

TEST

Testing was conducted in TC 875 using the same load level, cycle, and temperature distribution as reported earlier. The test procedure and setup were identical to the previous tests.

During BU 9 there were three automatic shutdowns after 109.9 thousand major cycles, but all were within the 1% tolerance on torque.

RESULTS

The failure mode of the compressor shaft in BU 9 was identical to that reported in earlier builds. Cracks originated at the compressor oil feed holes and propagated fore and aft along a line 45 deg from the axis of shaft rotation. Crack growth was monitored until the maximum crack length reached approximately 1.5 in. Figure A-9 describes the system windup for the shafts in BU 9, and the crack growth data are shown in Figure A-10.

The following summarizes the results of the testing:

BU	Shaft S/N	Service hours	Major cycles at 1/8 in crack	Major/minor cycles/ length at end of test
9	DN10273	3378	73K	112.1K/26.9M/1.4 in.

This report contained results from four shaft configurations. Only two of the shafts had the configuration of interest for this lifing example. All reference to the other two shafts has been removed.

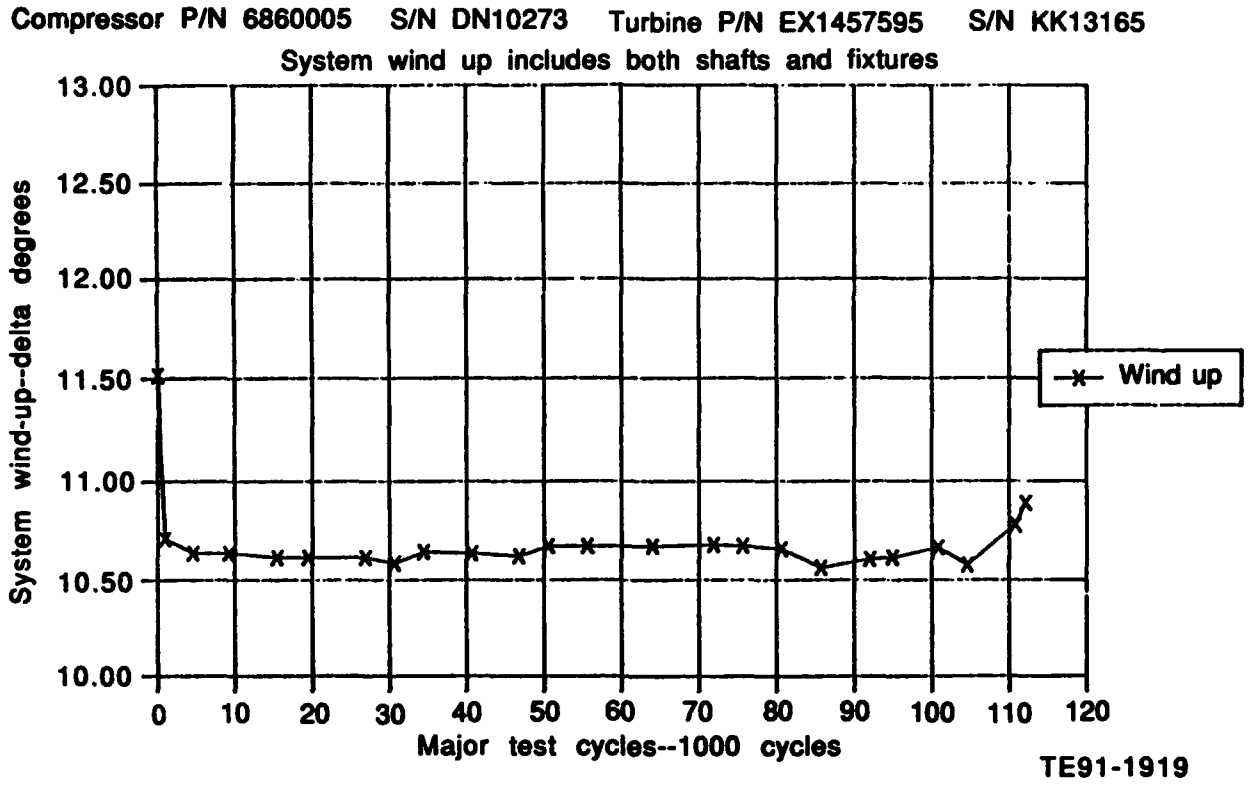

Fig. A-9. TF41 LP mainshaft LCF rig XA18286, BU 9.

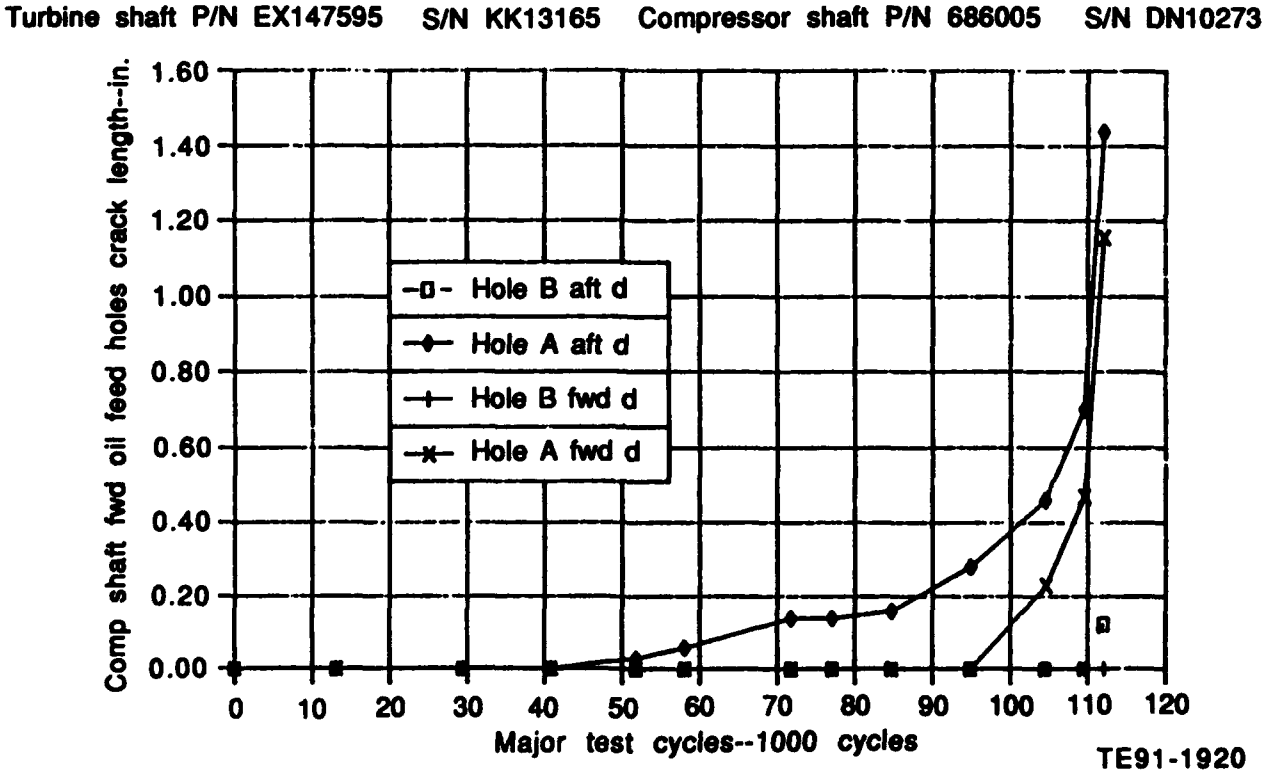

Fig. A-10. TF41 LP mainshaft LCF rig XA18286, BU 9.

TECHNICAL DATA REPORT

Allison Gas Turbine Division, General Motors Corporation, P.O. Box 420, Indianapolis, Indiana 46206-0420	EDO NO. REF.	PAGE 1 OF PAGES 24	REPORT NO. AF.0226-009
TITLE EVALUATION OF LCF TORSION TESTS OF TF41 LP COMPRESSOR SHAFTS.		PREPARED R.C. Klug DATE	
		CHECKED K. N. Ryan	
		APPROVED 4/24/85	

85 FAB-74
MATERIALS DEVELOPMENT LABORATORY
MATERIALS AND PROCESSES DEPARTMENT

REFERENCE: TR: AF0020-15-507

IDENTIFICATION:

PART NAME: L. P. Compressor Drive Shaft
PART NUMBER: A & B - 6860005

PART SERIAL NUMBER: A - D0092
B - DP10356

PART TIME: A - 3434 eng. hrs. 75,540 rig cycles
B - 3410 eng. hrs. 43,457 rig cycles

MATERIAL: EMS 64500
CONDITION: AMS 2485 (black oxide)

ENGINE MODEL: TF41 (Torsion Test Rig)
USER/REMOVAL STATION: Allison Gas Turbine

ABSTRACT:

Compressor Shaft B had multiple fatigue origin sites initiating in corrosion pits on the ID of the forward oil hole. Compressor Shaft A had single fatigue origin sites associated with the forward oil hole surface imperfections.

The hardness measurements for Shaft B was just below the HRC 41-45 limits specified while the other Shaft hardness measurements were within the specified limits.

Chemistry and microstructural evaluations of the Compressor Shafts indicated conformance to the drawing requirements.

TECHNICAL DATA REPORT

Allison Gas Turbine Division	EDO NO. REF.	PAGE 2 OF PAGES 24	REPORT NO. AF.0226-009
TITLE		PREPARED R.C. Klug	DATE
		CHECKED	
		APPROVED	

85 FAB-74

FOREWORD:

A series of LCF torsion tests of the TF41 engine LP section resulted in Compressor Shaft failures (multiple cracks) at the forward oil holes. Two (2) LPC Shafts, P/N 6860005, S/N's D0092 & DP10356, had just over 3400 engine hrs. (see Ident. section) prior to the applied test rig cycles.

The Shafts were received in the Allison Materials Development Laboratory for investigation.

CONCLUSIONS:

1. Compressor Shaft B had multiple fatigue origin sites initiating from corrosion pits on the I.D. of the forward oil hole.

2. Compressor Shaft A had fatigue origin sites initiating at surface irregularities in the forward hole.

4. Hardness measurements of Shaft B were just below the specified limits while the other shaft met the limits specified.

5. Chemical and microstructural evaluations indicated conformance to the drawing requirements.

RESULTS:

Visual, and F.P.I. Examination

Figure 1 shows the as-received condition of the Compressor Drive Shafts. Visual and F.P.I. examination, with a ZL-30 penetrant, did not reveal any cracks or areas of distress in the Shafts other then the torsion cracks found in the forward oil holes and indicated in Figure 1.

Macroscopic and Scanning Electron Microscopic (SEM) Investigation

A. L.P. COMPRESSOR SHAFT, P/N 6860005, S/N D0092

Black light photographs of the Shaft A forward oil hole cracks are shown in Figure 2. The fractures in oil holes #1 and #2 were both opened in the laboratory and are shown in Figures 3 and 4 respectively. The fatigue fracture origin sites are indicated and labeled. In most cases the fatigue was from a single origin site. The fatigue fracture origins in all cases were located in the outer 50% of the shaft wall thickness and were associated with surface imperfections.

TECHNICAL DATA REPORT

	EDO NO. REF.	PAGE / PAGES	REPORT NO.
Allison Gas Turbine Division, General Motors Corporation, P.O. Box 420, Indianapolis, Indiana 46206-0420		3 OF 24	AF.0226-009
TITLE		PREPARED R.C. Klug	DATE
		CHECKED	
		APPROVED	

85 FA8-74

B. L.P. COMPRESSOR SHAFT, P/N 6860005, S/N DP10356

Figure 5 shows the black light photographs of the Shaft B forward oil hole cracks. Fractures in oil holes #1 and #3 were opened in the laboratory. Figures 6 and 7 show the #1 hole fracture while the #3 hole fracture is shown in Figure 8. In both cases the fractures had multiple fatigue origins initiating in corrosion pitts on the oil hole surfaces.

Metallographic Examination

Selected forward oil hole fractures from shafts A through were sectioned and are shown in Figure 18. No microstructural abnormalities which could have contributed to the fractures or fracture origin sites were noted. Micrographs showing the microstructure typical to the shafts are shown in Figure 20.

Hardness Measurements

The hardness measurements for the Compressor Shafts were on the low end of the limits specified in drawings (EPS 292), with shaft B falling just below the limits. The average hardness measurements were as follows;

EPS 292 spec. limits	Shaft A.	Shaft B.
41-45 HRC	43 HRC	40 HRC

TECHNICAL DATA REPORT

	EDO NO. REF.	PAGE / PAGES	REPORT NO.
		4 OF 24	AF.0226-009
TITLE		PREPARED R.C. Klug	DATE
		CHECKED	
		APPROVED	

85 FA8-74

Chemistry

Quantitative (Spectrographic) Analysis of the Compressor Drive Shafts met the EMS 64500 specifications as follows;

	EMS 64500 spec.		Compressor Shaft Samples	
	min.	max.	A.	B.
Carbon	0.35	0.45	0.37	0.39
Silicon	0.10	0.35	0.21	0.19
Manganese	0.45	0.70	0.51	0.51
Nickel	----	0.30	0.20	0.18
Chromium	3.00	3.50	3.42	3.20
Molybdenum	0.80	1.10	1.07	1.07
Vanadium	0.15	0.25	0.24	0.18
Phosphorus	----	0.020	0.011	0.009
Tin	----	0.025	----	----
Phosphorus + Tin, Total	----	0.025	----	----
Sulfur	----	0.020	<0.01	<0.01

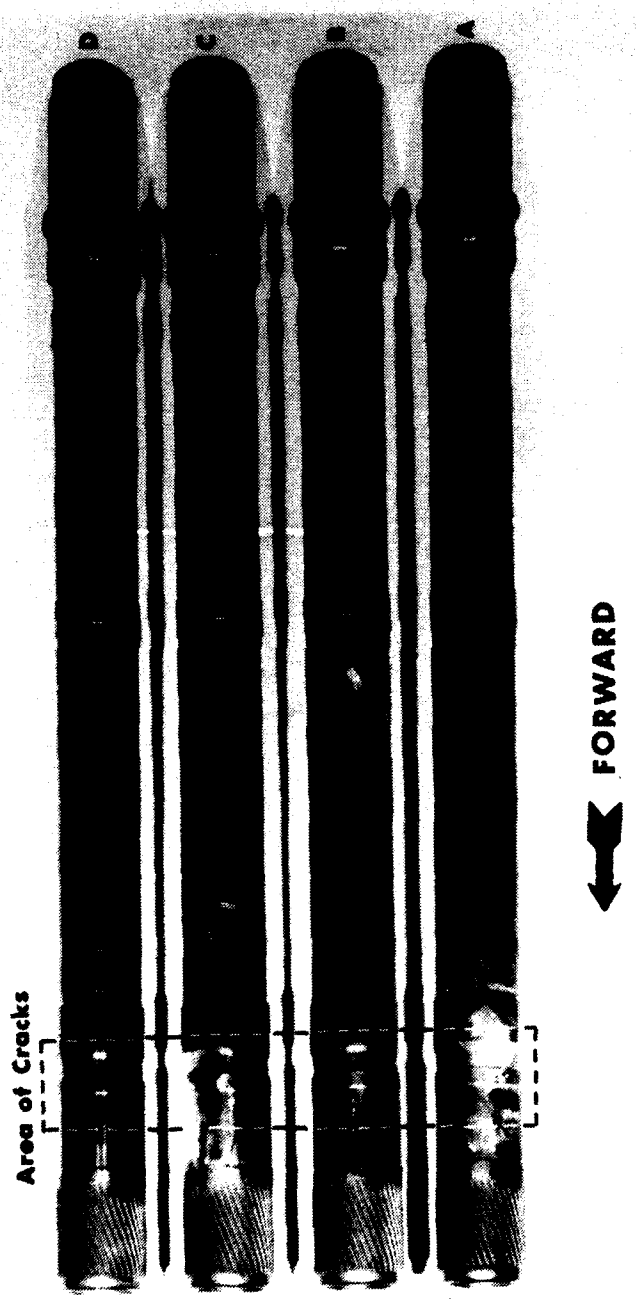

Figure 1. As received photographs of the L.P. Compressor Drive Shafts;

A - P/N 6860005, S/N D0092
B - P/N 6860005, S/N DP10356
C - P/N EX142075, S/N KK12578
D - P/N EX142969, S/N DN12713

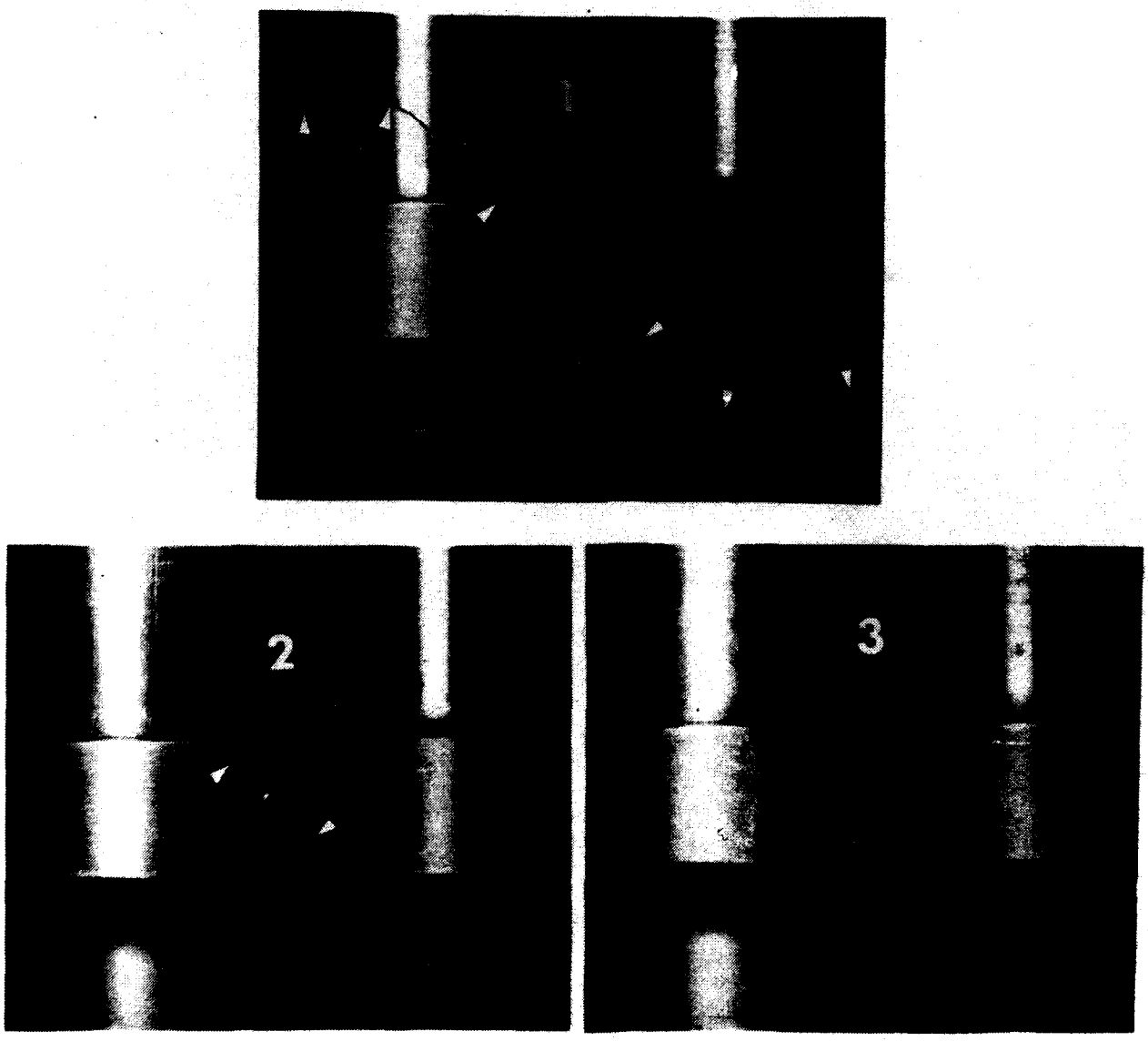

Figure 2. Blacklight photographs of the forward oil holes and associated cracks, indicated by arrowheads, on shaft A. Magn. 2X

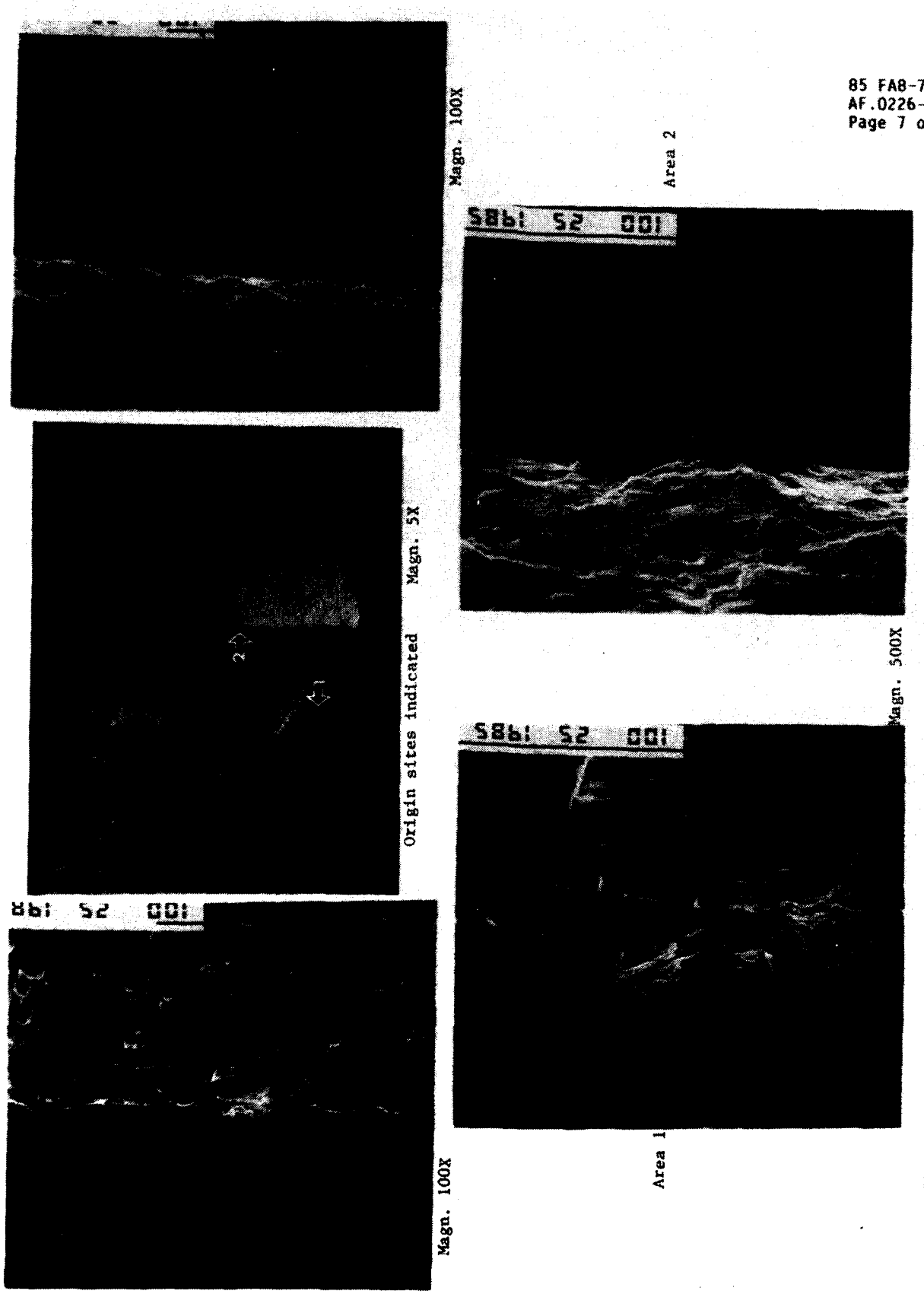

Figure 3. Macroscopic and SEM photographs of #1 fracture shaft A.

Area 2 Magn. 100X

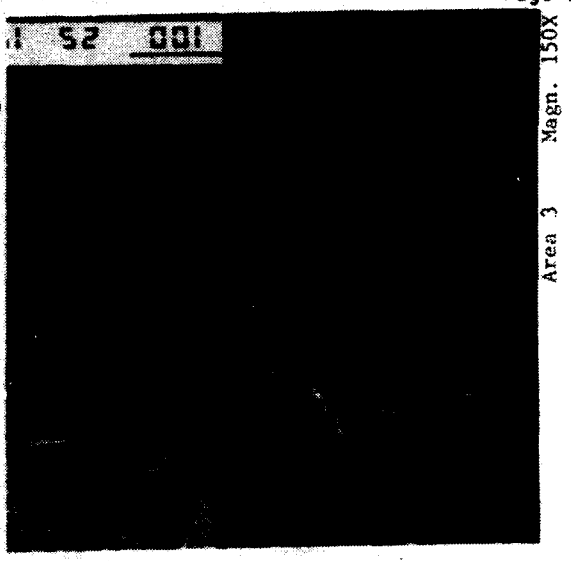

Area 3 Magn. 150X

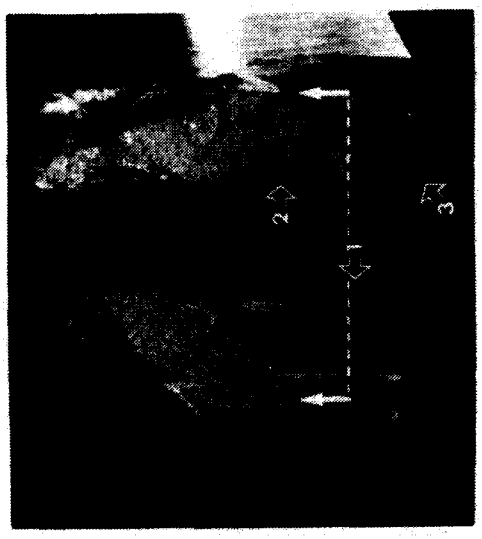

Origin sites and metallographic section indicated. Magn. 2X

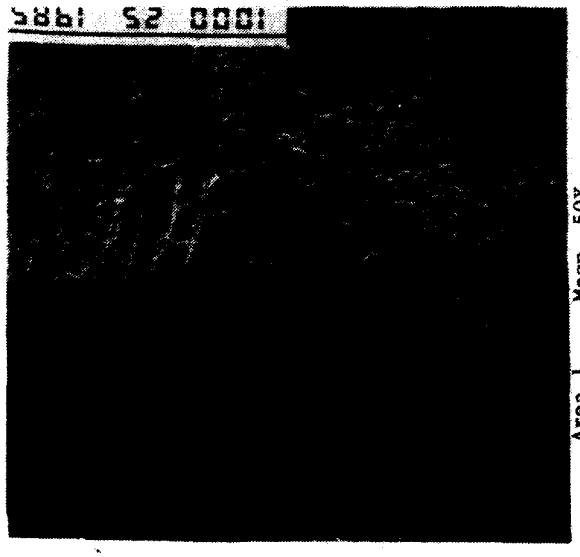

Area 1 Magn. 50X

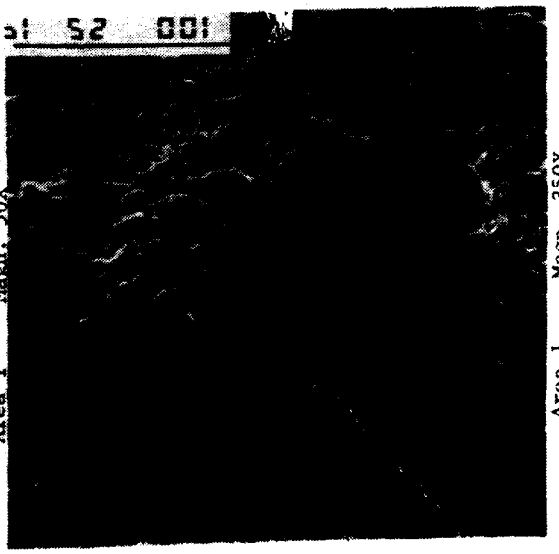

Area 1 Magn. 350X

Figure 4. SEM and macroscopic photographs of #2 fracture shaft A.

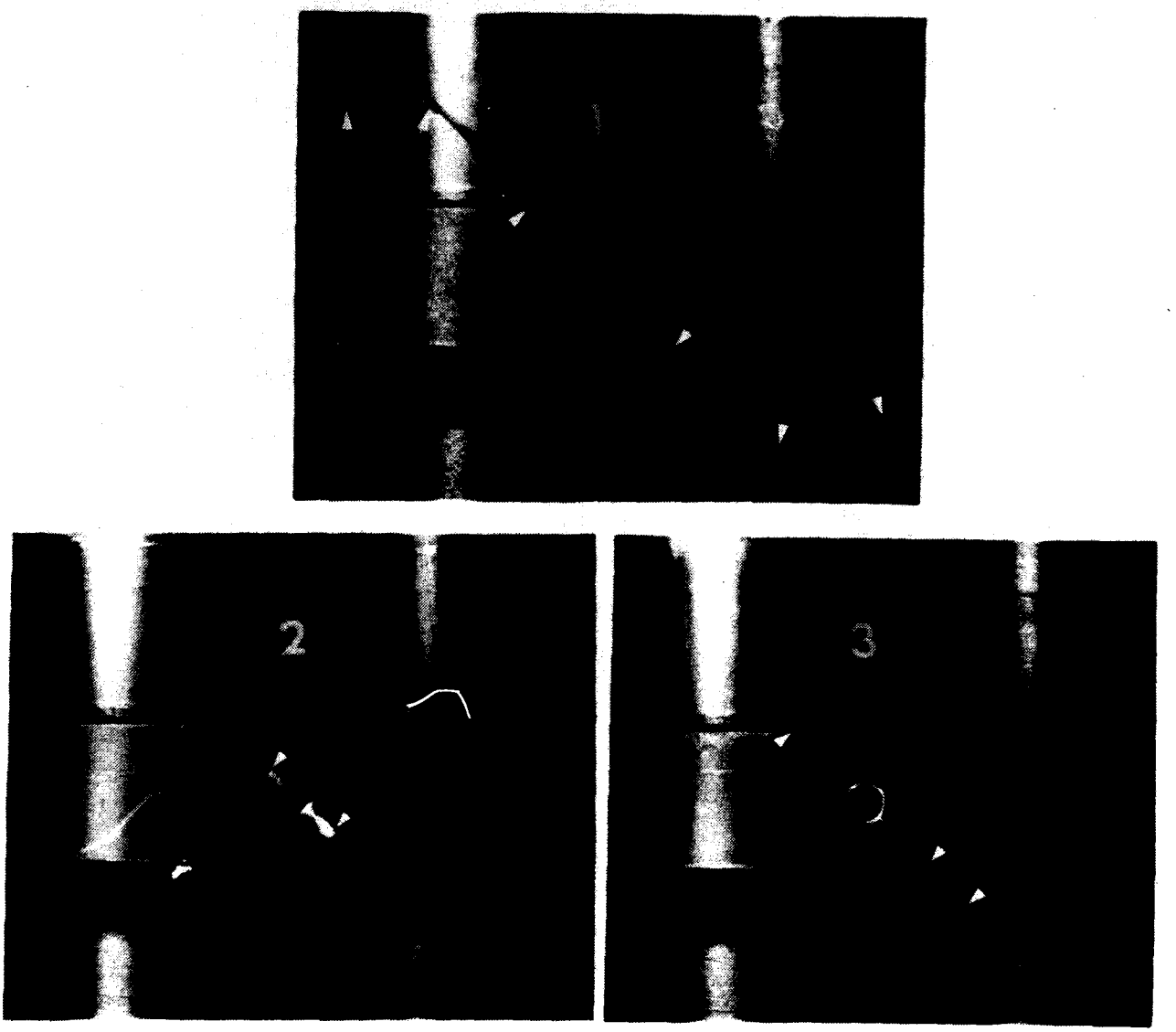

Figure 5. Blacklight photographs of the forward oil holes and associated cracks, indicated by arrowheads, on shaft B. Magn. 2X

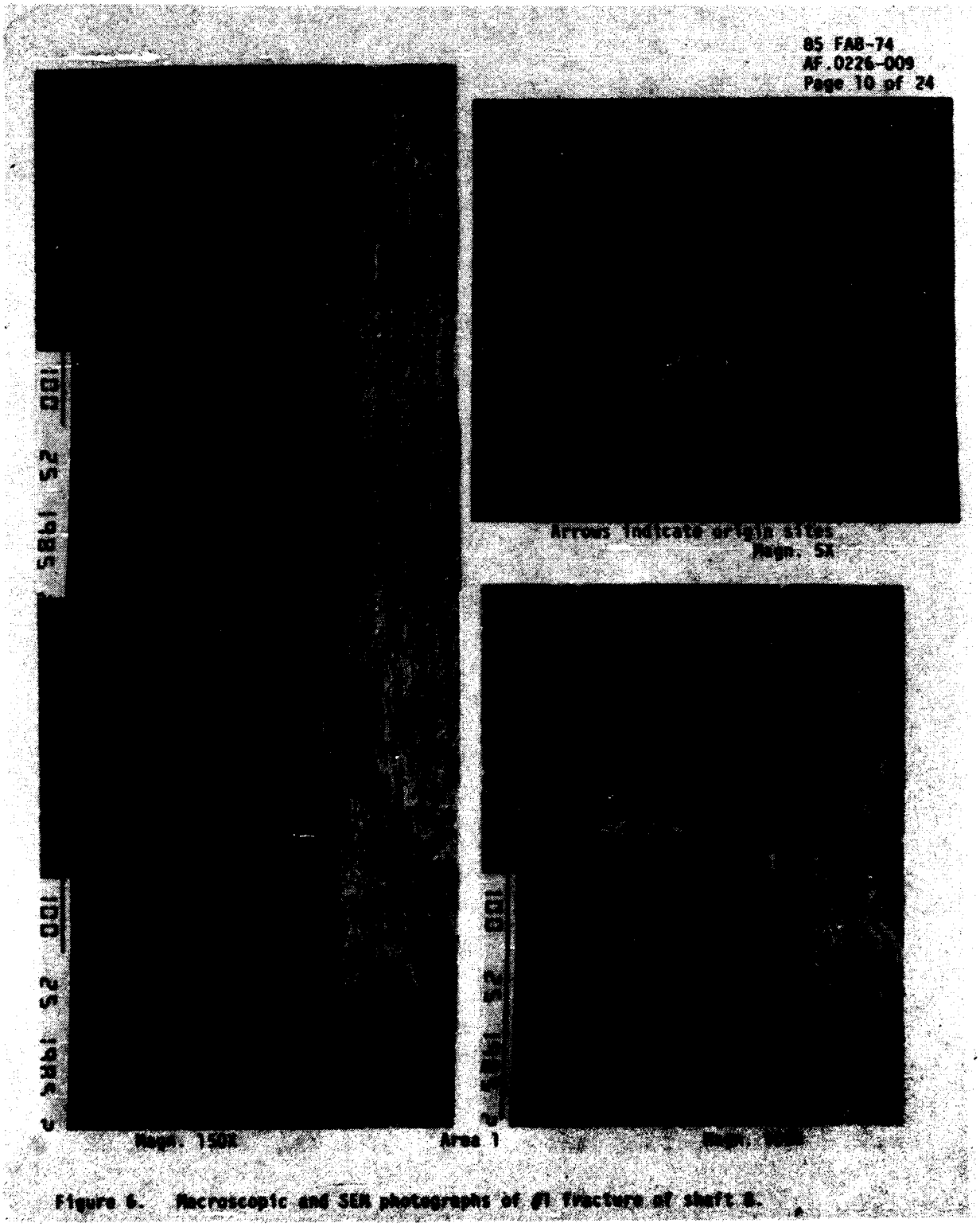

Figure 6. Macroscopic and SEM photographs of #1 fracture of shaft 8.

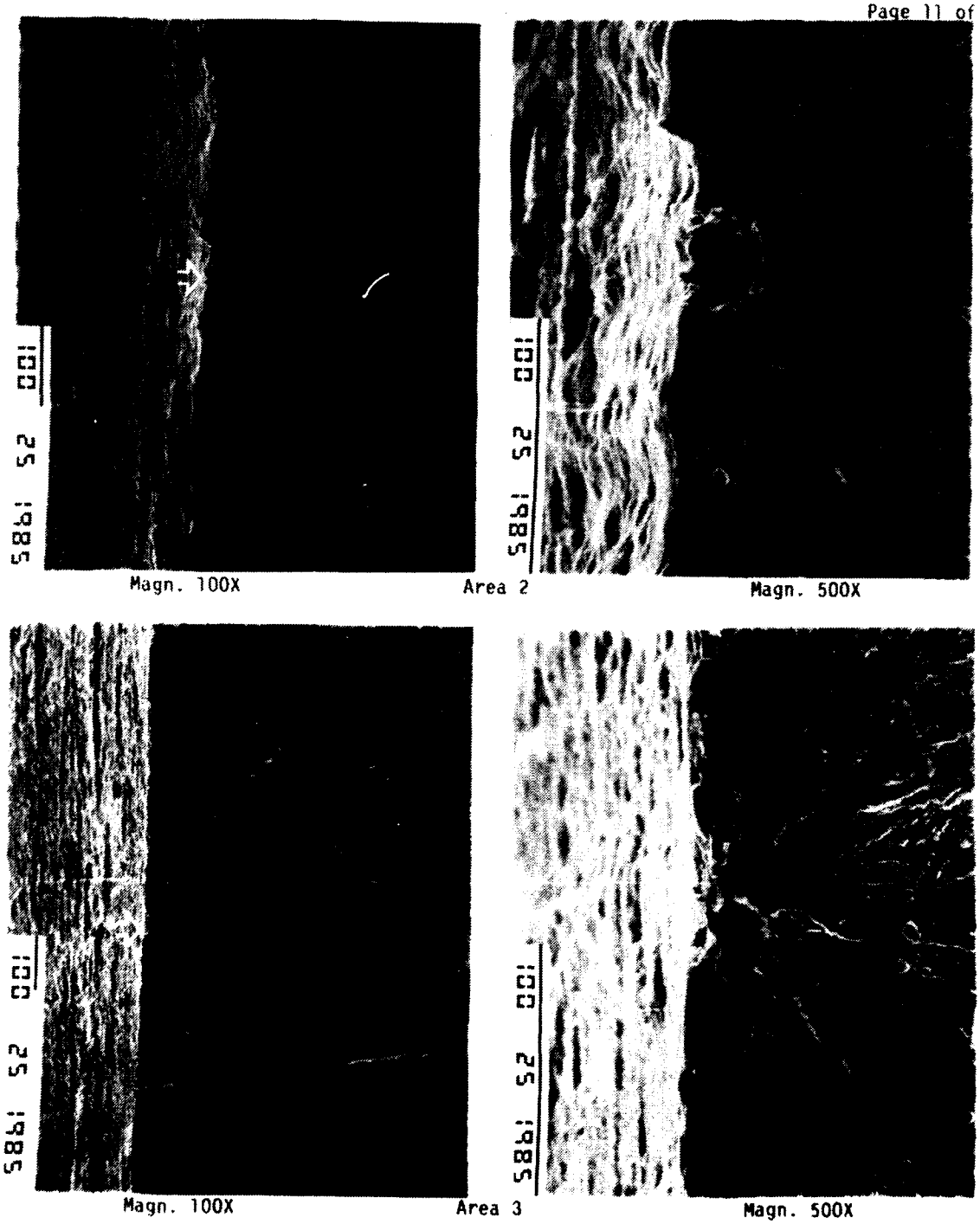

Figure 7. SEM photographs of the #1 fracture of shaft B.

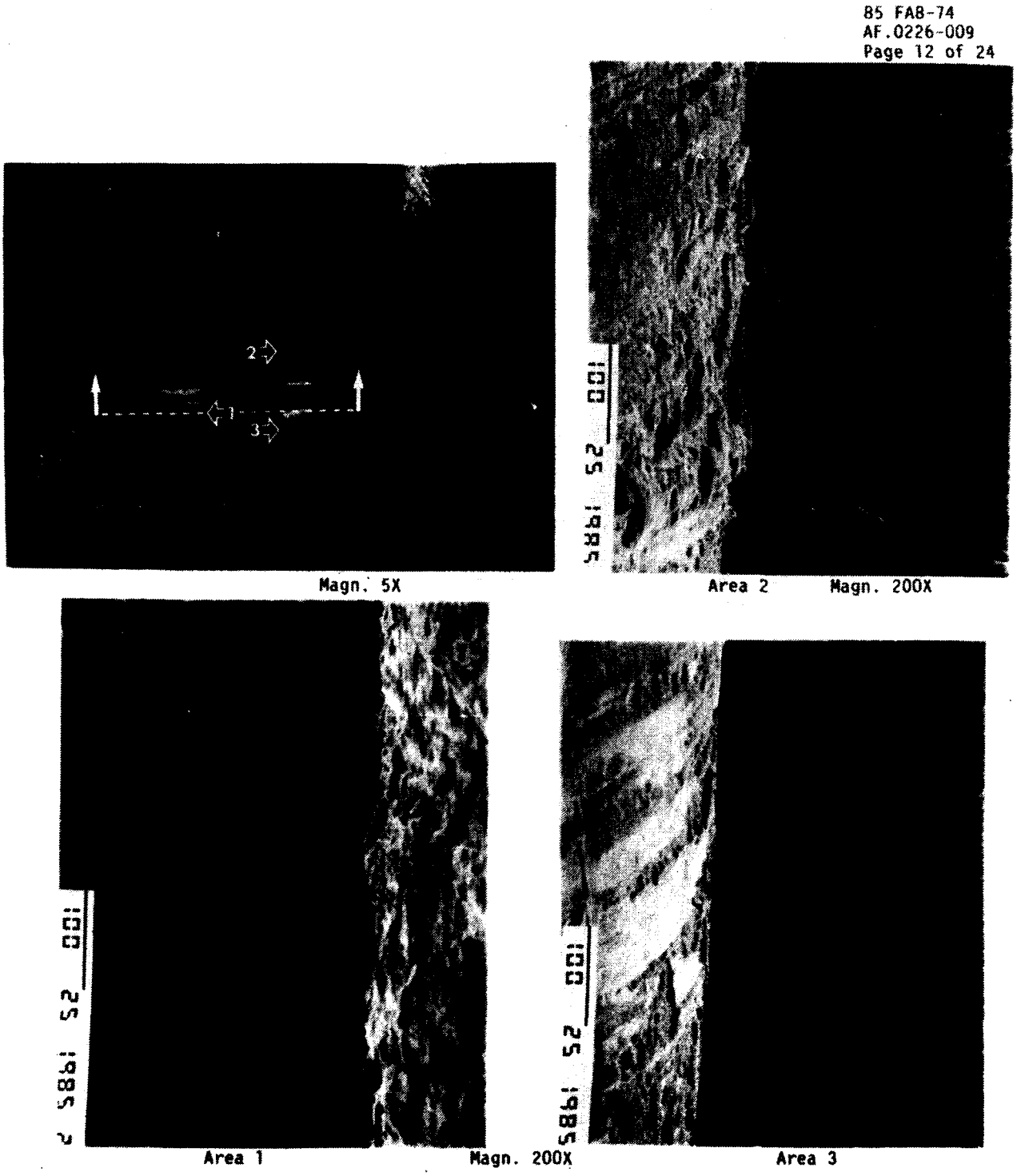

Figure 8. Macroscopic and SEM photographs of fracture #3 on shaft B.

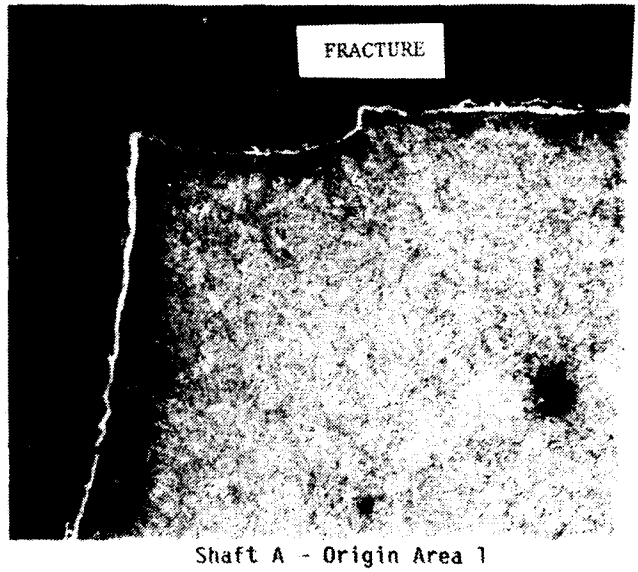

Shaft A - Origin Area 1

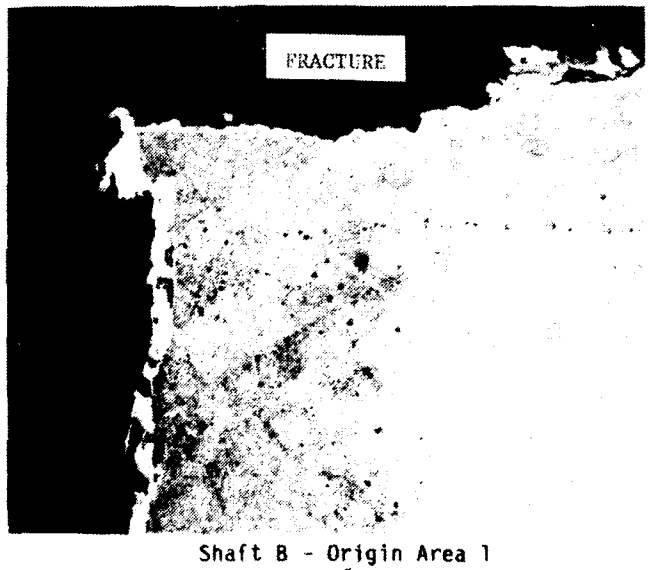

Shaft B - Origin Area 1

Figure 18. Micrographs of the fracture at the oil hole surface for the sections shown in Figures 4 and 8. Magn. 200X
(Etchant: 5% Nital)

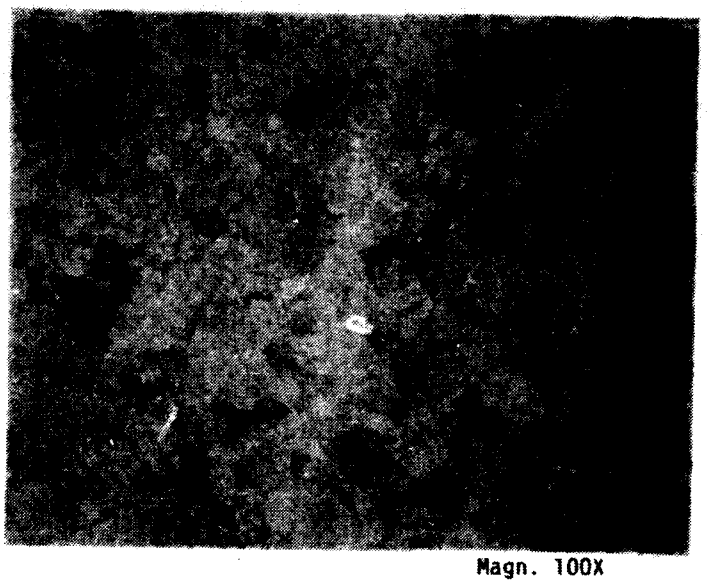

Magn. 100X

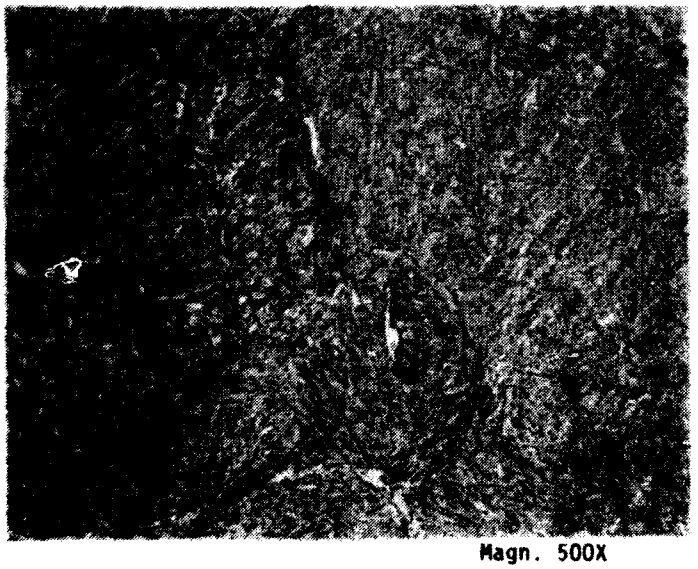

Magn. 500X

Figure 20. Micrographs of the typical microstructure found in the four Compressor Shafts.
(Etchant: 5% Nital)

Chapter 7

F100 2nd Stage Fan Disk Bolthole Crack Propagation Ferris Wheel Test

By
T. E. Farmer
Pratt & Whitney, Government Engine Business
P.O. Box 109600,
West Palm Beach, FL 33410-9600, USA

1. INTRODUCTION

The F100 2nd Stage fan disk test case provides the opportunity for the evaluation and verification of residual crack propagation life capability for a typical "fracture critical" gas turbine engine titanium rotor component.

A bill of material F100 2nd fan disk, redesigned to optimize damage tolerance capability, was subjected to residual life testing to verify the design goal life and prediction methodology. The component bolthole life limiting location was precracked and subjected to simulated low cycle fatigue (LCF) mission cycle loading to assess the residual crack propagation life. In addition, a "hot prespin" treatment of the disk was assessed to evaluate further enhancement of residual life capability by imposing beneficial compressive surface and near surface residual stresses at the disk boltholes.

This test case provides the opportunity to verify crack propagation life prediction methodology for the baseline reconfigured disk as well as the residual stress enhanced "hot prespin" treated disk. Ferris wheel testing provides the residual life data (crack dimension versus accumulated mission cycles) to which the prediction is correlated. A total of 10 holes per disk were preflawed, precracked, and monitored to assess the statistical variation in residual life data.

The test case can be assessed in two phases: (1) an evaluation of the redesigned Damage Tolerance Design (DTD) disk without prespin treatment, and as an option (2) an evaluation of the stress enhanced hot prespin treatment of the same disk configuration.

Complexities Of The Test Case Include:

- Actual engine hardware configuration (titanium material, engine part).
- Evaluation of a complex local stress gradient.
- Residual crack propagation life prediction at a feature exposed to constrained local plasticity.
- Variable amplitude (simulated mission) test cycle.
- Evaluation of induced beneficial residual stresses and their subsequent impact on residual life of the component.
- Damage tolerance residual life assessment of "fracture critical" component.

Limitations Of The Test Case Include:

- Isothermal, continuous (no dwell), ferris wheel and partial vacuum spin pit test.
- Artificial crack starter notches.
- Rigorous stress analysis is required, including the evaluation of the rotor elastic-plastic stress state after local plasticity.
- Interpolative crack growth rate model (da/dN versus delta K) covering positive and negative R-ratios is required.
- Material stress-strain definition is required.

ASSESSMENT ANALYSIS

This test case was independently reviewed and found to provide sufficient information to conduct the

required stress analyses, develop the necessary stress gradients at the bolthole location, predict mission cycle residual life at the bolthole O.D. location, and compare the predictions to the ferris wheel test results.

The component geometry description was utilized to generate an 3–D finite element analysis of a 45 degree section of the disk. This model used as a baseline to establish justification of modelling a 9 degree section of the disk allowing elimination of the necessity of modelling live rim region details and the hub holes. This smaller section required less elements to model the overall part and enabled the analyst to mesh the area much finer at the bolt hole without having an inordinate number of degrees of freedom in the model.

The test case provided the necessary boundary conditions and material properties to conduct both elastic and elastic–plastic analyses of the component. Stress gradients established using these analyses provide the input utilized in prediction of the fatigue crack progression. Sufficient room temperature crack growth rate data is provided, including plots of crack growth rate data for various stress ratios with corresponding sinh model superimposed and tabulated sinh model coefficients.

2. COMPONENT GEOMETRY

This section provides the basic part geometry and includes the details of the test assemblies for both the ferris wheel and the spin pit rigs.

The overall F100 engine cross section and a detail of the low pressure compressor (fan) module are shown in figures 1 & 2, respectively. The overall goal of the design program was to develop a Damage Tolerant Design (DTD) 2nd disk configuration capable of operating with 0.030 inch surface length cracks for three overall periods. In addition, the impact of the prespinning procedure was assessed. Changes to the original design included thickening of the bore and web for reduced stress in the critical locations and specification of AMS 4928 (Ti 6–4) material. The Bill of Material 2nd disk configuration versus Damage Tolerant Design (DTD) configuration are shown in figure 3. A cross section showing the F100 2nd Stage fan disk and bolthole location of interest is shown in figure 4.

The DTD 2nd Stage fan disk detail drawing is provided as figures 5A thru 5D and represents the geometry of the prespin test article (hereafter referred to as disk 1). Prior to the ferris wheel test, the prespun disk 1 bore area was remachined (fore and aft face material removed) to achieve proper nominal disk stresses within the limits of ferris wheel drawbar load capability (see figure 6, hereafter referred to as the ferris wheel configuration). The "non–treated" baseline disk was machined directly into the ferris wheel configuration (hereafter referred to as disk 3).

The ferris wheel (F/W) test set–up is illustrated in figure 7. The F/W rig consists of the F/W modified 2nd stage fan disk (preflawed), drawbars (60) to apply simulated blade load, hydraulic actuators, actuator control system, and facility main frame. Prior to ferris wheel testing, disks 1 and 3 were preflawed in ten boltholes at the outer diameter (OD) centerline location calculated to have the maximum hoop stress.

The spin pit (S/P) set–up is illustrated in cross section (figure 8). The S/P rig consists of the DTD 2nd stage fan disk, complete set of 2nd stage blades (60), 2nd stage blade retaining ring, and spin pit arbor assembly (arbor, adapter, nut and safety wire bolt). The blade retaining ring was joined to the disk with six (6) threaded pin rivets. The blade retaining plate detail drawing is provided as figure 5E. The S/P rig is suspended vertically from the drive turbine assembly which is mounted on the spin pit lid. The spin pit lid is sealed against the vacuum can and partial vacuum provided. Near isothermal conditions are provided throughout the disk via an oven assembly suspended form the spin pit lid and surrounding the body of the disk.

3. PART PROCESSING INFORMATION

Material was procured from one heat of Ti–6Al–4V in the form of disk forgings sufficient to provide for the fabrication of the damage tolerant design disks. The material analysis report is presented in table 1.

Table 1. Material Analysis Report

Mechanical property acceptance of listed forgings based on results from integral test ring per forging

which conforms to the listed material specifications are:

Serial Number	Testing Identity	Yield (ksi) 0.2% Offset	Ultimate (ksi) Strength	Elongation in./in.	Reduction of Area(%)
2022	112	141.1	152.8	11	32
2023	112	141.9	153.4	14	40
2024	112	141.5	152.3	13	41
Spec Min.	20.0	130.0	10	20	
Des.Typ.	140.0	150.0	15	42	

Specification: AMS4928H SUPP PWA S–4928G

This specification differs from the AMS 4928 specification in that disk forgings shall be produced by multiple melting using vacuum consumable electrode practice in each melting cycle. In addition, microstructure shall be that resulting from processing below the beta transus, consisting of well dispersed primary alpha particles in a transformed matrix and shall be free from segregation. The finished product shall be free of any oxygen–rich layer or other contamination.

Conditions of Forgings: Forgings were solution treated at 1745 °F +/– 15 °F for 1 hr, water–quenched, annealed at 1300° F +/– 15 °F, for two(2) hours, then, aircooled.

Both 2nd stage disks were fully machined and boltholes were finished using a standard reciprocating spindle method.

Disk 1 was machined to the damage tolerant design disk configuration and "hot prespun" in the spin pit to induced beneficial residual stresses. After prespin, disk 1 was machined to the ferris wheel configuration. The baseline disk 3 was machined directly to the ferris wheel configuration.

4. OPERATING CONDITIONS

A description of the ferris wheel test and spin pit cycle and the associated operating environments is provided in this section.

Ferris Wheel Test Description

Ferris wheel testing was conducted on the disk 3 to provide baseline results for bolthole O.D. residual life capability. Ferris wheel testing was conducted on the disk 1 after it was the "hot prespun" in the spin pit rig (spin pit test is discussed later).

Elox damage (approximately 0.020 in. long X 0.005 in. width X 0.010 in. deep) was provided in ten (10) of the twenty (20) boltholes to hasten initiation to a 0.030 in. surface length precrack. All ferris wheel testing was conducted in ambient air conditions. The disk was then cycled with simple sawtooth loading to initiate and grow the elox starter cracks to the required 0.030 in. surface length, before mission cycle testing began.

Maximum load was 18,890 lbs/slot with simple sawtooth cycles (5% maximum load, up to 100%, unload to 5%, repeat). Cycles were continuous with linear load–unload at 10 cycles per minute. Growth of the starter notches to the required 0.030 in. surface length was monitored using replication techniques. When required crack lengths were verified the precracking load cycle was terminated and mission cycle testing started.

The mission cycle testing involved the application of a simulated mission cycle block representing the equivalent low cycle fatigue damage for a typical fighter engine mission. Each mission cycle block consisted of nine load cycles to 100% maximum loading (18,890 lbs/slot) with the first (1) from 0.05% maximum load, the next four (4) from 36% maximum load, and the final four (4) from 25% maximum load (see figure 9). The load blocks were applied continuously with the exception of periodic replication of the cracks under partial load to monitor growth during the test. The actual number of sawtooth and mission cycles applied is provided in Section 8 (Operation History).

The test of disk 3 was run with the intent of stopping the test when the largest crack reached approximately 0.200 in. surface length. The objective was to preserve the disk for additional rim crack propagation testing (possible follow–on work).

After termination of the mission cycle testing, representative bolthole cracks were trepaned from the disks (1 and 3) to provide photos and SEM analysis of typical crack propagation behavior.

"Hot Prespin" Test Description Of The Disk 1

The disk was hot–spun to induce beneficial residual stress at the stress concentration features. The disk was instrumented with thermocouples and eight high temperature strain gages. The instrumentation was concentrated at the peak stress locations at the bolthole O.D. and the rimslot bottom. A temperature and strain gage survey was completed prior to the actual "hot prespin".

The disk was then prespun at 500°F to the analytically predicted speed required to achieve the optimum bolthole residual stresses while remaining within allowable growth tolerances. The 500 °F insured that spin induced residuals severe enough to provide local reverse yielding during unloading will not relax at hot shut–down engine operating temperatures (200° – 300 °F).

The bolt circle radius received special inspection before and after the prespin to quantify the amount of permanent radial growth. The spin speed had been selected by declaring 0.002 – 0.004 in. to be the acceptable range of growth and by selecting the initial spin speed using the results of a elastic–plastic analysis. This analysis predicted that 12,150 rpm would yield the minimum acceptable growth (0.002 in.) although this elastic–plastic prediction was recognized as having significant error band due to hub geometry. Postspin growth results indicated 0.0038 in. change in the bolt circle radius and substantiated the adequacy of the spin. Due to the large plastic deformation in the boltholes, the strain gages failed during upload. Because the analytical prediction (assumed Neuber upload and kinematic hardening with perfect plasticity unload) indicated that significant reverse yielding would accompany 0.002 in. growth, it was concluded that a near–optimum beneficial residual had been successfully induced in the boltholes.

5. BOUNDARY CONDITIONS FOR STRESS ANALYSIS

The boundary conditions required to complete the stress analysis for ferris wheel cyclic testing and hot prespin spin pit cycle are included in this section. (Note that disk 3 provides the baseline and disk 1 represents the the impact of ferris wheel cyclic testing after exposure to the hot prespin.)

Boundary Conditions For Ferris Wheel Stress Analysis

Ferris wheel cyclic testing was conducted for both disks 1 and 3. The test was run in isothermal ambient air conditions. The ferris wheel is a "static" load rig with radial load applied at the blade attachment slots via drawbars. Only external disk loads are applied (radial only in this case) and, therefore, simulation of normal disk stress distributions are only approximate (no body loads due to rotor speed were present, rpm = 0.). A maximum (100%) load of 18,890 lbs/slot for each of the 60 slots was applied. Ferris wheel live rim load summary is presented in table 2. Ferris wheel sawtooth and mission cycle description is shown in figure 9. Actual cyclic load history was applied as described in Section 8.

The ferris wheel rig stress analysis requires modelling only the disk with either 2D or 3D finite element analysis being the recommended tools. The bolthole region of the disk is far enough removed from the applied radial load that it is recommended modelling the disk to the "live rim". The "live rim" radius of a disk is defined as the outermost continuous (axisymmetric) fiber. The total radial load is applied as a uniformly distributed load at the live rim radius (7.699 inch).

Modelling the disk only to the live rim radius eliminates the necessity of detailed modelling of the attachment region, does not reduce the quality of the solution at bolthole, and allows more efficient distribution of elements density/reduced model size/faster execution. If the complete ferris wheel disk configuration is modelled including the disk rim attachment region, the 18,890 lbs/slot should be applied at the bearing surface centerplane of the disk

rim attachment. Axial offset of the drawbar load was established to minimize the moment placed on the disk rim (see figure 11 for axial offset).

Boundary Conditions For Spin Pit Stress Analysis

Hot prespin was conducted on disk 1 only. Required stress analysis and associated boundary conditions follow in this section.

Spinpit load summary is presented in Table 2. The hot prespin treatment disk bolthole analysis requires several steps including: (1) elastic–plastic analysis of the full spin pit disk configuration up to maximum load conditions (12,150 rpm at temperature of 500 °F (isothermal)), (2) unload analysis to 0 rpm at 500 °F reflecting the elastic–plastic residual stress state due to the unload characteristic of Ti 6–4 (consider kinematic or combined hardening (Bausinger effect)), and (3) analysis of the ferris wheel configuration to evaluate the resulting bolthole stress gradient for ferris wheel cyclic testing accounting for the residual stresses induced from the 500 °F spin pit cycle.

It should be noted that the bolthole stress concentration factor (ie. stress concentration factor = local concentrated stress / reference nominal stress) will vary slightly for the spin pit versus the ferris wheel modified configuration. This variation is due primarily to the difference in loading conditions, not the result of any geometric difference (ie. loss of the hub). Disk body and rim loads for spin pit versus rim load only for ferris wheel rig generate different ratios of hoop (circumferential) and radial nominal stress at the bolthole location resulting in a change in the stress concentration factor. In addition, some of the beneficial spin–induced residual stress at the bolthole location was sacrificed when the bore faces were removed to make ferris wheel testing possible.

6. HEAT TRANSFER INFORMATION

All ferris wheel testing was conducted in ambient air lab conditions. No heat transfer analysis was required.

No heat transfer analysis was performed for the 500 F prespin conducted in the spin pit facility. The spin pit rig thermal profile was monitored using thermocouples and close to isothermal conditions of 500 F were achieved in the plane of the disk during the prespin test. The thermocouple results indicated temperatures ranging from 491 F to 520 F in the disk plane. An approximate 150 F temperature differential between the bore and hub was measured, however, this thermal gradient was determined to have no significant impact on the disk bolthole stresses.

7. MATERIALS DATA

Physical And Mechanical Property Data

All physical and mechanical property data necessary to complete the analysis of the test case is included in the section.

Tensile properties include: typical yield and ultimate strength, modulus of elasticity, coefficient of thermal expansion (alpha), poissons ratio, and density (table 3); plastic strain versus stress (table 4).

Crack Growth Rate Data include: a plot of the Ti 6–4 (AMS 4928) design system model R–ratio (R=minimum stress/maximum stress) trends at room temperature (figure 12); tabulated SINH design system model coefficients for Ti 6–4 model, explanation of the SINH model coefficients, and English–to–metric conversion factors for the SINH models (table 5); individual plots of pre–contract database versus design system models (figures 13 to 21).

Positive R–ratio constant amplitude crack growth rate data is generally developed using the standard compact tension specimen type. The preferred test specimen type for negative R–ratio constant amplitude crack growth rate data is the thick–section center notched specimen. The thick–section center notched specimen has threaded end grips is approximately 4.5 inches long, 1.0 inch diameter with rectangular mid section 1.0 inch by 0.150 inch containing a thru thickness slot approximately 0.100 inch by 0.010 inch precracked with a thru thickness crack. The negative R–ratio data trends provided in this test case were developed using radial hollow tube specimen types. The hollow tube specimen was approximately 6 inches long with threaded end grips,

3/4 inch O.D. diameter, 1/8 inch wall thickness, and precracked with a thru thickness crack. These negative R–ratio trends were checked against negative R–ratio data generated with thick threaded end center flaw specimens obtained from a Grumman open literature report on Ti 6–4 (AFFDL–TR–74–129). The Ti 6–4 design system sinh curve provides conservative crack growth rates compared to this data (Figure 21).

8. OPERATION HISTORY

Background And Objectives

A damage tolerant design system was developed in a previous effort and applied to the redesign of an F100 fan disk, life assessment tests were required in order to evaluate the actual bolthole residual crack propagation life and to verify the design system predictions. The critical location selected for life testing was the bolthole outer diameter (BHOD). Test disk No. 1 received the spin treatment and was tested to determine BHOD residual life. Test disk No. 3 provided BHOD residual life without the benefit of the spin treatment.

Test Configuration, Procedure And Results

Strain gages and chromel/alumel thermocouples were installed to measure the strain and temperature distribution on disk 1 at 500 F. A three leadwire system was installed to minimize strain gage drift due to temperature variations. Disk 1 was instrumented to establish the strain and oven calibration (figures 22 and 23, respectively). A layout of oven and spin assembly in the spin rig configuration is shown in figure 8. The first spin acceleration of disk 1 was conducted only to 10,000 rpm to corroborate analytical design predictions prior to the full speed test. The complete strain data and corresponding test temperatures are in table 6. The resultant room temperature residual strain values are also contained in table 6. Figures 25 through 28 are plots of table 6 for disk 1.

Ferris Wheel Test Portion

Prior to the ferris wheel test, the two prespun DTD disks had their bores removed to create proper nominal disk stresses within the limit of drawbar pull load capability. Disk 3 was the "non–treated" baseline disk for disk 1 and therefore not spin tested; it was machined directly into the ferris wheel configuration. Prior to ferris wheel testing, disks 1 and 3 were elox preflawed in ten boltholes (figure 24).

A ferris wheel strain survey was first carried out on disk 1 instrumented per figure 24, with resultant strains in table 7. Figure 7 shows the ferris wheel setup for disk 1. In figures 29 and 30, ferris wheel strain data for the bolthole O.D. location from table 7 are plotted.

Inspection techniques applied to the ferris wheel LCF portion of this test included replication and fluorescent penetrant inspection (FPI). Replication was used as the primary inspection method. FPI was discontinued after use only on disk 1, as the elox flaws caused excessive bleedout of the penetrant and therefore inaccurate measurements. Replications (acetyl cellulose plastic film, 0.034 mm thick) were taken for all elox flaws to determine initial baseline preflaw dimensions. Figure 31 shows a typical elox flaw for each disk. After cycling began, periodic replications were performed under partial load in the ferris wheel to enhance crack detail. Replication photos in figure 32 show a typical bolthole crack growth progression.

The disks were first sawtooth load cycled to attain about 0.030 inch crack initiation and then mission cycled for crack propagation evaluation (cycles defined in figure 9). Replication crack propagation data are detailed in tables 8 and 9 for disks 1 and 3, respectively. Figures 33 and 34 contain crack growth data from tables 8 and 9. Disk 1 was LCF tested to failure, while LCF testing on disk 3 was discontinued at imminent fracture.

Five cracked boltholes in disk 1 and three in disk 3 were: (1) sectioned out of the respective disks; (2) heat–tinted for one hour at 600 °F; (3) and broken open to expose the fracture faces. This was to determine crack depths at test termination. This data

is contained in table 10. Figures 35 and 36 show a representative bolthole fracture face set for each disk. Data from tables 8 and 9 were converted to change in crack growth per change in number of cycles (da/dN) tables 11 and 12, respectively. The two boltholes on disk 1 which failed through (10 and 20) were viewed by the scanning electron microscope (SEM). These fractures are shown in figures 37 through 39.

DISCUSSION OF RESULTS

Spin Test

At 8,000 rpm, the last speed where all readable gages were operable on disk 1, the maximum strain occurred in the bolthole (gage 5, figure 22). It reached 4300 microinch/in. However, extrapolating the data for gages 3, 5, 6, 7 to 12,150 rpm (by linear regression, which resulted in a fair amount of conservatism) indicated strains well into yielding for the bolthole gages. At 500 °F, minimum strain to cause 0.2 percent yield is about 6440 microinch/in. for AMS 4928. The extrapolated strains for gages 3, 5, 6 and 7 were 5150, 9180, 9500, and 8880 microinch/in., respectively. This yielding resulted in a reported residual growth of about 0.004 inches in the bolt circle diameter for disk 1.

Comparing rim slot bottom stresses on disk 1 (strain gages 1, 2, 3 and 4) to those previously measured on the B/M disk at 10,000 rpm showed significant differences. Stresses were lowered about 34 percent on the front side in the slot room bottom (live rim) for disk 1 versus the B/M. They were reduced about 48 percent on the rear side. These lowered stresses, compared to the B/M disk, are due to the thickened bore and web on the DTD disk. This fact should increase life in the rim for the DTD disk. Data were not available in the boltholes on the B/M disk for similar comparison.

The spin strain data, plotted in figures 25 through 28, showed yielding occurred somewhere above 11,000 rpm. Note also in figures 25 through 28 (rim slot locations) that some residual tension occurred at the end of the deceleration portion of the run. The plastic yielding of the bore to the bolt circle area (about 0.004 inch growth in the bolt circle diameter and the elastic material around it (rim) should cause the bore to bolthole area to be in compression and the rim in tension. Rim gages 1, 3 and 4 showed this tension in the rim after the residual spin. This will lower the operating stresses at the boltholes and thereby increase bolthole life.

FERRIS WHEEL TEST

Strain Survey

Disks 1 and 3 were designated for bolthole testing. Disk 1 was predominantly strain gaged in the boltholes. Disk 3 (not strain gaged) was the baseline disk for disk 1.

The highest strain occurred in the midspan of the bolthole, outboard side. It peaked at 9770 microinch/in. for 18,890 lbs/slot (gage 11, figures 24 and 29). This was well beyond the 0.2 percent yield point at room temperature (8500 microinch/in.). However, the bolthole was starting from a compressive residual state. If the residual compressive strain values of gages 5 or 6 of If the residual compressive strain values induced by the prespin were added, net peak strain would be somewhat reduced resulting in elastic response. This would provide additional ferris wheel LCF life in the residual treated DTD disk 1 over the baseline DTD disk 3.

Strains decreased moving outboard of the bolthole edges (shown in figure 30). Peak strain occurred on the front side, and reached 6190 microinch/in. at 18,890 lbs/slot (strain gage 5, figure 24).

Bore (modified for ferris wheel test) midspan strains (circumferential) were repeatable to within 1 percent, where maximum strain reached 6050 microinch/in. (strain gage 30, figure 24).

The web strains were repeatable to about 3 percent. The circumferential web stresses at 18,890 lbs/slot attained 71,500 psi and 71,800 psi (front and rear, respectively, using averages and $E = 16.6 \times 106$ psi, $\nu = 0.35$). The radial web stresses at the same load were measured at 60,150 psi with a small +/−3450 psi bending stress toward the rear (drawbar load axis positioned to minimize bending).

No strains other than bolthole values approached the minimum required strain to yield AMS 4928. This

implied these other measured areas should have sufficiently more ferris wheel life than the bolthole and therefore be of lesser concern.

Ferris Wheel Test

Tables 8 and 9 contain the ferris wheel crack history (via replication) for disks 1 and 3 (the residual spun disk and its baseline, respectively). Bolthole cracks propagated noticeably faster during ferris wheel sawtooth cycling in disk 3 than disk 1, even though started from a shorter mean elox length (0.0141 inches vs. 0.020 inches). Figure 33 shows this well. Tables 10 and 12 also confirmed the crack growth rate for baseline disk 3 was always higher than disk 1 for sawtooth cycling.

Figure 34 shows the same events occurred in mission cycling. Up to the point where disk 1 mean crack lengths became much larger and closer to failure than disk 3 (past 445 mission cycles, table 8), disk 3 had higher ferris wheel mission cycle crack growth rate than disk 1 (comparing tables 11 and 12).

Past 445 mission cycles, the crack growth rate for disk 1 took a quick turn toward failure, which occurred after a total of 2091 sawtooth and 568 mission cycles. Primary failure site was bolthole 20. The failure resulted in the separation of disk 1 into two halves. Disk 3 approached this comparable point, then further testing on it was discontinued (after a total of 1200 sawtooth and 275 mission cycles). The final mean aspect ratio for the residually treated disk 1 was 1.94:1, 10 percent higher than the average for baseline (untreated) disk 3. (For reference, both disk 1 and 3 were 0.530 inches thick in the bolthole section and had twenty (20) 0.461 inch diameter holes equally spaced at 9.000 inch diameter.)

Boltholes 10 and 20 were studied with a SEM (scanning electron microscope). This was to assure no material anomalies existed. Figure 37 shows a clearly defined thumbnail shaped fatigue crack for bolthole 10 (secondary failure hole), and that the fatigue had progressed normally for Ti–6Al–4V (AMS 4928). This is clearly shown by the transgranular fatigue with striations well defined in many areas. Bolthole 20 (primary failure hole) showed a poorly defined thumbnail pattern (figure 38). In region B of bolthole 20 located the same distance from the elox slot as region A in bolthole 10, similar transgranular fatigue with well defined striations in many areas was seen (figure 38). Figure 39 views the crack surface progressing from a transition region C (reference figure 38) containing few striated areas with very little intergranular or tensile (dimpled) fatigue to a region D of overstress. This region 'D' of overstress has within it areas of mixed tensile (dimpled) and intergranular fatigue. Bolthole 6 on baseline disk 3 was examined by SEM for comparison and showed the same fatigue pattern as bolthole 10 on disk 1.

As a point of interest, bolthole 12 on disk 1, inboard side, had an elox flaw similar to the others on the disk. After disk failure, replication of this location showed no cracks propagating from this elox flaw.

9. SUMMARY

This test case provides the opportunity for the evaluation of the overall stress state in a typical "fracture critical" gas turbine engine rotor component and residual crack propagation life assessment at the bolthole for a simulated low cycle fatigue engine operation mission cycle. Ferris wheel testing provides the crack propagation data to which the prediction is correlated. In addition, an overload hot prespin treatment of the disk is evaluated as a means of establishing an induced beneficial near surface compressive residual stress at the bolthole to enhance the crack propagation life. The F100 2nd stage fan disk was tested as part of the US Air Force Damage Tolerant Design for Cold–section Turbine Engine Disks Program AFWAL–TR–81–2045 in the late 70s.

The component geometry, part processing, test rig set–up, operating conditions and environment, and materials data are presented in sufficient detail to allow users to model the component and predict the state of stress throughout the body of the disk with particular attention to the bolthole outer diameter location of interest. Solution of the stress state at the bolthole O.D. for the simulated mission cycle and use of crack propagation rate models allow prediction of the residual life from precracks and make comparisons to actual test data.

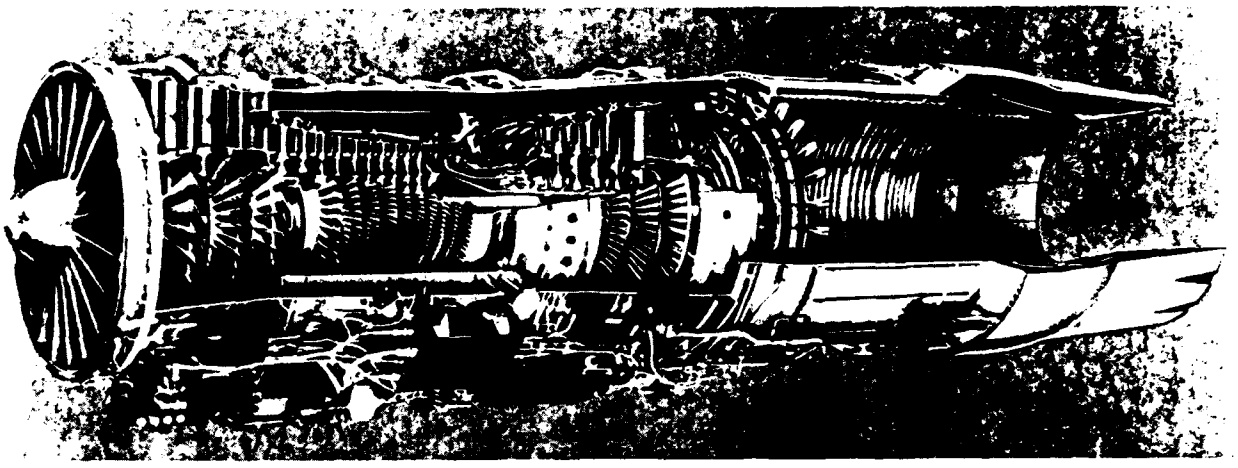

Figure 1. F100 Engine Cross Section

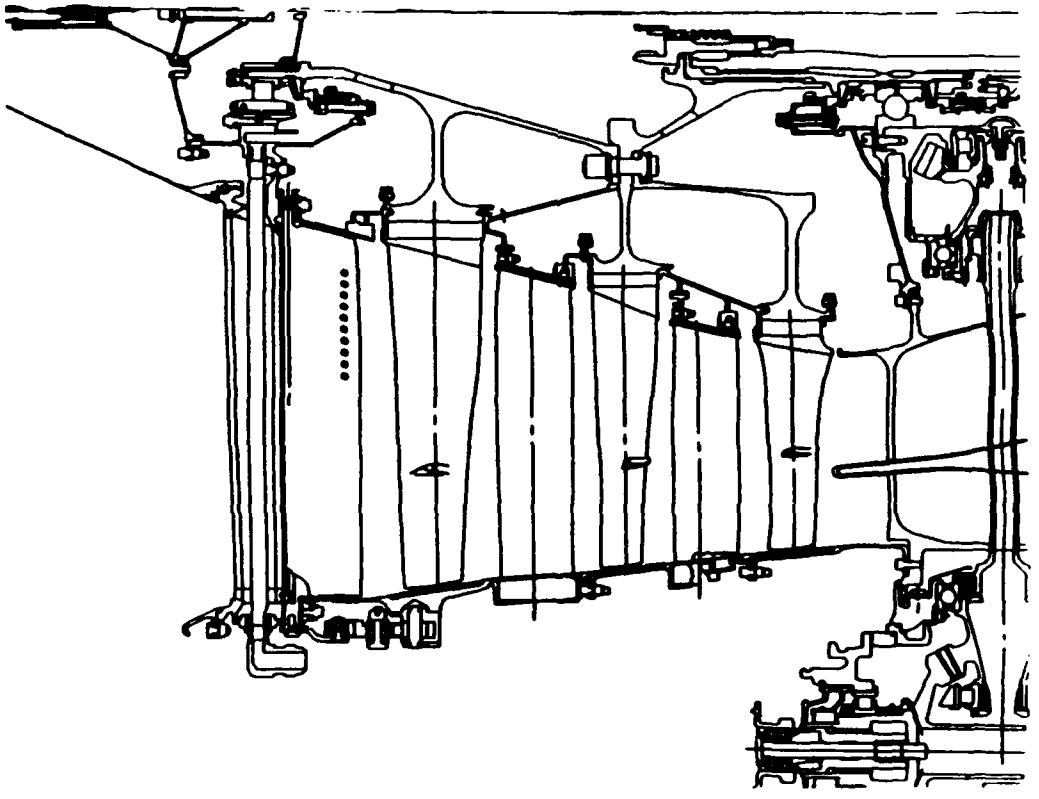

Figure 2. F100 Fan Module (1–3 Stage) Cross Section

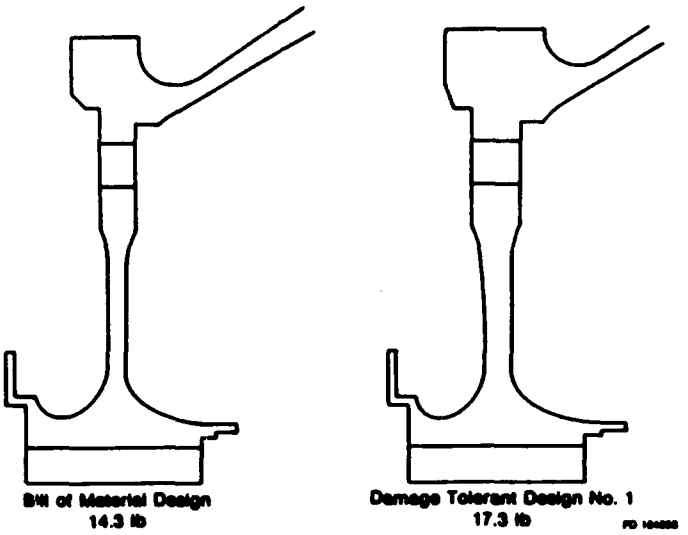

F100 2nd-Stage Fan Disk Designs.

Figure 3. Bill of Material Versus Damage Tolerant Design (DTD) Configuration

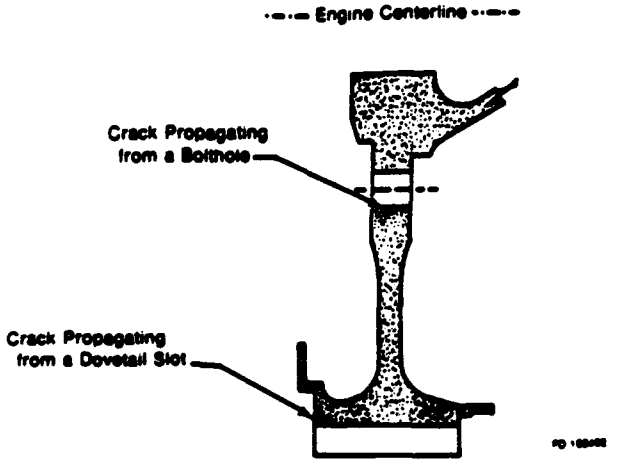

Life-Limiting Features of Damage-Tolerant Disk.

Figure 4. Life Limiting Location On Damage Tolerant Disk

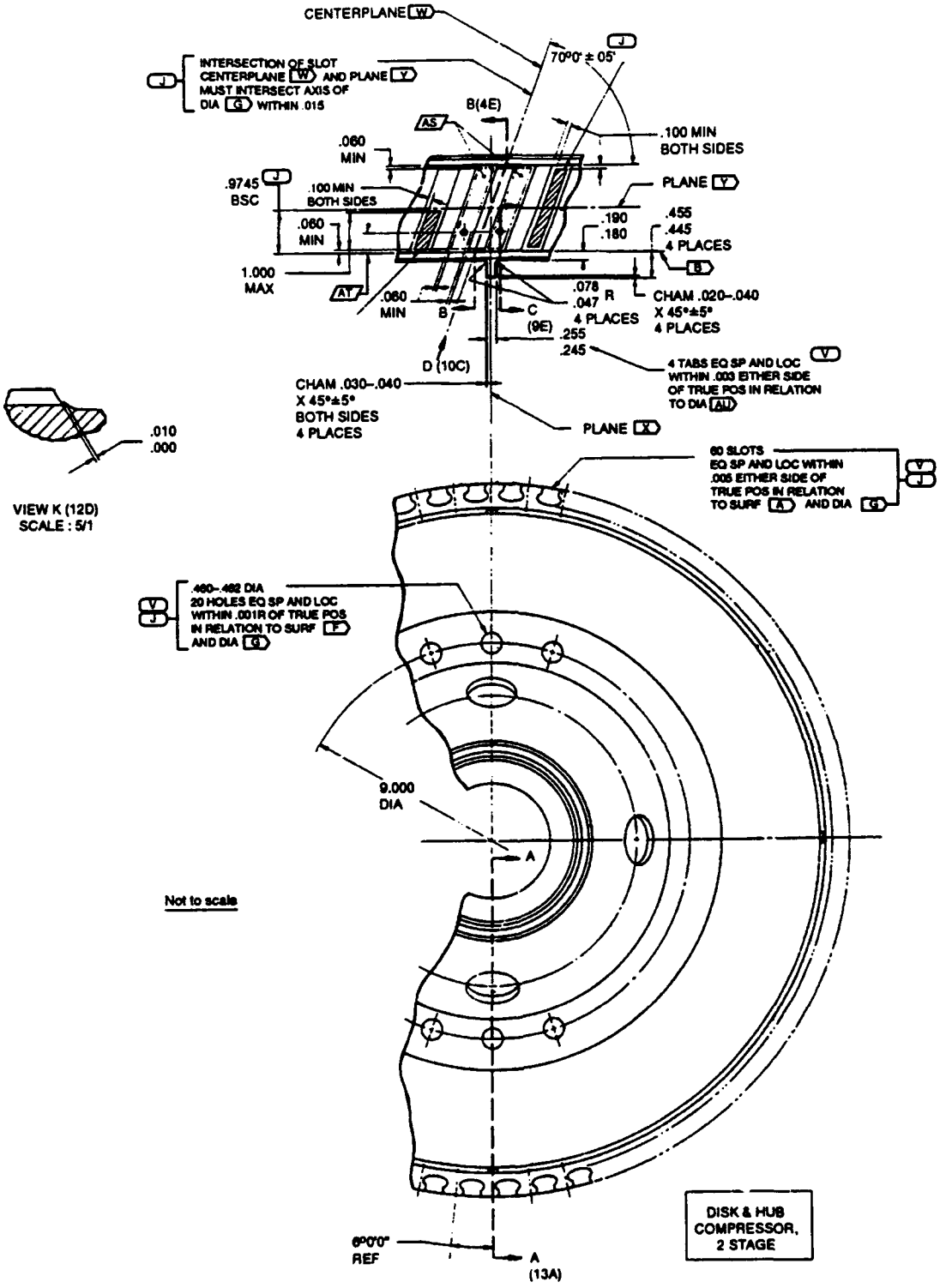

Dimensions Provided for Modeling Purposes Only.

9176

Figure 5A. Disk & Hub, Compressor, 2 Stage

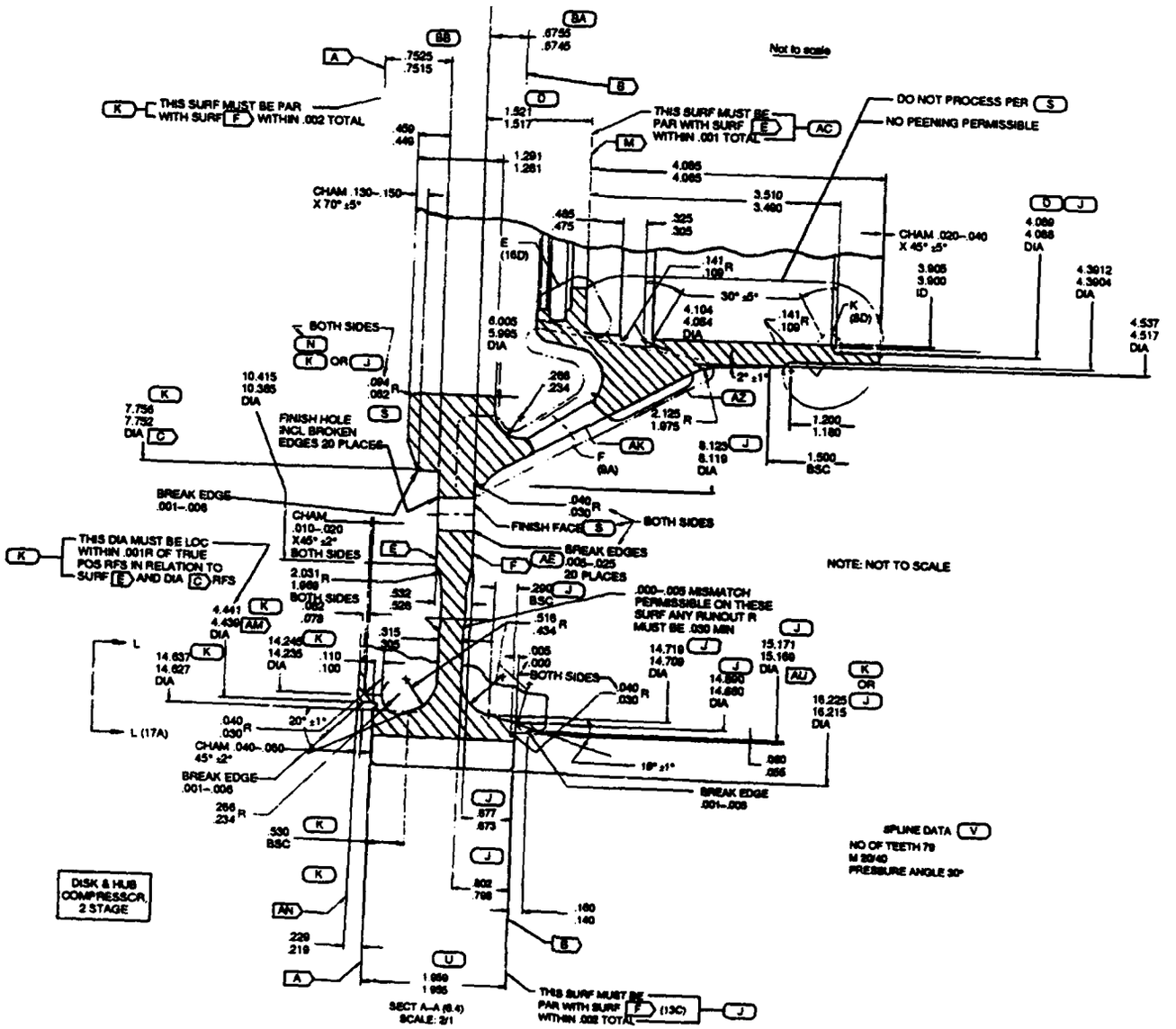

Dimensions Provided for Modeling Purposes Only.

Figure 5B. Disk & Hub, Compressor, 2 Stage

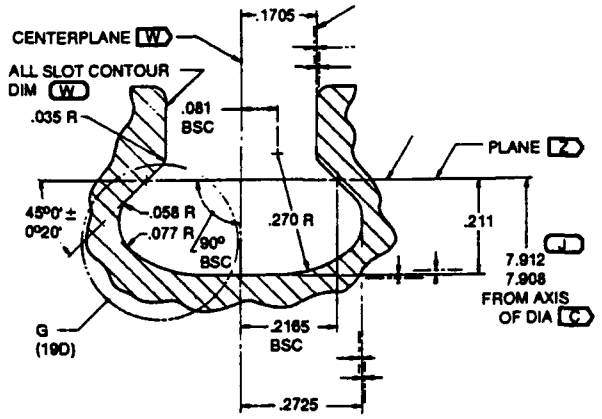

ENLARGED VIEW OF SLOT PROFILE (ROTATED) ALONG CENTERPLANE W
SCALE: 10/1

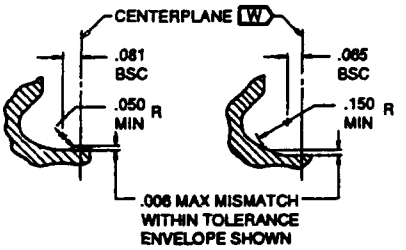

OPTIONAL VIEW AREA G (22E)
TYP BOTH SIDES
SCALE: 5/1

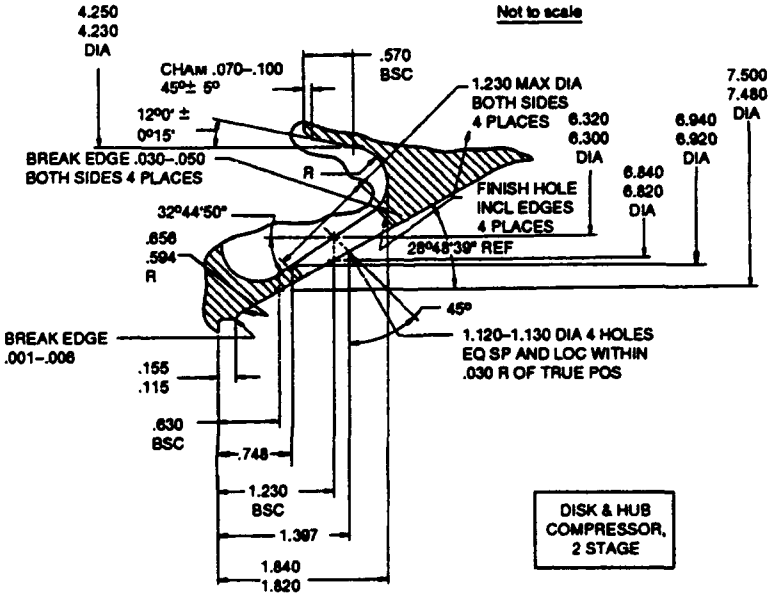

VIEW F (13C)
SCALE: 2/1

Dimensions Provided for Modeling Purposes Only.

Figure 5C. Disk & Hub, Compressor, 2 Stage

9177

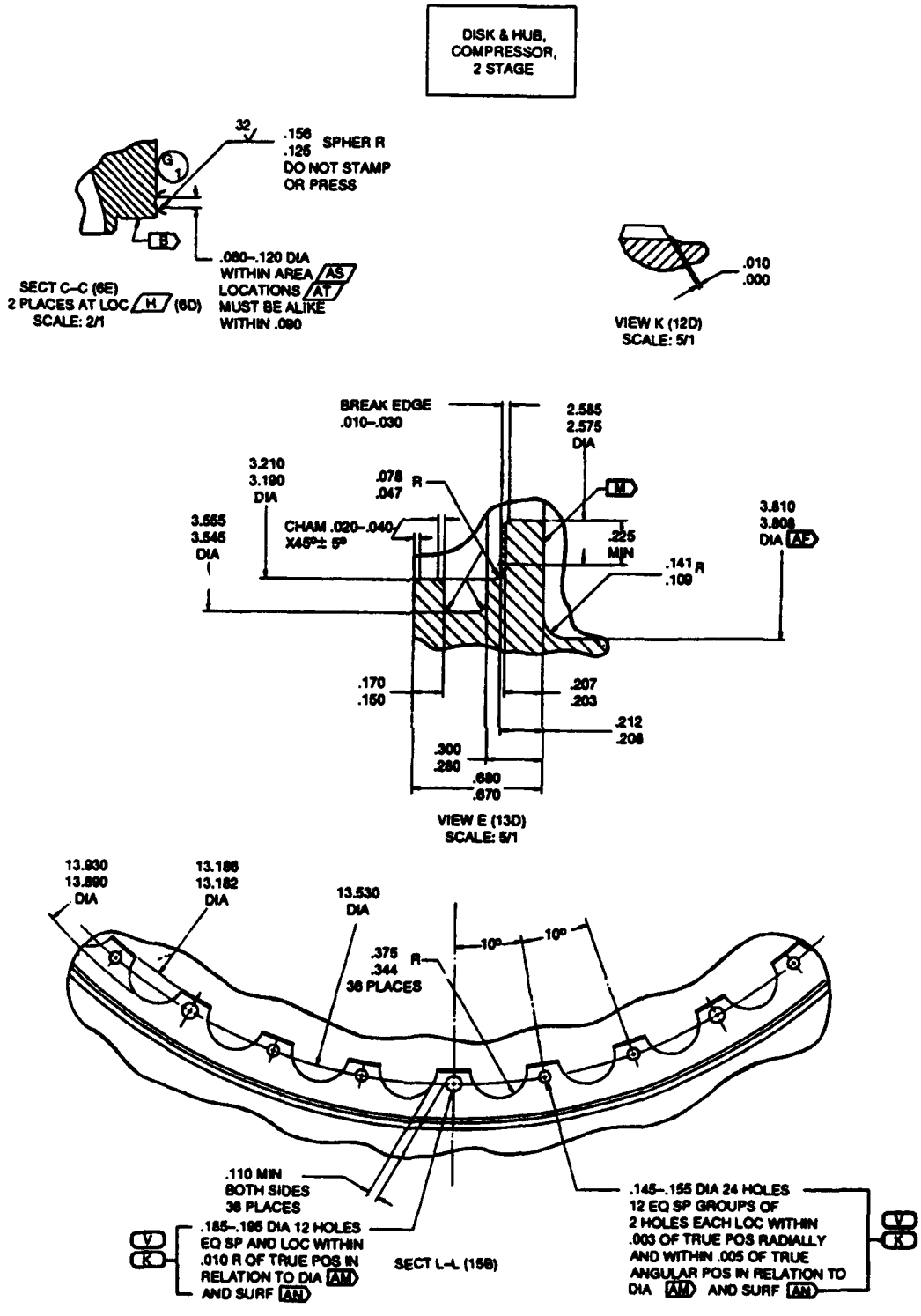

Dimensions Provided for Modeling Purposes Only.

9178

Figure 5D. Disk & Hub, Compressor, 2 Stage

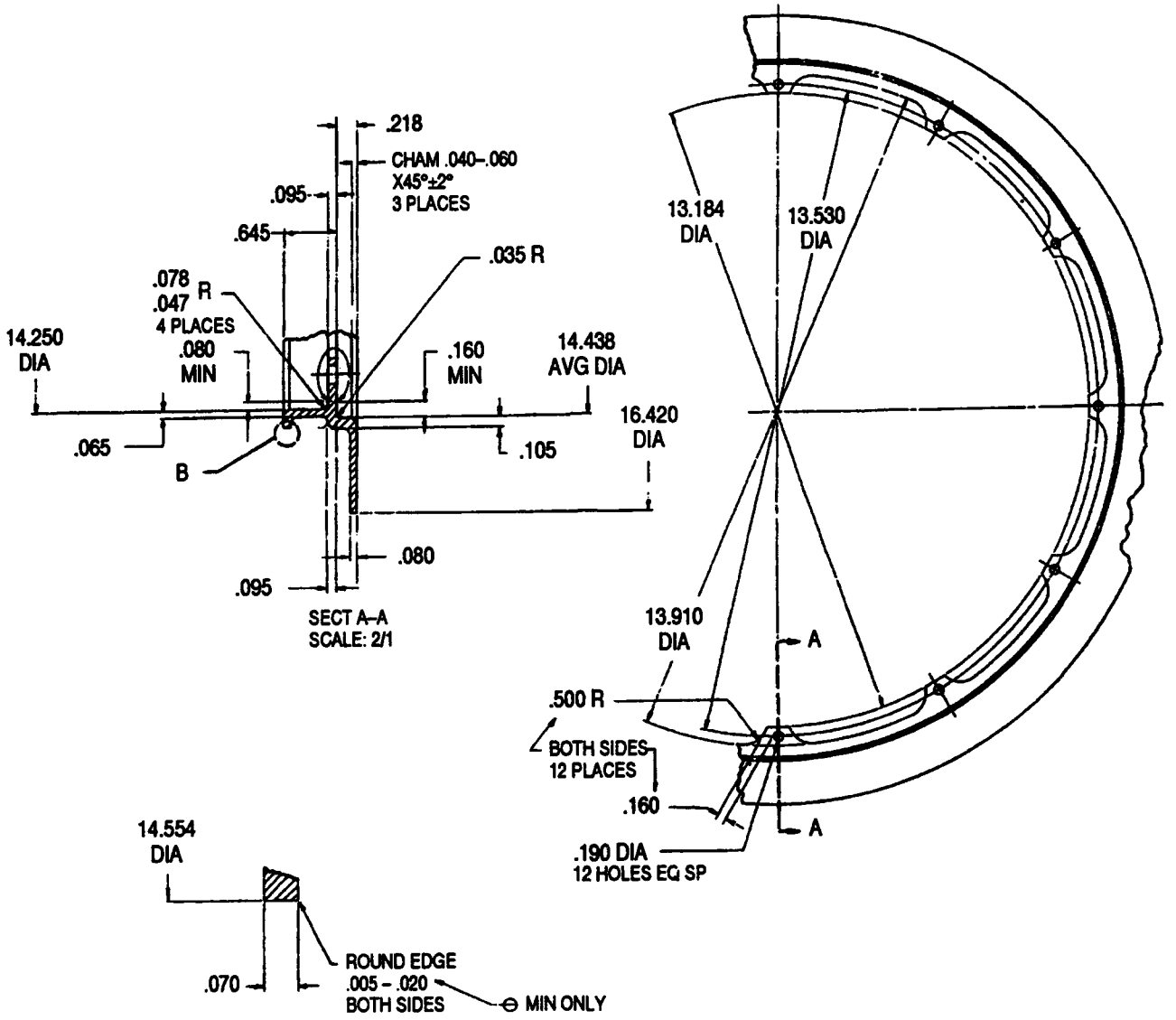

NOT TO SCALE

Dimensions Provided for Modeling Purposes Only.

9179

Figure 5E. Disk & Hub, Compressor, 2 Stage

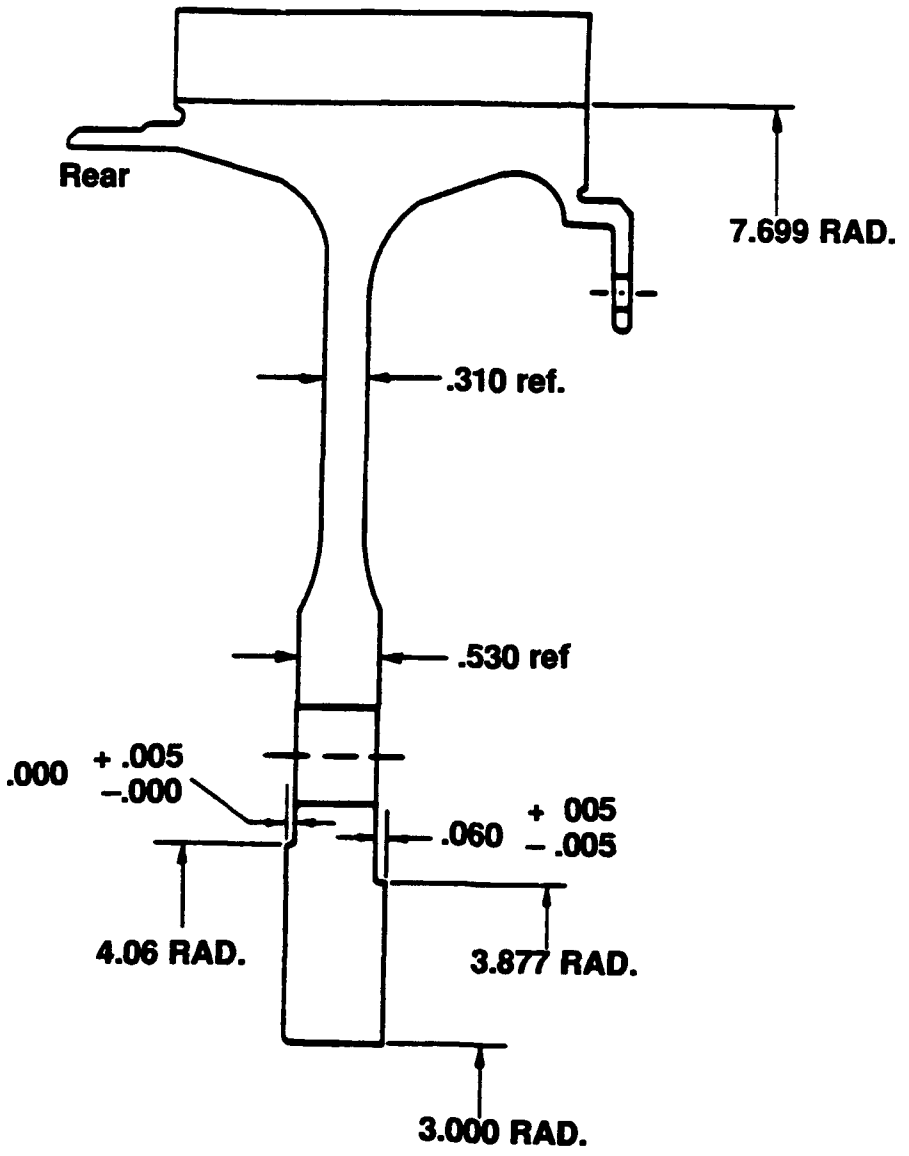

Figure 6. Ferris Wheel 2nd Disk Configuration

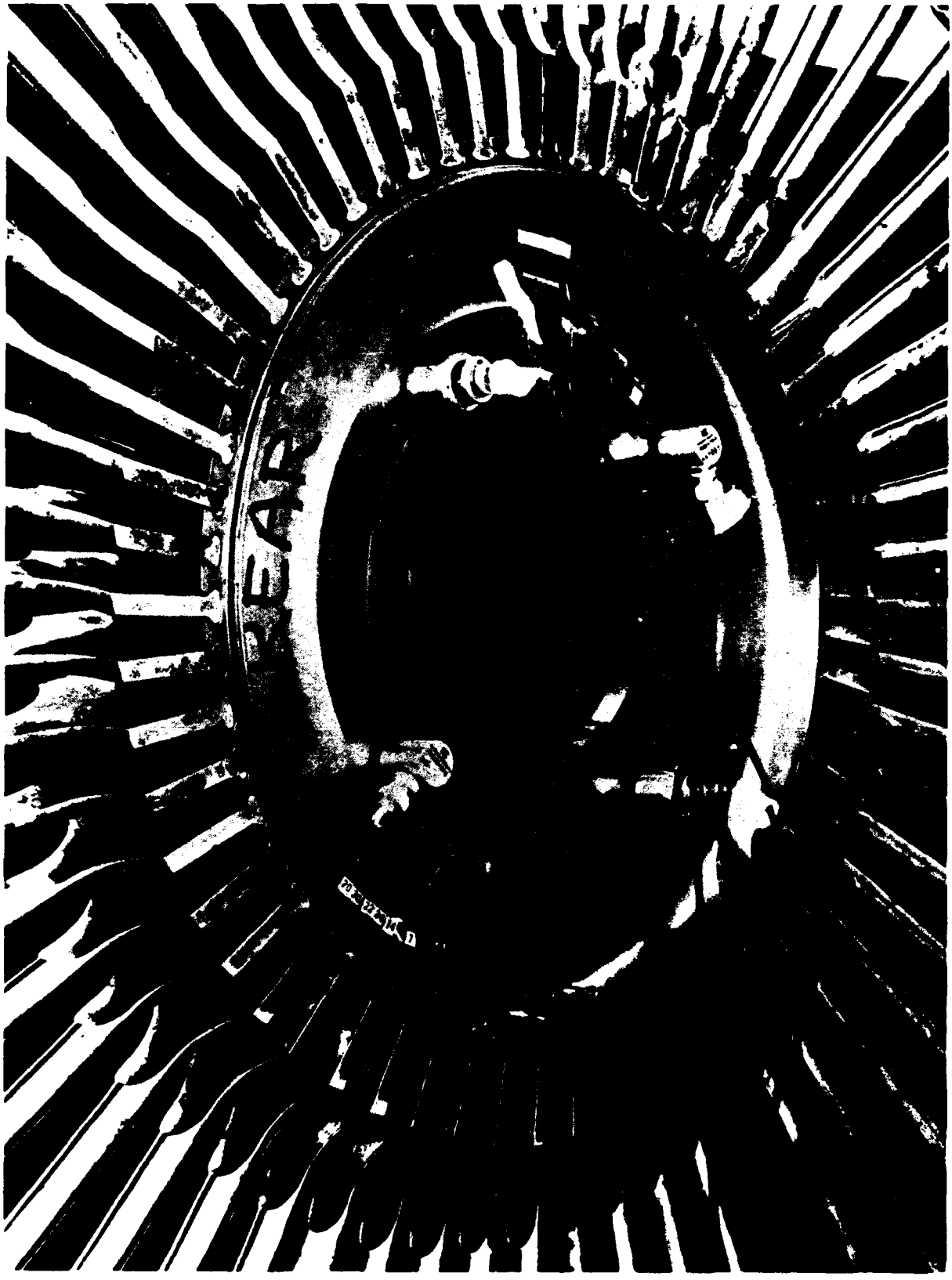

Figure 7. Ferris Wheel Test Set–up

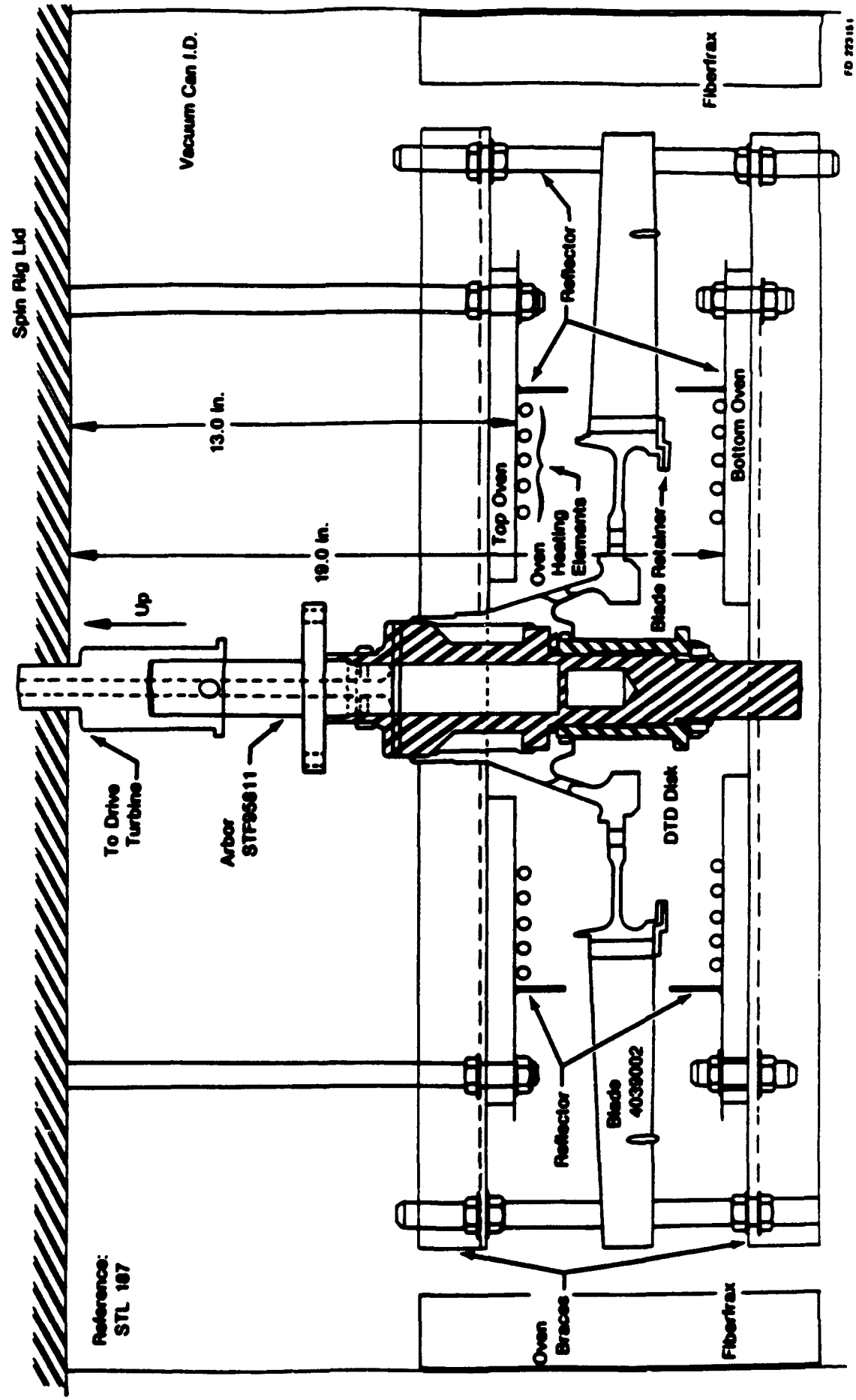

Figure 8. Oven Assembly for Hot Spin Test at 500°F. AMS 4928 Titanium Disk Derived From F100 2nd Stage Fan Design. Damage Tolerant Design Disk 1

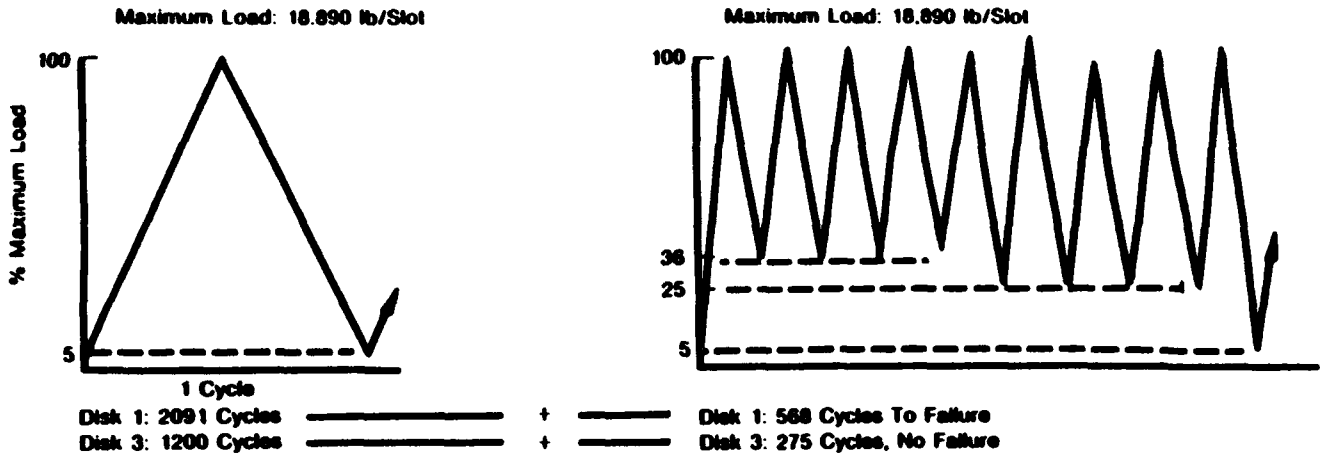

Figure 9. Load Cycle Definition for Ferris Wheel LCF Test

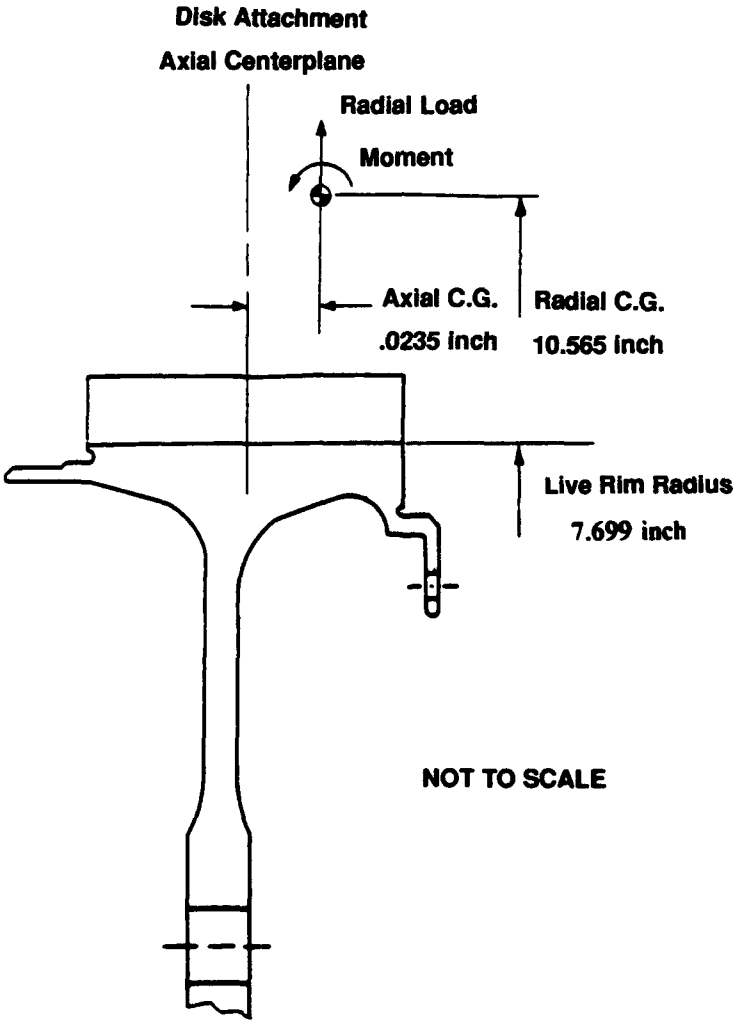

Figure 10. Live Rim Load Summary

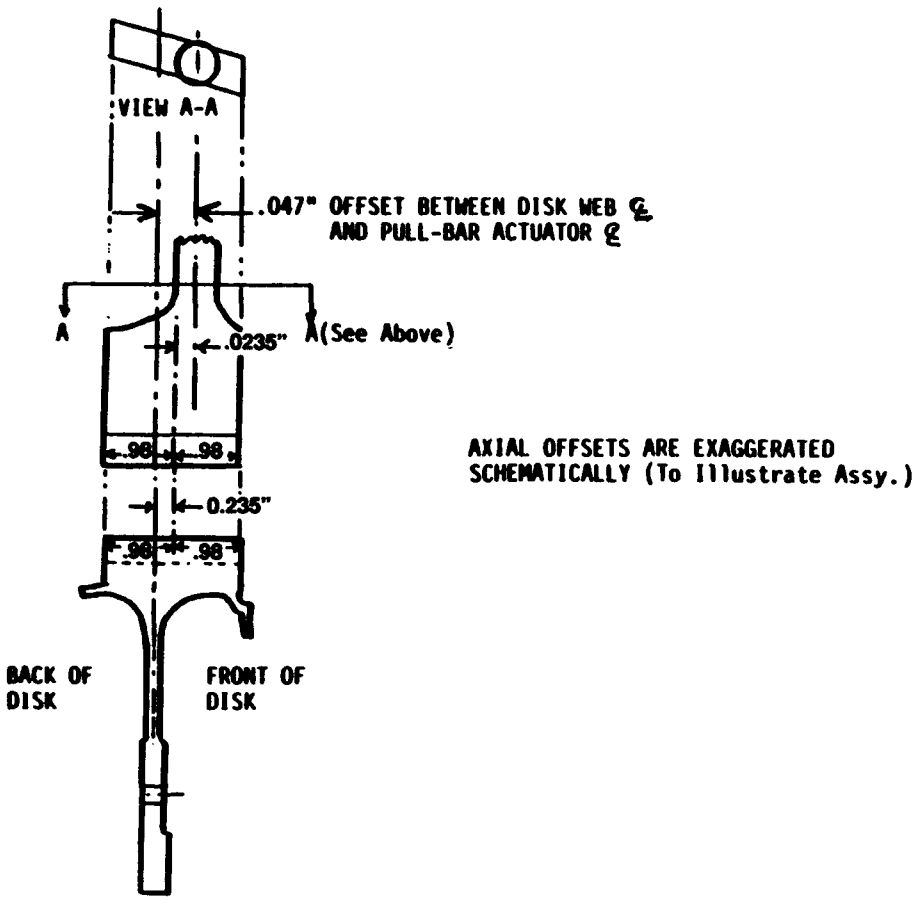

Figure 11. Ferris Wheel Load Summary

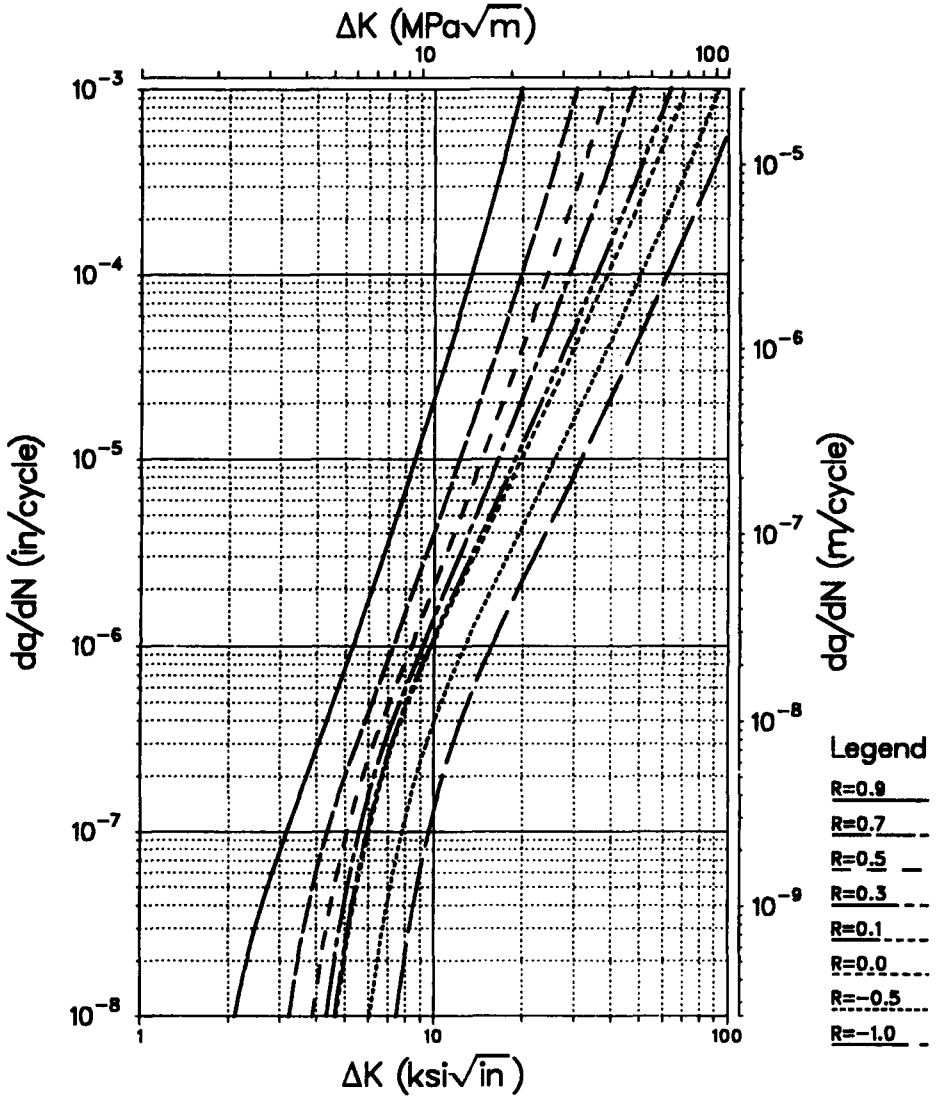

Figure 12. AMS 4928 Design System Model (Ti 6-4) Room Temperature, R-ratio = 0.9, 0.7, 0.5, 0.3, 0.1, 0.0, – 0.5, –1.0

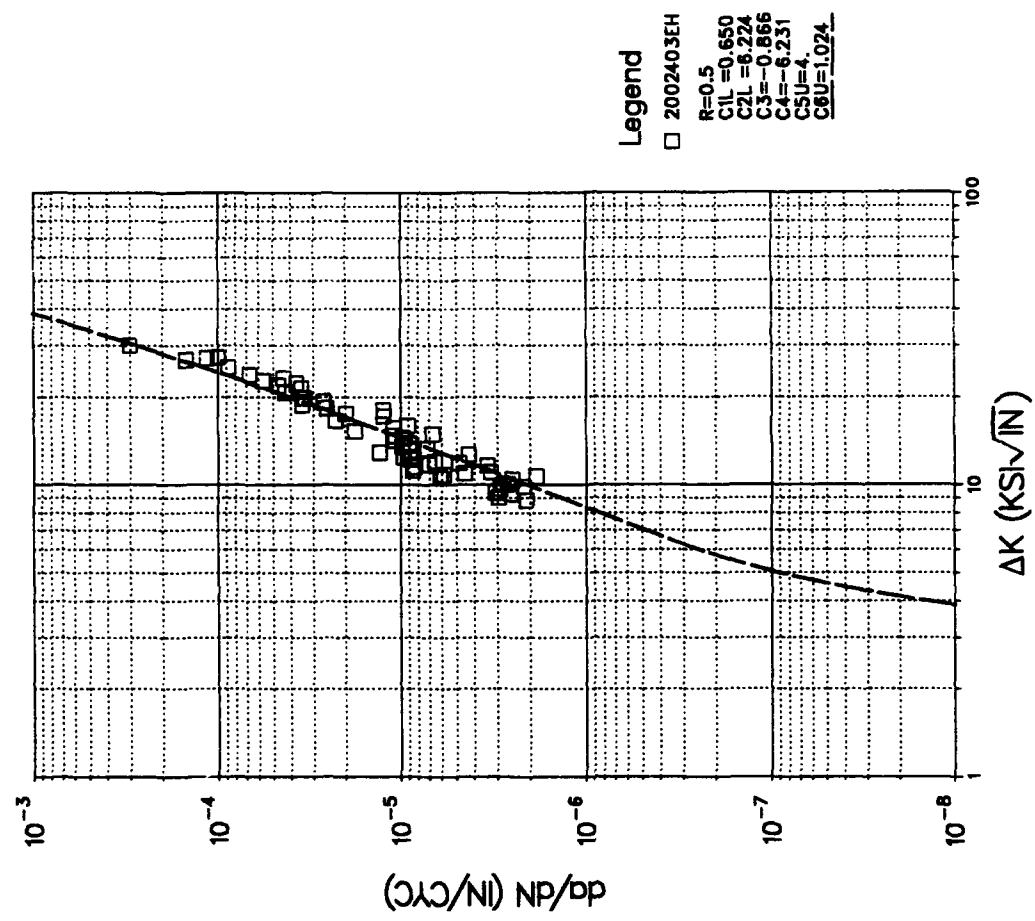

Figure 14. Ti 6-4, RT, R-ratio = 0.5, 10 cpm

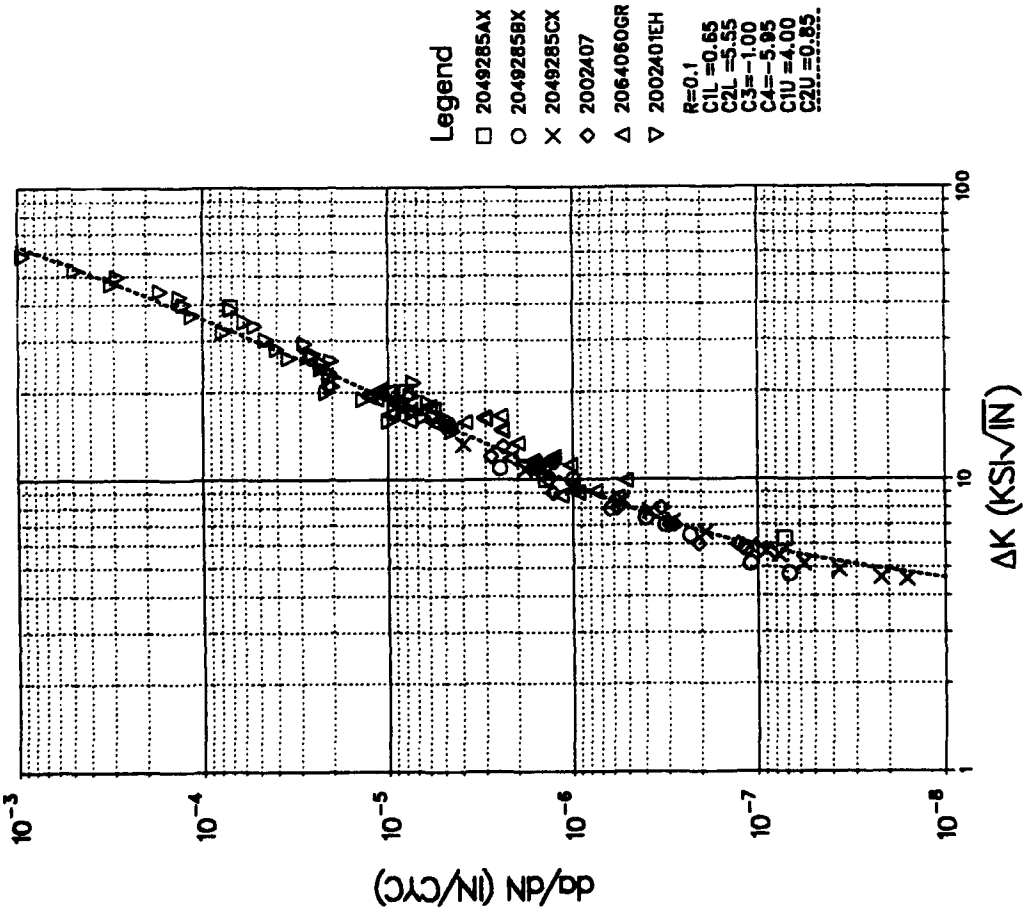

Figure 13. Ti 6-4, RT, R-ratio = 0.1, 10 cpm

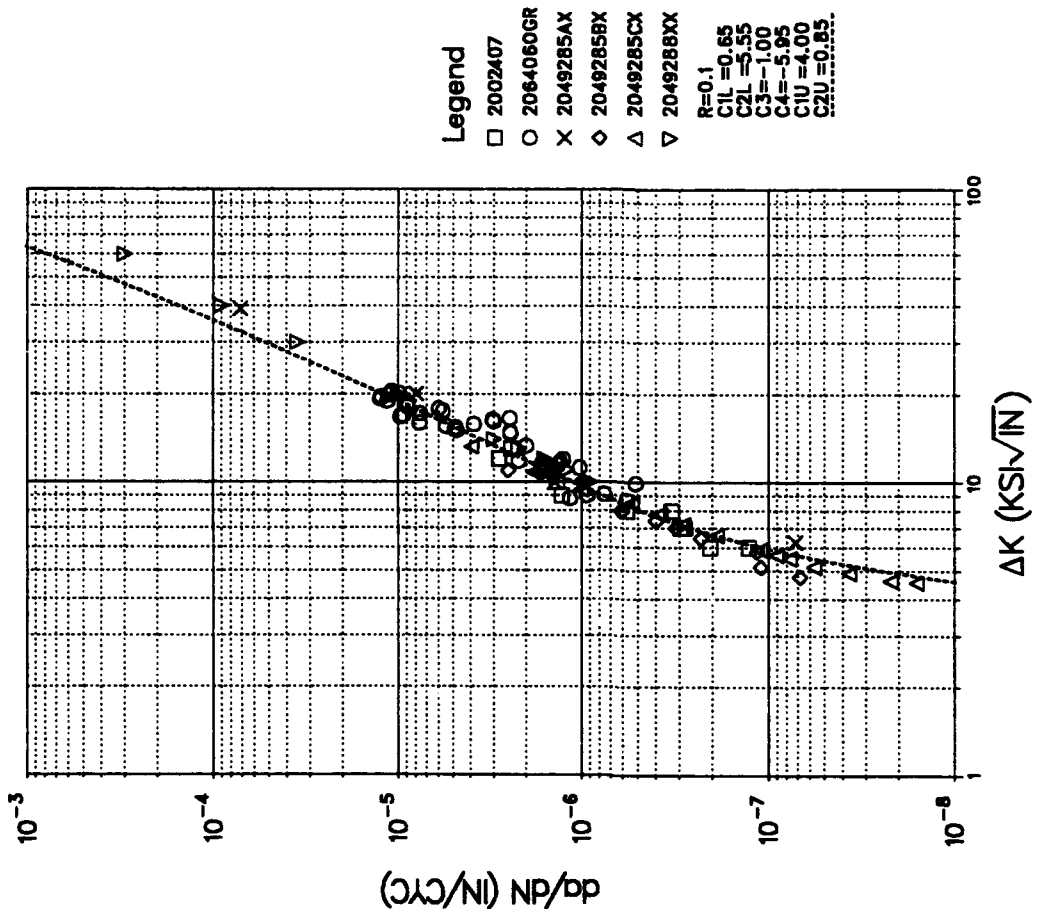

Figure 16. Ti 6–4, RT, R-ratio = 0.1, 1–30 Hz

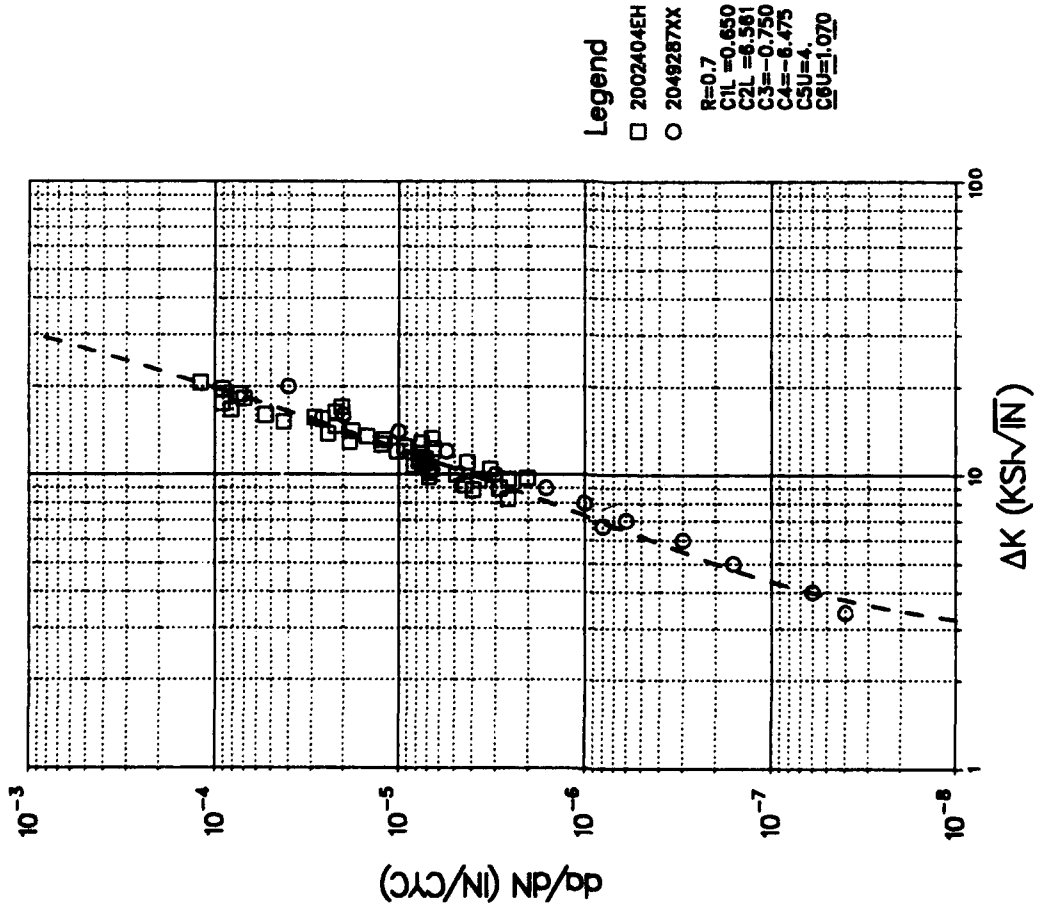

Figure 15. Ti 6–4, RT, R-ratio = 0.7, 10 cpm

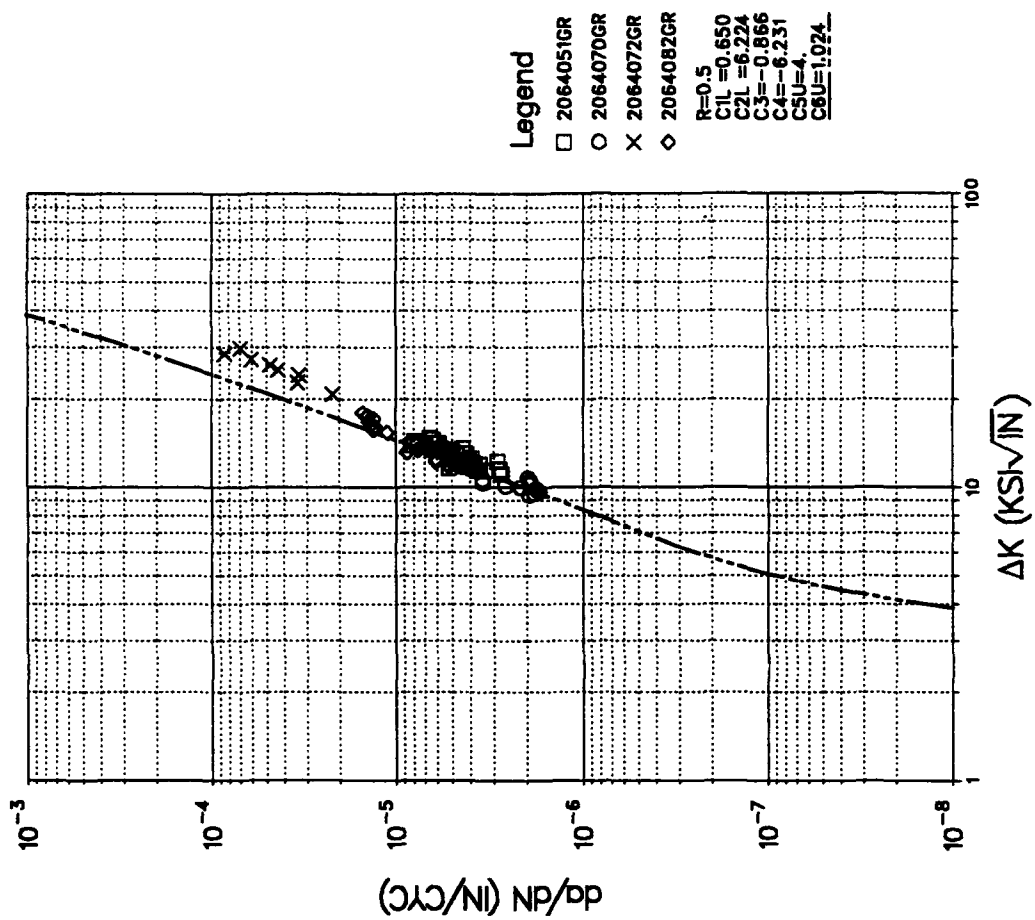

Figure 18. Ti 6-4, RT, R-ratio = 0.5, 1-30 Hz

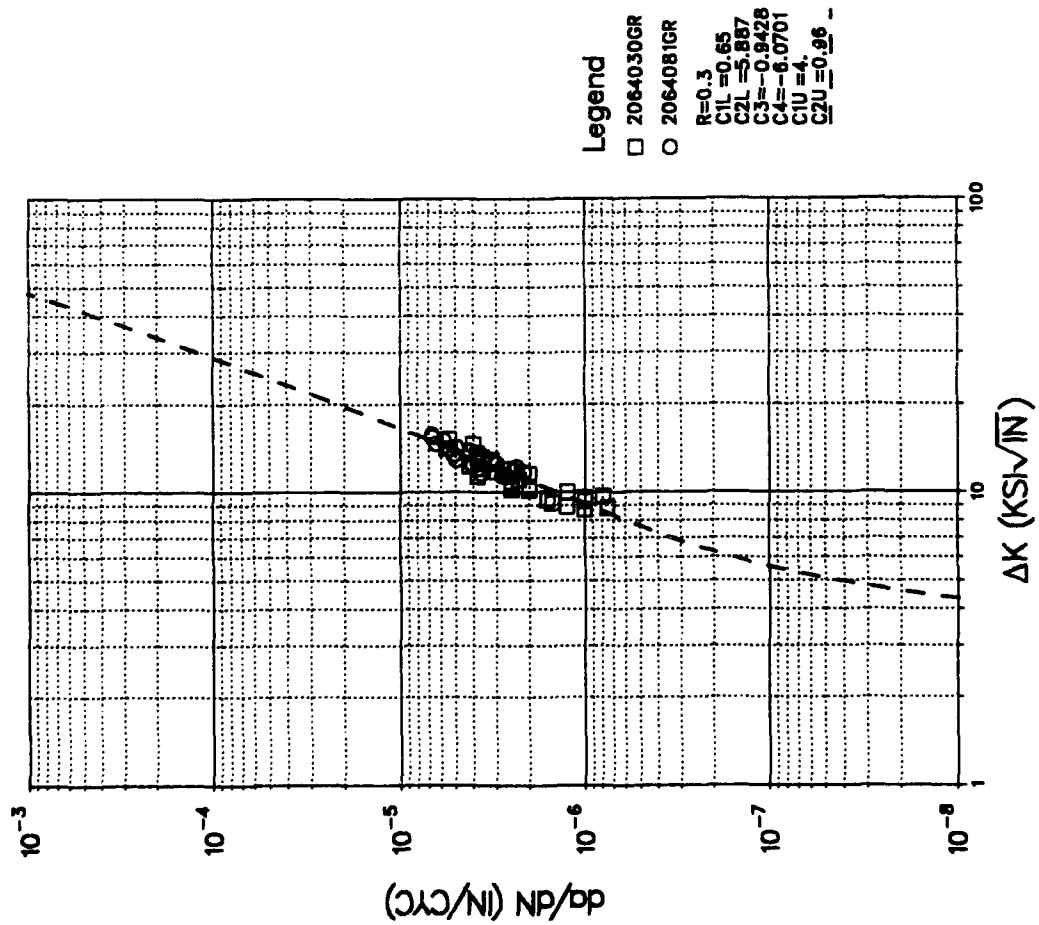

Figure 17. Ti 6-4, RT, R-ratio = 0.3, 1-30 Hz

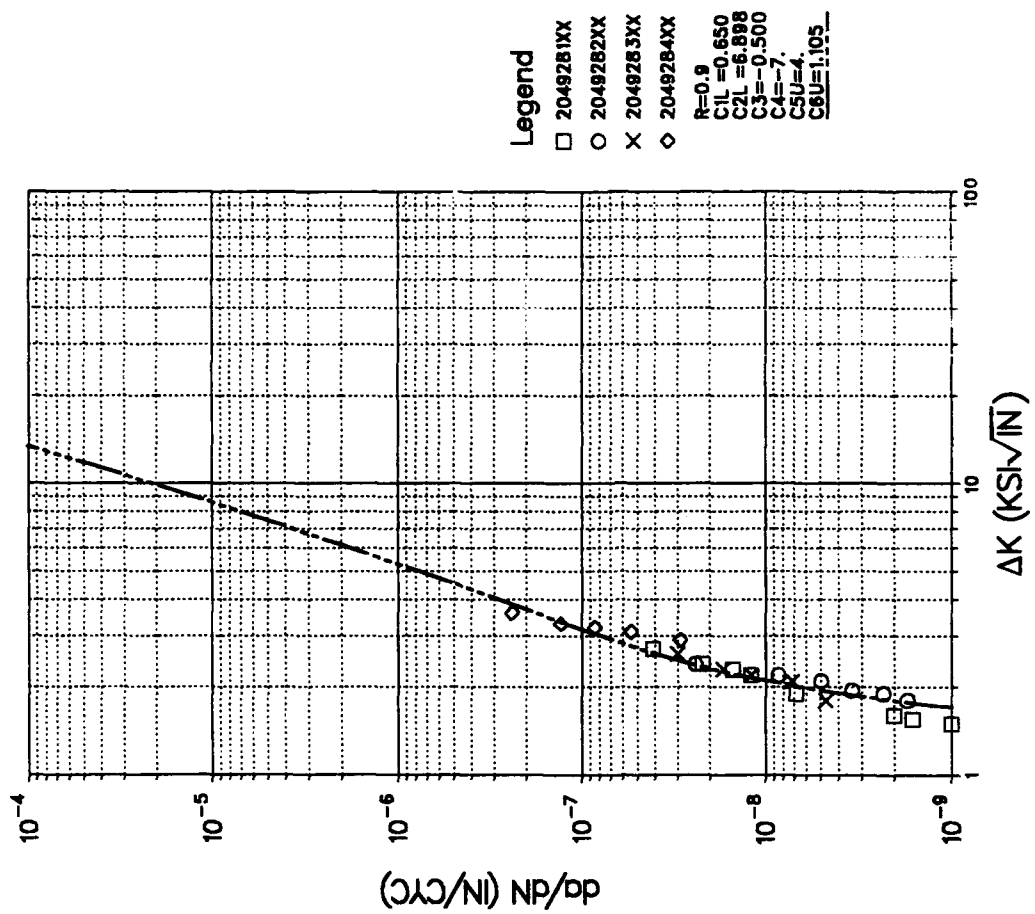

Figure 20. Ti 6–4, RT, R-ratio = 0.9, 1–30 Hz

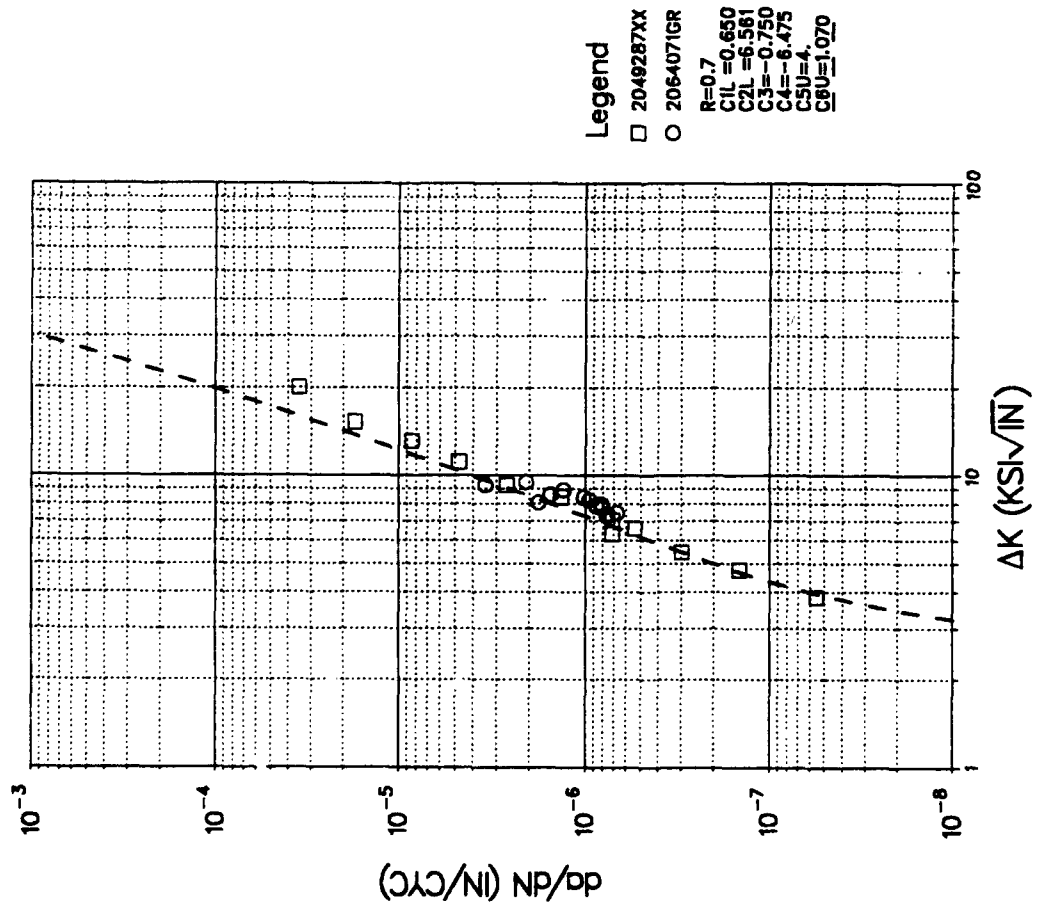

Figure 19. Ti 6–4, RT, R-ratio = 0.7, 1–30 Hz

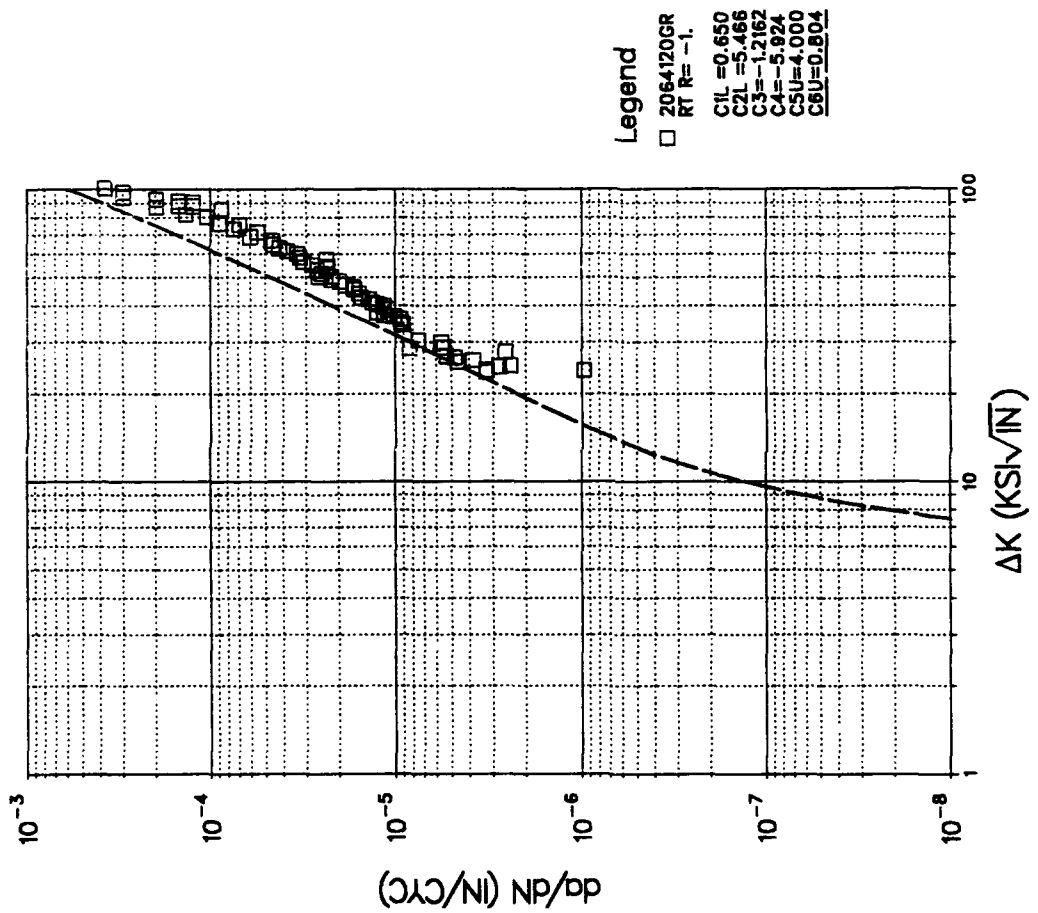

Figure 21. Ti 6-4, R-ratio = -1, 10 cpm

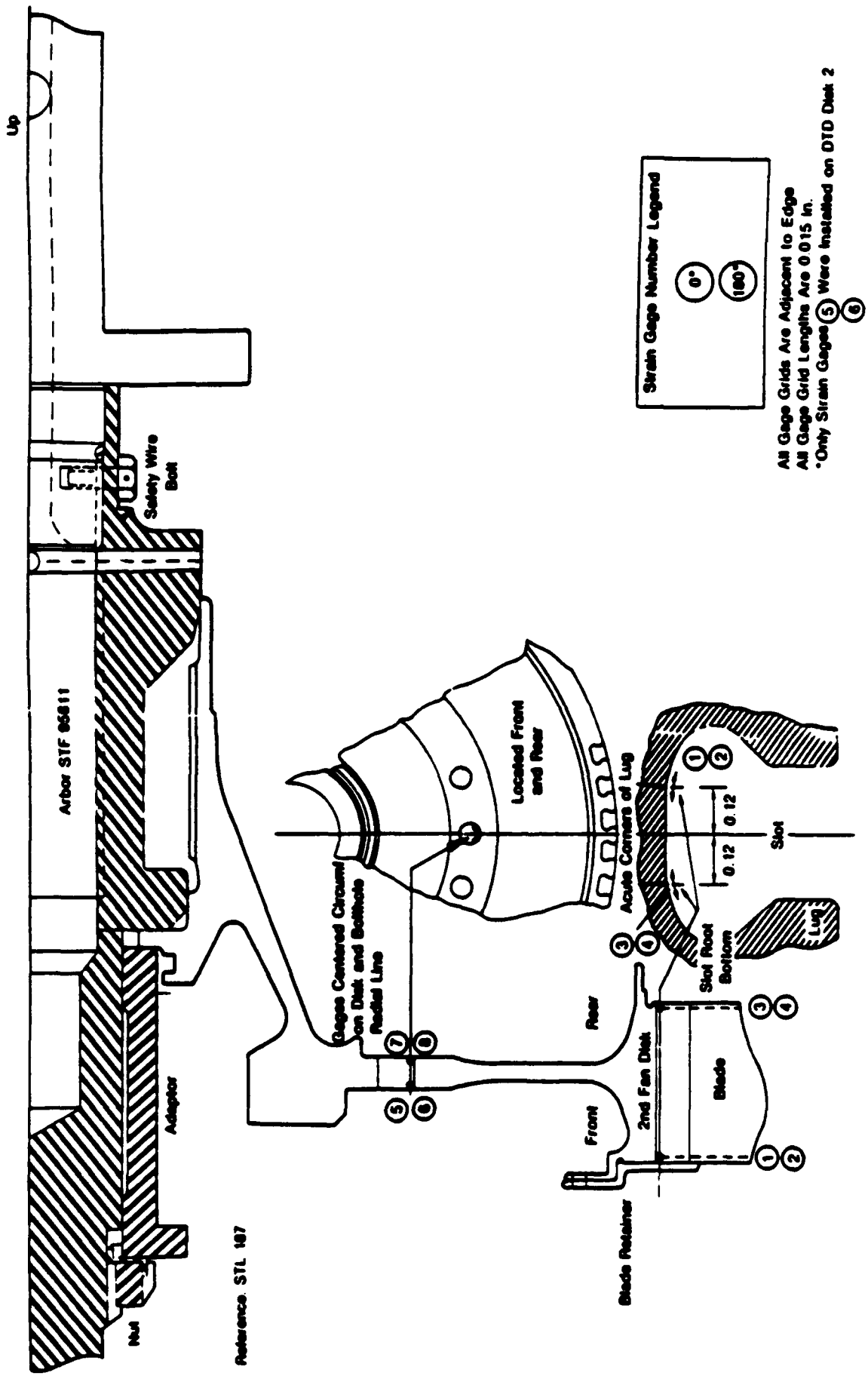

Figure 22. Strain Gage Locations
AMS 4928 Titanium Disk Derived From F100 2nd Stage Fan Design.

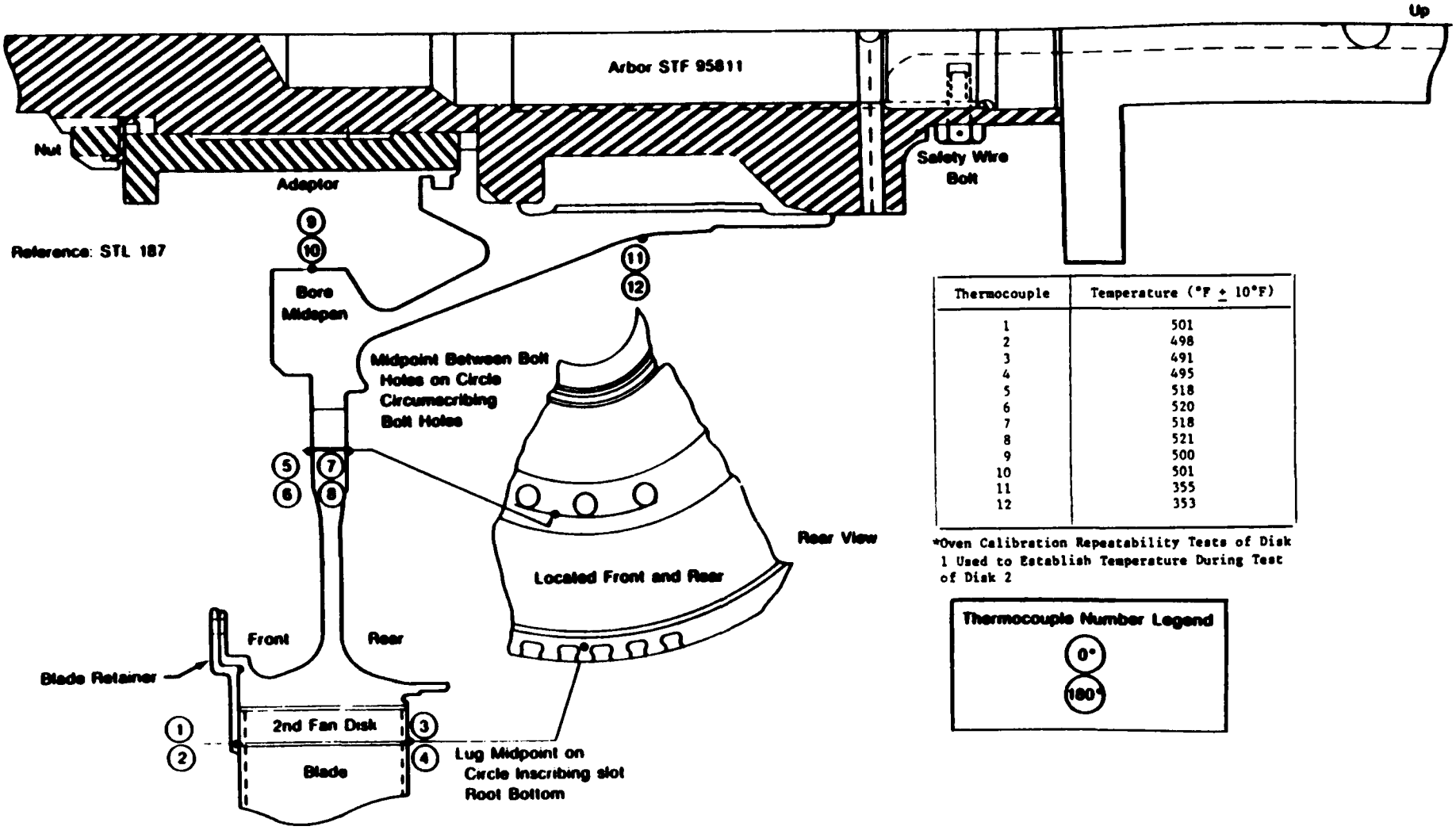

Thermocouple	Temperature (°F ± 10°F)
1	501
2	498
3	491
4	495
5	518
6	520
7	518
8	521
9	500
10	501
11	355
12	353

*Oven Calibration Repeatability Tests of Disk 1 Used to Establish Temperature During Test of Disk 2

Figure 23. Thermocouple Locations for Oven Calibration AMS 4928 Titanium Disk Derived From F100 2nd Stage Fan Design.

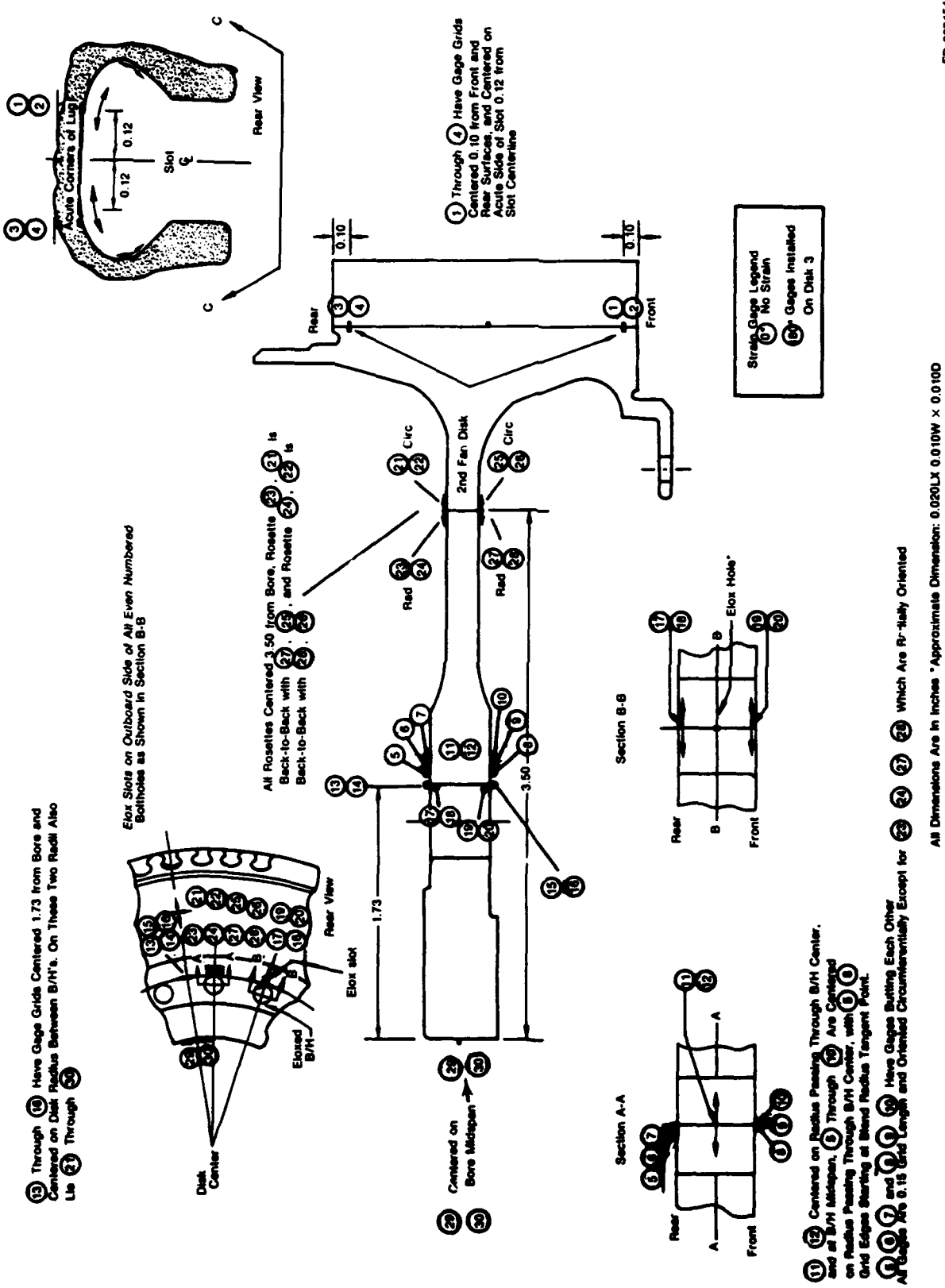

Figure 24. Strain Gage and Elox Locations AMS 4928 Titanium Disk Derived From F100 2nd Stage Fan Design.

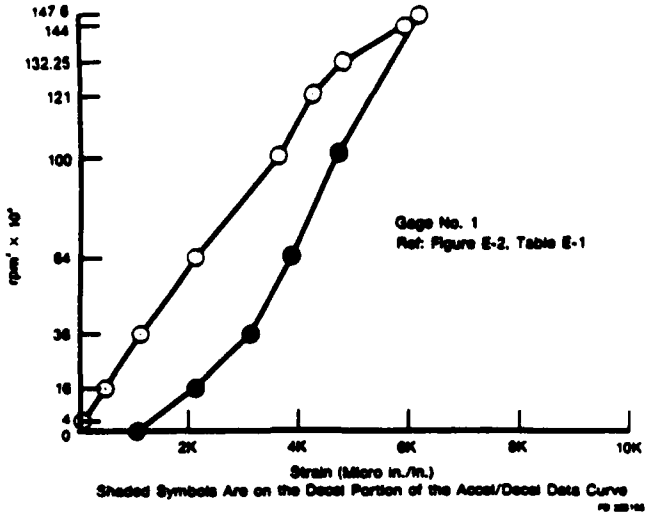

Figure 25. RPM² vs Spin Strain Accel/Decel Data at 500°F to 12,150 RPM, Damage Tolerant Design Disk 1.

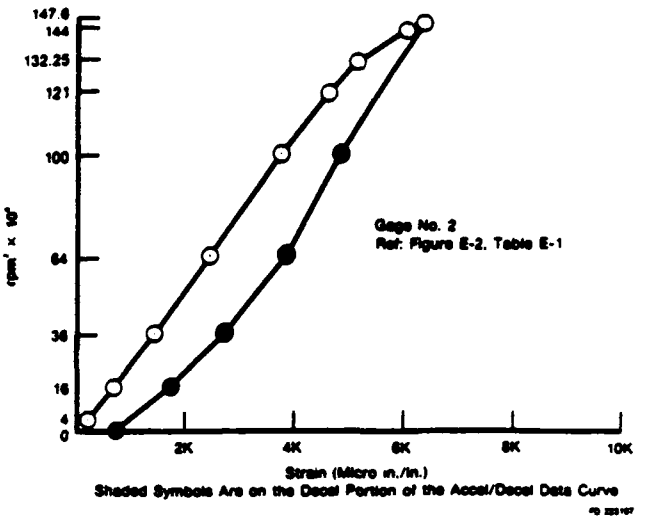

Figure 26. RPM² vs Spin Strain Accel/Decel Data at 500°F to 12,150 RPM Damage Tolerant Design Disk 1.

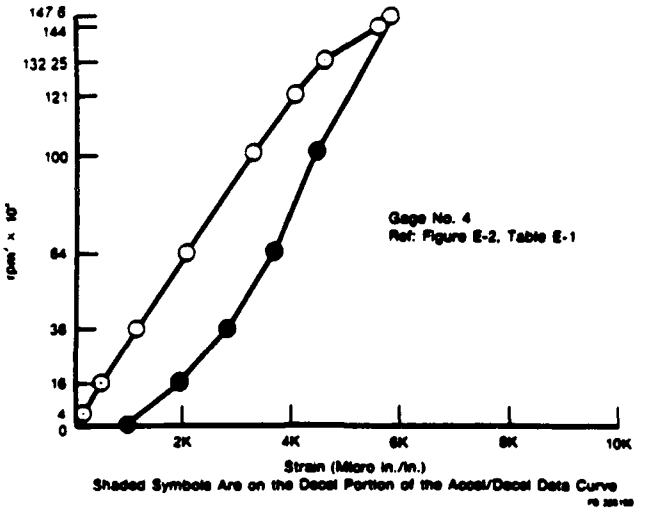

Figure 27. RPM² vs Spin Strain Accel/Decel Data at 500°F to 12,150 RPM Damage Tolerant Design Disk 1.

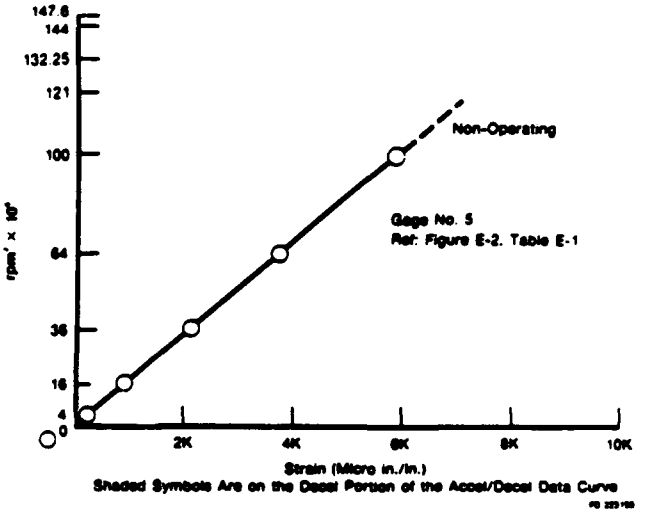

Figure 28. RPM² vs Spin Strain Accel/Decel Data at 500°F to 12,150 RPM Damage Tolerant Design Disk 1.

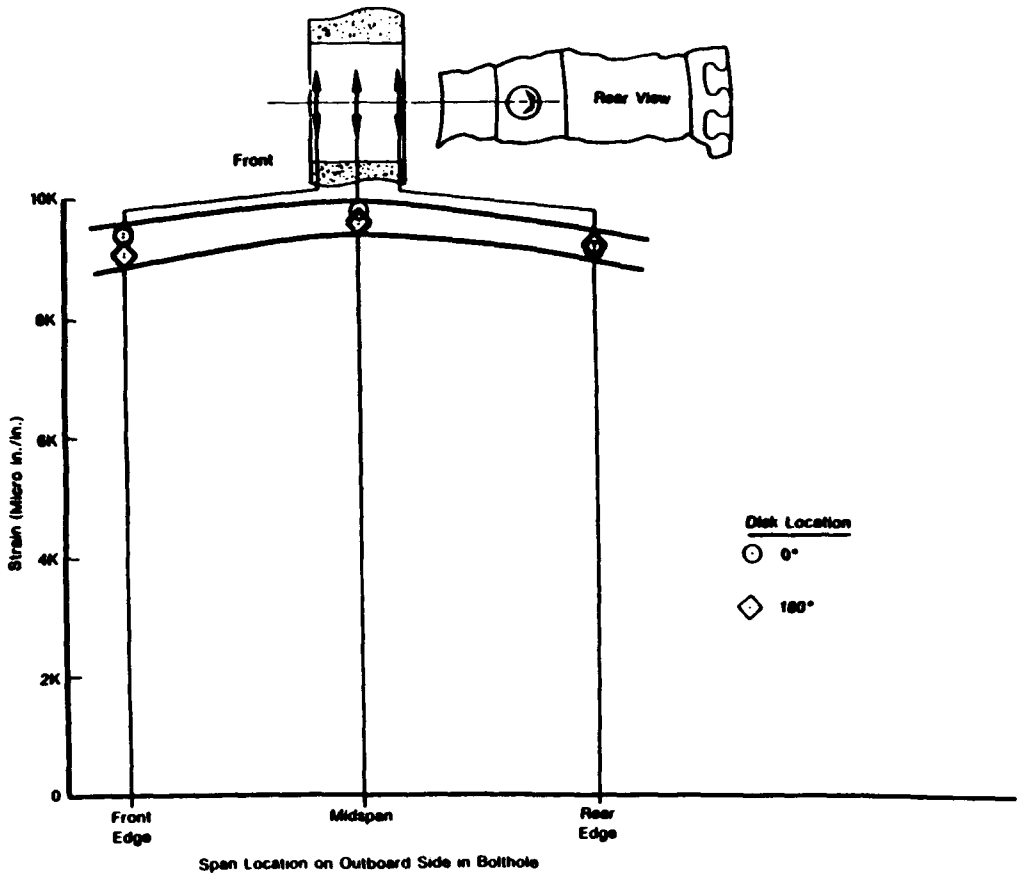

Figure 29. Static Strain Profile Outside Bolthole Edge. Room Temperature Ferris Wheel Test at 18,890 lb/slot. Damage Tolerant Design Disk 1. (Reference Figure 24 for Strain Gage Locations).

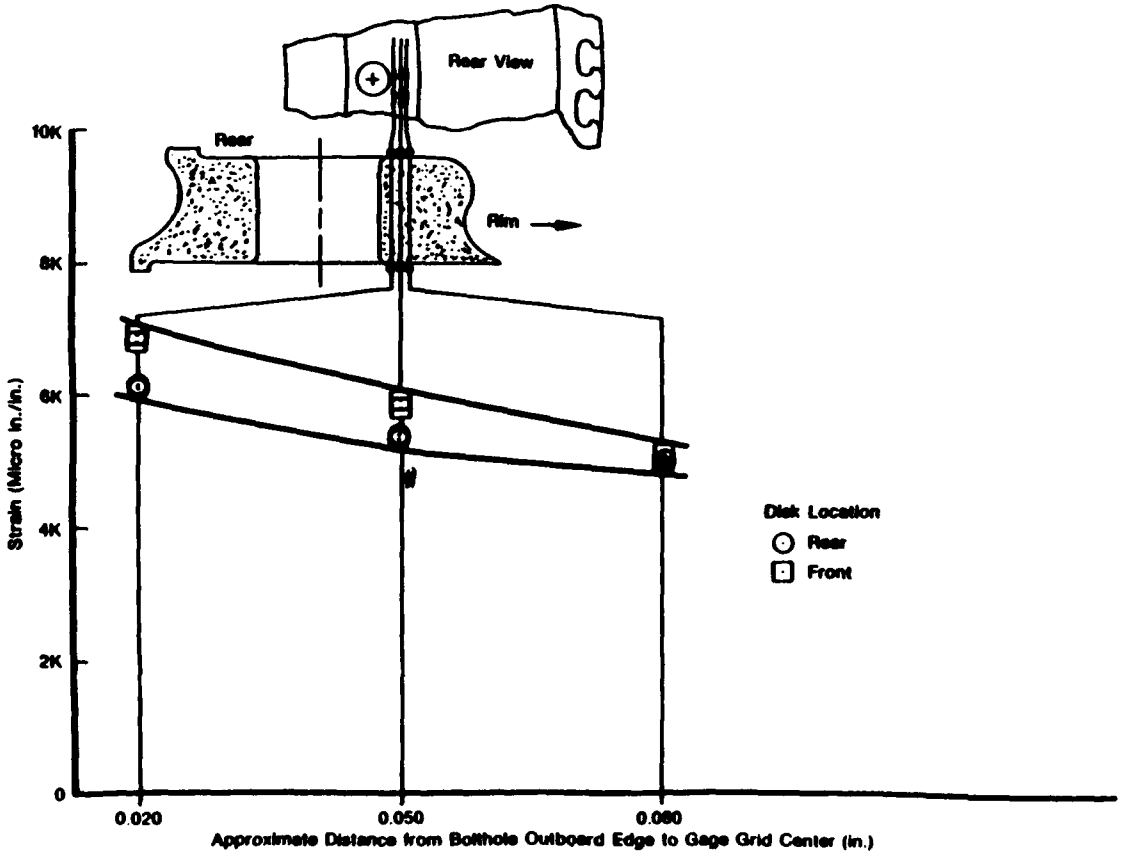

Figure 30. Static Strain Profile Outside Disk Bolthole Outboard Edge. Room Temperature Ferris Wheel Test at 18,890 lb/slot. Damage Tolerant Design Disk 1.

Disk 1

Mag: 100X

Elox Slot in Bolthole 4,
Outboard Side

Disk 3

Mag: 100X

Elox Slot in Bolthole 6,
Outboard Side

FD 208992
810704
bt3-830
FMMT 22361

Figure 31. Typical Baseline Elox Slot Pre-Flaw Indications Room Temperature Ferris Wheel LCF Test Damage Tolerant Design Disks 1 and 3

Baseline

Mag: 50X

500 Sawtooth Cycles

Mag: 50X

1100 Sawtooth Cycles

Mag: 50X

1200 Sawtooth + 100 Mission Cycles

Mag: 50X

1200 Sawtooth + 275 Mission Cycles

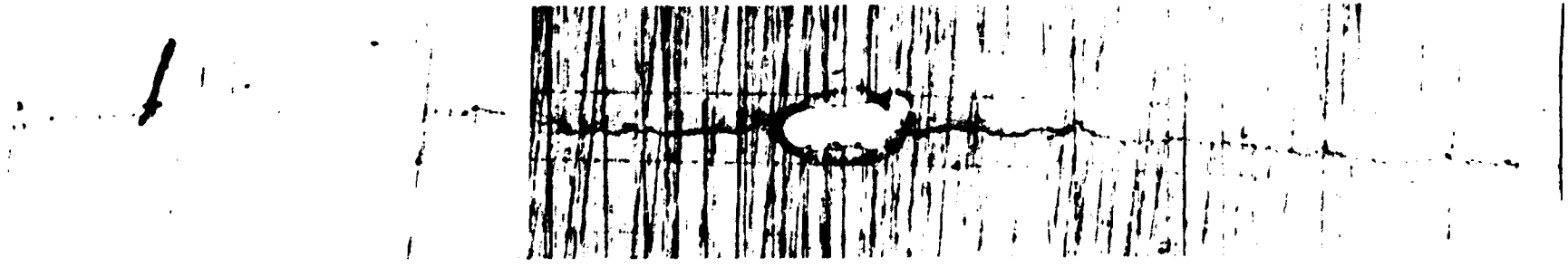

Mag: 50X

FD 214241
810704
bt3-831
FMMT 22361

Figure 32. Replication Crack Growth Progression of Bolt Hole 6 Outboard Side Room Temperature Ferris Wheel LCF Test DamageTolerant Design Disk 3

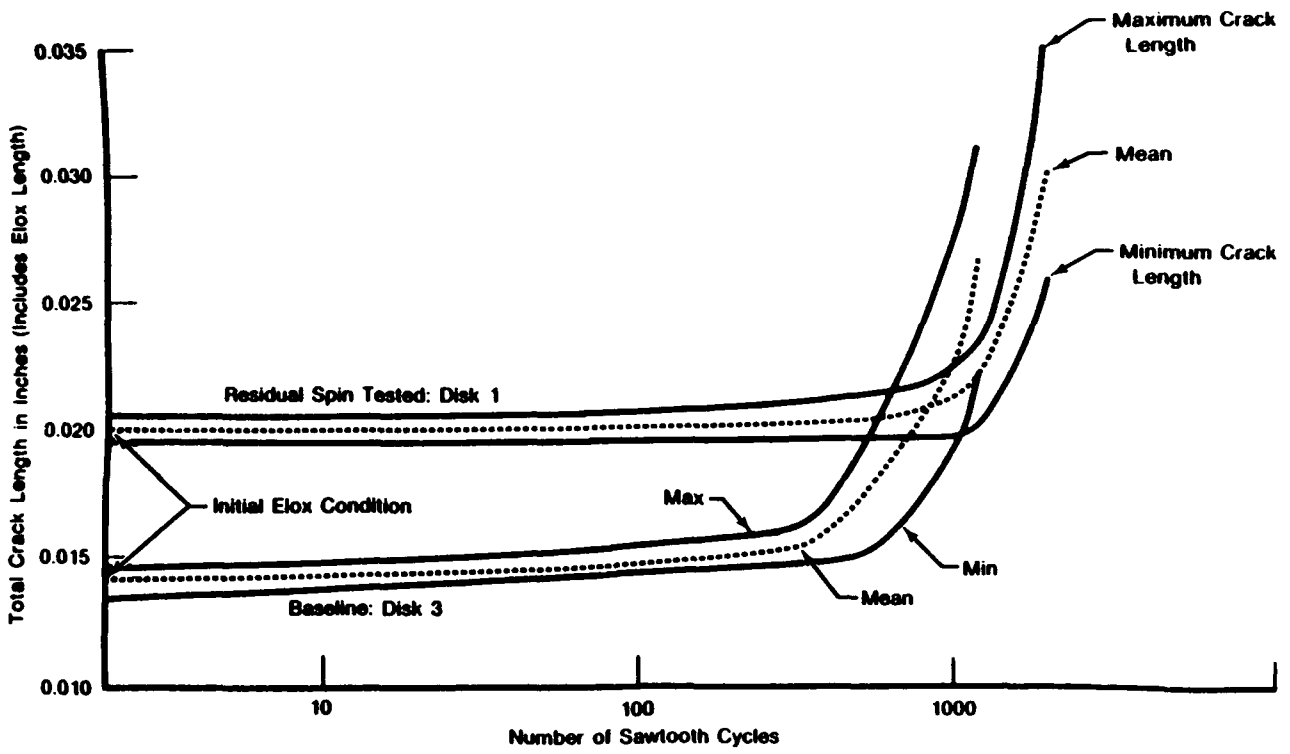

Figure 33. Bolthole Crack Growth to 1/32 in. Initiation vs Ferris Wheel Sawtooth Cycles. Room Temperature Ferris Wheel LCF Test (Maximum Load at 18,890 lb/slot). Damage Tolerant Disk 1 and Baseline Disk 3 (Data Taken From Tables 8 and 9).

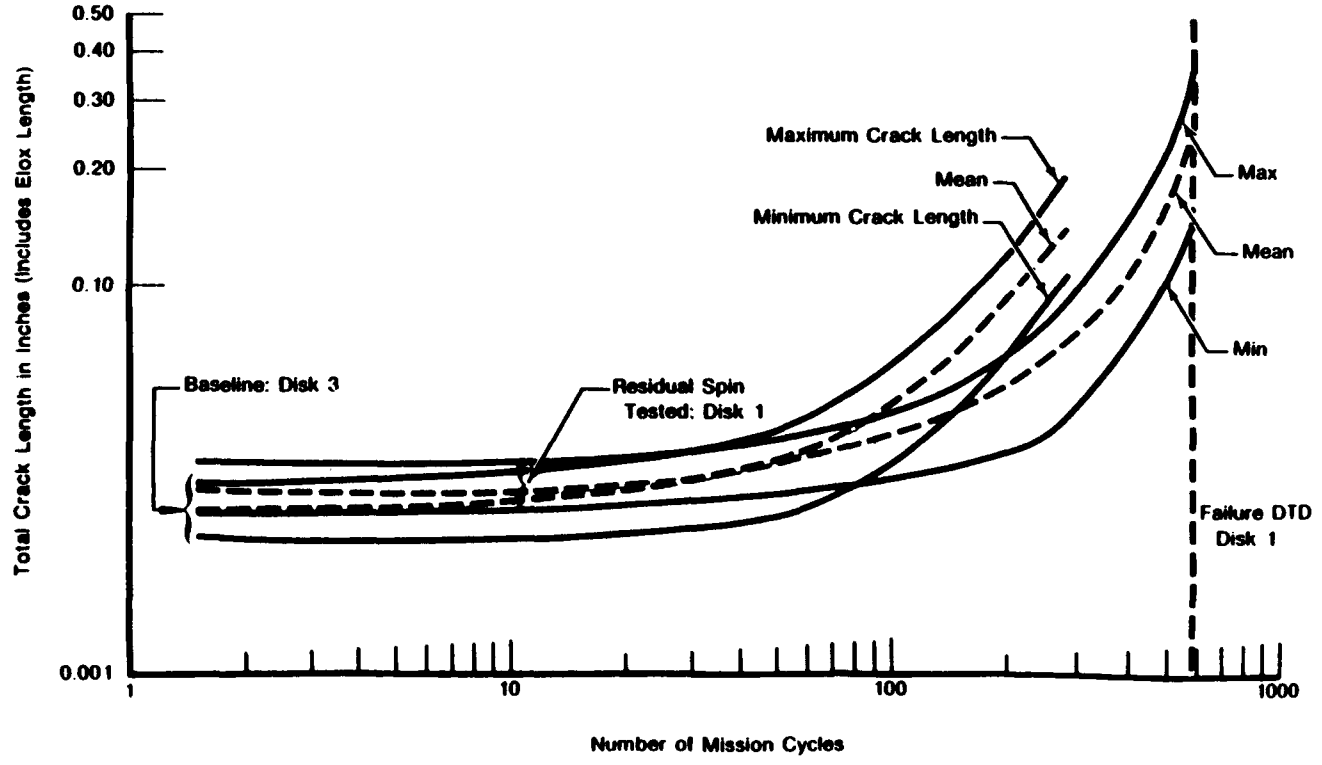

Figure 34. Bolthole Crack Growth to 1/32 in. Initiation vs Ferris Wheel Mission Cycles. Room Temperature Ferris Wheel LCF Test (Maximum Load at 18,890 lb/slot) (Data Taken from Tables 8 and 9).

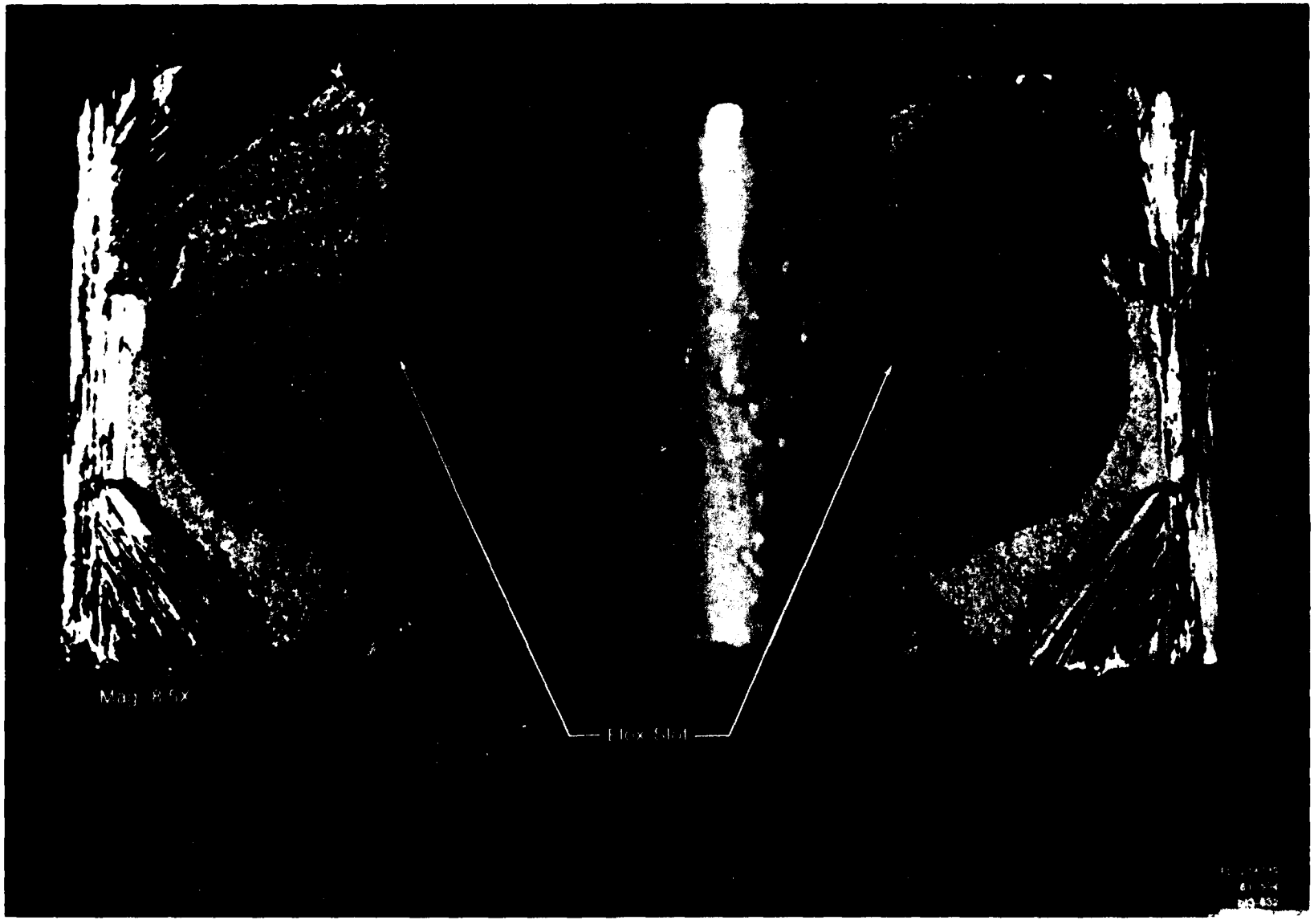

Figure 35. Close–up View of Heat Tinted Fracture Face of Elox Initiated Crack in Bolthole 6, Room Temperature Ferris Wheel LCF Test, Damage Tolerant Design Disk 1

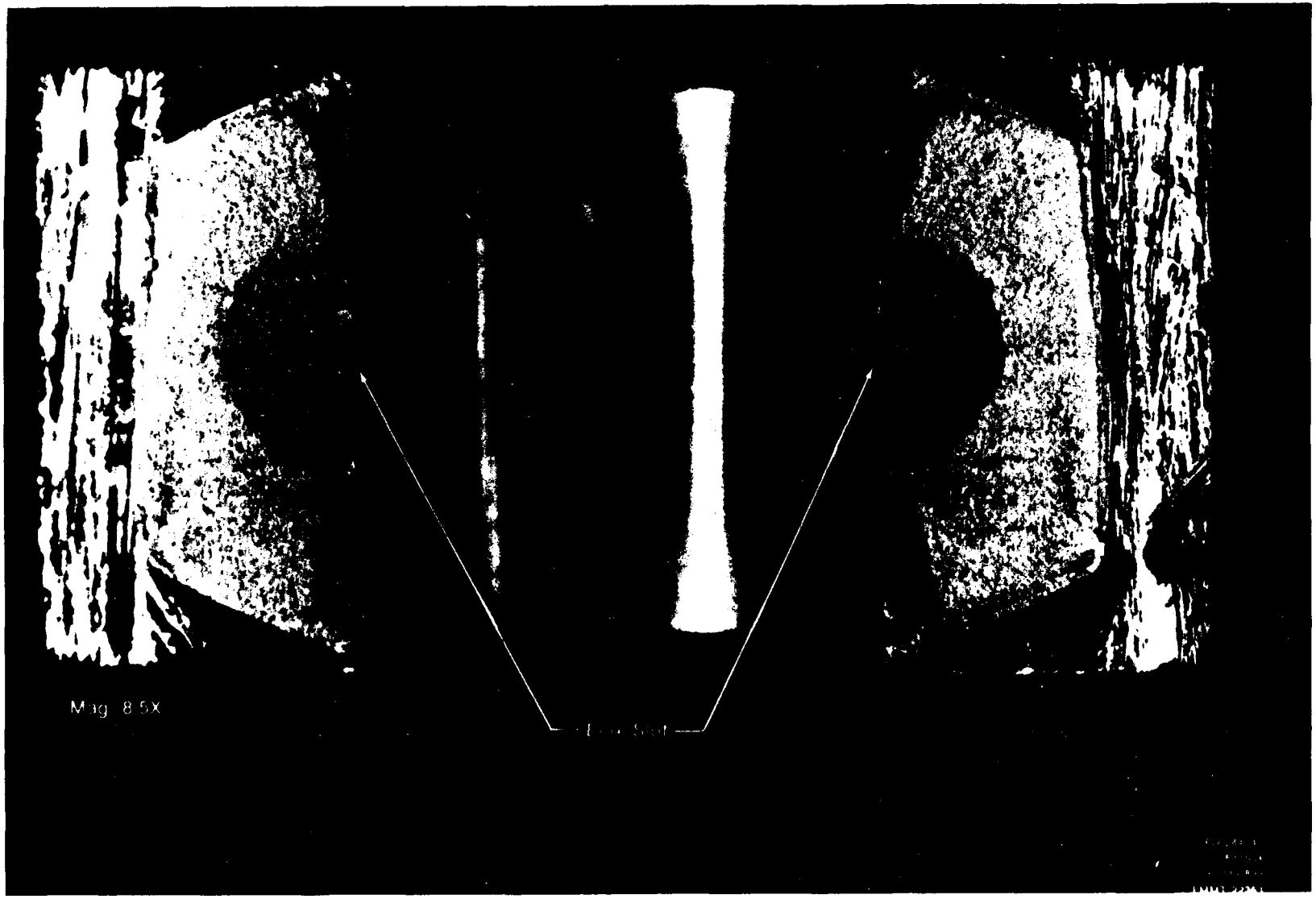

Figure 36. Close–up View of Heat Tinted Fracture Face of Elox Initiated Crack in Bolthole 6, Room Temperature Ferris Wheel LCF Test, Damage Tolerant Design Disk 3

Bolthole 10 With Region A Inset

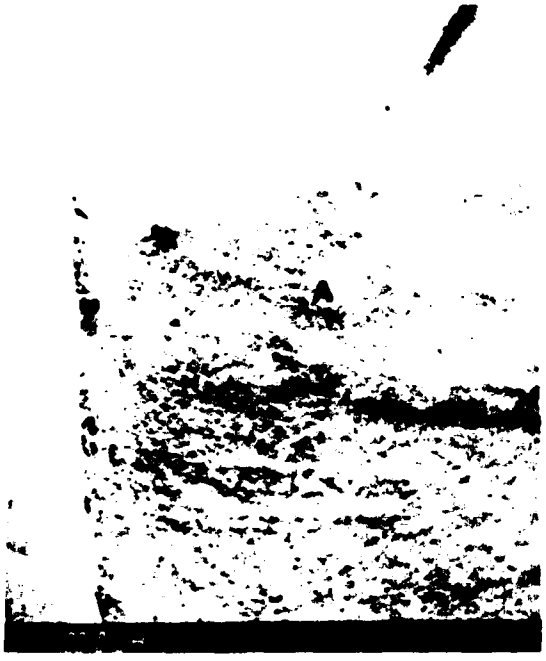

Mag: 10X

Region A With A1, A2 Insets

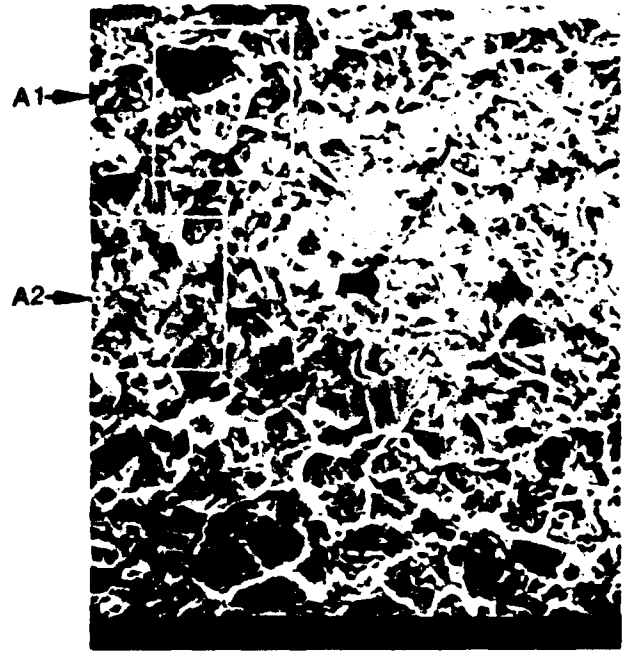

Mag: 500X

A1 Inset

Mag: 2000X

A2 Inset

Mag: 2000X

FD 214234
811504
bl3-834
FMMT 22361

Figure 37. Scanning Electron Microscope Views of Bolthole 10 Fracture Face Room Temperature Ferris Wheel LCF Test, Damage Tolerant Design Disk 1 Clearly Defined Thumbnail Pattern Containing Transgranular Fatigue With Well Defined Striations

Poorly Defined Thumbnail Pattern Containing Mixed Types of Fatigue
Bolthole 20 With Region B, C, D Insets

Region B: Located Same Distance From Elox Slot as Region A.
This Area Shows Transgranular Fatigue With Well Defined Striations

Region B With B1 Inset

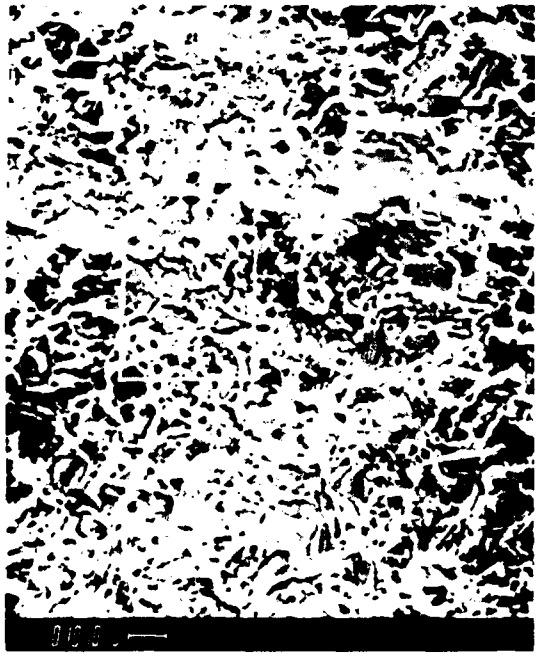

Mag: 500X

B1 Inset

Mag: 2000X

FD 214235
810704
bl3-835
FMMT 22361

Figure 38. Scanning Electron Microscope Views of Bolthole 20 Fracture Face Room Temperature Ferris Wheel LCF Test, Damage Tolerant Design Disk 1

Region C: Shows a Transition Area Containing Some Striated Areas

Region C With C1 Inset

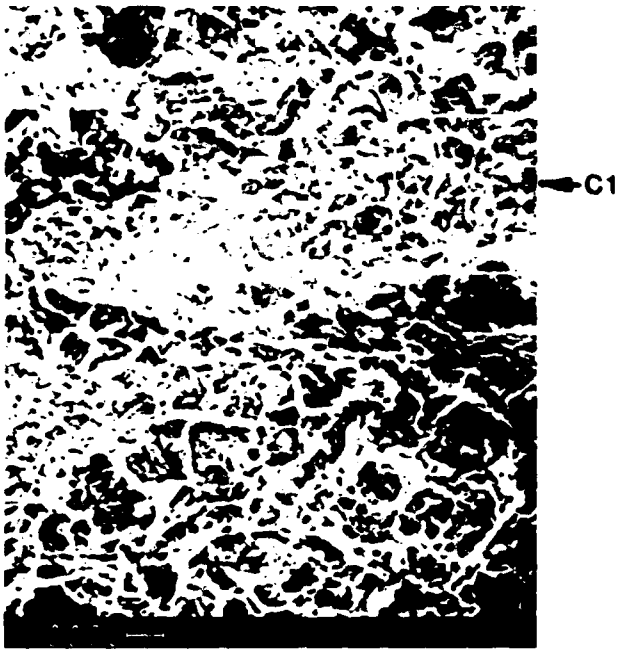

Mag: 500X

C1 Inset

Mag: 2000X

Region D: Shows Overstress With Mixed Tensile (Dimpled) and Intergranular

Region D

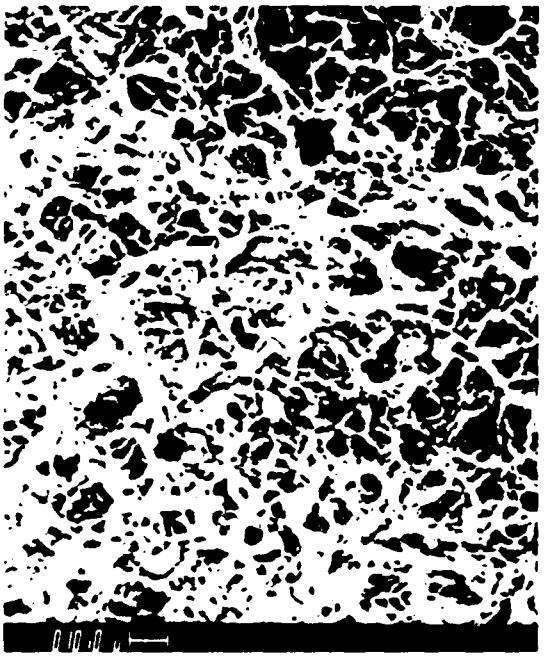

Mag: 500X

Enlargement of an Area in Region D

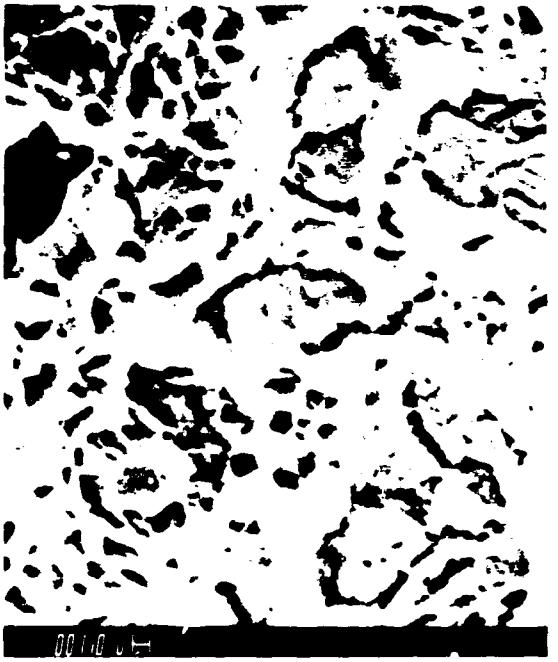

Mag: 2000X

FD ...14236
B10704
bf1-836
FMMT 22361

Figure 39. Scanning Electron Microscope Views of Bolthole 20 Fracture Face Room Temperature Ferris Wheel LCF Test, Damage Tolerant Design Disk 1

Table 2. Boundary Conditions for Stress Analysis

Load conditions for spin pit analysis:

Maximum speed: 12150 rpm

Temperature: 500F (isothermal)

Spin pit live rim loads:

Live rim loads include blade pull and dead rim load
(radial load due to disk material outboard of the live rim radius)
at the reference rotor speed.
Note: for other speeds, ratio radial load by (rpm/10,000)**2

See figure 10 for illustration of spin pit live rim load condition.

Live rim radius = 7.699 in

Radial load 10,000 rpm = 19,196 lb/in circumference at live rim radius

Radial C.G. = 10.565 in (included for reference)

Axial C.G. = 0.0235 in (forward of disk attachment axial centerplane)

For example:

Radial load 12,150 rpm = 19,196 lb/in*(12,150/10,000)**2 = 28,338 lb/in

Loads for ferris wheel test:

Maximum (100%) load = 18,890 lbs/slot for each of 60 slots

The total radial load is applied as a uniformly distributed load
at the live rim radius.

Live rim radius = 7.699 in
Total radial load = (18,890 lbs/slot) * 60 slots = 1,133,400 lbs
Circumference at live rim radius = 2*PI*R = 2*PI*7.699 = 48.37 in,
Total radial load per inch of liverim circumference =
(1,133,400 lbs) / (2*PI*7.699 in) = 23,430 lbs/in

See figure 11 for illustration of spin pit live rim load condition.

See Section 4 for ferris wheel sawtooth and mission cycle description.

Table 3. AMS 4928 Elastic Material Properties

Material	=	AMS 4928
Number of values	=	7
Density	=	0.160 Lbm/cu.in
Poissons Ratio	=	0.350
Interpolation	=	Quintic

Temperature (F)

0.0	100.0	200.0	300.0	400.0	500.0	600.0

Coefficient of Thermal Expansion (Alpha) (in/in/ F)

0.4550E-05	0.4690E-05	0.4805E-05	0.4910E-05	0.4990E-05	0.5050E-05	0.5110E-05

Modulus of Elasticisty (E) (psi)

0.1635E+08	0.1603E+08	0.1568E+08	0.1530E+08	0.1485E+08	0.1445E+08	0.1400E+08

Table 4. AMS 4928 Stress Versus Strain (Typical)

Plastic Strain (in/in)	RT	500 F
0.00001	98.0	67.0
0.000015	99.4	67.7
0.00002	100.1	68.3
0.00003	101.5	69.6
0.00004	103.3	70.6
0.00006	105.7	72.0
0.00007	107.1	72.6
0.00008	108.5	73.3
0.00010	110.6	74.1
0.00013	114.1	75.6
0.00016	116.2	76.7
0.00020	119.0	78.2
0.00030	123.9	80.8
0.00040	126.7	83.1
0.00050	128.8	84.6
0.00070	131.9	86.3
0.00100	134.7	88.2
0.00150	137.9	89.3
0.00200	139.9	90.9
0.00300	142.1	92.7
0.00500	144.2	95.0
0.00700	145.3	96.5
0.01000	145.9	98.3
0.01500	147.0	100.0
0.02500	147.7	102.2
0.04000	148.4	103.6
0.06000	148.5	105.1
0.10000	148.8	106.7

Table 5. Ti 6–4 Crack Growth Rate Design System Model (AMS 4928)

$$\log(da/dN) = C1 \times \sinh[C2 \times (\log(\Delta K) + C3)] + C4$$

where $C1 = C1L$ and $C2 = C2L$ for $\Delta K \leq 10^{|C3|}$

and $C1 = C1U$ and $C2 = C2U$ for $\Delta K > 10^{|C3|}$

Material model = AMS 4928
Temperature = 80.00

Positive stress ratios:

R	C1L	C2L	C3	C4	C1U	C2U
0.0	0.6500	5.4657	-1.0123	-5.9241	4.0000	0.8043
0.10	0.6500	5.5500	-1.0000	-5.9500	4.0000	0.8500
0.20	0.6500	5.7185	-0.9732	-6.0062	4.0000	0.9143
0.30	0.6500	5.8870	-0.9428	-6.0701	4.0000	0.9600
0.40	0.6500	6.0555	-0.9078	-6.1437	4.0000	0.9954
0.50	0.6500	6.2240	-0.8663	-6.2309	4.0000	1.0243
0.60	0.6500	6.3925	-0.8155	-6.3375	4.0000	1.0488
0.70	0.6500	6.5610	-0.7500	-6.4750	4.0000	1.0700
0.80	0.6500	6.7295	-0.6577	-6.6687	4.0000	1.0887
0.90	0.6500	6.8980	-0.5000	-7.0000	4.0000	1.1054

Negative stress ratios: $C3 = -1. \times \log[6.17 \times (1. - R) + 4.11]$

R	C1L	C2L	C3	C4	C1U	C2U
-1.00	0.6500	5.4660	-1.2162	-5.9240	4.0000	0.8040
-0.90	0.6500	5.4660	-1.1996	-5.9240	4.0000	0.8040
-0.80	0.6500	5.4660	-1.1823	-5.9240	4.0000	0.8040
-0.70	0.6500	5.4660	-1.1643	-5.9240	4.0000	0.8040
-0.60	0.6500	5.4660	-1.1456	-5.9240	4.0000	0.8040
-0.50	0.6500	5.4660	-1.1260	-5.9240	4.0000	0.8040
-0.40	0.6500	5.4660	-1.1054	-5.9240	4.0000	0.8040
-0.30	0.6500	5.4660	-1.0839	-5.9240	4.0000	0.8040
-0.20	0.6500	5.4660	-1.0612	-5.9240	4.0000	0.8040
-0.15	0.6500	5.4660	-1.0494	-5.9240	4.0000	0.8040
-0.10	0.6500	5.4660	-1.0373	-5.9240	4.0000	0.8040
-0.05	0.6500	5.4660	-1.0248	-5.9240	4.0000	0.8040

Note: Above coefficients for English units

Metric conversions follow:
C1 Metric = C1 English
C2 Metric = C2 English
C3 Metric = C3 English - 0.04935
C4 Metric = C4 English - 1.40483

Disk #1 — 500°F Strain (micro in/in.) for Speed (rpm) of:

Gage	Run	0*	2000	4000	6000	8000	10000**	11000	11500	12000	12150	10000	8000	6000	4000	2000	0	Ort***
1	1	0	-	720	1430	2390	3660	-	-	-	-	-	-	-	-	-	0	0
	2	0	110	490	1160	2150	3640	4250	4780	5820	6100	4700	3890	3170	2140	-	1040	1100
2	1	0	-	750	1490	2470	3770	-	-	-	-	-	-	-	-	-	0	0
	2	0	200	700	1440	2450	3740	4550	5060	5980	6260	4810	3820	2780	1740	-	760	870
3	1	0	-	480	1240	2190	3460	-	-	-	-	-	-	-	-	-	0	0
	2	0	-	-	-	-		.	.	INOPERATIVE		.	.	.	-	-	-	
4	1	0	-	570	1230	2130	3300	-	-	-	-	-	-	-	-	-	0	0
	2	0	120	480	1110	2040	3230	4000	4520	5450	5690	4400	3630	2800	1920	-	950	1040
5	1	0	-	1100	2490	4300	6180	-	-	-	-	-	-	-	-	-	0	0
	2	0	230	960	2100	3710	5790	-	-	.	.	INOPERATIVE			.	.	-	
6	1	0	-	1130	2440	4180	-	-	-	-	-	-	-	-	-	-	0	0
	2	0	-	-	-	-	.	-.	.	INOPERATIVE		.	.	.	.	-	-	
7	1	0	-	960	2160	3850	-	-	.	INOPERATIVE		.	.	.	.	-	-	
	2	0	-	-	-	-	.	.	.	INOPERATIVE		.	.	.	.	-	-	
8	1	0	-	-	-	-	.	.	.	INOPERATIVE		.	.	.	.	-	-	
	2	0	-	-	-	-	.	.	.	INOPERATIVE		.	.	.	.	-	-	

Table 6. Steady State Spin Strain Data at 500°F
AMS 4928 Titanium Disk Derived
From F100 2nd Stage Fan
Design Damage Tolerant Design Disk 1
(Reference Figure 22 for S/G Locations)

* Recording System set for zero initial output prior to acceleration

**** Run #1 to only 10,000 rpm for preliminary design analysis check prior to full speed run #2

*** Residual strain measured after test at room temperature

Strain (Micro in./in.) for Load (lbs) at Each Blade Slot of:

Gage	Run	8000	12000	16000	17000	18000	18890	18000	17000	16000	12000	8000
1	1	2180	3380	4630	4910	5220	5470	5200	4920	4630	3540	2550
	2	2260	3440	4630	4970	5280	5530	5250	4970	4650	3540	2580
2	1	1990	3020	4080	4310	4570	4650	4530	4210	3900	2900	2000
	2	2020	3020	4070	4320	4580	4770	4510	4170	3870	2850	1960
3	1	1860	3000	4180	4460	4750	4980	4710	4450	4200	3190	2250
	2	1950	3030	4190	4490	4780	5010	4730	4480	4190	3140	2230
4	1	1920	2910	4000	4230	4510	4700	4470	4140	3800	2770	1890
	2	1940	2920	3990	4260	4520	4720	4460	4090	3780	2720	1850
5	1	2510	-	-	-	-	6150	-	-	-	-	2540
	2	2560	-	-	-	-	6190	-	-	-	-	2460
6	1	2190	-	-	-	-	5380	-	-	-		2210
	2	2250	-	-	-	-	5410	-	-	-	-	2140
7	1	2020	-	-	-	-	4890	-	-	-	-	2000
	2	2060	-	-	-	-	4930	-	-	-	-	1950
8	1	2790	-	-	-	-	6920	-	-	-	-	2910
	2	2860	-	-	-	-	6970	-	-	-	-	2790
9	1	2390	-	-	-	-	5880	-	-	-	-	2460
	2	2450	-	-	-	-	5930	-	-	-	-	2380
10	1	2110	-	-	-	-	5130	-	-	-	-	2120
	2	2150	-	-	-	-	5160	-	-	-	-	2050
11	1	3760	5730	7900	8450	9120	9620	9360	8770	8200	6250	4230
	2	3830	5830	8100	8650	9270	9770	9340	8710	8160	6150	4130
12	1	3800	5770	7860	8390	9030	9530	9200	8650	8080	6170	4170
	2	3880	5820	7970	8520	9130	9620	9070	8470	7930	5970	3990
13	1	1040	-	-	-	-	2460	-	-	-	-	980
	2	1040	-	-	-	-	2440	-	-	-	-	930
14	1	1070	-	-	-	-	2520	-	-	-	-	1030
	2	1070	-	-	-	-	2500	-	-	-	-	980
15	1	1040	-	-	-	-	2500	-	-	-	-	1020
	2	1050	-	-	-	-	2490	-	-	-	-	990
16	1	.	.	.	.		INOPERATIVE		.	.	.	.
	2	-	.	.	.		INOPERATIVE		.	.	.	.
17	1	3550	5430	7500	8040	8660	9150	8900	8330	7800	5950	4070
	2	3630	5500	7630	8190	8720	9280	8870	8280	7750	5830	3960
18	1	3700	5620	7650	8130	8720	9160	8820	8250	7690	5820	3910
	2	3780	5660	7710	8220	8720	9230	8720	8130	7600	5680	3790
19	1	3710	5640	7730	8260	8900	9370	9100	8500	7940	6030	4100
	2	3780	5680	7810	8360	8880	9440	9010	8390	7840	5860	3940
20	1	3610	5500	7510	8000	8600	9040	8760	8190	7640	5800	3920
	2	3680	5520	7570	8070	8580	9100	8640	8070	7550	5670	3790
21	1	1340	-	-	-	-	3450	-	-	-		1070
	2	1350	-	-	-	-	3280	-	-	-	-	1290
22	1	1200	-	-	-	-	2900	-	-	-	-	1190
	2	1210	-	-	-	-	2890	-	-	-	-	1160
23	1	790	-	-	-	-	1960	-	-	-	-	820
	2	800	-	-	-	-	1970	-	-	-	-	810
24	1	760	-	-	-	-	1840	-	-	-	-	750
	2	780	-	-	-	-	1830	-	-	-	-	730
25	1	1240	-	-	-	-	2980	-	-	-	-	1180
	2	1250	-	-	-	-	2900	-	-	-	-	1140
26	1	1250	-	-	-	-	3010	-	-	-	-	1240
	2	1250	-	-	-	-	2980	-	-	-	-	1200
27	1	990	-	-	-	-	2340	-	-	-	-	1010
	2	1000	-	-	-	-	2330	-	-	-	-	980
28	1	980	-	-	-	-	2310	-	-	-	-	940
	2	1000	-	-	-	-	2300	-	-	-	-	930
29	1	2230	-	-	-	-	5360	-	-	-	-	2210
	2	2260	-	-	-	-	5370	-	-	-	-	2090
30	1	2490	-	-	-	-	6030	-	-	-	-	2480
	2	2530	-	-	-	-	6050	-	-	-	-	2530

Table 7. Ferris Wheel Steady State Strain Data At Room Temperature AMS 4928 Titanium Disk Derived From F100 2nd Stage Fan Design Damage Tolerant Design, Disk 1 (Reference Figure 24)

Bolthole	Beginning Elox Width	Beginning Elox Length	Sawtooth Cycles			Mission Cycles				
			1177	1500	2000	250	420	445	545	568
2	0.0073	0.0196	0.0212	0.0237	0.0270	0.0413	0.0790	0.0855	0.1220	0.1370
4	0.0075	0.0205	0.0210	0.0222	0.0282	0.0656	0.1355	0.1470	0.2250	0.2670
6	0.0075	0.0205	0.0228	0.0241	0.0298	0.0794	0.1439	0.1630	0.2764	0.3450
8	0.0073	0.0198	0.0223	0.0264	0.0311	0.0647	0.0960	0.1135	0.1610	0.1933
10	0.0073	0.0200	0.0220	0.0260	0.0281	0.0535	0.0769	0.0880	0.1580	0.1866
12	0.0075	0.0195	0.0225	0.0230	0.0288	0.0760	0.1360	0.1525	0.2250	0.3266
14	0.0074	0.0200	0.0220	0.0238	0.0258	0.0604	0.1176	0.1278	0.1810	0.2115
16	0.0070	0.0195	0.0201	0.0242	0.0349	0.0777	0.1386	0.1418	0.2260	0.2610
18	0.0070	0.0200	0.0220	0.0267	0.0312	0.0588	0.1036	0.1278	0.1850	0.2090
20	0.0070	0.0202	0.0225	0.0263	0.0314	0.0794	0.1662	0.1805	0.3000	0.4200*
Minimum Crack Length										
B/H		0.0195 12	0.0201 16	0.0222 4	0.0258 14	0.0413 2	0.0769 10	0.0855 2	0.1220 2	0.1370 2
MEAN (Average)		0.02000	0.0218	0.0246	0.0296	0.0657	0.1193	0.1327	0.2059	0.2559
Maximum Crack Length										
B/H		0.0205 6	0.0228 6	0.0267 18	0.0349 16	0.0794 20	0.1662 20	0.1805 20	0.3000 20	0.4200 20

*Primary Failure Site

Table 8. Crack Length Vs. Number of Ferris Wheel Cycles
Outboard Bolthole Elox
Replication Inspection Data
AMS 4928 Titanium Disk Derived From F100 2nd Stage
Fan Design Damage Tolerant Design Disk 1
(See Figure 9 for Ferris Wheel Duty Cycle Definition)

Bolthole	Mission Cycles									
	125	135	150	165	175	190	200	210	220	225
2	-	0.0580	-	-	-	0.0876	-	-	-	-
4	-	0.0704	-	-	-	0.0974	-	-	-	-
6	0.0697	0.0754	0.0850	0.0943	0.1022	0.1086	0.1146	0.1240	0.1316	0.1360
8	0.0743	0.0818	0.0890	0.0992	0.1060	0.1140	0.1224	0.1268	0.1354	0.1416
10	-	0.0685	-	-	-	0.0910	-	-	-	-
12	-	0.0448	-	-	-	0.0631	-	-	-	-
14	-	0.0482	-	-	-	0.0686	-	-	-	-
16	-	0.0613	-	-	-	0.0834	-	-	-	-
18	-	0.0530	-	-	-	0.0762	-	-	-	-
20	-	0.0581	-	-	-	0.0764	-	-	-	-
Minimum Crack Length B/H	-	0.0448 12	-	-	-	0.0631 12	-	-	-	-
Mean	-	0.0620	-	-	-	0.0866	-	-	-	-
Maximum Crack Length B/H	-	0.0818 8	-	-	-	0.1140 8	-	-	-	-

Table 9. Crack Length Vs. Number of Ferris Wheel Cycles Outboard Bolthole Elox Replicationinspection Data AMS 4928 Titanium Disk Derived From F100 2nd Stage Fan Design Damage Tolerant Design Disk 3 (See Figure 9 for Ferris Wheel Duty Cycle Definition)

Bolthole	Mission Cycles					
	230	235	245	255	265	275
2	-	0.1126	-	0.1304	-	0.1400
4	-	0.1240	-	0.1360	-	0.1488
6	0.1404	0.1492	0.1568	0.1670	0.1784	0.1892
8	0.1444	0.1520	0.1608	0.1710	0.1820	0.1882
10	-	0.1090	-	0.1174	-	0.1268
12	-	0.0826	-	0.0921	-	0.1012
14	-	0.0936	-	0.0988	-	0.1076
16	-	0.1052	-	0.1162	-	0.1266
18	-	0.0960	-	0.1070	-	0.1176
20	-	0.0950	-	0.1054	-	0.1146
Minimum Crack Length		0.0826		0.0921		0.1012
B/H	-	12	-	12	-	12
MEAN	-	0.1119	-	0.1241	-	0.1361
Maximum Crack Length		0.1520		0.1710		0.1892
B/H	-	8	-	8	-	6

Bolt-Hole	Beginning Elox Width	Beginning Elox Length	Sawtooth Cycles					Mission Cycles		
			300	500	900	1100	1200	50	100	115
2	0.0053	0.0138	0.0148	0.0165	0.0213	0.0232	0.0261	0.0352	0.493	-
4	0.0048	0.0133	0.0153	0.0178	0.0218	0.0242	0.0274	0.0385	0.0545	-
6	0.0060	0.0142	0.0162	0.0192	0.0252	0.0282	0.0310	0.0427	0.0605	0.0642
8	0.0053	0.0142	0.0153	0.0183	0.0230	0.0267	0.0300	0.0430	0.0647	0.0685
10	0.0052	0.0143	0.0152	0.0177	0.0230	0.0258	0.0287	0.0377	0.0530	-
12	0.0055	0.0145	0.0150	0.0152	0.0182	0.0202	0.0222	0.0259	0.0357	-
14	0.0055	0.0142	0.0158	0.0168	0.0207	0.0230	0.0247	0.0293	0.0405	-
16	0.0048	0.0143	0.0154	0.0173	0.0208	0.0225	0.0253	0.0350	0.0594	-
18	0.0050	0.0140	0.0150	0.0167	0.0200	0.0222	0.0243	0.0303	0.0428	-
20	0.0053	0.0141	0.0150	0.0179	0.0215	0.0232	0.0262	0.0324	0.0456	-
Minimum Crack Length		0.0133	0.0148	0.0152	0.0182	0.0202	0.0222	0.0259	0.0357	-
B/H		4	2	12	12	12	12	12	12	
MEAN		0.0141	0.0153	0.0173	0.0216	0.0239	0.0266	0.0350	0.0506	-
Maximum Crack Length		0.0145	0.0162	0.0192	0.0252	0.0282	0.0310	0.0430	0.0647	-
B/H		12	6	6	6	6	6	8	8	

Table 9. Crack Length Vs. Number of Ferris Wheel Cycles Outboard Bolthole Elox Replication Inspection Data
AMS 4928 Titanium Disk Derived From F100 2nd Stage Fan Design Damage Tolerant Design Disk 3
(See Figure 9 for Ferris Wheel Duty Cycle Definition) (Cont.)

Disk 1 Bolthole	Final Crack Length[3]	Final Crack Depth[3]	Elox Slot Depth	Final Aspect Ratio
2	0.1480	0.0750	0.0105	1.97:1
6[1]	0.3780	0.2050	0.0098	1:84:1
10	0.1960	0.1010	0.0098	1:94:1
16	0.2720	0.1360	0.0097	2.00:1
20	0.4300	0.2230[2]	0.0100	1:93:1
Mean				1:94:1
Disk 3				
Bolthole				
2	0.1480	0.0820	0.0104	1.80:1
6[1]	0.2030	0.1150	0.0106	1.77:1
12	0.1075	0.0630	0.0114	1.71:1
Mean				1.76:1

(1) Figures E-24 and E-25 show heat tinted fracture faces of each, respectively.

(2) Normal crack pattern depth was about 0.2230 inches; however, the last several cycles produced additional striations for a total depth of about 0.38 inches.

(3) Includes elox length and depth.

Table 10. Ocular Examination Data. Final Crack Length Vs. Depth of Several Boltholes for Ferris Wheel LCF Test of AMS 4928 Titanium Disk Derived From F100 2nd Stage Fan Design (See Figure 9 for Ferris Wheel Duty Cycle Definition)

Bolthole	Sawtooth Cycles			Mission Cycles				
	0-1177	1177-1500	1500-2000	0-250	250-420	420-445	445-545	545-568
2	0.0014	0.0077	0.0066	0.0572	0.2218	0.2600	0.3650	0.6522
4	0.0004	0.0037	0.0120	0.1496	0.4112	0.4600	0.7800	1.8261
6	0.0020	0.0040	0.0114	0.1984	0.3794	0.7640	1.1340	2.9826
8	0.0021	0.0127	0.0094	0.1344	0.1841	0.7000	0.4750	1.4043
10	0.0017	0.0124	0.0042	0.1016	0.1376	0.4440	0.7000	1.2435
12	0.0025	0.0015	0.0116	0.1888	0.3529	0.6600	0.7250	4.4174
14	0.0017	0.0056	0.0040	0.1384	0.3365	0.4080	0.5320	1.3261
16	0.0005	0.0127	0.0214	0.1712	0.3582	0.1280	0.8420	1.5217
18	0.0017	0.0146	0.0090	0.1104	0.2635	0.9680	0.5720	1.0435
20	0.0020	0.0118	0.0102	0.1920	0.5106	0.5720	1.1950	5.2174
Minimum da/dN	0.0004	0.0015	0.0040	0.0572	0.1376	0.1280	0.3650	0.6522
B/H		12	14	2	10	16	2	2
Mean da/dN	0.0016	0.0086	0.0100	0.1442	0.3156	0.5364	0.7320	2.1635
Maximum da/dN	0.0025	0.0146	0.0214	0.1984	0.5106	0.9680	1.1950	5.2174
B/H	12	18	16	6	20	18	20	20

Table 11. Crack Growth Rate for Ferris Wheel LCF Test of AMS 4928 Titanium Disk Derived From F100 2nd Stage Fan Design (Reference Table 8 for Data Used in Table 11)

da/dN (Mils/Cycle)

Bolthole	Sawtooth Cycles					Mission Cycles				
	0-300	300-500	500-900	900-1100	1100-1200	0-50	50-100	100-115	115-125	100-135
2	0.0033	0.0085	0.0120	0.0095	0.0290	0.1820	0.2820	-	-	0.2486
4	0.0067	0.0125	0.0100	0.0120	0.0320	0.2220	0.3200	-	-	0.4543
6	0.0067	0.0150	0.0150	0.0150	0.0280	0.2340	0.3560	0.2467	0.5500	0.1629
8	0.0037	0.0150	0.0118	0.0185	0.0330	0.2600	0.4340	0.2533	0.5800	0.2143
10	0.0030	0.0125	0.0133	0.0140	0.0290	0.1800	0.3060	-	-	0.4429
12	0.0017	0.0010	0.0075	0.0100	0.0200	0.0740	0.1960	-	-	0.2600
14	0.0053	0.0050	0.0098	0.0115	0.0170	0.0920	0.2240	-	-	0.2200
16	0.0037	0.0095	0.0088	0.0085	0.0280	0.1940	0.4880	-	-	0.0543
18	0.0033	0.0085	0.0083	0.0110	0.0210	0.1200	0.2500	-	-	0.2914
20	0.0030	0.0145	0.0090	0.0085	0.0300	0.1240	0.2640	-	-	0.3571
Minimum da/dN	0.0017	0.0010	0.0075	0.0100	0.0170	0.0740	0.1960	-	-	0.0543
B/H	12	12	12	12	14	12	12			16
Mean da/dN	0.0040	0.0120	0.0106	0.0119	0.0267	0.1682	0.3120	-	-	0.2706
Minimum da/dN	0.0067	0.015	0.0150	0.0185	0.0330	0.2600	0.4880	-	-	0.4543
B/H	6	6	6	8	8	8	16			4

Bolthole	Mission Cycles									
	125-135	135-150	150-165	165-175	135-190	175-190	190-200	200-210	210-220	220-225
2	-	-	-	-	0.5382	-	-	-	-	-
4	-	-	-	-	0.4909	-	-	-	-	-
6	0.5700	0.6400	0.6200	0.7900	0.6036	0.4267	0.6000	0.9400	0.7600	0.8800
8	0.7500	0.4800	0.6800	0.6800	0.5855	0.5333	0.8400	0.4400	0.8600	1.2400
10	-	-	-	-	0.4091	-	-	-	-	-
12	-	-	-	-	0.3327	-	-	-	-	-
14	-	-	-	-	0.3709	-	-	-	-	-
16	-	-	-	-	0.4018	-	-	-	-	-
18	-	-	-	-	0.4218	-	-	-	-	-
20	-	-	-	-	0.3327	-	-	-	-	-
Minimum da/dN	-	-	-	-	0.3327	-	-	-	-	-
B/H					12					
Mean da/dN	-	-	-	-	0.4487	-	-	-	-	-
Maximum da/dN	-	-	-	-	0.6036	-	-	-	-	-
B/H					6					

Bolthole	Mission Cycles								
	225-230	190-235	230-235	235-245	235-255	245-255	255-265	255-275	265-275
2	-	0.5556	-	-	0.8900	-	-	0.4800	-
4	-	0.5911	-	-	0.6000	-	-	0.6400	-
6	0.8800	0.9022	1.7600	0.7600	0.8900	1.0200	1.1400	1.1100	1.0800
8	0.5600	0.8444	1.5200	0.8800	0.9500	1.0200	1.1000	0.8600	0.6200
10	-	0.4000	-	-	0.4200	-	-	0.4700	-
12	-	0.4333	-	-	0.4750	-	-	0.4550	-
14	-	0.5556	-	-	0.2600	-	-	0.4400	-
16	-	0.4844	-	-	0.5500	-	-	0.5200	-
18	-	0.4400	-	-	0.5500	-	-	0.5300	-
20	-	0.4133	-	-	0.5200	-	-	0.4600	-
Minimum da/dN	-	0.4000	-	-	0.2600	-	-	0.4400	-
B/H		10			14			14	
Mean da/dN	-	0.5620	-	-	0.6105	-	-	0.5965	-
Maximum da/dN	-	0.9022	-	-	0.9500	-	-	1.1100	-
B/H		6			8			6	

Table 12. Crack Growth Rate for Ferris Wheel LCF Test of AMS 4928 Titanium Disk Derived From F100 2nd Stage Fan Design Reference Table 9 for Data Used in Table 12

Chapter 8

IN-SERVICE CONSIDERATIONS AFFECTING COMPONENT LIFE

by

Dr R. Thamburaj
Orenda Division
Hawker Siddeley Canada Inc.
3160 Derry Road East
Mississauga, Ontario
Canada

The test cases presented in earlier chapters have dealt with a variety of gas turbine engines and have spanned a wide range of test conditions. The objective of this Working Group has been to initially address test cases that would be easier to define thoroughly and this purpose has been achieved in the various rig tests that have been proposed. Users of the information presented in these test cases would benefit from the fact that the data relate to test results on actual engine components, since life predictions based on specimen testing alone are unlikely to represent in-service behaviour of engine components.

It is believed that this initial effort will be the forerunner of a number of future studies dealing with more complex combinations of factors that need to be considered to assess the life of a gas turbine component in actual service.

Some of these considerations are discussed here, in relation to the test cases detailed in earlier chapters. While the focus is upon discs and spacers, to maintain a close relationship with the test cases presented earlier for other engines, blade life prediction is also discussed. Where appropriate, examples have been drawn from experience on J85 and F404 engines operated in Canada.

Considered here are various practical aspects of life prediction which merit further investigation, namely,

I. Small crack behaviour
II. Effect of Loading Conditions
  (i) Multiaxial Loading
  (ii) HCF-LCF Interactions
  (iii) Creep-Fatigue and Creep-Fatigue-Environment Interactions
III. Microstructural Effects
  (i) Long Term Service Exposure Effects
  (ii) Grain Size, and Grain Shape Effects
  (iii) Anisotropic Behaviour and Single Crystal Turbine Blades
IV. Coating Effects
V. Defects and Damage Tolerance
VI. Inspection Sensitivity and Reliability Effects
VII. Residual Stress Effects
VIII. Effects of Repair
IX. Usage Monitoring

I. SMALL CRACK BEHAVIOUR

The behaviour of "small" cracks or "short" cracks has been recognized to be of significant importance in recent years (1), and has substantial relevance to some of the test cases presented earlier. The Snecma High Pressure (HP) Turbine Disc (Inconel 718) test case in particular might lend itself to short crack growth modelling and it would be useful to evaluate the differences in life prediction for this test case using conventional crack propagation models as compared to short crack growth models taking into account effects such as closure. Room temperature cyclic life of Astroloy turbine discs based on short crack life predictions has been shown (1) to be approximately a factor of two below large crack predictions for an initial crack size of 0.2 x 0.4 mm. Similar evaluations need to be carried out for the case of elevated temperature conditions for varying Stress Ratio (R) and microstructure,

with hold cycles and multiaxial loading conditions.

Grain size is an important variable affecting short crack growth behaviour, and this should be included as part of the data package in future test cases dealing with crack growth kinetics. It would be particularly useful to evaluate single crystal materials in this light, since there is some concern (1) that this microstructure would not be optimum for minimizing the growth of small fatigue cracks.

II. MULTIAXIAL AND COMBINED LOADING EFFECTS

(i) Multiaxial Loading

A number of engine components could be subject to multiaxial cyclic loading conditions resulting in biaxial/triaxial stress states. Out of phase loading and mean stress effects further complicate the task of life prediction.

Past work (2) has demonstrated that a successful uniaxial mean-stress life prediction method can result in erroneous multiaxial fatigue life estimates as large as an order of magnitude if the physical basis for the parameter is not consistent with the damage mechanism observed for the material. Since in many materials multiaxial fatigue damage accumulation manifests itself in the formation and growth of shear cracks, shear based multiaxial fatigue criteria tend to be more appropriate for predicting the fatigue life of these materials.

While a number of such damage parameters have been proposed in the literature (3, 4), it would be useful to develop documented test cases of application of some of these models to in-service engine component life prediction.

The Allison TF-41 engine Low Pressure (LP) shaft test case and the Snecma HP Turbine Disc test case provide some opportunity to verify analytical life prediction models for multiaxial loading under the controlled conditions of rig testing. It would have been preferable however, to have data on more than one rig test to minimize the effects of scatter.

In future studies, data needs to be compiled from several multiaxial rig tests and the life prediction models that successfully correlate with rig test data should be validated against actual service experience. It would be of considerable value to elucidate the reasons why a particular prediction model does or doesn't correlate well with service experience.

(ii) HCF-LCF Interactions

Loading profiles experienced by engine discs may consist of a group of low frequency cycles associated with thermal gradients and/or centrifugal forces and superimposed high frequency loading associated with blade passage. While the low cycle (low frequency) loading is of the order of seconds to several hundred seconds, the high cycle (high frequency) loading would typically involve frequencies of the order of hundreds to several thousand hertz (5).

In such situations, it is important to establish,

* the cumulative damage rules that should apply when combined high cycle/low cycle loading conditions contribute to crack growth,
* the degree to which the high cycle and low cycle loading influence each other's contribution to crack growth.

Although the effect of major and minor cycles was addressed by the Allison TF-41 test case, the aspect of HCF-LCF interactions at elevated temperatures has not been addressed in the test cases presented earlier.

Past work (5) on the interactive effects of high and low cycle loading on crack growth for the alloy Inconel 718, has shown that distinct regimes of high and low frequency dominated behaviour exist at 649°C under combined cycle loading with a 10 Hz high frequency component. Crack

retardation effects were observed when high frequency loading was applied in the low cycle dominated regime. Thus, a linear summation of crack growth on a cycle-by-cycle basis for a given loading profile can lead to erroneous predictions for certain combinations of high/low cycle fatigue loading conditions. The task of crack growth prediction under combined high/low cycle loading is complicated by the transient effects associated with hold time and the transient effects associated with high cycle growth rate retardation. Since the effects of crack retardation from such interaction are not reliably estimated, designers have resorted to approximations which provide conservative, but consistent predictions of combined cycle crack growth rates (5).

It would be useful to see the extent of benefit or detriment such approximations would result in, in actual application to an engine Retirement For Cause (RFC) program. Knowledge of the nature of the effect of such load interactions upon crack growth kinetics is critical to the success of an RFC program, and future work in this area would be most valuable.

(iii) Creep-Fatigue And Creep-Fatigue Environment Interactions

The interaction of creep and fatigue is another complex topic involving transient phenomena that depend upon a number of variables. Creep crack growth following fatigue could be characterized by an initially high growth rate that decays to steady state behaviour in a few minutes. This initially high growth rate has been observed (6) when K_{max} in fatigue was less than, or equal to the stress intensity, K under sustained loading. When K_{max} in fatigue was greater than K during the hold time, an incubation period was observed.

The frequency of prior fatigue cycling is another variable affecting initial creep crack growth rates. In order to explain the differences observed, it has been proposed that:

* at high frequencies, crack growth rate is primarily cycle dependent, and high rate of mechanical damage due to fatigue cycling overshadows the time dependent processes of environmental degradation and creep, or stress relaxation. In this instance, the crack tip stresses are high, but the damage zone is marginally affected by the creep and environment with little or no crack growth transient behaviour.

* at intermediate frequencies, the fatigue damage is significantly enhanced by the environment, while creep deformations are probably still quite limited. Since the stresses remain high because creep is limited, the crack tip damage prior to the hold time is maximized, resulting in the maximum crack growth transient behaviour.

* at low frequencies, the environmental effect is still present but creep deformation has become significant, allowing stress relaxation to occur at the crack tip. In this situation, the reduced stress levels result in a lower crack driving force and reduce the transient behaviour.

This explanation based on a competition between environmental and creep mechanisms is hypothetical and is yet to be substantiated with data. Several such effects occur due to the interactions between creep, fatigue and environmental oxidation, carburization or sulphidation and these complex interrelationships do not appear to lend themselves to simple analyses that utilize constant amplitude fatigue and creep crack growth data and linear damage summation algorithms.

* Some progress is being made in this direction, using micro mechanistic models. In one model (7), fatigue crack extension is estimated on the basis of the kinetics of grain boundary diffusion at elevated temperatures, grain boundary oxidation and microrupture of a crack tip grain

boundary. The time δt for a crack extension of δa through one such microrupture is estimated as,

$$\delta t = (B/D_{gb})\ (\delta a/\beta B)^{1/n} \quad (1)$$

where,

B = magnitude of the diffusion jumping vector or interatomic spacing

D_{gb} = grain boundary diffusion coefficient

β, β' = proportionality constants

n = positive exponent (less than unity)

The number of microruptures during a holding period Δt_H is,

$$m = \Delta t_H/\delta t = (\Delta t_H\ D_{gb}/B)(\beta B/\delta a)^{1/n} \quad (2)$$

where m is linearly proportional to the holding period and is inversely proportional to frequency, f.

Fatigue crack growth per cycle is the sum of microruptures during the holding period and is inversely proportional to the frequency.

Fatigue crack growth per cycle is the sum of the microruptures during the holding period

Hence, $da/dN = m\ \delta a \quad (3)$

From equations (1) - (3) we obtain

$$da/dN = \beta' \Delta t_H\ D_{gb}\ (B/\delta a)^{1-n/n}$$

$$= \beta'(D_{gb}/f)\ (B/\delta a)^{1-n/n}$$

Fig. 1 , illustrates the comparison of predicted and actual crack growth rates in various materials. It appears that the model is more successful in correlating crack growth rates in the more environmentally sensitive alloys such as Inconel 718. Excellent correlation is obtained with Astroloy at 760°C since at this temperature this alloy would be quite susceptible to environmental attack by way of grain boundary oxidation. Thus the model seems to provide good results when the dominant mechanism of crack extension is environmental embrittlement of the grain boundaries. However, the usefulness of such models and their validity for engine component lifing needs to be rigorously tested by exercises such as the test cases addressed by this Working Group.

There is a clear need for test cases that would help validate life prediction models that take creep-fatigue-environment interactions into account. Test cases that involve rig tests would be a sufficient challenge, considering the complexity of the phenomena involved. Such test cases should address the effect of microstructure in detail as well, since microstructural effects e.g. whether grain boundaries are planar or serrated or whether the material is polycrystalline, directionally solidified or cast as a single crystal, would have substantial impact on elevated temperature creep-fatigue and environmental interactions.

III. MICROSTRUCTURAL EFFECTS

A variety of microstructural effects have a significant impact on damage accumulation of components in service. Discussed below are some topics which require further effort.

(i) Long Term Service Exposure

Material properties generated from accelerated specimen tests do not necessarily reflect the effects of long term exposure that the actual component would see. Particularly in the case of a mature engine for which a user wishes to exercise a Retirement For Cause option, care should be taken to use a material property data base which includes new as well as high time service exposed materials.

(ii) Grain Size and Grain Shape Effects

Grain size has been shown to be a key parameter that controls deformation and environmental embrittlement effects at elevated temperature (8). Grain size can be an important consideration in components such as turbine blades experiencing crack initiation in thin walled areas, where the ratio of thickness to grain size could be an

important consideration. Serrated grain boundaries can substantially reduce crack propagation rates (8), a finding which could find application in the development of damage tolerant turbine discs.

(iii) Anisotropic Behaviour and Single Crystal Turbine Blades

Single crystal casting technology has been proven to provide substantial turbine blade life improvements as compared to conventional casting. Process repeatability is still a difficult goal in single crystal casting and a number of problems can arise, including recrystallization, deviation of crystal plane from ideal radial direction, stray grain and porosity (9).

With single crystal castings the anisotropy in creep properties becomes large depending upon which crystal axis is parallel to the stress direction. The creep properties of individual alloys do not vary consistently and, this variation of the rupture strength with crystallographic orientation is incompletely understood. It appears that the variation in rupture strength produced by crystallographic orientation could be augmented by anisotropy in dendrite strength. The strength in a particular direction could then vary depending on the arrangement of the dendrites (10).

Fatigue crack propagation in single crystal blade materials could be characterised by an effective ΔK, defined on the basis of strain energy release rate and taking into account elastic anisotropy (11). This effective local crack driving force is affected by crack deflection, branching and roughness induced closure, all of which seem to play a significant role in single crystal materials.

IV. COATING EFFECTS

The author's experience has been that in a number of cases, crack initiation in aluminide coated turbine blades is initiated in the brittle interdiffusion zone between the base material and the protective coating (Fig. 2)

However, very few life prediction models have been developed that reliably model the behaviour of coated superalloys. A recent attempt (7), by Pratt and Whitney Aircraft for overlay coated single crystal superalloys models the total life N_f to crack initiation as,

$$N_f = N_c + N_{sc} + N_{sp}$$

or

$$N_f = N_{si} + N_{sp}$$

where,

N_c = cycles to initiate a crack through the coating
N_{sc} = cycles for coating initiated crack to penetrate a small distance into the substrate
N_{si} = cycles to initiate a substrate crack due to macroscopic slip, oxidation effects, or defects
N_{sp} = cycles to propagate substrate crack
N_f = total cycles to crack initiation through coating and through substrate

For calculating N_c, the following model was proposed:

$$N_c = C(\Delta W_t)^{-b} . \upsilon^m$$

where,

$$\upsilon = \frac{1}{\Sigma \frac{r(T_i)}{r(T_o)} . t_i - D_o} \quad ; \upsilon \leq 1.0$$

$r(T) = r_o \exp(-Q/T)$ = temperature and time dependent damage rate

W_t = tensile hysteretic energy, N-m/m^3

T_i = individual temperature levels in the cycle, K

t_i = time (min) at T_i, including 100 percent of tensile hold and 30 percent of compressive hold times in the cycle, if any.

T_o = threshold temperature for temperature dependent

damage (assumed to be 1088°K)

D_o = "incubation damage"

Q = effective activation energy for temperature and time dependent damage

Model constants were derived from thermal tests and coating hysteresis loops were predicted using a constitutive one-dimensional model. This model takes into account the differences in the coefficients of thermal expansion between the coating and the substrate and determines the stress-strain states of the coating and substrate by imposing an equivalent displacement history. It is believed that a similar approach based on hysteretic energy would apply for aluminide coatings as well. This task is likely to be considerably more difficult from the point of view of constitutive modelling.

Although a complex and challenging task, life prediction models which take coating behaviour into account are essential. An understanding of the interaction between the coating and substrate would not only improve life prediction capability but also allow designers to match coating composition and process with the properties of the substrate to achieve optimum life under a given set of operating conditions.

While a substantial amount of specimen test data has been published on the effect of various coatings upon thermal fatigue life, there is very limited information involving tests on actual engine components. Future work is strongly recommended in this direction, documenting test cases of coated blades with polycrystalline, directionally solidified and single crystal microstructures, for which thermal fatigue life prediction models were developed, initially using rig tests and subsequently validated through service experience.

V. DEFECTS & DAMAGE TOLERANCE

Crack propagation from a sub-surface inclusion was considered in the RB-211-524 HPT disc test case. Since the crack at the inclusion was a rather unexpected event, data could not be documented in steps on the nucleation and propagation phases of the crack development. Although the inclusion was not the life limiting factor in this case (the disc failed at a feature other than this embedded defect), understanding the approach to analyzing the impact of potential defects upon component life is a key factor for improved life prediction methods.

In practice, a variety of defects can occur and have substantial impact upon component life. Such defects could be created in material processing, component fabrication or during service. Examples of these are,

(i) tool marks in a turbine wheel cooling air hole (Fig. 3),
(ii) crack initiation from corrosion pitting in a compressor blade tang,
(iii) crack initiation from an inclusion in a compressor disc,
(iv) temperature and/or strain induced precipitation of harmful phases in turbine wheels,
(v) shrinkage cavities in a turbine blade (Fig. 4),
(vi) defects in braze joints (microporosity, microcracks),
(vii) fretting damage in blade dovetail/disc rim slots.

In several instances, the presence of such defects is discovered after a few years of the engine being introduced into service, with drastic reduction in life limits if a "safe life" approach were to be followed. Alternatively, a detailed Damage Tolerance Assessment may be carried out and the user might be able to exercise a "Retirement For Cause" (RFC) option. For the RFC option to be applied successfully a comprehensive understanding of several factors is required.

It is considered that the probability of failure from a defect can be considered as the combination of at least seven statistical factors:

(i) the probability of a component containing a critical size flaw: P1
(ii) the probability of such a flaw not being detected by the NDI technique used: P2
(iii) the probability of the flaw falling in a zone of the component which is sufficiently highly stressed to result in failure of the component from that flaw within the required life: P3
(iv) the probability of the flaw showing no nucleation life: P4
(v) the probability of the crack growing from the flaw at a faster rate than assumed: P5
(vi) the probability of the fracture toughness of the material being lower than anticipated: P6
(vii) the probability of various unknowns (P7) such as,
* inadequate knowledge of service operating condition
* inadequate knowledge of material property data
* lack of knowledge of past usage history of a component

Therefore, a comprehensive analysis of the impact of a certain type of defect upon the life of a component requires a substantial amount of data, relating to P1 - P7 above on:

(i) processing and fabrication history (P1)
(ii) reliability and sensitivity of non destructive inspection (P2)
(iii) usage severity (P3)
(iv) knowledge of the type of interaction between the defect and the surrounding alloy material and hence its impact on crack initiation behaviour (P4 and P7)
(v) defect size and distribution and its effect on short crack growth and long crack propagation behaviour (P5, P6, and P7)

Material property data obtained from specimens need to be applied very carefully, since substantial differences in crack propagation data can be observed depending upon the type of specimen used. It is generally accepted that rig tests should be used in addition to specimen tests, as a more representative vehicle for developing lifing models. Yet, the environment that the component would see in actual service would be considerably more complex than most rig tests can simulate and it is service experience that is more likely to tell the whole truth.

Hence, it would be valuable to have documented test cases that would provide the opportunity to analyze and predict the influence of a certain type of defect in an engine component, evaluate the impact on maintenance operations, and verify the results with past history and experience with the engine. Such test cases would provide a systematic means for calibrating an incomplete engineering model with in-service data in order to minimize the effects of analytical modelling errors or missing laboratory or structural simulation data (12).

VI. INSPECTION SENSITIVITY AND RELIABILITY EFFECTS

Besuner (13, 14) notes that in the life prediction of a turbine disc, the knowledge of the maximum crack depth to within a factor of three (or crack area to within a factor of nine) is equivalent to knowledge of effective stresses in the disc rim slot, to within 7-8%. Given the complexity of the loading conditions for an in-service turbine disc, it would be easier to measure the area of a large rim crack to within a factor of nine than to estimate, by analytical methods alone, the operating stresses in a specific disc rim slot to within 7-8%. Thus, one cannot over emphasize the merit of life prediction methodologies which rely heavily upon the accuracy and comprehensiveness of inspection data to calibrate the analytical stress and lifing models. The situation that many an engine designer faces, is the

difficulty of obtaining such accurate and comprehensive inspection data from various users who may not have the equipment or expertise to generate such a comprehensive inspection data base.

The sensitivity and reliability of the inspection techniques used would have a very strong impact upon the life limits developed for various fracture critical components in an engine. A study carried out in Canada on J85 compressor discs has borne this out quite clearly (15). The J85 and F404 engines operated by the Canadian Forces still rely mainly upon Fluorescent Penetrant Inspection for detection of cracks in fracture critical components and this is likely to be a similar situation for various mature engines operated in different parts of the world. In the event that RFC were implemented, would be most useful to formulate test cases to illustrate how improved inspection techniques such as eddy current testing were used to effect substantial life extension.

In particular, it would be useful to evaluate the effect of,

(i) multiple inspections rather than a single inspection,
(ii) automated vs manual inspection techniques,
(iii) statistical models used to process Probability of Detection (POD) data.

The author's laboratory in conjunction with the National Research Council of Canada is actively developing the knowledge base that would assist the Canadian Forces in making decisions regarding the adoption of an inspection based Retirement For Cause lifing approach for J85 and F404 engines operated in Canada. The J85 engines are being addressed initially and the approach is very similar to that developed by the USAF for damage tolerance assessment of gas turbine engines (Fig. 5).

A particularly valuable body of data could be assembled if inspection of parts that have exceeded their life limits were undertaken. These parts are normally discarded without inspection. Even disks periodically inspected in ENSIP life management are not inspected one final time upon reaching the safe life limit. Inspection would identify parts whose actual lives were somewhat less than the predicted lives and thereby help improve prediction methods.

VII. RESIDUAL STRESS EFFECTS

The effects of compressive residual stress from shot peening was addressed by the CF6-6 HP Compressor Spool Test Case. The effect of shot peening on fatigue life, although generally beneficial, is rather unpredictable in a quantitative sense due to the potentially wide range of scatter in the results. It is the author's experience that such scatter is particularly pronounced in the case of titanium alloy fretting fatigue. Fretting fatigue is a potential failure mechanism for titanium alloy fan blades and discs, the blade dovetail and disc rim slot areas being particularly susceptible. Uncertainties associated with the residual stresses produced by shot peening were found to substantially complicate the task of life prediction under these conditions.

Further work is required to establish fretting fatigue testing standards that represent engine conditions, achieve better control of shot peening parameters that produce relatively uniform results and develop quantitative life prediction methods that take into account the effect of shot peening on fretting fatigue life.

Cold expansion is another technique that has been successfully used to improve fatigue life, but most of the work to date has been performed on aluminum alloys and very little data has been reported on application to engine components. This technique is being actively investigated in the author's laboratory, and excellent results have been seen in specimen tests on Ti-6Al-4V material. The application of this technique is being considered for bolt holes on J85 compressor discs and spacers and turbine wheels.

Concerns remain however, regarding,

(i) shifting the fracture critical location from the bolt holes to another location which could be difficult to inspect and/or in which crack propagation could be more rapid and catastrophic,
(ii) quality assurance in producing uniform results.

Intensive work is underway in the author's laboratory to resolve these issues.

VIII. EFFECTS OF REPAIR

Repair operations add a substantial number of additional variables and complexities to the task of life prediction. Advanced repair technologies are now being used extensively for a number of gas turbine components and coming years may see a substantial further increase in their application. Operations involved in repair or refurbishment involve a number of steps that alter the microstructure of the component, and thereby affect the life of the component. Hot Isostatic Pressing, when used for refurbishment to heal shrinkage cavities, braze porosity, and weld microcracks can be a beneficial influence on component life. However, weld repair and braze repair on the other hand, while they would be useful in refurbishing an unserviceable component to a serviceable condition, are likely to limit the life of a repaired component to a lower life than a new component. The task of estimating the life of a repaired/refurbished component is an important challenge, with substantial economic rewards. Future work in predicting life limits for repaired components is expected to have a synergistic effect in bringing newer, improved repair technologies to the market.

IX. USAGE MONITORING

Life prediction methods developed taking into account the various considerations mentioned above are put to best use through accurate usage monitoring techniques. Experience with fighter aircraft engine usage in Canada and the U.S. has indicated that life consumption based on flying hours varies considerably for the same type of aircraft and engine due to mission profile variations. Other users have found (16) that differences of a factor of 10 from flight to flight are not uncommon. Thus, the task of life prediction is not complete unless the design **and** utilization scenarios are taken into consideration.

As mentioned by Breitkopf and Speer (16), there are three basic methods for determining usage, namely;

(i) the use of overall cyclic exchange rates for converting the flying hours into the number of completed reference cycles or sequences,

(ii) the use of different cyclic exchange rates depending upon the nature of the mission flown, using speed characteristics as the primary criterion,

(iii) in-flight usage monitoring on the basis of the time history of the relevant flight and engine parameters.

The use of overall cyclic exchange rates can be valid only when the mission mix of all the aircraft is known and all engines undergo the same mission mix and the life consumption for this mission mix is known.

Evaluation of the flown missions using different cyclic exchange rates based on speed characteristics is probably the most commonly used method. In contrast to the method of using the overall cyclic exchange rates, this method offers substantially better accuracy. However, a satisfactory level of accuracy is likely to be achieved only in the case of cold section components with this method. Hot section parts need to be treated differently since load sequence effects and thermal effects

are very critical. Two types of missions which may cause very minimal difference in life consumption of cold section components may affect hot section components quite differently.

Thus, the risk of overshooting the approved usage period or the economic penalties of under utilization of component life can be avoided only through on-line computation of life consumed during the flight, from measured relevant flight and engine parameters.

However, such a system would be practical only if simple algorithms were developed to approximately calculate, in real-time, the life consumption calculated by a complex finite element and fracture mechanics based numerical analysis package. This makes the calculation effort substantially faster and simpler for the purpose of in-flight monitoring. MTU has developed a system based on these considerations, and have succeeded in being able to closely follow disk temperature and stress variations with their usage monitoring algorithms.

As our knowledge of life prediction improves, we need to implement improved methods of usage monitoring as well. There is a need for developing advanced usage monitoring systems for fighter aircraft engines operating in Canada and a major effort is underway at present in this direction, as a cooperative program between the author's company and the National Research Council of Canada. This effort is being funded by the Department of National Defence in Canada.

X. CONCLUSIONS

The discussion above clearly indicates that a substantial amount of work remains to be undertaken to improve our understanding of life prediction as applied to actual service experience. Test cases developed on the basis of recommendations made here would be of substantial value in helping engine designers and users calibrate their lifing models and improve on them. The author's company is very active in a number of the areas proposed here for future work and welcomes cooperation from other institutions in this regard.

References

1/ J. Lankford and S.J. Hudak Jr., "Relevance of the Small Crack Problem to Lifetime Prediction in Gas Turbines", Int. J. of Fatigue, Vol. 9, No. 2, 1987, pp 87-93.

2/ A. Fatemi and P. Kurath, "Multiaxial Fatigue Life Predictions Under the Influence of Mean Stresses", Trans. of the ASME, Vol. 110, October 1988, pp.380-388.

3/ Y.S. Garud, "Multiaxial Fatigue: A Survey of the State of the Art", J. of Testing and Evaluation, Vol. 9, No. 3, 1981, pp. 165-178.

4/ E. Krempl, "The Influence of State of Stress on Low Cycle Fatigue of Structural Materials: A Literature Survey and Interpretive Report", ASTM STP 549, American Society for Testing and Materials, Philadelphia, 1974, 46 pp.

5/ A. Petrovich and W. Zeigler, "The Influence of Several Combined High/Low Cycle Loading Parameters on the Crack Growth of a Turbine Disk Alloy", Transactions of the ASME, J. of Vibration, Acoustics, Stress and Reliability in Design, Vol. 108, July 1986, pp. 262-267.

6/ J.M. Larsen and T. Nicholas, "Load Sequence Crack Growth Transients in a Superalloy at Elevated Temperature", Fracture Mechanics: Fourteenth Symposium - Vol. II, Testing and Applications, ASTM STP 791, Eds: J.C. Lewis and G. Sines, American Society For Testing and Materials, 1983, pp. II-536-II-552.

7/ G.R. Halford, T.G. Meyer, R.S.

Nelson, D.M. Nissley and G.A. Swanson, "Fatigue Life Prediction Modelling for Turbine Hot Section Materials", Proc. of Conf. on "Toward Improved Durability in Advanced Aircraft Engine Hot Sections", 33rd ASME International Gas Turbine and Aeroengine Congress and Exposition, Ed: D.E. Sokolowski, American Society of Mechanical Engineers, 1988, pp. 97-107.

8/ R. Thamburaj, T. Terada, A.K. Koul, W. Wallace and M.C. de Malherbe, "The Influence of Microstructure and Environment upon Elevated Temperature Crack Growth Rates in Inconel 718, Proc. Int. Conf. on Creep, April 14-18 1986, JSME, I.MechE, ASME ASTM.

9/ A.G. Dodd, "Mechanical Design of Gas Turbine Blading in Cast Superalloys", Materials Science and Technology, Vol. 2, May 1986, pp. 476-485.

10/ P.N. Quested and S. Ogersby, "Mechanical Properties of Conventionally Cast, Directionally Solidified and Single Crystal Superalloys", Materials Science and Technology, Vol. 2, May 1986, pp. 461-475.

11/ K.S. Chan, J.E. Hack and G.R. Leverant, "Fatigue Crack Growth in MAR-M200 Single Crystals:, Metallurgical Transactions, Vol. 18A, April 1987, pp. 581-591.

12/ P.M. Besuner, K.G. Sorenson and D.P. Johnson, "A Workable Approach For Extending The Life Of Turbine Rotors", Proc. of the 22nd Annual International Gas Turbine Conference, Philadelphia, March 27-31, 1977, ed. T.A. Cruse and J.P. Gallagher, ASME.

13/ K.G. Sorenson and P.M. Besuner, "A Workable Approach For Extending the Life of Expensive Life-Limited Components", Failure Data and Failure Analysis, Proc. of the Energy Technology Conference on Power and Processing Industries, September 18-23, 1977, ed: A.C. Gangadharan, and S.J. Brown, Jr., The Pressure Vessels and Piping Division, ASME.

14/ C.A. Rau Jr., and P.M. Besuner, "Quantitative Decisions Relative to Structural Integrity", Trans. of the ASME, Vol. 102, January 1980, pp. 56-63.

15/ A.K. Koul, A. Fahr, G.M. Gould and N.C. Bellinger, "Influence of Sensitivity and Reliability of NDI Techniques on Damage Tolerance Based Life Prediction of Turbine Discs", National Research Council Technical Report, LTR-ST-1665, March 1988.

16/ G.E. Breitkopf and T.M. Speer, "In-Flight Evaluation of LCF Life Consumption of Critical Rotor Components Subjected To High Transient Thermal Stress", Proc. 63rd Specialists' Meeting of the Propulsion and Energetics Panel on Engine Cyclic Durability by Analysis and Testing, AGARD-CP-368, 1984.

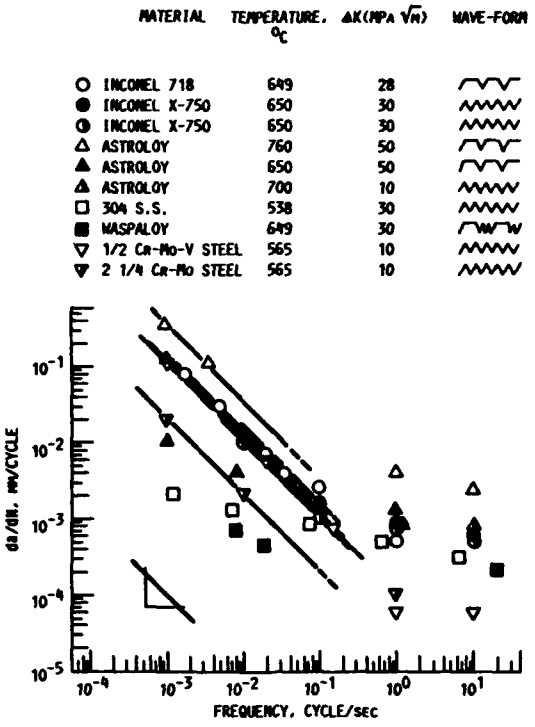

Fig. 1 Evaluation of the micro-mechanistic oxidation crack extension model of Liu and Oshida (7)

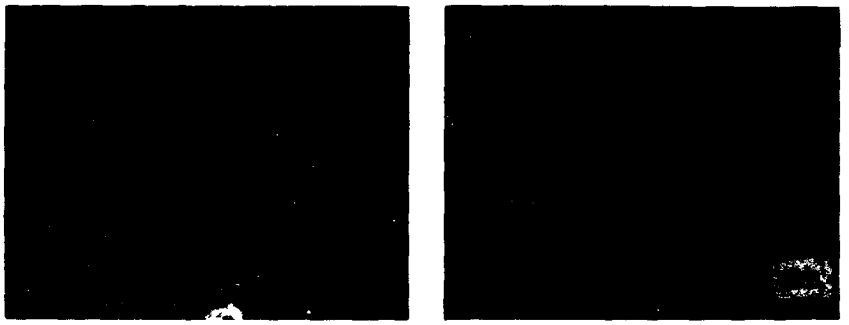

Fig. 2 Crack initiation at aluminide coating on a nickel base superalloy turbine blade

(a) initiation of thermal fatigue crack at the coating near a leading edge cooling hole

(b) preferential oxidation attack at the diffusion zone

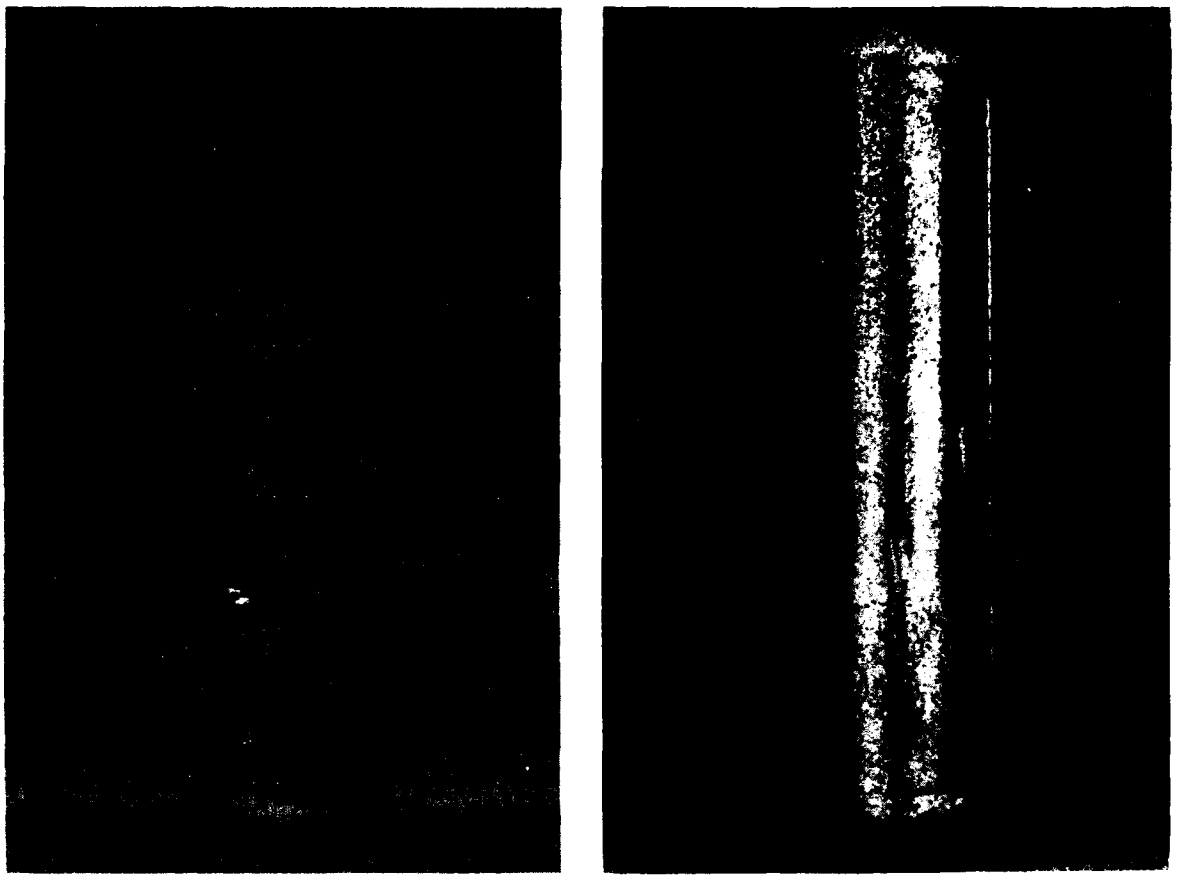

Fig. 3 Tool marks in a turbine wheel cooling air hole

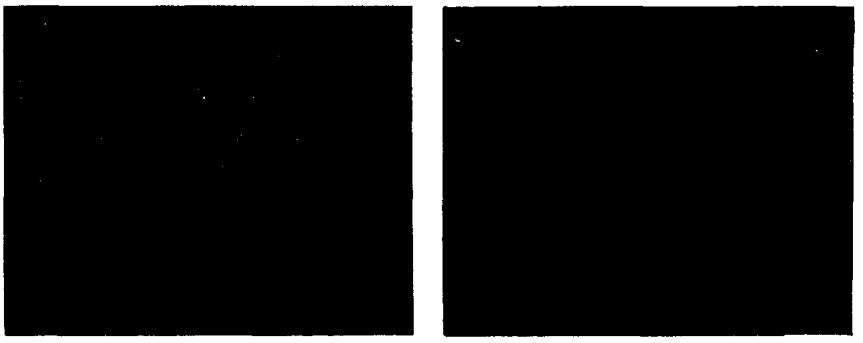

(a) (b)

Fig. 4 Shrinkage cavities in a cast turbine blade

(a) cavities at coating/alloy substrate interface

(b) oxidation attack of substrate alloy around a shrinkage cavity located near the coating/alloy substrate interface

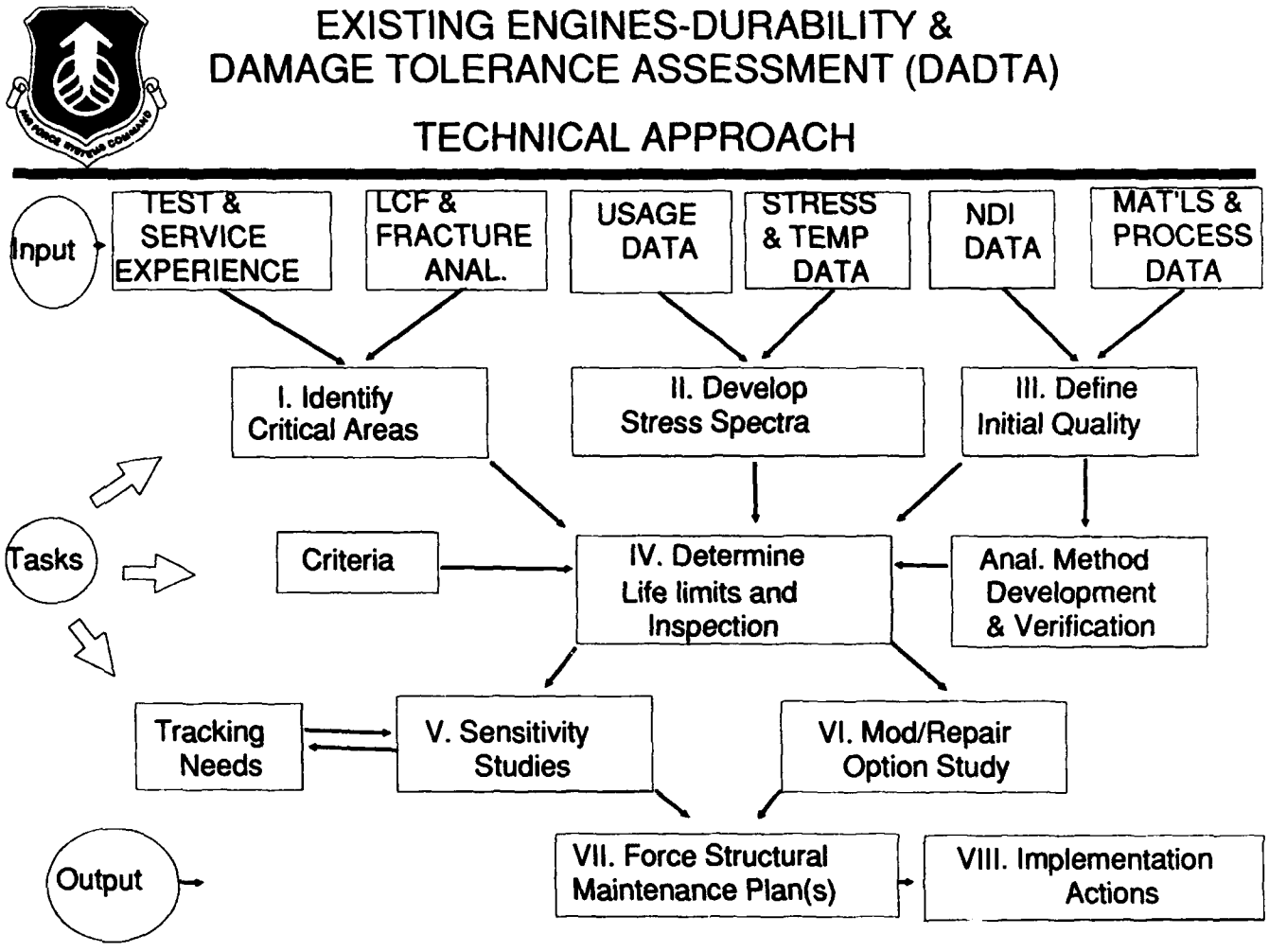

Fig. 5 USAF Damage Tolerance Assessment Technical Approach For Mature Engines

Chapter 9

FUTURE DIRECTIONS

by

Dr Robert C. Bill

As follow-up to the accomplishments of Working Group 20, test case usage will be monitored and feedback from users collected. At an appropriate time, defined by accumulated test case usage, a workshop involving test case authors and users would be mutually beneficial. The workshop will serve as a forum for discussing essential features of structural analysis and life prediction codes needed to capture the phenomena documented in the test cases. It will also serve as a guide to the development of future test cases addressing more complex phenomena and more recently emerged materials. Some specific technical areas of concern, that the six test cases in this report did not document, were discussed in some detail in the preceding section. It appears reasonable to consider some of these areas as a starting point for identifying topics for the "next generation" test cases.

The test cases comprising this report all addressed crack initiation phenomena in the elastic or elasto-plastic loading regime. Furthermore, all of the materials involved were conventional isotropic alloys. With the widespread application of single crystal materials to turbine airfoils, and the development of advanced constitutive models that describe in detail time dependent material mechanical behavior, the appropriateness of test cases involving anisotropic materials under creep-fatigue interactive loading is apparent. The challenges of course are the extent of the data base necessary to support such test cases at the engine component level, including coating effects and the shear difficulty of obtaining realistic component thermo-mechanical loading information. Indeed, the difficulties were considerable in the six test case assembled under this cover especially in the area of documenting the appropriate material data and crack initiation/growth information. Future efforts like those of Working Group 20 should concentrate on building just one well constructed test case in the category.

Within the structural analysis and life prediction research and development community, there is an increasing level of interest in probabilistic methodologies. This interest is partly stimulated by the development of structural ceramic materials wherein statistical approaches to critical flaw existence are mandatory. Statistical life prediction methodologies, however, are also applicable to high strength superalloy disks and other structures--rolling element bearing life prediction has been approached statistically for 60 years. A well formed statistical life prediction test case should address at least the seven statistical factors outlined in the previous section, and incorporate sufficient data to permit definition of necessary statistical parameters.

Pending definitive user feedback and other developments, future AGARD Propulsion Energetics Panel support of the development of engine life assessment test cases is probably a few years off. The support would have to take the form of a whole new Working Group which would maintain some continuity in philosophy and direction with Working Group 20. In the meantime, it is intended that a loose interaction between Working Group 20 members be maintained, and that at least one workshop will be undertaken.

REPORT DOCUMENTATION PAGE

1. Recipient's Reference	2. Originator's Reference	3. Further Reference	4. Security Classification of Document
	AGARD-AR-308	ISBN 92-835-0686-3	UNCLASSIFIED

5. Originator Advisory Group for Aerospace Research and Development
North Atlantic Treaty Organization
7 rue Ancelle, 92200 Neuilly sur Seine, France

6. Title TEST CASES FOR ENGINE LIFE ASSESSMENT TECHNOLOGY

7. Presented on

8. Author(s)/Editor(s)	9. Date
Various	September 1992
10. Author's/Editor's Address	**11. Pages**
Various	232

12. Distribution Statement This document is distributed in accordance with AGARD policies and regulations, which are outlined on the back covers of all AGARD publications.

13. Keywords/Descriptors

Compressor stage tests
Crack propagation
Ferris wheel tests
Gas turbine life
In-service life
Life assessment of engines
Spin tests
Test cases
Torsional fatigue of shafts
Turbine disk cracks
Turbine engine life

14. Abstract

This report presents a set of six test cases intended to provide support for the development and validation of structural analysis and life prediction codes applicable to gas turbine components. The test cases are based on actual engine simulation tests. The data bases comprising the test cases include geometric design information describing the component, rig interface information, material data, and test condition data including steady, dynamic, and thermal loading. Crack initiation and propagation data are also included. Hence, these test cases, for the first time, make available all of the component and loading information required to verify that existing codes or codes in development yield meaningful and consistent predictions.

This Advisory Report was prepared at the request of the Propulsion and Energetics Panel of AGARD.

AGARD A ory Report 308
Advisory G. for Aerospace Research and Development, NATO
TEST CASES FOR ENGINE LIFE ASSESSMENT TECHNOLOGY
Published September 1992
232 pages

This report presents a set of six test cases intended to provide support for the development and validation of structural analysis and life prediction codes applicable to gas turbine components. The test cases are based on actual ngine simulation tests. The data bases comprising the test cases include geometric design information describing the component, rig interface information, material data, and test condition data including steady, dynamic, and thermal

P.T.O.

AGARD-AR-308

Compressor stage tests
Crack propagation
Ferris wheel tests
Gas turbine life
In-service life
Life assessment of engines
Spin tests
Test cases
Torsional fatigue of shafts
Turbine disk cracks
Turbine engine life

AGARD Advisory Report 308
Advisory Group for Aerospace Research and Development, NATO
TEST CASES FOR ENGINE LIFE ASSESSMENT TECHNOLOGY
Published September 1992
232 pages

This report presents a set of six test cases intended to provide support for the development and validation of structural analysis and life prediction codes applicable to gas turbine components. The test cases are based on actual engine simulation tests. The data bases comprising the test cases include geometric design information describing the component, rig interface information, material data, and test condition data including steady, dynamic, and thermal

P.T.O.

AGARD-AR-308

Compressor stage tests
Crack propagation
Ferris wheel tests
Gas turbine life
In-service life
Life assessment of engines
Spin tests
Test cases
Torsional fatigue of shafts
Turbine disk cracks
Turbine engine life

AGARD Advisory Report 308
Advisory Group for Aerospace Research and Development, NATO
TEST CASES FOR ENGINE LIFE ASSESSMENT TECHNOLOGY
Published September 1992
232 pages

This report presents a set of six test cases intended to provide support for the development and validation of structural analysis and life prediction codes applicable to gas turbine components. The test cases are based on actual engine simulation tests. The data bases comprising the test cases include geometric design information describing the component, rig interface information, material data, and test condition data including steady, dynamic, and thermal

P.T.O.

AGARD-AR-308

Compressor stage tests
Crack propagation
Ferris wheel tests
Gas turbine life
In-service life
Life assessment of engines
Spin tests
Test cases
Torsional fatigue of shafts
Turbine disk cracks
Turbine engine life

AGARD Advisory Report 308
Advisory Group for Aerospace Research and Development, NATO
TEST CASES FOR ENGINE LIFE ASSESSMENT TECHNOLOGY
Published September 1992
232 pages

This report presents a set of six test cases intended to provide support for the development and validation of structural analysis and life prediction codes applicable to gas turbine components. The test cases are based on actual engine simulation tests. The data bases comprising the test cases include geometric design information describing the component, rig interface information, material data, and test condition data including steady, dynamic, and thermal

P.T.O.

AGARD-AR-308

Compressor stage tests
Crack propagation
Ferris wheel tests
Gas turbine life
In-service life
Life assessment of engines
Spin tests
Test cases
Torsional fatigue of shafts
Turbine disk cracks
Turbine engine life

loading. Crack initiation and propagation data are also included. Hence, these test cases, for the first time, make available all of the component and loading information required to verify that existing codes or codes in development yield meaningful and consistent predictions.

This Advisory Report was prepared at the request of the Propulsion and Energetics Panel of AGARD.

ISBN 92-835-0686-3

loading. Crack initiation and propagation data are also included. Hence, these test cases, for the first time, make available all of the component and loading information required to verify that existing codes or codes in development yield meaningful and consistent predictions.

This Advisory Report was prepared at the request of the Propulsion and Energetics Panel of AGARD.

ISBN 92-835-0686-3

loading. Crack initiation and propagation data are also included. Hence, these test cases, for the first time, make available all of the component and loading information required to verify that existing codes or codes in development yield meaningful and consistent predictions.

This Advisory Report was prepared at the request of the Propulsion and Energetics Panel of AGARD.

ISBN 92-835-0686-3

loading. Crack initiation and propagation data are also included. Hence, these test cases, for the first time, make available all of the component and loading information required to verify that existing codes or codes in development yield meaningful and consistent predictions.

This Advisory Report was prepared at the request of the Propulsion and Energetics Panel of AGARD.

ISBN 92-835-0686-3

AGARD
NATO OTAN
7 RUE ANCELLE · 92200 NEUILLY-SUR-SEINE
FRANCE
Téléphone (1)47.38.57.00 · Télex 610 176
Télécopie (1)47.38.57.99

DIFFUSION DES PUBLICATIONS
AGARD NON CLASSIFIEES

L'AGARD ne détient pas de stocks de ses publications, dans un but de distribution générale à l'adresse ci-dessus. La diffusion initiale des publications de l'AGARD est effectuée auprès des pays membres de cette organisation par l'intermédiaire des Centres Nationaux de Distribution suivants. A l'exception des Etats-Unis, ces centres disposent parfois d'exemplaires additionnels; dans les cas contraire, on peut se procurer ces exemplaires sous forme de microfiches ou de microcopies auprès des Agences de Vente dont la liste suite.

CENTRES DE DIFFUSION NATIONAUX

ALLEMAGNE
Fachinformationszentrum,
Karlsruhe
D-7514 Eggenstein-Leopoldshafen 2

BELGIQUE
Coordonnateur AGARD-VSL
Etat-Major de la Force Aérienne
Quartier Reine Elisabeth
Rue d'Evere, 1140 Bruxelles

CANADA
Directeur du Service des Renseignements Scientifiques
Ministère de la Défense Nationale
Ottawa, Ontario K1A 0K2

DANEMARK
Danish Defence Research Board
Ved Idraetsparken 4
2100 Copenhagen Ø

ESPAGNE
INTA (AGARD Publications)
Pintor Rosales 34
28008 Madrid

ETATS-UNIS
National Aeronautics and Space Administration
Langley Research Center
M/S 180
Hampton, Virginia 23665

FRANCE
O.N.E.R.A. (Direction)
29, Avenue de la Division Leclerc
92322 Châtillon Cedex

GRECE
Hellenic Air Force
Air War College
Scientific and Technical Library
Dekelia Air Force Base
Dekelia, Athens TGA 1010

ISLANDE
Director of Aviation
c/o Flugrad
Reykjavik

ITALIE
Aeronautica Militare
Ufficio del Delegato Nazionale all'AGARD
Aeroporto Pratica di Mare
00040 Pomezia (Roma)

LUXEMBOURG
Voir Belgique

NORVEGE
Norwegian Defence Research Establishment
Attn: Biblioteket
P.O. Box 25
N-2007 Kjeller

PAYS-BAS
Netherlands Delegation to AGARD
National Aerospace Laboratory NLR
Kluyverweg 1
2629 HS Delft

PORTUGAL
Portuguese National Coordinator to AGARD
Gabinete de Estudos e Programas
CLAFA
Base de Alfragide
Alfragide
2700 Amadora

ROYAUME UNI
Defence Research Information Centre
Kentigern House
65 Brown Street
Glasgow G2 8EX

TURQUIE
Milli Savunma Başkanlığı (MSB)
ARGE Daire Başkanlığı (ARGE)
Ankara

LE CENTRE NATIONAL DE DISTRIBUTION DES ETATS-UNIS (NASA) NE DETIENT PAS DE STOCKS DES PUBLICATIONS AGARD ET LES DEMANDES D'EXEMPLAIRES DOIVENT ETRE ADRESSEES DIRECTEMENT AU SERVICE NATIONAL TECHNIQUE DE L'INFORMATION (NTIS) DONT L'ADRESSE SUIT.

AGENCES DE VENTE

National Technical Information Service
(NTIS)
5285 Port Royal Road
Springfield, Virginia 22161
Etats-Unis

ESA/Information Retrieval Service
European Space Agency
10, rue Mario Nikis
75015 Paris
France

The British Library
Document Supply Division
Boston Spa, Wetherby
West Yorkshire LS23 7BQ
Royaume Uni

Les demandes de microfiches ou de photocopies de documents AGARD (y compris les demandes faites auprès du NTIS) doivent comporter la dénomination AGARD, ainsi que le numéro de série de l'AGARD (par exemple AGARD-AG-315). Des informations analogues, telles que le titre et la date de publication sont souhaitables. Veuiller noter qu'il y a lieu de spécifier AGARD-R-nnn et AGARD-AR-nnn lors de la commande de rapports AGARD et des rapports consultatifs AGARD respectivement. Des références bibliographiques complètes ainsi que des résumés des publications AGARD figurent dans les journaux suivants:

Scientifique and Technical Aerospace Reports (STAR)
publié par la NASA Scientific and Technical
Information Division
NASA Headquarters (NTT)
Washington D.C. 20546
Etats-Unis

Government Reports Announcements and Index (GRA&I)
publié par le National Technical Information Service
Springfield
Virginia 22161
Etats-Unis

(accessible également en mode interactif dans la base de données bibliographiques en ligne du NTIS, et sur CD-ROM)

Imprimé par Specialised Printing Services Limited
40 Chigwell Lane, Loughton, Essex IG10 3TZ